STRUCTURAL BEHAVIOUR OF GEOPOLYMER CONCRETE BEAMS AND COLUMNS REINFORCED WITH GLASS FIBRE REINFORCED POLYMER BARS

A thesis submitted by

Ginghis Bautista Maranan, M Eng

For the award of

Doctor of Philosophy

2016

Abstract

In Australia, the environments are severe to use steel as reinforcement to concrete structures from the viewpoint of corrosion damage. With the limited resources of the state and the federal governments to maintain existing infrastructures, a new approach for construction of more durable infrastructures is required. As a result, glass fibre reinforced polymer (GFRP) bars have gained considerable worldwide interest for use as internal reinforcement to concrete structures that operate in highly aggressive environments. At the same time, the use of geopolymer cement as an alternative to ordinary portland cement (OPC) is currently attracting increasingly widespread attention because its manufacture does not directly create CO_2 emissions. However, there is inadequate scientific research undertaken to substantiate the benefit of the combined use of these materials in actual infrastructure, which has been the key motivation for this research. Therefore, this study investigated the suitability and structural behaviour of geopolymer concrete structures reinforced with GFRP bars to allow the safe and responsible introduction of this technology in construction and civil infrastructure.

Firstly, the bond between geopolymer concrete and GFRP bar was investigated as this is a critical factor that influences the strength and long-term behaviour of reinforced concrete structures. The results obtained from the direct pullout test showed that the sand-coated GFRP bars have sufficient bond to geopolymer concrete through the sand-particles coated around its surface that provide the necessary mechanical interlock and friction forces. The bond between GFRP bars and geopolymer concrete was found comparable to deformed steel bars and was higher than GFRP-ordinary concrete bond. Generally, as the embedment length and bar diameter increases, the bond stress between the GFRP bars and geopolymer concrete decreases. The use of anchor heads further enhanced the pullout load resistance of the GFRP bars by as much as 49-77%, owing to the mechanical bearing resistance of the anchor heads.

The flexural behaviour of geopolymer concrete beams reinforced with GFRP bars was investigated as the second stage. The results showed that the serviceability performance of the beams is affected by the amount of reinforcement. The beams with a higher longitudinal reinforcement ratio exhibited lower deflection and narrower crack width, than the beams with lower reinforcement ratio. The reinforcement ratio and bar diameter, however, did not significantly influence the flexural strength of the beams. The beams with headed GFRP bars yielded similar flexural strength and serviceability performance as the beam with straight

GFRP bars. The GFRP-reinforced geopolymer concrete (GFRP-RGC) beams yielded higher flexural strength than both steel-reinforced geopolymer concrete (S-RGC) and GFRP-reinforced concrete (GFRP-RC) beams but inferior serviceability performance to S-RGC beams, owing to the higher tensile strength but lower elastic modulus of GFRP bars compared to steel bars.

The shear behaviour of geopolymer concrete beams reinforced with GFRP stirrups at different spacing was investigated in the third stage. The results showed that the GFRP web reinforcement doubled both the shear strength and deflection capacities of the beam without stirrups. The spacing of GFRP stirrups did not directly influence the strength and deflection capacities; however, it did affect the shear-crack width development, wherein the increase in stirrups spacing was accompanied by an increase in crack width. The beams with GFRP stirrups yielded relatively similar strength, deflection capacity, and stiffness as the beam with steel stirrups; however, wider shear cracks occurred in the former beams because of the lower elastic modulus of GFRP bars compared to that of steel bars. In addition, the shear capacity of the tested GFRP-RGC beams was higher than that of the FRP-RC beams.

The compression behaviour of circular GFRP-RGC columns subjected to concentric axial loads was investigated at the last stage. From the experimental outcomes, the provision of GFRP ties enhanced the compression performance of the geopolymer concrete column without transverse reinforcements. The columns with closely spaced ties yielded higher strength and deformation capacities and failed in a more ductile manner than the columns with widely spaced ties. The spiral-confined columns showed higher confinement efficiency and ductility compared to their counterpart hoop-confined columns, owing to the continuous nature of the spiral that enables it to distribute the stresses uniformly around and along the height of the column. The short columns yielded higher axial strength and stiffness compared to slender columns. This can be expected since the short columns failed due to crushing, a material type of failure, while the slender columns failed due to buckling, a geometric type of failure, owing to the effects of slenderness ratio. Generally, the GFRP-RGC beams and columns yielded better load-carrying capacity than their counterpart GFRP-reinforced concrete (GFRP-RC) with similar configurations and material properties. This could be attributed to the higher elastic modulus of geopolymer concrete compared to normal concrete of the same grade, resulting in better compatibility in the GFRP-RGC system that in a GFRP-RC system.

Prediction equations that reliably describe the structural behaviour of geopolymer concrete structures reinforced with GFRP bars were developed in each stage of the study. Cosenza, Manfredi, and Realfonzo (CMR)-based bond-slip laws were developed to model the ascending segment of the bond-slip curve while an analytical model was proposed to estimate the pullout load capacity of the straight and headed GFRP bars embedded in geopolymer concrete. Similarly, new analytical equations based on equivalent stress block and the parabolic stress block were developed to predict the flexural strength of the GFRP-RGC beams. In these equations, the usable concrete strain is 0.0048 and the compression contribution of top bars are included. The deflection of the beam, on the other hand, was estimated accurately by incorporating the constants β_a and β_b, both functions of actual and balanced reinforcement ratios, to the effective moment of inertia formula suggested by Branson. In terms of shear capacity, the ACI 318-14 strut-and-tie model yielded the most accurate predictions among the design equations employed in the study. Finally, a strength reduction of 0.90 and the compression contribution of GFRP bars up to a strain of 0.002 were considered in the proposed equation to estimate the nominal capacity of the columns. The comparison and validation of the developed analytical models showed good agreement with experimental results.

From this study, it is concluded that the GFRP-RGC system is a promising application. An enhanced understanding of the behaviour of geopolymer concrete beams and columns reinforced with GFRP bars is an outcome of this investigation. The analytical equations developed in this study can be important tools for design engineers permitting the safe design and development of GFRP-RGC system, enabling their increased acceptance and utilisation in the mainstream construction applications.

Certification of Thesis

I certify that the ideas, experimental work, results, analyses, and conclusions reported in this thesis are entirely my own effort, except where otherwise acknowledged. I also certify that the work is original and has not been previously submitted for any award, except where otherwise acknowledged.

_____ / /

Signature of Candidate Date

Endorsement

_____ / /

Signature of Principal Supervisor Date

_____ / /

Signature of Associate Supervisor Date

Acknowledgements

I would like to express my deepest gratitude to,

***Dr. Allan C. Manalo**, my principal supervisor, for giving me the opportunity to do a PhD at the University of Southern Queensland. I owe him an unbelievable amount of gratitude for his patient guidance, encouragement and advice all throughout these years. I have been extremely lucky to have a supervisor who cared so much about my work, and who responded to my questions and queries so promptly.*

***Prof. Warna (Karu) Karunasena**, my associate supervisor, and **Prof. Brahim Benmokrane** and **Prof. Priyan Mendis**, my advisers, for their valuable comments and suggestions that were essential in improving the quality of this research.*

*The **Faculty of Engineering, Health and Sciences (FoHES)** and the **Centre of Excellence in Engineered Fibre Composites (CEEFC)** for the academic, financial and technical support that made this research possible.*

*The **Office of Research and Graduate Studies (ORGS)** for the awarding me with USQ PhD scholarships to pursue my PhD study.*

***Prof. Thiru Aravinthan**, Associate Dean of Research and Research Training and Director of CEEFC, for the helpful discussions and suggestions.*

***Mr. Wayne Crowell**, **Mr. Martin Geach** and to all the **staff and postgraduate students at CEEFC** for their technical assistance during the fabrication, construction and testing of specimens and for their support and friendship.*

***Mr. Darren Lutze** and **V-Rod® Australia**, for the technical and materials support.*

***My family**, especially my **mother (Candida B. Maranan)** and **father (Bernardino M. Maranan)**, for your love, understanding, encouragement, and moral and financial supports that made me reach this success. You are the major driving force that keeps me pushing on in pursuing my goals in life.*

*And last but the not the least, our **ALMIGHTY GOD**, for giving me good health, courage, knowledge, and strength.*

Ginghis Bautista Maranan

Statements of Contributions

The following detail the share of co-authors in the presented publications in this thesis:

- **Maranan, G. B.,** Manalo, A. C., Karunasena W. M., and Benmokrane, B. (2015). Bond stress–slip behavior: Case of GFRP bars in geopolymer concrete. Journal of Materials in Civil Engineering, Vol. 27, Issue 1, pp. 04014116-1-9. (IF: 1.296, SNIP: 1.668)

  GBM was responsible for 70% of designing the experimental set-up, 80% of experimental works, 90% analysis and interpretation of data, and 100% of drafting and revising the final submission; ACM was responsible for 20% of designing the experimental set-up, 20% of experimental works, 10% of analysis and interpretation of data, and 80% of editing the manuscript and providing important technical inputs; WMK was responsible for 10% of designing the experimental set-up and 10% of editing the manuscript and providing important technical inputs; BB was responsible for 10% of editing the manuscript and providing important technical inputs

- **Maranan, G. B.,** Manalo, A. C., Karunasena W. M., and Benmokrane, B. (2015). Pullout behaviour of GFRP bars with anchor head in geopolymer concrete. Composite Structures, Vol. 132, pp. 1113-1121. (IF: 3.318, SNIP: 2.486)

  GBM was responsible for 80% of designing the experimental set-up, 90% of experimental works, 90% of analysis and interpretation of data, and 100% of drafting and revising the final submission; ACM was responsible for 10% of designing the experimental set-up, 10% of experimental works, 10% of analysis and interpretation of data, and 80% of editing the manuscript and providing important technical inputs; WMK was responsible for 10% of designing the experimental set-up and 10% of editing the manuscript and providing important technical inputs; BB was responsible for 10% of editing the manuscript and providing important technical inputs

- **Maranan, G. B.,** Manalo, A. C., Benmokrane, B., Karunasena W. M., and Mendis, P. (2015). Evaluation of the flexural strength and serviceability of geopolymer concrete

beams reinforced with glass-fibre-reinforced polymer (GFRP) bars. Engineering Structures, Vol. 101, pp. 529-541. (IF: 1.838, SNIP: 2.396)

GBM was responsible for 90% of designing the experimental set-up, 90% of experimental works, 90% of analysis and interpretation of data, and 100% of drafting and revising the final submission; ACM was responsible for 5% of designing the experimental set-up, 10% of experimental works, 10% of analysis and interpretation of data, 60% of editing the manuscript and providing important technical inputs; WMK was responsible for 5% of designing the experimental set-up and 10% of editing the manuscript and providing important editorial inputs; BB was responsible for 20% of editing the manuscript and providing important technical inputs; PM was responsible for 10% of editing the manuscript and providing important technical inputs.

- **Maranan, G. B.,** Manalo, A. C., Benmokrane, B., Karunasena W. M., and Mendis P. (S-2015-269.R3, accepted for publication). Shear behavior of geopolymer concrete beams reinforced with GFRP bars. ACI Structural Journal. (IF: 1.089, SNIP: 1.926)

  GBM was responsible for 90% of designing the experimental set-up, 90% of experimental works, 90% of analysis and interpretation of data, and 100% of drafting and revising the final submission; ACM was responsible for 5% of designing the experimental set-up, 10% of experimental works, 10% of analysis and interpretation of data, 60% of editing the manuscript and providing important technical inputs; WMK was responsible for 10% of editing the manuscript and providing important technical inputs; BB was responsible for 5% of designing the experimental set-up and 20% of editing the manuscript and providing important technical inputs; PM was responsible for 10% of editing the manuscript and providing important editorial inputs.

- **Maranan, G. B.,** Manalo, A. C., Benmokrane, B., Karunasena W. M., and Mendis P. (2016). Behavior of concentrically loaded geopolymer concrete columns reinforced longitudinally and transversely with GFRP bars. Engineering Structures, Vol. 117, pp. 422-436. (IF: 1.838, SNIP: 2.396)

GBM was responsible for 90% of designing the experimental set-up, 90% of experimental works, 90% of analysis and interpretation of data, and 100% of drafting and revising the final submission; ACM was responsible for 10% of designing the experimental set-up, 10% of experimental works, 10% of analysis and interpretation of data, 60% of editing the manuscript and providing important technical inputs; WMK was responsible for 10% of editing the manuscript and providing important technical inputs; BB was responsible for 20% of editing the manuscript and providing important technical inputs; PM was responsible for 10% of editing the manuscript and providing important technical inputs.

Table of Contents

List of Figures

List of Tables

1. INTRODUCTION

1.1. Research background and motivation

Reinforced concrete (RC) is one of the most widely adopted composite materials in the construction of civil infrastructure such as the multi-storey buildings, roads, bridges, retaining walls, and underground structures. It has, however, several disadvantages, including the corrosion of internal reinforcing steel bars and the sustainability issue of cement, which drive engineers and researchers to look for viable alternatives. Steel corrosion is the main contributing factor that causes the deterioration of concrete (PCA 2002) as shown in **Figure 1.1**, resulting in the early strength degradation and loss of serviceability of RC structures. In addition, the maintenance, repair, and rehabilitation of damaged and deteriorating RC structures are costly (Achillides and Pilakoutas 2004) and bear heavily to one's economy. The sustainability issue of cement, on the other hand, is also one of the main disadvantages of RC materials because the production of 1.0 tonne of cement releases approximately 1.0 tonne of CO_2 in the atmosphere (Mehta 2010). In fact, cement industry contributes around 8% of the worldwide yearly CO_2 emissions (Olivier *et al.* 2015). Furthermore, the cement manufacturing is a resource- and energy-intensive process. Approximately, 2.8 tonnes of virgin raw materials and 110-120 kWh are needed to manufacture 1.0 tonne of cement (Guo *et al.* 2010; Mejeoumov 2007). With the stated drawbacks of the conventional RC system, engineers and researchers were driven to modify the existing system and/or to develop new but more effective alternatives. Among the current solutions that are being employed are to replace steel bars with glass fibre reinforced polymer (GFRP) bars or to replace ordinary concrete with geopolymer concrete.

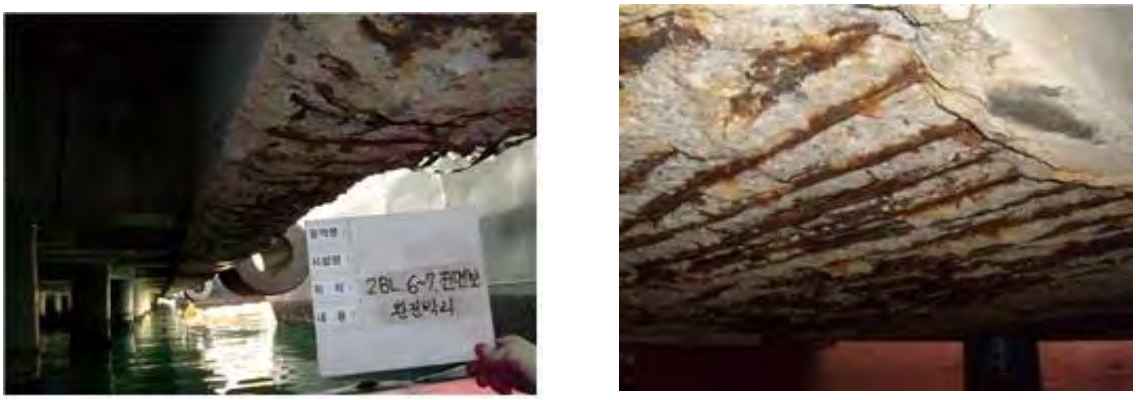

Figure 1.1 Corrosion problems of concrete structures

Fibre reinforced polymer (FRP) composite bars have gained considerable worldwide interest and growing acceptance in the construction industry as internal reinforcement in concrete structures to enhance the durability and prolong the service life of these structures. This composite material which typically consists of strong fibres embedded within a light polymer matrix has become an attractive construction material because of its corrosion resistant, light weight, high tensile strength, and nonmagnetic properties (Gangarao *et al.* 2007; Robert and Benmokrane 2009), with the added benefits of rapid and ease of construction. Among the existing FRP bars, however, GFRP bars are the most popular because they are more economical than carbon FRP (CFRP) and aramid (AFRP) bars (Robert and Benmokrane 2010). Based on the previous studies (Arias *et al.* 2012; Okelo and Yuan 2005), the GFRP bars can be properly anchored in concrete through the provision of sand coating, which provide the mechanical interlock and friction forces to resist pullout stresses. Moreover, several researchers (Alsayed 1998; Alsayed *et al.* 2000; Benmokrane *et al.* 1995; Masmoudi *et al.* 2012; Matos *et al.* 2012) suggest that FRP bars can be as effective as steel bars for reinforcement in concrete beams but require different design considerations. In the same way, GFRP bars are found suitable for transversely reinforcing the concrete beams because web reinforcements are more susceptible to corrosion as they are nearer to concrete outer surface compared with the longitudinal bars (Ahmed *et al.* 2010b). In fact, the ACI 440.1R-15 (2015) guidelines and CAN/CSA S6-14 (2014) codes encouraged the use of FRP stirrups as transverse reinforcement for concrete members. While experimental and developmental activities conducted on the behaviour of GFRP bars as longitudinal reinforcement for concrete structures under compression are still limited (M.Z. Afifi *et al.* 2013; De Luca *et al.* 2010; H.M. Mohamed *et al.* 2014; Tobbi *et al.* 2012), all studies concluded that the GFRP-reinforced concrete columns exhibited almost the same strength to their steel reinforced counterparts. These activities have resulted in the widespread applications of GFRP bars in many parts of the world.

Geopolymer concrete, on the other hand, is considered as a viable alternative to the traditional cement-based concrete for the development of environment-friendly and sustainable structures because the geopolymer binders can be manufactured using alkali-activated industrial waste materials that are rich in silica and alumina (e. g. slag and fly ash) (Lloyd and Rangan 2010). Davidovits (1991) coined the term “geopolymer” since the chemical reaction that takes place between the source materials and the activating alkaline liquid is a polymerisation process. The use of geopolymer concrete is currently attracting increasingly widespread attention in the construction industry because its manufacture reduces the CO_2

emission by 80-90% compared to those of ordinary portland cement (OPC)-based concrete (Duxson *et al.* 2007). Furthermore, this material has highly desirable properties that can lead to significant cost savings in many structural members (Lloyd and Rangan 2010). The cost of one ton of fly ash is only a small fraction, approximately 10% to 30 %, of the cost of one ton of OPC (Hardjito and Rangan 2005; Kambic and Hammaker 2012). Hardjito and Rangan (2005) estimated that the chemicals (sodium silicate solution and sodium hydroxide solids) needed to react one tonne of fly ash is significantly lower than that of OPC, which is approximately 50 AUD. To date, most researches have focused only on geopolymer concrete mix design and durability (Palomo and Glasser 1992; Rangan 2008; Sofi *et al.* 2007; Xu and van Deventer 2000) with a few research works reported on bond strength between geopolymer concrete and steel reinforcement (Sarker 2011; Selby 2011) and behaviour of beams and columns made up of steel-reinforced geopolymer concrete (S-RGC) (Abraham *et al.* 2013; Murugavel and Mala 2014; Sarker 2009; Sujatha *et al.* 2012; Sumajouw and Rangan 2006). It is necessary therefore to extend the understanding into the behaviour of full-scale structure made up of geopolymer concrete to increase its acceptance and utilisation in the mainstream construction applications.

A logical solution, therefore, is to combine GFRP bars and geopolymer concrete to construct structures with increased durability and substantially reduced embodied carbon while providing requisite of strength and stiffness. However, there is inadequate scientific research undertaken to substantiate the benefit of the combined use of these materials in actual infrastructure. This has been the key motivation for undertaking this research. Specifically, no research work has been reported on the bond behaviour of GFRP reinforcement in geopolymer concrete and on the effect of anchor heads on the bond resistance of GFRP reinforcement. While there are a number of studies that dealt with the shear performance of GFRP-RC slender beams (Ahmed *et al.* 2010a; Bentz *et al.* 2010; El-Sayed and Soudki 2011; Oller *et al.* 2015), limited studies have focused on short/deep beams, especially the influence GFRP transverse reinforcement in these beams. Furthermore, the use of GFRP bars for compression member is not recommended by most of the current design codes and standards, mainly because of the perceived low compression contribution of GFRP bars. With the advances in FRP technology, however, the new generation of GFRP bars have enhanced physical and mechanical properties that has high potential for reinforcing geopolymer concrete columns.

In this study, the structural behaviour of GFRP-reinforced geopolymer concrete (GFRP-RGC) system was experimentally and analytically investigated. A better understanding

on its bond mechanism was gained first because it is the critical factor that controls the structural performance of any reinforced concrete members. The effects of bar diameter, embedment length, and anchorage system on the bond performance of GFRP bars in geopolymer were assessed. The results of this initial study provided the necessary information to extend the understanding into the flexural, shear, and compression behaviour of full-scale beams and columns made up of geopolymer concrete reinforced longitudinally and transversely with GFRP bars. The test results were then compared to that of the published results on RC, FRP-RC, and S-RGC systems to assess the acceptability of the proposed system. Furthermore, new analytical equations were proposed whenever the current design equations for RC and FRP-RC systems (e.g. ACI, CSA, etc.) were not applicable. It is anticipated that engineering data generated from this study will provide useful information on the performance behaviour of this construction system that can be utilised by designers and engineers in designing GFRP-RGC structures more effectively and comply with the safety requirements.

1.2. Research questions

The main research questions that were addressed through the course of this study are:

- What are the effects of embedment length, bar diameter, and anchorage system on the bond performance of GFRP bars in geopolymer concrete?
- How do geopolymer concrete beams reinforced with GFRP bars and stirrups behave under flexural and shear loading?
- How do geopolymer concrete columns reinforced with GFRP bars and ties behave under compressive loads?
- What are the similarities and/or differences of the structural behaviour of GFRP-RGC system compared to the conventional RC, GFRP-RC, and S-RGC systems?
- Are the existing design codes and analytical models for the conventional RC and FRP-RC system applicable to GFRP-RGC system?

1.3. Research objectives

This thesis aimed at evaluating the structural behaviour of geopolymer concrete beams and columns reinforced with glass-fibre-reinforced polymer (GFRP) bars through experimental and analytical investigations. The specific objectives of this study were:

1. To investigate the effects of the bar diameter, embedment length, and anchorage system on the bond performance of GFRP bars in geopolymer concrete;

2. To determine the flexural and shear behaviour of GFRP-RGC beams with varying reinforcement ratios, bar diameters, anchorage systems, stirrups spacing, and shear-span-to-effective-depth ratio using the four-point bending test;
3. To examine the behaviour of GFRP-RGC circular columns under concentric loading with different slenderness ratios, tie spacing, and tie configurations;
4. To determine the similarities and/or differences of the GFRP-RGC system in comparison with the GFRP-RC and S-RGC systems; and
5. To evaluate the applicability of the existing design codes and analytical models for the conventional RC and FRP-RC system to the GFRP-RGC system and, if not, to develop prediction equations for the proposed system.

1.4. Scope and limitations

This thesis investigated the structural performance of geopolymer concrete beams and columns internally reinforced with GFRP bars. The straight and bent GFRP bars used in this study were high modulus bars and were made through the pultrusion process of continuous E-glass fibres embedded in a modified vinyl ester resin. The mechanical properties of the GFRP bars (straight, headed, ties and spiral) used in this thesis resulted from numerous actual tests conducted by Pultrall Inc. (the bar manufacturer) and by researchers at the University of Sherbrooke. These information were provided by Prof. Brahim Benmokrane of the University of Sherbrooke. The geopolymer concrete, on the other hand, is a commercially produced concrete, under ambient curing, with a proprietary mixture consisting of fine and medium sands, 10 mm and 20 mm coarse aggregates, water, plasticizer, and a geopolymer binder produced from the alkali-activation of two industrial by-product materials, the fly ash and slags.

The bond mechanism between the GFRP bars and the geopolymer concrete was investigated using the direct pullout test in accordance with ACI 440.3R-04 with some modifications. Firstly, the length of the concrete cube was increased from 200 mm to 300 mm to accommodate the longest embedment length of $15d_b$ = 300 mm. Secondly, the specimens were cast horizontally to concentrically align the bar and to make the loaded surface of the geopolymer concrete as plane as possible to minimize errors on the measured slip. Moreover, this casting procedure simulate that of beams that are normally prepared horizontally. Lastly, the overall slip was measured by placing an LVDT in the unloaded end of the bar as recommended by RILEM 7-II-128 (1994). The direct pullout test was adopted in this study because, relatively, it is simpler, more convenient, and more economical compared to the other tests. Similarly, this test method had been successfully used in numerous studies (Achillides

and Pilakoutas 2004; Al-Zahrani *et al.* 1999; Baena *et al.* 2009; Bakis *et al.* 1998; Benmokrane and Tighiouart 1996; Ganesan *et al.* 2015; Kim and Park 2014; Okelo and Yuan 2005; Robert and Benmokrane 2010) to evaluate the influence of concrete strength, surface conditions of the bar, bar diameter, concrete cover, and embedment length on the bond behaviour of reinforcement in concrete. In fact, various provisions and test procedures had already been developed for direct pullout test such as ACI 4403.3R B.3, CSA S806 Annex H, JSCE E-539 and RILEM 7-II-128. The state of stresses around the bars have been the issue of using the direct pullout test; however, the study conducted by Filho *et al.* (2008) showed that the results obtained from pullout test were similar to that of beam test for concrete with compressive of 30.10 MPa to 32.02 MPa. This strength was similar to that of the geopolymer concrete used in the pullout test (around 33 MPa). The flexural and shear behaviour of GFRP-RGC beams, on the other hand, were investigated using the four-point static bending test to minimise stress concentration at the loading points and to expose a larger portion of the beams. The columns were subjected to concentric loads. This loading condition is an initial step to understand whether GFRP bars can be used as internal reinforcement for RC columns.

The structural behaviour of the members made of GFRP-RGC were compared to that of the conventional RC, GFRP-RC, and S-RGC members to assess the adoptability of the GFRP-RGC system for the fabrication of structural members. In addition, the applicability of the analytical equations formulated by several researchers (M.Z. Afifi *et al.* 2013; Cosenza *et al.* 1997; Han *et al.* 2003; Mihaylov *et al.* 2013; H.M. Mohamed *et al.* 2014; Popovics 1973) and the current design procedures for RC and FRP-RC systems (ACI 318-14 2014; ACI 440.1R-15 2015; CAN/CSA S806-12 2012; JSCE 2007), was evaluated and, if not applicable, new prediction equations, calibrated from the experimental results, were developed.

1.5. Thesis organisation

This thesis is composed of an introduction that present the research theme, an extensive review of related literature, five major studies which address the main objective of this research and with results that are presented in high quality international journals, a conclusion that summarises the general findings and contributions of this study, and some recommendations for future works. The five journal manuscripts that resulted from this research are the following:

- **Paper I: Maranan, G. B.,** Manalo, A. C., Karunasena W. M., and Benmokrane, B. (2015). Bond stress–slip behavior: Case of GFRP bars in geopolymer concrete. Journal

of Materials in Civil Engineering, Vol. 27, Issue 1, pp. 04014116-1-9. (IF: 1.296, SNIP: 1.668)

- **Paper II: Maranan, G. B.,** Manalo, A. C., Karunasena W. M., and Benmokrane, B. (2015). Pullout behaviour of GFRP bars with anchor head in geopolymer concrete. Composite Structures, Vol. 132, pp. 1113-1121. (IF: 3.318, SNIP: 2.486)
- **Paper III: Maranan, G. B.,** Manalo, A. C., Benmokrane, B., Karunasena W. M., and Mendis, P. (2015). Evaluation of the flexural strength and serviceability of geopolymer concrete beams reinforced with glass-fibre-reinforced polymer (GFRP) bars. Engineering Structures, Vol. 101, pp. 529-541. (IF: 1.838, SNIP: 2.396)
- **Paper IV: Maranan, G. B.,** Manalo, A. C., Benmokrane, B., Karunasena W. M., and Mendis, P. (S-2015-269.R3, accepted for publication). Shear behavior of geopolymer concrete beams reinforced with GFRP bars. ACI Structural Journal. (IF: 1.089, SNIP: 1.926)
- **Paper V: Maranan, G. B.,** Manalo, A. C., Benmokrane, B., Karunasena W. M., and Mendis, P. (2016). Behavior of concentrically loaded geopolymer concrete columns reinforced longitudinally and transversely with GFRP bars. Engineering Structures, Vol. 117, pp. 422-436. (IF: 1.838, SNIP: 2.396)

In addition, the significant findings from this research were presented in related national and international conferences, which are summarised in Appendix B.

The **first specific objective** was successfully addressed and the results were presented in **Papers I and II**. **Paper I** gives an overview of the bond stress-slip behaviour of sand-coated GFRP bars in geopolymer concrete using the direct pullout test. The effects of the bar diameter and embedment length on the pullout load capacity, mode of failure, and bond stress-slip behaviour of GFRP-geopolymer-concrete pullout specimens were evaluated. **Paper II**, on the other hand, presents of the effects of anchor head on the pullout behaviour of the GFRP bars in geopolymer concrete. The headed GFRP bars embedded in a geopolymer concrete cube were subjected to direct pullout test. The effects of the embedment length and bar diameter were also evaluated. The test results such as the mode of failure, average bond stress, pullout load-slip relationship, and tensile stress developed in the bars were examined and were compared to that of the straight GFRP bars. From the result of this study, it was found that sufficient bond exists between the GFRP bar and geopolymer concrete to effectively transfer the stresses from one to the other and secure a composite action. This validated the acceptability of GFRP bars

as alternative reinforcement to geopolymer concrete structures such as beams and columns, which are investigated to address the key objectives of the study.

Paper III and **IV** addressed the **second specific objective** of the study. **Paper III** focuses with the flexural strength and serviceability performance of the geopolymer concrete beams reinforced with glass fibre reinforced polymer (GFRP) bars using the four-point static bending test. The parameters investigated were the nominal bar diameter, reinforcement ratio, and anchorage system. The test results were reported in terms of load-deflection relationship, mode of failure, flexural capacity, midspan deflection, strain distribution and cracking behaviour. Conversely, **Paper IV** shows the influence of stirrups, stirrup spacing, stirrup type, longitudinal reinforcement ratio, and shear-span-to-depth ratio (a/d) on the shear performance of the geopolymer concrete beams longitudinally and transversely strengthened with GFRP reinforcement using similar test setup used for flexural investigation. The behaviour of the beams was described in terms of the crack pattern and propagation, failure mode, load-deflection response, cracking load, shear and deflection capacities, and geopolymer concrete and reinforcement strains. These results suggest that GFRP bars can be as effective as steel bars for reinforcement in geopolymer concrete beam structures but some considerations should be considered in their design. The effectiveness of GFRP- reinforced geopolymer concrete structure subject to compressive loading, i.e. columns was then investigated to address another objective of the study.

The **third specific objective**, the behaviour of concentrically loaded circular geopolymer concrete columns reinforced longitudinally and transversely with GFRP bars, is covered in **Paper V**. Initially, the compression contribution of longitudinal GFRP bars was determined. Then, the effects of tie, tie spacing and tie configuration to the confinement and ductility of the geopolymer concrete core and stability of the longitudinal reinforcement were studied, including the influence of the slenderness ratio. The load-deformation response, mechanism of failure, strength and deformation capacity, geopolymer concrete and reinforcement strains were thoroughly investigated. The results of the extensive experimental programs presented in Papers I to V have demonstrated that GFRP bars are effective reinforcement to geopolymer concrete structures. A comparison was then conducted to determine the similarities and/or differences of the GFRP-RGC system to that of GFRP-RC and S-RGC systems.

The **fourth specific objective** was successfully addressed in each paper. The bond of performance of the sand-coated GFRP bars in geopolymer concrete was compared to that of steel bars embedded in geopolymer concrete and to that of GFRP bars bonded in normal

concrete to check whether the anchorage system used for GFRP bars could match the pullout resistance coming from the mechanical bearing of the deformed steel bars. The flexural, shear, and compression test results of the GFRP-RGC system were also compared to that of the experimental results obtained from S-RGC system and the published results on FRP-RC system to assess the viability of the proposed system for structural applications. Analytical equations were then developed to describe the behaviour of geopolymer concrete members reinforced with GFRP bars accurately.

The **fifth specific objective** of this study was successfully accomplished. Constitutive analytical models for the ascending branch of bond-slip curve, based on the Cosenza, Manfredi, and Realfonzo (CMR) model, were developed to provide tools for evaluating the bond performance of GFRP bars in geopolymer concrete at the service condition. These models were presented in **Paper I**. An analytical equation that can estimate both the pullout load capacity of the straight and headed GFRP bars was formulated and presented in **Paper II**. The derived equation was basically dependent on the bonded length and nominal diameter of the bar and the concrete cover. The flexural strength and serviceability performance of the GFRP-RC beams were assessed using the equations prescribed by the CSA S806-12 (2012), ACI 440.1R-15 (2015), and ACI 318-14 (2014); however, none of these codes provided accurate estimates. Hence, new prediction equations were developed, which are summarised in **Appendix A**. Different shear design provisions were employed to identify which of the existing codes could be used to predict the capacity of the tested beams, including the ACI 318-14 (2014) and CSA S806-12 (2012) strut-and-tie models, the JSCE-07 (JSCE) shear formula for RC beams, and the kinematic model for deep beams developed by Mihaylov et al. (2013). Based on the results presented in **Paper IV**, the ACI 318-14 gave the most accurate predictions among the considered equations. Finally, various equations were used to determine which among these equations could accurately estimate the nominal capacity of the tested columns. A stress-strain model for the confined GFRP-RGC column was proposed and is summarised in **Paper V**.

2. REVIEW OF RELATED LITERATURE

2.1. Reinforced concrete and its challenges

Reinforced concrete (RC) is one of the most widely used composite materials in the construction of civil infrastructures like buildings, roads, bridges, retaining walls, and underground structures. It is generally composed of high compressive strength concrete that is longitudinally and transversely reinforced with high tensile strength and ductile steel bars and stirrups, respectively. In fact, the advantages of concrete compensate for the disadvantages of steel bars and vice versa. Concrete, in general, have high compressive strength that made them suitable for members primarily subjected to compression, such as columns. However, it lacks ductility and its tensile strength is small, approximately 8-15% of its compressive strength. To counteract this limitation, high tensile strength and ductile steel bars are used to reinforce the concrete. The concrete cover, on other hand, prevents the occurrence of steel corrosion.

A concrete structure is basically composed of beams, columns, slabs, walls, and foundations (MacGinley and Choo 1990). In general, columns are regarded as the most critical and important structural members, followed by beam-column joints and beams, while slabs are generally less critical and relatively easy to replace or strengthen (Wasti and Ersoy 2006). Columns and beams are typically the two main component members of a rigid-frame that provides the lateral stability of the structure (e.g. multi-storey buildings) and hold the structure together. The beams carry the external transverse loads, from the floors and roofs, and transfer these loads to columns by bending and shear actions. The columns, on the other hand, transfer these loads to foundations through axial compression or tension plus bending and shear actions. A damaged beam or column will most likely cause the instability of the whole structure. Hence, the strength and stiffness of these members, including the rigidity of their connections, must be designed properly.

The bond interaction between the reinforcement and concrete is one of the critical factors that controls the structural performance of RC members, aside from the properties of its constituent materials. An adequate bond must exist between these two materials to achieve a composite action, such that the forces are transferred effectively from one to the other and vice versa (Foster *et al.* 2010). The bond strength of deformed steel bars is mainly provided by the mechanical interlock of the surface deformations or indentations, with little contribution from the chemical adhesion and the mechanical friction between the reinforcement and concrete

(Nilson *et al.* 2003). The deformations enhance the bending, shear, and torsion resisting mechanisms of RC members and control the width of the cracks by minimising the slip of the reinforcement relative to concrete. In addition to deformations, the provision of bends and hooks at the end of the reinforcement provide additional bearing resistance that enhance the bar anchorage and prevent slippage. The use of standard hooks, however, would likely result in steel congestion, particularly in the exterior or corner beam-column joints, with the difficulty of steel fabrication, especially when high strength-steel are used, and concrete placement and compaction during casting (Dhake *et al.* 2015; Sung-Gul *et al.* 2007). Nowadays, the use of headed bars is becoming a more popular alternative to standard hooks since it provides a solution to the construction problem of steel congestion (Kang and Mitra 2012).

The prevalent global adoption of RC material can be attributed to the following: 1) its relatively lower cost compared to the other building materials; 2) the widespread accessibility to its component materials such as cement, sand, gravel, water, and reinforcing steel bars; 3) its ability to be moulded to different shapes and sizes according to the desired structural forms; and 4) the relatively simpler skills required in erecting RC structures (Nilson *et al.* 2003; Wight and MacGreggor 2009). However, it has two principal disadvantages, including the corrosion of steel bars and sustainability issue of cement, which made engineers and researchers to look for viable alternatives.

2.1.1. Corrosion of steel reinforcement

The corrosion of steel reinforcement is one of the major factors that causes the deterioration of concrete that consequently result to the early strength degradation, loss of serviceability, and sometimes failure of RC structures, especially those that are located in or near marine, mining, and industrial environments and those that are constantly exposed to de-icing salts (Otieno *et al.* 2016). The expected service life of RC structures is usually around 50 years; however, their lifespan in aggressive environments was being reduced by 20 to 30 years or even more due to steel corrosion (Mehta 1997). Generally, there are two major types of corrosion in RC structures, the local and general corrosions (Capozucca 1995; Pantazopoulou and Papoulia 2001). The local corrosion, also known as pitting corrosion, happens when the chloride ions penetrate into the concrete and reach a critical threshold value at the reinforcement depth, given that there is a sufficient amount of moisture and oxygen at the steel surface (Tang *et al.* 2008; Tao *et al.* 1992; Tighiouart *et al.* 1998; Torres-Acosta *et al.* 2007). The chlorides may be introduced into concrete “internally” by unknowingly or deliberately using chloride-contaminated mixing water, gravels, and admixtures or “externally” from the seawater and

other chloride-contaminated environments. The general corrosion, on the other hand, transpires through the carbonation of concrete. Carbonation happens when the carbon dioxide in the atmosphere penetrates the concrete and reacts with calcium hydroxides to form calcium carbonates (Bertolini 2008). This chemical reaction lowers the pH of concrete from its normal values (13 to 13.8) to neutral values (as low as 8.5) that destabilizes the steel's passive film, a protective oxide layer surrounding the steel that shields it from corrosion (PCA 2002). When the neutralization process reaches the steel surface, the protective layer breaks down and corrosion becomes possible, again, if enough amounts of oxygen and moisture are available. The chloride-induced corrosion, however, is more dominant than carbonation-induced corrosion (Otieno *et al.* 2016).

Once the corrosion of the steel bars commenced, the rust products can expand to a volume of approximately four times the original volume of steel with the same mass (Isgor and Razaqpur 2006). The expansion of the corroding steel generates internal bursting or tensile stresses that cause the cracking, delamination, and spalling of the concrete surrounding the reinforcement, since concrete is physically weak in tension. This phenomenon together with the reduction of load–bearing capacity of the reinforcement, owing to the loss of steel cross section, and the weakening of the of steel-to-concrete bond directly affect the residual strength and serviceability of the structural elements, and hence, of the whole RC structure (Cabrera 1996; Rodriguez *et al.* 1997). The range of the remaining service life of a corroding RC structure is generally influenced by the rate of corrosion (Ahmad 2003). Even though the corrosion process can be delayed by providing adequate concrete cover or by the high alkalinity of the concrete solution, still, it cannot be "prevented" due to the degradation of concrete cover with the passage of time, presence of concrete pores, inadequate material specifications, and poor workmanship.

In addition to the degradation of strength and structural integrity, the economic loss associated with the expenditures for the repair, rehabilitation, and maintenance of damaged and deteriorating RC structures caused by steel corrosion is also one the major problems faced by the asset owners. Worldwide, billions of dollars are spent every year in repairing and strengthening concrete structures whose reinforcement has deteriorated due to corrosion (Achillides and Pilakoutas 2004). In the year 2006, the International Federation for Structural Concrete ((fib Bulletin 40 2007)) estimated that more than 100 billion euros are needed to repair and maintain existing infrastructures around the world and a large portion of this budget was spent to address the durability problems in concrete structures. In the United States, the

total financial loss caused by the reinforcement corrosion in RC structures is about 2.8 billion dollars annually – approximately 4% of its gross national product (GNP) (Sung-Ho and Rak-Hyun 2011). In Ontario, Canada, it was estimated that around $57 billion was spent to repair the 10,000 structurally-deficient RC bridges due to steel corrosion (Bruun 2014). In the year 2009, Ratcliff (2009) reported that the corrosion may have cost Australia up to $32 billion per annum which translates to more than $1,500 per person per year in Australia. In view of the enormous cost involved in the initial construction and in the repair and rehabilitation of RC structures, it is imperative, therefore, to develop more durable and cost-effective alternative to steel reinforcement.

2.1.2. Sustainability issue of cement

Cement-based concrete is the most commonly used construction material in the world, and next to water as the mostly consumed material (Sakulich 2011). **Figure 2.1** shows the yearly global production of cement from 1994 to 2014 as reported by the United States Geological Survey or USGS (van Oss 1996-2016), with China contributing the largest portion with a yearly average of 44% of the total production in the world. From the figure, it is apparent that the worldwide manufacture of cement increases yearly in the previous years. In fact, it will keep on increasing in the coming years as reported by the Portland Cement Association (PCA 2015), wherein they estimated that the world cement consumption increased by 2.2 % in 2015 and would increase by 3.7% and remain near 4.0% in 2016 and during 2017-2018, respectively. This rise on cement production could be attributed to the continuing growth of world population and the expansion of the construction industry to meet the increasing global demand for new residential and non-residential buildings. Cement manufacturing, however, has been always one of the chief sources of anthropogenic CO_2, wherein 50% originate from the calcination process or decomposition of $CaCO_3$ to CaO and CO_2, 40% come from the combustion of fossil fuels, and the remaining 10% from the works related to raw materials transportation and electricity consumption (Mahasenan *et al.* 2003). As a matter of fact, approximately 0.90 tonne of CO_2 arise from the production of one tonne of cement, 0.53 tonne were derived from grinding and crushing of raw materials and 0.37 tonne from the combustion of fossil fuel (Mehta 2010), suggesting that if we adapt the data provided by the USGS, the cement industry had already discharged a total of around 46 giga-tonne (Gt) of CO_2 into the atmosphere from 1994 to 2014. The billions of tonnes of cement produced every year accounts for about 8% of the world's total yearly CO_2 emissions (Olivier *et al.* 2015). It is a well-known fact that CO_2 is one of the major greenhouse gases (GHGs) that causes global warming, a

worldwide phenomenon that is considered as the major environmental and economic threat in our time because of its negative impacts such as the extinction of 20-30% of plants and animals, extreme weather events, and rise of sea level (Benhelal *et al.* 2013). This factor had led to the research and development for low emission binding agents for concrete to mitigate the amount of CO_2 emitted into the atmosphere to subside the threat of global warming.

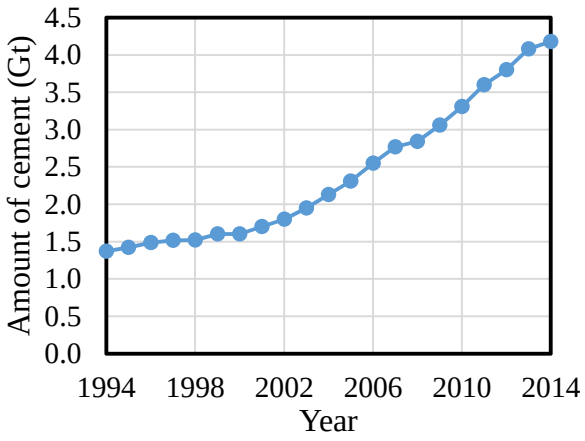

Figure 2.1 Global yearly production of cement (Gt) as reported by the USGS

The production of cement is also a resource-exhausting process. Large amounts of virgin materials such as limestone, clay, and marl, which contain the four essential elements of cement (Calcium (Ca), Silicon (Si), Aluminium (Al), and Iron (Fe)), are consumed to manufacture clinkers for cement. For every one tonne of cement produced, approximately 2.8 tonnes of raw materials (fuel and other materials) are needed (Guo *et al.* 2010). The concrete industry also utilises a large volume of fresh water, with a yearly consumption of around one trillion litres of mixing water (Mehta 2001).

Further, next to aluminium and steel, cement is the most energy-intensive building materials. In a typical cement plant alone, around 110-120 kWh is consumed per tonne of produced cement (Mejeoumov 2007). Sixty percent of this total energy account for the electrical energy use to crush and grind the raw and final materials to achieve the desired specific size. Twenty-five percent, in the form of thermal energy, are utilise for pyro-processing or clinker calcination – the heart of the manufacturing process – by burning fossil fuels in the calciner and kiln while the remaining 15%, in the form of electrical energy, are consume to run the auxiliary equipment like kiln motors and air blowers (Madlool *et al.* 2011). In fact, the expenditure for energy accounts for 50-60% of the total cost of cement manufacturing (Wang *et al.* 2009).

Considering the excessive CO_2 emissions and the resource- and energy-intensive process of producing cement products, Mehta (2002) suggested the use of environmentally friendly concrete that would necessitate fewer natural resources, less energy, and minimise carbon dioxide emissions and he categorised these short-term efforts as 'industrial ecology'.

2.2. Current methods used to address the issues on the use of conventional reinforced concrete

2.2.1. Replacement of steel bars with GFRP bars

The adoption of FRP composites in the construction industry is mainly for the purpose of repairing and rehabilitating in-service structures. The recent advances in FRP composite technologies, however, have resulted in the application of FRP as internal reinforcement for concrete structures, primarily to enhance the durability and to prolong the serviceability of these structures. The corrosion-induced durability problems could be eliminated if chemically inert or non-metallic reinforcement like fibre-reinforced polymer (FRP) bars could replace steel bars as the primary reinforcement within concrete structures (Aiello and Ombres 2000; Mufti *et al.* 2007). Furthermore, GFRP bars seems to be the best option when low electric conductivity and electromagnetic neutrality are sought or lightweight is an important design factor. They also have high tensile strength (2-3 times that of steel), high strength-to-weight and stiffness-to-weight ratios, high fatigue resistance, and good thermal insulation, with the added benefits of ease in fabrication, transportation, and handling and the potential for real-time monitoring (Gangarao *et al.* 2007; Robert and Benmokrane 2009). In comparison with steel reinforcement, however, FRP reinforcement have lower elastic modulus, shear strength, and compressive strength compared to steel bars. Furthermore, unlike steel, they behave linearly-elastic up to failure and lack ductility (Castro and Carino 1998).

The apparent higher initial expenditures, specifically the material costs, of FRP bars over steel bars is one of the major reasons for its slow uptake in the construction industry. Yet, a direct comparison on the unit price basis may not be appropriate. The life cycle cost analysis performed by Najm (2012) on concrete bridge decks reinforced with FRP bars highly recommended the use of FRP reinforcement in corrosive environments. According to Nkurunziza et al. (2005), FRP bars are more economical and more adequate than epoxy-coated or galvanized steel when used for concrete structures under corrosive environments. The use of FRP bars as reinforcement in concrete structures is also particularly suitable when transportation cost increase significantly with the weight of the materials. Furthermore, the

inconvenience of retrofitting damaged members and the costly repair and maintenance are the other economic factors that must be considered in adopting FRP bars (Mousavi and Esfahani 2012).

Research and development on FRP-reinforced concrete (FRP-RC) structures had become tantamount that several countries had developed their own design guidelines such as JSCE-1997 (Machida and Uomoto 1997) in Japan; ISIS 3(2)-01 (2006), CAN/CSA S6-14 (2014) and CAN/CSA S806-12 (2012) in Canada; CNR-DT 203/06 (2007) in Italy and fib Bulletin 40 (2007) in Europe; and ACI 440.1R-15 (2015) in the USA. Most of these codes were derived from the provisions for the traditional RC members, with several modifications to account for the different physical and mechanical properties between FRP and steel bars.

2.2.1.1 GFRP reinforcement properties

Among the various FRP reinforcement available, the glass FRP (GFRP) bars are the most widely used and accepted because of their low cost-to-performance advantage (Robert and Benmokrane 2010) and their successful application in bridge deck slabs, barrier walls, parking garages, continuous pavement, and other concrete structures (Ahmed *et al.* 2010a). **Figure 2.2** shows the typical configuration of a GFRP bar, which is generally manufactured using the well-known pultrusion process to produce a bar with a constant cross-section. The reinforcing glass fibres are pulled through a resin bath to saturate the fibres with liquid polymer resin and then through a shaping die to cure the resin. The properties of the bars are mainly dependent on the characteristics, amounts, and bond interaction between the fibres and the matrices. **Table 2-1** summarises the physical and mechanical properties of the high modulus (HM) GFRP bars manufactured by V-Rod® Australia (2012) according to the CSA S807-10 FRP Specification (2010), the reinforcement employed in this study. The bars were made of continuous longitudinal E-glass fibre strands bound together with a thermosetting vinylester resin using a pultrusion process.

The initial studies on first-generation of GFRP bars reported that the bars have low durability and highly prone to alkaline corrosion; however, with the recent advances in FRP technology, the durability of the latest generation of GFRP bars is significantly improved. Alkali-resistant glass fibres with proper sizing and matrix were adopted while the manufacturing quality were enhanced, specifically the fibre/matrix interphase. Furthermore, the bars in these previous studies are subjected to idealized and simulated harsh environment, with high pH concentration often involving high temperatures, and would behave differently

in the actual field conditions (Mufti *et al.* 2007). In fact, Robert et al.(2009) confirmed that the laboratory-based durability performance of GFRP bars in concrete do not accurately represent the actual service life of the bars in concrete environments. The recent study conducted by Benmokrane et al. (2015) showed that the glass/vinylester (G/V) FRP bars exhibited the best bond between the fibres and resin, flexural strength and elastic modulus, and interlaminar shear, which is governed by the fibre/matrix interface, compared to the basalt/vinylester (B/V) and basalt/epoxy (B/E) FRP bars. They also showed the lowest moisture intake and superior durability in the alkaline environment at elevated temperature.

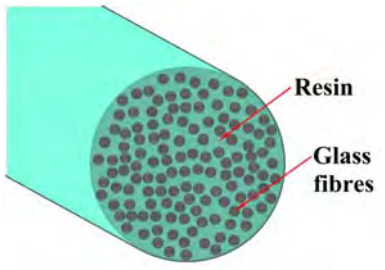

Figure 2.2 Typical configuration of a GFRP bar

Table 2-1 Physical and mechanical properties of GFRP bars manufactured by V-Rod® Australia

Property	Unit	#3	#4	#5	#6
Bar diameter	Mm	9.5	12.7	15.9	19.0
Unit weight	kg/m	0.243	0.380	0.558	0.811
Cross-sectional area	mm^2	71.3	126.7	197.9	285.0
Tensile strength	MPa	1372	1312	1184	1105
Tensile modulus	GPa	65.1 ± 2.5	65.6 ± 2.5	62.6 ± 2.5	63.7 ± 2.5
Tensile strain	%	2.11	2.00	1.95	1.99
Poisson's ratio	-	0.25	0.26	0.25	0.25
Flexural strength	MPa	1734	1377	1239	1196
Flexural modulus	GPa	65.5	64.9	63.5	60.2
Flexural strain	%	2.65	2.12	1.95	1.99
Transverse shear capacity	kN	41	67	94	127
Nominal bond strength	MPa	14			
Glass content by volume	%	65			
Glass content by weight	%	83			
Longitudinal thermal expansion	$x10^{-6}/C$	6.2			
Transverse thermal expansion	$x10^{-6}/C$	23.8			
Glass type	-	E			
Resin type	-	Vinylester			

Note: The numbers reflected in the table represent the nominal values.

2.2.1.2 Bond behaviour of GFRP bars in concrete

The interaction phenomena between the FRP reinforcement and the concrete is a critical factor that controls the structural performance of FRP-RC members. In fact, the design of FRP-

RC system is generally governed by the serviceability requirements, such as the control of crack widths and deflections, which involves the evaluation of the tension-stiffening effects that is directly influenced by the bond between the FRP bars and concrete. The magnitude of slip of FRP bars relative to concrete is larger than that of steel bars, owing to the lower elastic modulus of the former reinforcement compared to the latter, and, unlike steel bars, the calculation of development length is based on the post-peak bond strength of FRP bars (Davalos *et al.* 2008). Furthermore, FRP bars are anisotropic, wherein the resin controls its transverse properties while the fibre dominates the longitudinal properties (Al-Zahrani *et al.* 1999). Hence, bond stress-slip laws, calibrated from the experimental results, were developed specifically for the FRP-RC system, including the BPE model (Eligehausen *et al.* 1982), Malvar model (Malvar 1994), CMR model (Cosenza *et al.* 1995), and modified BPE model (Cosenza *et al.* 1996).

According to the previous studies (Achillides and Pilakoutas 2004; Benmokrane and Tighiouart 1996; Chaallal and Benmokrane 1993; Malvar 1994; Nanni *et al.* 1995; Tang *et al.* 2008; Tao *et al.* 1992; Tighiouart *et al.* 1998), the mechanism of stress transfer through the bond between the GFRP bars and the ordinary concrete is mainly influenced by the bar diameter, embedment length, confinement, and concrete compressive strength. The bond strength decreases when the embedment length increases, owing to the nonuniform distribution of bond stresses over the anchorage length of the bar. Similarly, an increase in the bar diameter is accompanied by a decrease in bond strength, which can be attributed to the Poisson and shear lag effects. Furthermore, larger bar diameter requires larger embedment, and hence, results to nonlinear stress distribution along the bonded length. An increase in confining pressure increases the maximum average developed bond stress. Achillides et al. (1997) , however, pointed out that a high bond stress obtained from a well-confined pullout tests does not mean a good bond can be achieved in a concrete member where the concrete splitting failure determines the ultimate failure load. On the other hand, the bond strength also increases with concrete compressive strength, however, the rate of increase declined with the rise in strength because the bond failure occurs at the surface of the bars when high strength concrete are used (Baena *et al.* 2009).

The bond of smooth GFRP bars in concrete can be enhanced through the provision of sand particles around the bar surface (Okelo and Yuan 2005). In fact, Soong et al. (2011) reported that the resistance from lugs or deformations to bar pullout is comparable to that from sand particles bonded to the bar. Arias et al. (2012) further stated that the use of coarse sand

produced higher bond strength, owing to the higher mechanical interlock and friction forces provided by coarse sand compared to fine sand. The anchorage of the bars in the concrete can be enhanced further by using longer embedment lengths; yet, this would incur additional costs and would lead to reinforcement congestion. Another option is to provide standard hooks at the end of the bars. Bending of GFRP bars on-site, however, is not possible. Furthermore, the GFRP bars have much lower strength at the bend portions, approximately 35-40% of the tensile strength of a similar straight bar (Ascione *et al.* 2014; Shehata *et al.* 2000), owing to the kinking of the innermost fibres compared to those at the outermost radius and the localised concentration at the bend due to curvature combined with the intrinsic weakness of fibres perpendicular to their axis (Ahmed *et al.* 2010a; El-Sayed and Soudki 2011). Given these limitations, the use of headed GFRP bars seems to be the most logical solution to achieve the required development. Limited studies (Ahmed and Benmokrane 2009; Mohamed and Benmokrane 2009; Sayed-Ahmed and Sennah 2014), however, were found in the literature regarding the pullout behaviour of headed GFRP bars in concrete. Nevertheless, these studies showed that the provision of anchor heads, which were made up of thermosetting polymer material cast onto the end of the straight GFRP bar and hardened at elevated temperatures, significantly enhanced the pullout load resistance of the bars, suggesting that the headed GFRP bars provide a suitable alternative to the bent bars in some applications

Direct pullout tests have been widely adopted for the evaluation of the bond performance of FRP bars in concrete, mainly because they are more economical and convenient to perform and they represent the concept of anchoring a bar in a simple manner (Achillides and Pilakoutas 2004; Robert and Benmokrane 2010; Zhou *et al.* 2011). In addition, this test permits access of the free-end of the rod which allows for the measurement of free-end slip and placement of instrumentation within the rod (Nanni *et al.* 1995). Hence, this method was adopted in this study to obtain the constitutive bond-slip relationship for the proposed system.

2.2.1.3 GFRP-reinforced concrete beams

The behaviour of concrete beams reinforced with GFRP bars is different from the traditional RC beams in many ways, mainly because of the differences between the physical and mechanical properties of the FRP and steel reinforcement (Alsayed 1998; Alsayed *et al.* 1999; Benmokrane *et al.* 1995; Masmoudi *et al.* 2012; Matos *et al.* 2012). Firstly, the GFRP-reinforced concrete (GFRP-RC) beams exhibited wider cracks, larger deflections, and lower

stiffness at service conditions, owing to the lower modulus of elasticity of the GFRP bars compared to steel bars, approximately 25-30 % of the steel bars. Thus, the design of GFRP-RC beams is generally governed by the serviceability design requirements. Secondly, the concrete crushing failure is more preferred rather than the FRP rupture failure because the former is less brittle and less catastrophic compared to the latter owing to the linear elastic behaviour up to the point of failure and non-ductile characteristics of the FRP bars. Thus, the FRP-RC beams are usually designed as over-reinforced. Thirdly, since the surface geometries and mechanical features of FRP bars are different from the steel bars, its bond to concrete is different from that of steel bars. Finally, the dowel action of the longitudinal FRP reinforcement is lower than that of steel reinforcement because the shear stress is perpendicular to the direction of the fibre orientation (Mallick 2007). Many researchers, therefore, recommended the modifications of the existing RC design codes to fit with the design of GFRP-RC beams (Alsayed *et al.* 2000; Barris *et al.* 2009; El-Mogy *et al.* 2010)

The flexural behaviour of concrete beams with longitudinal GFRP bars are predominantly influenced by the reinforcement ratio, concrete strength, elastic modulus of the bar, effective depth of the beam, and surface configuration of the bar. According to the previous research works (Adam *et al.* 2015; Barris *et al.* 2009; El-Gamal *et al.* 2011; Kassem *et al.* 2011; Pecce *et al.* 2000; Theriault and Benmokrane 1998), smaller deflections and narrower cracks are obtained from the beams with higher amount of GFRP reinforcement, owing to the enhancement of the reinforcement's axial stiffness, and vice versa. The concrete strength did not show strong influence on the flexural strength of over-reinforced GFRP-RC beam; however, wider cracks occurred in beams with higher concrete strength (Adam *et al.* 2015; Theriault and Benmokrane 1998). Furthermore, the beams with lower effective depths yielded larger deflections (Barris *et al.* 2009). On the other hand, the beams with sand-coated bars exhibited more cracks and less average crack spacing compared to beams reinforced with ribbed-surface bars, indicating that the sand-coated bars had better bond than the ribbed-surface bars (Kassem *et al.* 2011). The information regarding the effects of bar diameter and anchorage system, such as the provision of anchor head at the end of the bar, on the structural performance of GFRP-RC beams were not yet available in the literature.

The FRP bars are particularly suitable for transversely reinforcing the concrete beams because web reinforcements are more susceptible to corrosion as they are nearer to concrete outer surface compared with the longitudinal bars. The strength of the FRP stirrup at the bend, however, is significantly lower than the strength of its straight portion. Nevertheless, with the recent development on FRP technology, the ACI 440.1R-15 (2015) guidelines and CAN/CSA

S6-14 (2014) codes encouraged the use of FRP stirrups as transverse reinforcement for concrete members. Similar to steel stirrups, the inclusion of GFRP stirrups increases the shear strength (Krall and Polak 2014; Mahmoud and El-Salakawy 2014) and reduced the crack width of the beam without stirrups, with the closely spaced stirrups yielding the highest capacity due to the confinement effect (Ahmed *et al.* 2010a). The inclination angle of GFRP stirrups was in good agreement with the traditional 45-degree truss model at shear failure (Ahmed *et al.* 2010a). According to the study conducted by Bentz et al. (2010), the beams with GFRP stirrups that failed in shear showed significantly more warning of failure than either type of flexural failure, concrete crushing and bar rupture. Most of these inferences were derived from slender members that were longitudinally and transversely reinforced with GFRP bars and stirrups, respectively. The use of GFRP bars and stirrups in short or deep beams, however, has not yet been studied extensively.

Short beams are commonly used as transfer girders, whose safety is often crucial for the whole structure's stability. Nagasaka et al. (1993) and Vijay et al. (1996) reported that the provision of GFRP stirrups in concrete deep beams enhanced both the load-carrying and deflection capacities of deep beams. However, they yielded contradicting findings regarding the influence of stirrup spacing. Vijay et al. (Vijay *et al.* 1996) mentioned that the stirrup spacing have no significant influence on the capacities of deep beams while Nagasaka et al. (1993) reported otherwise, wherein they found that the strength of deep beams increased as the stirrup spacing decreased. On the contrary, Mohamed at el. (2014) found that the strength of deep beams did not improved with the provision of GFRP stirrups; yet, the GFRP stirrups limits the width and number of flexural and shear cracks in concrete deep beams, owing to the stirrups clamping effect. Farghaly and Benmokrane (2013) reported that by increasing the longitudinal reinforcement ratio, the strength of deep beams was enhanced; however, according to Yost et al., the reinforcement ratio had no significant influence on the shear capacity of the beams. El-Sayed et al. (2012), on the other hand, reported that the cracked stiffness of deep beams increases with the amount of longitudinal reinforcement. These different findings regarding the influence of the GFRP stirrups and its spacing and the amount of longitudinal GFRP bars in deep beams leave a research gap that needs to be addressed by scrutinizing the factors that caused the variation of the results in the previous studies.

2.2.1.4 GFRP-reinforced concrete columns

Very few experimental and developmental activities have studied the behaviour of GFRP bars as longitudinal reinforcement for concrete structures under compression. In fact, among the

current design provisions for FRP-RC system, only the JSCE (Sonobe *et al.* 1997) had developed a design protocol for concrete compression members with FRP bars (De Luca *et al.* 2010). The ACI 440.1R-15 (2015) and CAN/CSA S6-14 (CAN/CSA S6-14 2014) do not recommend the use of FRP bars in reinforced concrete columns. The CAN/CSA S806-12 (2012) recommended an equation to calculate the axial load resistance of confined columns, similar to CAN/CSA A23.3-04 (2004); yet, the compression contribution of FRP bars was ignored.

De Luca (2009) reported that the behaviour of GFRP-RC columns reinforced longitudinally was very similar to that of the conventional concrete columns reinforced with steel bars. The GFRP bars, however, contributed less than 5% of the peak load, which is significantly lower than that of steel bars (approximately 12%). This could be attributed to the lower compression properties the GFRP bars and the smaller amount of longitudinal reinforcement ratio (1.0%) they adopted in their studies. The GFRP ties, on the other hand, strongly influenced the failure mode of the columns by delaying the buckling of longitudinal bars, initiation and propagation of unstable cracks, and crushing of the concrete core. With the advances in the manufacturing processes and the enhancement of the properties of the component materials of GFRP bars, however, the latest generation of GFRP bars have improved physical and mechanical properties that can match that of steel bars. The recent study conducted by Tobbi et al. (2012), showed that the GFRP bars contributed 10% of the column capacity, which was practically analogous to steel's contribution (12%). Hence, they concluded that GFRP bars could be adopted as longitudinal reinforcement for concrete column members, if adequate confinement was provided to eliminate bar buckling, and that the strength reduction factor of 0.85, typically used for steel-reinforced concrete columns, can be adopted for GFRP-RC columns. They also reported that the GFRP ties effectively enhanced the strength, toughness, and ductility of the confined concrete core. Furthermore, the experimental investigation performed by Afifi (2013) also showed that the compression performance of circular concrete columns reinforced with longitudinal GFRP bars and stirrups is similar to that of the traditional RC columns. The GFRP stirrups provided satisfactory restraint against the buckling of the longitudinal GFRP bars and provided good confinement of the concrete core in the post-peak stages. Mohamed et al. (2014) evaluated the performance of columns with GFRP bars and confined with GFRP hoops and spirals. Based on the experimental results, they concluded that GFRP-RC columns exhibited similar behaviour as the conventional RC columns. The use of GFRP hoops and spirals effectively confined the concrete in post peak

stages, with similar degree of efficiency. These current findings suggest the suitability of GFRP bars and ties as reinforcement for concrete column members.

2.2.2. Replacement of OPC concrete with geopolymer concrete

Geopolymer concrete is considered as a viable alternative to the traditional cement-based concrete for the development of greener and more sustainable structures because, instead of cement paste, the geopolymer binder can be manufactured using by-product materials that are rich in silica and alumina, such as fly ash and blast furnace slag (Lloyd and Rangan 2010). Davidovits (Davidovits 1991) coined the term "geopolymer" since the chemical reaction that takes place between the source materials and the activating alkaline liquid is a polymerisation process. The geopolymer concrete reduce the CO_2 emission by 80-90% compared to those of OPC-based concrete (Duxson *et al.* 2007). The production of geopolymer can also minimise the landfill necessary for fly ash that is reportedly abundant worldwide, but limitedly utilised worldwide; however, its utilization is limited. Furthermore, the geopolymer binder can immobilise approximately 90% of heavy metals within its matrices (Fernández-Jiménez and Palomo 2003; Khale and Chaudhary 2007).

2.2.2.1 Geopolymer and geopolymer concrete properties

The mechanical strength of geopolymer system depends on several factors. The pH of the activating solution is the major parameter that controls the compressive strength of a geopolymer. According to Khale and Chaudhary (Khale and Chaudhary 2007), the activating solution with a pH range of 13-14 is the most suitable for the formation of the geopolymers with better mechanical strength. The properties of source materials also affect the strength of geopolymers. Source materials with a high reactivity produce geopolymer systems with a high compressive strength (Xu and van Deventer 2002). Geopolymers with higher amount of reactive silica also yielded high mechanical strength, owing to the formation of larger amount of geopolymeric or alumino-silicate gel (Chen-Tan *et al.* 2009; Criado *et al.* 2007; Deb *et al.* 2015). The particle size distribution directly affects the reactivity of fly ash. The fly ash reactivity increases with the amount of fine particles, owed to higher surface area, which in turn yields geopolymer system with higher compressive strength (Diaz *et al.* 2010). The early strength development of geopolymer system, on the other hand, can be enhanced by using NaOH with higher molarity but with low alkali content and by using elevated temperature for curing (Khale and Chaudhary 2007).

Geopolymer binders exhibited superior mechanical properties to those of OPC binders (Palomo and Glasser 1992; Xu and van Deventer 2000). Furthermore, geopolymer concrete have strength, stiffness, and other mechanical properties that are comparable and, most of the time, superior to that of OPC-based concrete (Rangan 2008; Sarker 2008; Sofi *et al.* 2007). Duxson et al. (2007) also reported that other desirable characteristics of geopolymer concrete such as rapid development of mechanical strength, fire resistance, dimensional stability, acid resistance, excellent adherence to aggregates and reinforcements, and have lower material cost, approximately 10-30% lower than that of OPC. Wallah et al. (2003) stated that geopolymer concrete undergoes very little drying shrinkage and creep and showed excellent resistance to sodium sulphate. With the highly desirable structural properties of geopolymer concrete, a significant cost savings in many structural members is expected (Aldred and Day 2012).

Several researchers have developed constitutive models for geopolymer concrete based on OPC concrete models with minor modification to the curve-fitting factor (Hardjito *et al.* 2004; Sarker 2008). In fact, the Concrete Institute of Australia published a practice handbook on the manufacture and use of geopolymer concrete technology. This handbook covers optimum mixed design, material characterisation and practical application of geopolymer concrete. Most of the research, however, is focused only on geopolymer concrete mix design and durability (Aleem and Arumairaj 2012; Duxson *et al.* 2007; Hardjito *et al.* 2004; Rangan 2008; Sumajouw *et al.* 2007). It is necessary therefore to extend the understanding into the structural behaviour of full-scale structures made up of geopolymer concrete to increase its acceptance and utilisation in the mainstream construction application.

The initial price of geopolymer concrete has been one of its main drawbacks compared to OPC concrete; however, they are expected to even up in the long run as the price of carbon dioxide emissions during the clinker production will be incorporated in the future costing of OPC concrete (Vasconcelos *et al.* 2011). Furthermore, since geopolymer concrete is a relatively new technology, it lacks design guidelines compared to OPC concrete; hence urgent research and experimental works are necessary. Lastly, geopolymer concrete, in general, requires heat for curing that made them not suitable for on-site pouring and casting. Interestingly, the geopolymer concrete used in this study, with a proprietary mixture, addresses these casting issues. The novelties of this geopolymer concrete is that its constituent materials could be mixed in the batching plant and remain completely dormant until the activator chemical are added and it could be cured under ambient conditions.

2.2.2.2 Bond behaviour of steel bars in geopolymer concrete

The pullout test conducted by Selby (2011) showed that the bond strength of geopolymer concrete was comparable to that of OPC-based concrete for both smooth and ribbed reinforcement. Yet, the chemical adhesion of geopolymer concrete was found to be much higher than OPC-based concrete. The current methods in calculating the bond strength and development lengths for OPC concrete can be applied conservatively to geopolymer concrete. Sarker (2011), on the other hand, stated that the geopolymer concrete had higher bond strength than OPC-based concrete for the same parameter, owing to the higher splitting tensile strength of geopolymer concrete compared to ordinary concrete, which suggest that the bond strength of geopolymer concrete can be conservatively estimated by using the bond equations for OPC concrete. For both concrete, the bond strength increases as concrete strength and concrete cover increase. Sofi et al. (2007) investigated the performance of steel reinforcing bars in geopolymer concrete, which they called inorganic polymer concrete (IPC), using beam-end and direct pullout tests. Based on their experimental results, the bond strength increases with the tensile strength of the concrete and with the reduction of rebar diameter. They further concluded that the current bond equations for the normal concrete specified by AS 3600-01 (2001), ACI 318-02 (2002), and EC2 (Beeby and Narayanan 1995) were applicable for IPC, with EC2 providing the most conservative estimates.

2.2.2.3 Steel-reinforced geopolymer concrete beams

Based on the experimental study done by Sumajouw and Rangan (2006), the geopolymer concrete beams made from low-calcium fly ash behaved similarly as the conventional RC beams. They also stated that the flexural design provisions contained in the AS3600-05 (2005) draft were applicable to the tested beams. Dattatreya *et al.* (2011) investigated the flexural behaviour of fly ash- and slag-based geopolymer concrete beams reinforced with steel bars. The results of their study showed that the load-carrying capacities of the steel-reinforced geopolymer concrete (S-RGC) beams were, in most cases, marginally higher than that of the corresponding conventional RC beams. The conventional RC beams, however, yielded higher cracking and service loads compared to S-RGC beams because the elastic modulus and flexural strength of the ordinary concrete were higher than that of the geopolymer concrete they manufactured. The S-RGC and RC beams failed similarly and developed same order of crack width and number and spacing of flexural cracks. Interestingly, Kumaravel and Thirugnanasambandam (2013) obtained similar results using fly ash-based geopolymer concrete beams. The experimental results obtained by Abraham et al. (Abraham

et al. 2013) showed that geopolymer concrete beams yielded higher first crack and ultimate loads, exhibited more number of narrow cracks with a closer spacing, and relatively better energy absorption and ductility than the conventional concrete beams.

Ambily *et al*. (2012) investigated the shear behaviour of geopolymer concrete T-beams with a shear span-to-effective depth ratio (*a*/*d*) of 1.9, considered as deep beams. The outcomes of their study revealed that the beams without stirrups failed by web crushing under diagonal compression while the failure of beams with stirrups ranged from diagonal compression to shear tension with longitudinal splitting depending on the stirrup spacing. They also stated that the structural behaviour of the S-RGC beams resembled that of the typical RC beams and that the S-RGC beams perform adequately as structural components. Murugavel and Mala (2014) carried out experiment studies on S-RGC beams considering two *a*/*d* of 1.9 and 2.5. Based on the experimental results, as the *a*/*d* increases, the shear capacity also increases and vice versa. The compressive strength, however, did not influence the shear capacity of the beams. The beams with closer stirrup spacing yielded higher ultimate load-carrying capacity than the beams with wider stirrup spacing or without stirrups. The beams with lower *a*/*d* yielded lower deflections at ultimate loads compared to the beams with higher *a*/*d*, owing to the arch action effect. All the beams failed when the measured diagonal compressive strain exceeds 3500 με. Hence, they suggested the adoption S-RGC beam in the construction of infrastructures such as buildings and bridges.

2.2.2.4 Steel-reinforced geopolymer concrete columns

Sumajouw and Rangan (2006) performed experimental and analytical studies on the behaviour reinforced geopolymer concrete columns. The results revealed that the crack pattern and failure modes observed for geopolymer concrete columns were similar to those reported for OPC-based concrete cement columns. As the longitudinal reinforcement ratio and concrete compressive strength increase, the failure load of the tested columns also increases. They also stated that the design provisions for the typical RC column contained in AS 3600-05 (2005) and ACI 318-02 (2002) were applicable to S-RGC columns. These findings were also reported by Sumajouw et al. (2007) for heat-cured slender geopolymer concrete columns made up of low-calcium fly ash. Similarly, Sarker (2009) stated that the analytical method for conventional RC columns could be used for S-RGC columns provided that an appropriate stress-strain relationship of geopolymer concrete could be obtained. The strength assessment of heat-cured geopolymer concrete column performed by Sujatha *et al.* (2012) showed that the geopolymer concrete columns behaved similar to OPC-based concrete columns regardless of the concrete

grade. The geopolymer concrete columns show less deformation than that of control columns of the same percentage of steel. These results demonstrate that fly ash- and/or slag-based geopolymer concrete has excellent potential for applications in the construction industry.

2.3. Summary

The adoption of GFRP bars in place of steel bars as the primary internal reinforcement for concrete structures is now commonly practiced to enhance the durability and prolong the serviceability of the structures while the use of geopolymer concrete, instead of cement-based concrete, is particularly suitable for the fabrication of environmentally friendly concrete structures. With the stated advantageous characteristics of the GFRP bars and the geopolymer concrete, including their successful applications in the construction of various civil infrastructures, combining them would offer a promising technology in building new structures with high durability and high sustainability and with adequate strength and structural integrity. The poor understanding of the overall behaviour and the lack of designers' experience with GFRP-reinforced geopolymer concrete (GFRP-RGC) system, however, may place this new and innovative technology at a disadvantage when considered against the existing FRP-RC and S-RGC systems. A logical step, therefore, is to investigate the important aspects of their structural behaviour such as the bond performance of GFRP bars in geopolymer concrete, the flexural and shear behaviour of geopolymer concrete beams longitudinally and transversely reinforced with GFRP bars and stirrups, respectively, and the compression behaviour of geopolymer concrete columns internally reinforced with GFRP bars and ties. As of this writing, however, there is no scientific research undertaken to substantiate the benefit of using GFRP-RGC system. This was the main research gap that was identified from the discussions above. Furthermore, the other gaps in the existing literature are as follows:

1. There is insufficient research work regarding the anchorage behaviour of headed GFRP bars in concrete.
2. A number of experimental and analytical works are available regarding the shear performance of beams with FRP bars; however, few studies have focused on the shear contribution of FRP stirrups, especially in short or deep beams.
3. There are limited studies that dealt with the compression behaviour of concrete columns reinforced with GFRP bars. In fact, the current design guidelines and provisions for FRP-RC system, except JSCE, do not recommend the use of FRP bars in compression members.

4. Despite the fact that geopolymer concrete was developed several years ago and has many advantageous characteristics, it has not yet been used in actual infrastructures as extensively as OPC concrete because, to date, most of the research is focusing only on geopolymer concrete mix design and durability.
5. While design procedures for FRP-RC members are well documented in countries like the USA and Canada in North America, Italy and Great Britain in Europe, and Japan in Asia, Australia has yet to develop its own standard, more so with GFRP-RGC system.

Hence, this study was designed to assess the suitability and structural behaviour of GFRP-RGC system and extend the understanding into the critical problems associated with their application, thereby filling the knowledge gap that currently exist in civil engineering.

3. PUBLICATIONS FORMING PART OF THIS THESIS

3.1. Paper I: Bond stress–slip behavior: Case of GFRP bars in geopolymer concrete

This paper presents the investigation of the bond behaviour of glass fibre reinforced polymer (GFRP) bars in geopolymer concrete. This study was conducted first because the bond between the concrete and reinforcement is a critical factor that affects the overall behaviour of the reinforced concrete (RC) system. The test parameters (bar diameter and embedment length) were evaluated carefully using the direct pullout test in accordance with ACI 440.3R-04 with some modifications. These modifications, including the justifications for adopting the test, were discussed in section "1.4 Scope and Limitations" of the thesis. The schematic diagram of the test set-up is shown in **Figure 1** of **Paper I.** In addition, the locations of the bonded and debonded lengths are shown in **Figure B.1** of **Appendix B**.

The summary of the failure load and failure mode of the pullout specimens is shown in **Table 2** of **Paper I**, wherein the symbol "±" stands for the standard deviation of the measured failure load. Furthermore, the bond stress-slip curves of all the tested specimens are shown in **Figure B.1** of **Appendix B**. From the experimental results, it can be generalised that the average bond stress at failure (termed as "average bond stress" in the text and in **Figures 10**, **11**, and **12** of **Paper I**) decreases as the bar diameter and embedment length increase. An opposite trend, however, was observed in terms of bond stiffness (**Table B-1** of **Appendix B**), wherein the bond stiffness increases with the increase of bar diameter and embedment length. The analytical models formulated in Paper I can be used to calculate the bond stress τ for a given slip in the bar. Using this stress value, the required development length (L_d) can be determined by using equation

$$L_d = \frac{d_b f_s}{4\tau}$$

where d_b and f_s correspond to nominal diameter and tensile stress of the GFRP bar. Overall, the modified direct pullout test employed in the study allowed the sufficient evaluation of the important parameters that affect the bond behaviour of GFRP bars in geopolymer concrete.

In cases were longer embedment lengths are inappropriate, the provision of anchor heads is a viable option. Limited studies, however, are available regarding the use of anchor heads especially in GFRP bars. Hence, the candidate investigated the influence of anchor heads

on the pullout resistance of GFRP bars following the test method employed in Paper I and the results were presented, analysed, and discussed in Paper II.

Bond Stress-Slip Behavior: Case of GFRP Bars in Geopolymer Concrete

Ginghis Maranan[1]; Allan Manalo[2]; Karu Karunasena[3]; and Brahim Benmokrane[4]

Abstract: The use of geopolymer concrete reinforced with fiber-reinforced polymer (FRP) bars is anticipated to address the concerns on the usage of traditional reinforced concrete structures, such as the corrosion of internal steel reinforcement, costly repair and rehabilitation, and development of sustainable infrastructures. To gain wide acceptance in the construction market, the bond between geopolymer concrete and the FRP bar should be investigated first because it is a critical factor that influences the behavior of structures, specifically its strength and long-term durability. In this study, the bond performance of sand-coated glass fiber-reinforced polymer (GFRP) bars into geopolymer concrete with a compressive strength of 33 MPa was investigated under a direct pullout test. The effects of parameters such as bar diameter (12.7, 15.9, and 19.0 mm) and embedment length (5, 10, and 15 d_b, where d_b is the bar diameter) were evaluated. The results showed that the maximum average bond stress obtained is around 23 MPa. As GFRP bar diameter increases, the average bond stress decreases. Similarly, the average bond stress decreases as the bond length becomes longer. The specimens with shorter embedment length failed because of pullout of the bars, whereas those with longer embedment lengths failed because the concrete split. The results further revealed that the geopolymer concrete reinforced with GFRP bars have a bond strength similar to that of steel-reinforced geopolymer concrete. Finally, bond-slip models for the ascending branch up to maximum bond stress of the bond-slip curves for GFRP bars and geopolymer concrete were proposed. **DOI: 10.1061/(ASCE)MT.1943-5533.0001046.**

Author keywords: Polymer; Concrete; Fiber-reinforced polymer; Bonding; Pullout; Analytical techniques.

Introduction

Cement-based concrete with internal steel reinforcement is one of the commonly used composite materials in the construction of civil infrastructures. However, there are several issues regarding its application that drive engineers and researchers to look for alternatives. First is the corrosion problem of steel reinforcement in the traditional reinforced concrete (RC) structures, especially those that are located in or near an aggressive environment. Second, there are many substandard and deteriorated structures that require costly repair or rehabilitation and, most of the time, need total replacement. And lastly, because of global warming, the use of cement is being discouraged, as the production of 1.0t of cement releases approximately 1.0t of CO_2 (McCaffrey 2002). In fact, 5–7% of the world's emission of CO_2 comes from cement production (McLellan et al. 2011).

The replacement of steel bars with fiber-reinforced polymer (FRP) bars as internal reinforcement to RC structures is now an accepted practice to enhance the durability and prolong the serviceability of these structures. In addition to ultra-high tensile strength and lightweight properties, the FRP composite materials are corrosion resistant, durable, and nonmagnetic (Gangarao et al. 2007). In comparison with steel, FRP materials have relatively lower ductility, lower bonding strength, and anisotropic properties. In effect, new and compatible design framework is necessary to ensure the safety and serviceability of concrete structures reinforced with FRP bars. Fico (2008) presented several FRP reinforced RC structures that were successfully built in Japan (e.g., floating marine structures, pontoon bridge, and magnetic levitation railway) and in other countries. Research and development on FRP reinforced RC structures had become tantamount that several countries developed their own design guidelines such as the Japan Society of Civil Engineers in Japan, ISIS and CSA-S806 [Canadian Standards Association (CSA) 2010] in Canada, and ACI 440.1R [American Concrete Institute (ACI) 2006] in the United States. Although the initial costs of using FRP are higher compared with those of steel, they will even up in the long run because the costly repair and maintenance from steel corrosion (Mazaheripour et al. 2013; Achillides and Pilakoutas 2004) will be avoided. The use of FRP materials is particularly relevant in cases where the design of RC structures is controlled by durability requirements (Tastani and Pantazopolou 2006) and long-term sustainable performance.

Geopolymer concrete is deemed as a viable alternative to traditionally used ordinary portland cement (OPC) concrete for the development of a greener and more sustainable structure. Instead of cement, the geopolymer utilizes by-product materials that are rich in silica and alumina, such as fly ash and rice husk ash, to produce binders (Lloyd and Rangan 2010). Davidovits (1988)

[1]Visiting Research Fellow, Centre of Excellence in Engineered Fibre Composites, Univ. of Southern Queensland, Toowoomba 4350, Australia. E-mail: Ging.Maranan@usq.edu.au

[2]Lecturer, Centre of Excellence in Engineered Fibre Composites, School of Civil Engineering and Surveying, Univ. of Southern Queensland, Toowoomba 4350, Australia (corresponding author). E-mail: allan.manalo@usq.edu.au

[3]Associate Professor, School of Civil Engineering and Surveying, Univ. of Southern Queensland, Toowoomba 4350, Australia.

[4]Professor, Dept. of Civil Engineering, Faculty of Engineering, Univ. of Sherbrooke, Sherbrooke, QC, Canada J1K 2R1. E-mail: Brahim.Benmokrane@USherbrooke.ca

Note. This manuscript was submitted on December 3, 2013; approved on January 30, 2014; published online on January 31, 2014. Discussion period open until December 11, 2014; separate discussions must be submitted for individual papers. This paper is part of the ***Journal of Materials in Civil Engineering***, © ASCE, ISSN 0899-1561/04014116(9)/$25.00.

named the binder as "geopolymer" because the chemical reaction that takes place in the activation of fly ash with alkaline liquid is a polymerization process. Duxson et al. (2007) reported several desirable characteristics of geopolymer, such as rapid development of mechanical strength, fire resistance, dimensional stability, acid resistance, and excellent adherence to aggregates and reinforcements. Furthermore, they stated that the material cost of fly ash–based geopolymer concrete is 10–30% lower than that of OPC.

With the advantageous characteristics of FRP and geopolymer concrete, combining them would offer a promising technology in the construction industry. However, for FRP reinforced geopolymer concrete to gain wide acceptance in the construction market, the bond between the geopolymer concrete and the FRP bar should be investigated, because it is a critical factor that influences the strength and long-term durability. Sufficient bond must exist between the FRP bar and geopolymer concrete to effectively transfer the stresses from one to the other and secure a composite action. Some of the pioneering studies on the mechanism of stress transfer through bond between the FRP and the ordinary concrete were performed by Tao et al. (1992), Chaallal and Benmokrane (1993), and Malvar (1994). Recent advances on FRP studies showed that the bond of FRP to concrete is dependent on several factors, such as surface roughness of the reinforcement, embedment length, bar diameter, and concrete strength (Okelo and Yuan 2005; Baena et al. 2009; Arias et al. 2012).

Sofi et al. (2007) initiated the investigation of the bond mechanics between the geopolymer concrete and deformed steel bar. They concluded that the bond performance of inorganic polymer concrete (IPC) are comparable with that of the OPC-based concrete and, therefore, the combination of steel and IPC can be used to resist not only compression but also tension stresses. Sarker (2011) made a comparison of the bond strength of geopolymer concrete and OPC concrete. He found that, although the compressive strength of OPC and geopolymer concrete are the same, the bond of geopolymer concrete is still higher than OPC concrete because of its higher tensile strength. In another study, Selby (2011) found that the bond strength of geopolymer concrete is at least as strong as that of OPC concrete on a relative basis. Furthermore, he added that the chemical adhesion of geopolymer concrete is two times greater than that of OPC concrete. This good chemical adhesion would prevent the early development of interfacial cracks between the FRP bar and the concrete, and within the longitudinal cracks in the surrounding concrete.

Although there are many studies that deal with the evaluation of bond performance between concrete and its reinforcement, e.g., FRP bars into OPC concrete and steel bars into geopolymer concrete, no research or experimental work has been conducted on the bond-slip relationship between the FRP and the geopolymer. This is the key motivation of this undertaking. In this study, the bond performance of sand-coated glass fiber-reinforced polymer (GFRP) bars into geopolymer concrete was evaluated using the direct pullout test. The influence of bar diameter and embedment length on the bond strength of geopolymer concrete reinforced with GFRP bars is determined. Also, the results are compared with that of steel-reinforced geopolymer concrete to validate the acceptability of GFRP as an alternative to steel as reinforcement for geopolymer concrete. Finally, analytical equations based on the Cosenza, Manfredi, and Realfonzo (CMR) model (Cosenza et al. 1997) are proposed to simulate the ascending behavior of the bond-slip curve and up to the maximum bond strength of GFRP bars embedded into geopolymer concrete.

Experimental Program

This section discusses the constituent materials and the test conducted to evaluate the bond performance of GFRP bars into geopolymer concrete.

Materials

Geopolymer Concrete

A ready-mix geopolymer concrete with a proprietary mixture, supplied by Wagners in Australia, was used in this study. It is composed of alkali-activated fly ash and ground granulated blast-furnace slag, gravel, and sand. The average compressive strength of the 28- to 32-day age geopolymer concrete is 33 MPa, with a standard deviation of 2.3 MPa.

The characterization of the mechanical properties of geopolymer concrete has been performed by Aldred and Day (2012). They found that geopolymer concrete tends to have higher tensile and flexural strength relative to the compressive strength than portland cement-based concrete. In addition, Sarker (2011) stated that geopolymer concrete has higher tensile strength than OPC concrete.

Reinforcing Bars

Three high-modulus GFRP bars (Grade III, CSA S807-10) of varying nominal diameter were investigated: 12.7 mm (#4), 15.9 mm (#5), and 19.0 mm (#6), which were provided by V-Rod Australia. The mechanical properties of these bars are presented in Table 1. The GFRP was used because glass fiber is relatively cheaper compared with other fibers such as carbon and aramid fibers (Gangarao et al. 2007). Other advantages include low susceptibility to moisture, high chemical resistance, and excellent insulating properties.

The bars were produced by a pultrusion process of continuous E-glass fibers impregnated in vinyl ester resin. The sand used to cover the GFRP bars are made up of Silica 24. Arias et al. (2012) stated that the provision of sand coating to GFRP bars improves its bond with the concrete through the friction and interlock forces provided by the sand. In addition, the study conducted by Tang et al. (2008) showed that the GFRP bars coated with sand have the highest bond strength values compared with smooth and mild steel bars. For the purpose of comparison, 16.0-mm-diameter deformed steel bar with a yield strength of 540 MPa was also embedded into geopolymer concrete and subjected to a direct pullout test.

Bond-Slip Specimens

Steel tubes with a diameter and a wall thickness of 33 and 3 mm, respectively, were sleeved at one end of GFRP bars using epoxy adhesive to protect them from the gripping force applied by the clamps of the machine during testing. This was done to ensure that bond failure will be achieved instead of bar failure because, unlike steel, the transverse strength of GFRP bars is weaker compared with its longitudinal strength. After the epoxy had cured, the bond-slip specimens were produced such that the steel and GFRP

Table 1. Mechanical Properties of GFRP Bars

Bar diameter (mm)	Guaranteed tensile strength[a] (MPa)	Modulus of elasticity (GPa)	Ultimate elongation (%)
12.7 (#4)	1,312	65.6 ± 2.5	2.00
15.9 (#5)	1,184	62.6 ± 2.5	1.89
19.0 (#6)	1,105	63.7 ± 2.5	1.71

[a]Guaranteed tensile strength: Average value $- 3 \times$ standard deviation (ACI 2006).

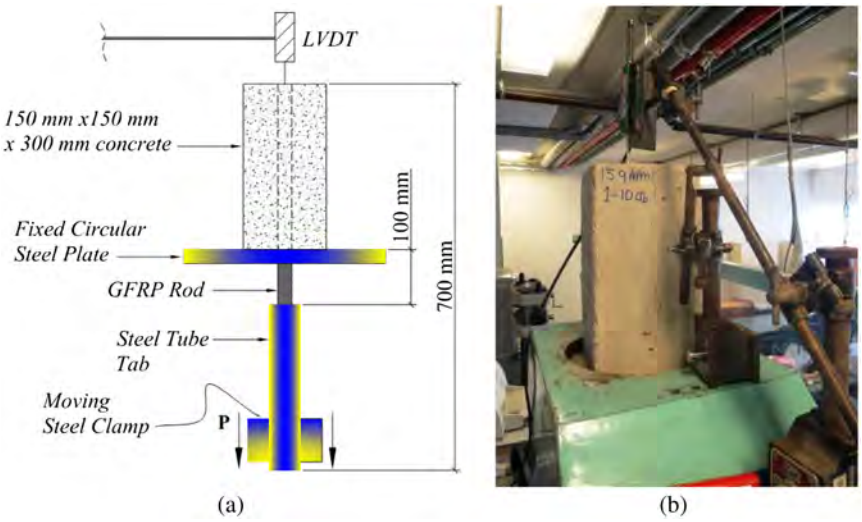

Fig. 1. Direct pullout test: (a) schematic diagram; (b) actual setup (image by Allan Manalo)

bars were embedded at the center of a horizontally cast 150 × 150 × 300-mm geopolymer concrete prism. The specimens are cast horizontally to maintain the concentric alignment (straightness) of the bars and to minimize the unevenness of the load concrete surface to minimize the errors during the initial loading. This is also done to simulate the standard practice for casting the reinforced concrete beam.

Three bond lengths were considered for each bar diameter: 5, 10, and 15 d_b, where d_b is the bar diameter. These lengths were achieved by using PVC pipes to debond the bars from concrete. Three samples were prepared for each embedment length, resulting into 27 GFRP–geopolymer (GG) and 9 steel–geopolymer (SG) bond-slip specimens. In addition, bond-slip specimens with 300-mm embedment length were cast for 12.7-mm ($23d_b$) and 15.9-mm ($18d_b$) GFRP bars and 16.0-mm ($18d_b$) steel bars. The specimens are labeled in the following manner: type of specimen-bar diameter-embedment length. For example, the specimen GG-12.7-5 d_b is a GFRP–geopolymer bond-slip specimen with a 12.7-mm diameter bar embedded $5d_b$ into geopolymer concrete.

All specimens were removed from formworks seven days after casting. This was done to ensure that the geopolymer concrete had cured properly to avoid damaging the specimens on their removal from formworks and during handling.

Direct Pullout Test

The direct pullout test in accordance with ACI 440.3R-04 (ACI 2004) was adopted in this study to evaluate the bond performance of GFRP-reinforced geopolymer concrete and steel-reinforced geopolymer concrete. Tastani and Pantazopolou (2010) stated that, because of differences in boundary conditions and stress state, the stress values obtained from direct pullout tests were not exactly the same as the stresses obtained in actual scenarios. However, the test was adopted in this study because it is simpler, more convenient, and costs less compared with other tests. This test setup is also practical as it represents the main longitudinal reinforcement, which is mostly subjected to tensile forces in a reinforced concrete beam. In fact, many researchers like Bakis et al. (1998), Zhang and Benmokrane (2002), and Achillides and Pilakoutas (2004) have used this test procedure to investigate the bond behavior between the concrete and the FRP bar.

The schematic diagram and actual setup configuration of the test are shown in Fig. 1. In the test conducted, the specimens are positioned in a reverse manner such that the concrete prism is on top while the bar is being pulled downward at a constant displacement rate of 1.2 mm/ min using AVERY testing machine with a loading capacity of 500 kN. The geopolymer concrete block is supported by a fixed circular steel plate that has a hole in the center where the bar can pass through. A linear variable differential transformer (LVDT) is placed on top of the unloaded end of bar to measure the overall slip of the bar. The stand of LVDT is independent of the test specimens to ensure that it will not be affected by the movement and failure of the specimen. The pullout load and end-slip displacement were measured and recorded using the System5000 data logger.

Results and Discussion

Failure Load

The pullout load in which the bond-slip specimens failed are summarized in Table 2. For GG-12.7 specimens, the failure load increases from 5 to $15d_b$ but decreases in 300 mm. The recorded average maximum failure loads for GG-12.7-5 d_b, GG-12.7-10 d_b, GG-12.7-15d_b, and GG-12.7-300 mm are 60.69, 117.00, 119.90,

Table 2. Failure Load and Failure Mode of GG and SG Specimens

Specimen	Failure load, P (kN)	Mode of failure
GG-12.7-5 d_b	60.69 ± 3.56	Bar pullout from concrete
GG-12.7-10 d_b	117.00 ± 2.20	Bar pullout from concrete
GG-12.7-15 d_b	119.90 ± 4.57	Concrete splitting
GG-12.7-300 mm	101.93 ± 0.00	Concrete splitting
GG-15.9-5 d_b	85.55 ± 5.13	Bar pullout from concrete
GG-15.9-10 d_b	144.49 ± 0.04	Concrete splitting
GG-15.9-15 d_b	163.32 ± 5.60	Concrete splitting
GG-15.9-300 mm	131.84 ± 0.00	Concrete splitting
GG-19.0-5 d_b	115.75 ± 7.13	Bar pullout from concrete
GG-19.0-10 d_b	158.76 ± 11.23	Concrete splitting
GG-19.0-15 d_b	138.93 ± 1.65	Concrete splitting
SG-16.0-5 d_b	94.20 ± 1.13	Bar pullout from concrete
SG-16.0-10 d_b	119.31 ± 4.35	Bar rupture
SG-16.0-15 d_b	126.37 ± 2.18	Bar rupture
SG-16.0-300 mm	126.68 ± 0.00	Bar rupture

and 101.93 kN, respectively. The same trend was observed in GG-15.9 specimens wherein the specimens with bond lengths of 5, 10, $15d_b$, and 300 mm failed at pullout loads of 85.55, 144.49, 163.32, and 131.84 kN, respectively. In the case of GG-19.0, the specimen with an embedment length of 10 d_b recorded the highest failure load of 156.76 kN, followed by GG-19.0–15 d_b (138.93 kN) and GG-19-5 d_b (115.75 kN), respectively. It is notable from the results that at an embedment length of 300 mm, the failure load of the specimens decreases. This is because, unlike the specimens with shorter embedment length, these specimens do not have unbonded geopolymer concrete in their loaded end that could prevent the early development of longitudinal cracks, thereby decreasing their pullout capacity. On the other hand, the SG specimens with an embedment length of $5d_b$ recorded the lowest failure load of 94.20 kN. The specimens with bonded lengths of 10 and $15d_b$, and 300 mm have relatively comparable results, as these specimens failed because of rupture of the steel.

Mode of Failure

A close observation of the failed specimens showed that no voids were created under the GFRP bar, indicating that the casting method is satisfactory. The entire surface of the embedded bars is bonded properly in the geopolymer concrete, showing physical evidence that there are no voids that have affected the bond behavior. This is supported by the consistent results of the failure load and failure mode observed for each type of specimens.

Two types of failure were observed in GG specimens: bar pullout and splitting of geopolymer concrete. Pullout type of failure was observed in the specimens with shorter embedment length. This happens because the development length for bonding is not enough, and thus the splitting tensile stress induced by bond is not sufficient to create wider longitudinal cracking. The longitudinal cracks that initiated at the surrounding geopolymer concrete (near the interface of the bar and the geopolymer concrete) did not propagate in the external surface. This resulted in a higher bond stress than calculated from the experiment. Concrete splitting type of failure, on the other hand, is exhibited by the specimens with relatively longer embedment length because they have enough length to develop high radial stresses. This high amount of stress leads to wider longitudinal cracks that can propagate to the external surface of the concrete, thereby eliminating the confinement capacity of geopolymer concrete. This failure contaminated the real bond strength of the specimens that resulted in a lower calculated bond stress than the specimens that failed because of bar pullout. The splitting of geopolymer concrete occurred in an explosive brittle manner, which was also observed by Sarker (2011) and Sofi et al. (2007). The longitudinal cracks are commonly localized to regions where the GFRP bar was bonded to geopolymer concrete.

Fig. 2 shows the failure mode of bond-slip specimens with a 12.7-mm GFRP bar. The specimens embedded 5 and $10d_b$ into geopolymer concrete failed because of bar pullout, whereas the specimens with embedment lengths of $15d_b$ and 300 mm failed because of concrete splitting. The mode of failure of pullout specimens with 15.9-mm diameter GFRP bar is depicted in Fig. 3. Only the specimens with the shortest embedment length experienced a pullout failure, whereas the rest failed because of concrete splitting. The same results were observed in specimens with 19.0-mm GFRP bar. As can be seen in Fig. 4, the specimens with bond length of $5d_b$ failed because of pullout, whereas those with longer embedment lengths failed because of concrete splitting. From these results, it can also be observed that, as the bar diameter increases, the concrete splitting type of failure became more dominant in specimens with longer embedment length. Furthermore, the formation of

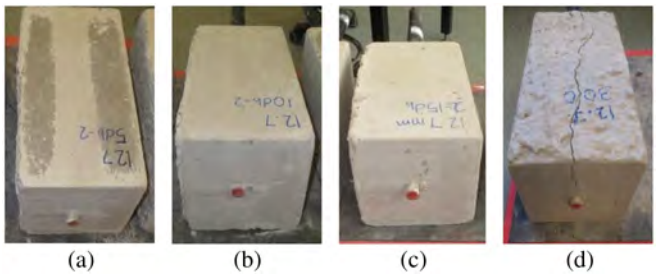

Fig. 2. Mode of failure of GG-12.7 specimens: (a) $5d_b$; (b) $10d_b$; (c) $15d_b$; (d) 300 mm (images by Ginghis Maranan)

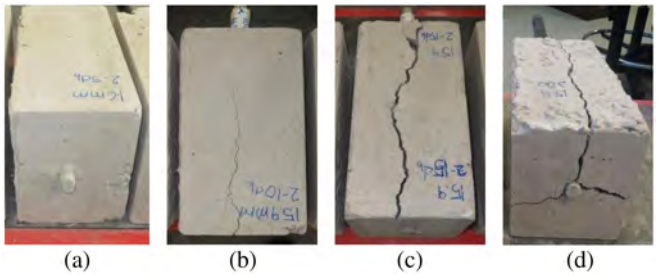

Fig. 3. Mode of failure of GG-15.9 specimens: (a) $5d_b$; (b) $10d_b$; (c) $15d_b$; (d) 300 mm (images by Ginghis Maranan)

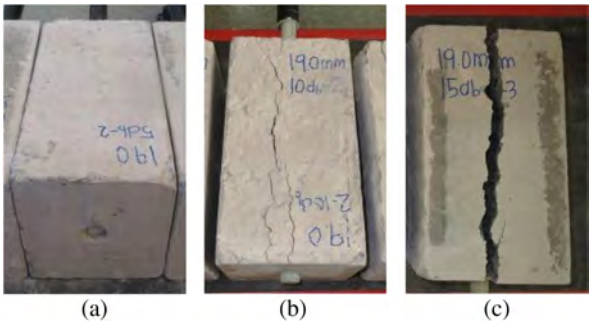

Fig. 4. Mode of failure of GG-19.0 specimens: (a) $5d_b$; (b) $10d_b$; (c) $15d_b$ (images by Ginghis Maranan)

longitudinal cracks is more pronounced in the specimens with longer bond length. Interestingly, the sand-coating did not debond from the GFRP bar, which indicates the effectiveness of the adhesive used to bind the sand around the surface of the GFRP bars.

The SG bond-slip specimens exhibited two types of failure: bar pullout and bar yielding. Fig. 5 shows that the specimens with shorter embedment length failed because of bar pullout from geopolymer concrete, whereas those with longer embedment length failed because of rupture of the bar. Table 2 summarizes the failure mode of the specimens.

Relation between Bond Stress and End-Slip Displacement

The bond stress-slip relationship is adopted to describe the bond performance of GFRP bars embedded into geopolymer concrete, as it is a commonly used representation of the bond behavior of reinforcement in concrete members wherein a constant stress

Fig. 5. Mode of failure of SG-16.0 specimens: (a) $5d_b$; (b) $10d_b$; (c) $15d_b$ (images by Ginghis Maranan)

distribution and the average bond stress are assumed. The relationship between the bond stress and end-slip displacement of the GG pullout test specimens is depicted in Figs. 6–8. The bond stresses reported in this study are the average of the three samples for each type of bond-slip specimen. The stress distribution is assumed constant along the bond length. With this assumption, the average bond stress (τ) is calculated using Eq. (1):

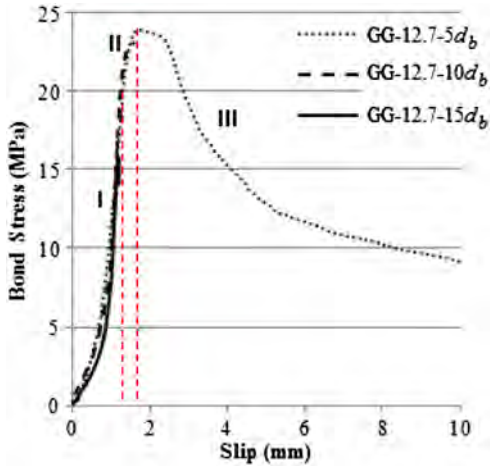

Fig. 6. Bond-slip diagram of 12.7-mm GFRP bar

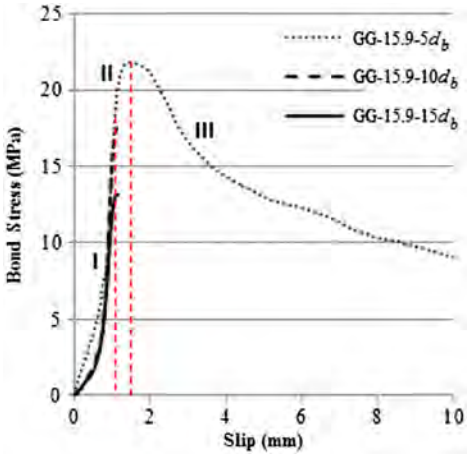

Fig. 7. Bond-slip diagram of 15.9-mm GFRP bar

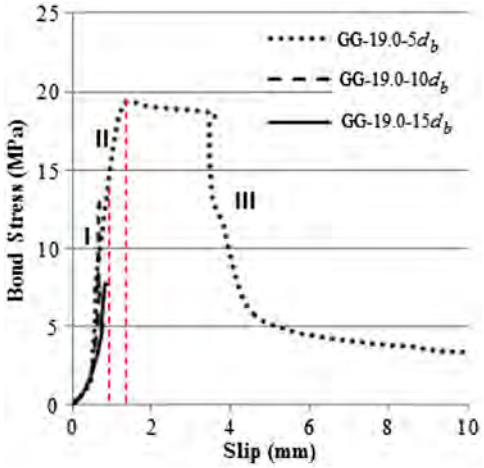

Fig. 8. Bond-slip diagram of 19.0-mm GFRP bar

$$\tau = \frac{P}{\pi d_b l_d} \tag{1}$$

where P = failure load (load when one of the following types of failure occurred enclosing geopolymer concrete splits, bar pullout from geopolymer concrete, and bar rupture); d_b = nominal bar diameter; and l_d = embedment length.

Generally, the bond stress-slip curve of GG specimens with a bond length of $5d_b$ that failed because of bar pullout is composed of three distinct regions: the linear, nonlinear, and softening regions. The first region (region I) is represented by a long linear ascending branch, wherein the load increases rapidly while end-slip increases slowly. In this region, it is the chemical adhesion and mechanical interlock between the sand coats and the geopolymer concrete that make up the main resisting mechanism of the specimen. However, during the initial loading, a low stiffness response was observed in the curves. This can be attributed to the settlement of the specimen during the initial loading caused by slight unevenness of the external face of the loaded end of geopolymer concrete. As the pullout load is applied, radial splitting stress develops, leading to simultaneous formation of interfacial cracks between the bar and the geopolymer concrete and longitudinal cracks in the surrounding geopolymer concrete. As the load is further increased, the bond stress-slip response shifted from linear to nonlinear (region II) up to peak load because of the increase of the size of longitudinal cracks. At this stage, it is still the mechanical interlock and the friction forces provided by the sand coating that resist the pullout load. The post peak phase (region III) is governed only by friction force between the bars and geopolymer concrete as characterized by a descending branch (softening region) of the bond stress with the increase of slip. The short bonded length of the bar did not induce sufficient tensile splitting stress that resulted in the pullout failure of the specimens. On the other hand, the bond-slip curves of GG specimens with embedment lengths of 10 and $15d_b$ that failed because of concrete splitting exhibited a linear response and a short portion of nonlinear region and no softening behavior.

In the case of SG specimens (Fig. 9), only the specimens bonded $5d_b$ into geopolymer concrete exhibited the three regions. In the linear region up to failure, the main resisting mechanism of these specimens is mostly governed by the mechanical bearing provided by the steel ribs. The remaining stresses are resisted by the friction between the bar and the concrete. On the contrary, the specimens with embedment length of 10 and $15d_b$ exhibited linear response up

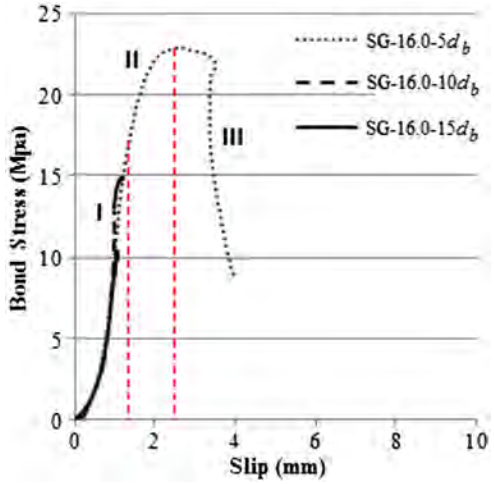

Fig. 9. Bond-slip diagram of 16.0-mm deformed steel bar

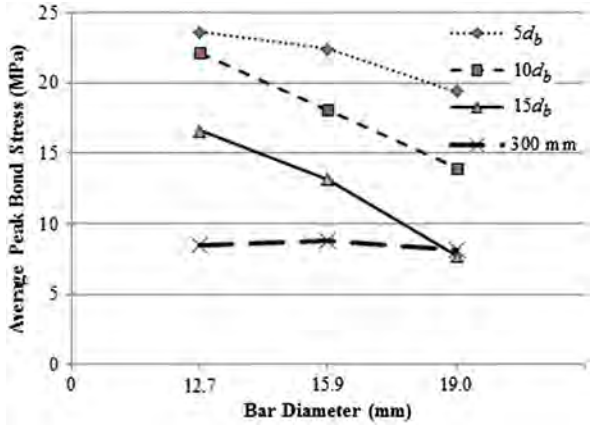

Fig. 10. Relationship between the average bond stress and bar diameter of GG specimens

to failure because of rupture of the steel bar. A notable observation from the graph is that the embedment length did not affect the linear stiffness behavior (region I) of bond-slip specimens that have the same bar diameter. In addition, as the GFRP bar diameter increases, the linear stiffness also increases. The range of bond stresses and slips per region are summarized in Table 3.

Discussion

Effect of Bar Diameter

The relationship between the average bond stress and the bar diameter of GG bond-slip specimens is presented in Fig. 10. From the graph, it can be observed from the specimens that failed because of bar pullout (specimens with embedment length of $5d_b$) that the increase in the bar diameter causes the peak average bond stress to decrease. This finding is in agreement with that of Cosenza et al. (1997), Tighiouart et al. (1998), and Arias et al. (2012), who studied the bond behavior of FRP bars in ordinary concrete. They suggested that the nonlinear distribution of stresses is more dominant in larger-diameter bars (requiring higher embedment length) that leads to a lower bond strength.

Achillides and Pilakoutas (2004) reported that, aside from the existence of nonlinear stress distribution, the observed behavior can also be attributed to Poisson's ratio and shear lag effects. Poisson's ratio leads to a decrease in bar diameter attributable to pullout load. Generally, the bars with a larger diameter experienced higher Poisson's ratio effect that leads to a lower mechanical interlock and/or friction between the GFRP bars and the geopolymer concrete. Shear lag, on the other hand, occurred when the GFRP is pulled in tension through its surface, which resulted in differential movement between the core and the surface of the bar. This movement resulted in a nonuniform distribution of normal stresses on the circular face of the GFRP bar that led to lower average stress in the core and higher surface normal stress. As the bar diameter increased, the difference between the two stresses also increased, which resulted into the reduction of bond strength between the concrete and the bar. Interestingly, the trend was also observed in the specimens that failed from bar pullout (specimens with embedment length greater than $5d_b$).

Effect of Embedment Length

Fig. 11 illustrates the correlation between the average bond stress and embedment length of all direct pullout specimens with GFRP bars. It can be seen from the figure that the bond stress of specimens with embedment length of $5d_b$ is higher than the specimens with embedment lengths of 10 and $15d_b$, regardless of bar diameter. This is attributed to two different types of failure exhibited by these specimens. The splitting type of failure exhibited by specimens with embedment lengths of 10 and $15d_b$ resulted in a lower average bond stress between the GFRP bars and the geopolymer concrete.

Comparing the specimens that failed because of concrete splitting (specimens with embedment length of 10 and $15d_b$), it can be observed that the computed bond stress decreases with an increase in embedment length. Tighiouart et al. (1998) explained that this behavior is a consequence of the nonlinear distribution of the stress (maximum at the loaded end and minimum at the unloaded end) along the bonded length that is more pronounced in bars with longer embedment. Furthermore, this nonlinear behavior was also reported by Cosenza et al. (1997), Arias et al. (2012), and Mazaheripour et al. (2013). Tang et al. (2008), on the other hand, explained that an increase in the embedment length leads to an increase in the perimeter area and, thus, a decrease in bond strength.

Table 3. Range of Bond Stresses and Slips per Region of the Bond-Slip Curves of Bond-Slip Specimens

	GG-12.7-5 d_b		GG-15.9-5 d_b		GG-19.0-5 d_b		SG-16.0-5 d_b	
Region	Slip (mm)	Bond stress (MPa)	Slip (mm)	Bond stress (MPa)	Slip (mm)	Bond stress (MPa)	Slip (mm)	Bond stress (MPa)
I	0.0–1.2	0.0–19.6	0.0–1.1	0.0–18.1	0.0–1.0	0.0–14.6	0.0–1.4	0.0–17.4
II	1.2–1.8	19.6–23.96	1.1–1.5	18.1–21.84	1.0–1.4	14.6–19.39	1.4–2.5	17.4–22.88
III	1.8–10.0	23.96–9.3	1.5–10.0	21.84–9.1	1.4–10.0	19.39–3.4	2.5–3.9	22.88–9.7

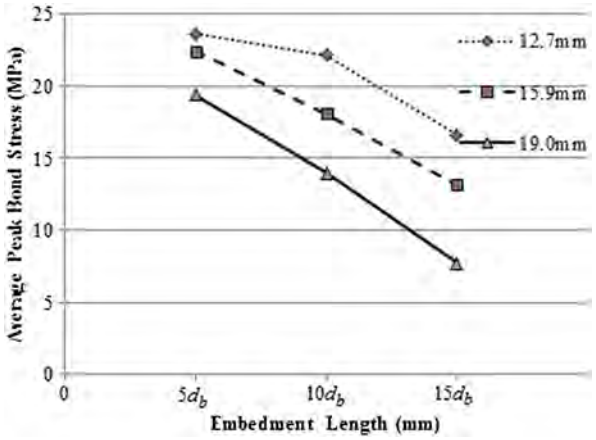

Fig. 11. Relationship between the average bond stress and embedment length of GG specimens

Comparison of GFRP-Geopolymer and Steel-Geopolymer Bond-Slip Specimens

The comparison of the average bond stress in GG and SG specimens is shown in Fig. 12. Based on the figure, the GG specimens have comparable bond strength compared with SG specimens at embedment length of $5d_b$. Therefore, it can be concluded that the sand-coated GFRP bar could be an effective alternative to steel as an internal reinforcement for geopolymer concrete structures. The bonding property of GFRP bars were improved through the mechanical interlock and friction forces provided by the sand coating as proven by Arias et al. (2012) and Tang et al. (2008). In the case of the specimens with longer embedment length, an indicative comparison is made because the mode of failure GG and SG specimens are different. The average bond stresses in GG specimens are greater than SG specimens because the SG specimens failed because of bar rupture. This is attributable to the lower tensile strength of steel used in the experiment compared with the tensile strength of the GFRP bars.

Analytical Model

Analytical models are normally developed to provide tools for evaluating the bond mechanisms of complex physical processes

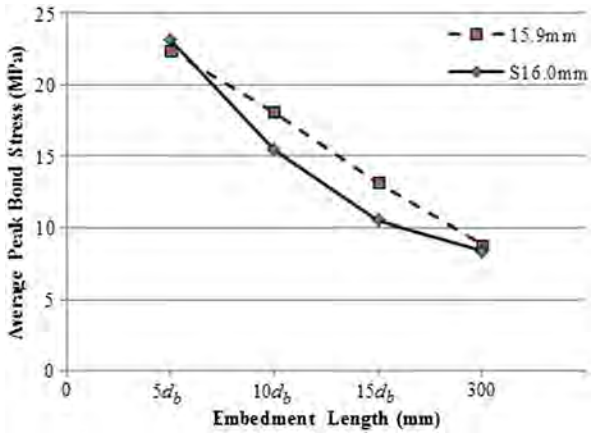

Fig. 12. Comparison of the relationship between the average peak bond stress and embedment length of GG-15.9 and SG-16.0

Table 4. Values of s_r and α Parameters

Bar diameter (mm)	s_r	α
12.7	0.20	9
15.9	0.14	5
19.0	0.12	4

happening during the bond-slip test and for the conduct of numerical modeling and simulations. Currently, there are four different models being used to simulate the actual bond-slip behavior of FRP-reinforced concrete. These models are the Malvar model, Bertero-Eligehausen-Popov (BEP) model, modified BEP (mBEP) model, and Cosenza-Manfredi-Realfonzo (CMR) model. Among these models, Cosenza et al. (1997) identified the CMR model as the most reliable model that can simulate the ascending behavior of the bond-slip curves. It is a modification of the ascending region of EBP model and is given as

$$\frac{\tau}{\tau_m} = [1 - e^{(-s/s_r)}]^{\alpha} \tag{2}$$

where τ = bond stress (MPa); τ_m = peak bond stress (MPa); s = corresponding slip at τ (mm); and s_r and α = parameters based on curve-fitting of the experimental data.

In this study, the constitutive analytical models of the ascending branch of bond-slip curve, generally used to investigate the behavior of structures at the serviceability state level, of the sand-coated GFRP bars embedded into geopolymer concrete were derived based on the CMR model and by considering the experimental bond stress versus slip curves of the specimens with an embedment length of $5d_b$. Specifically, these equations represent the bond behavior from regions II (linear) to III (nonlinear up to peak stress) of the bond stress-slip curves of GG specimens obtained from the experiment.

Table 4 shows the values of s_r and α parameters obtained by employing the curve-fitting method suggested by Tighiouart et al. (1998) for 12.7, 15.9, and 19.0-mm nominal diameter GFRP bars. The parameter s_r defines the slope of linear stiffness (region II) of the bond-slip curve, whereas α controls the nonlinear to peak stress shape (region III) of the curve. According to Table 4, the value of α decreases with an increase in bar diameter. On the other hand, an increase in bar diameter leads to a decrease of s_r.

A comparison of the curves between the analytical model and experimental results for GG-15.9-5 d_b specimen is shown in Fig. 13. It can be seen that there is a good agreement between

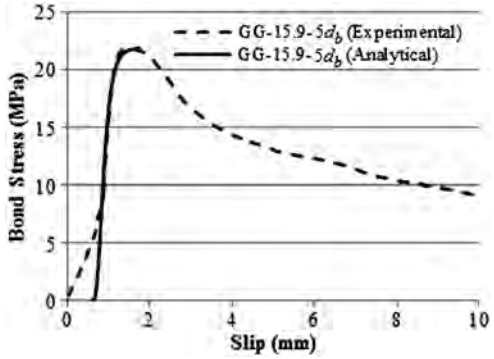

Fig. 13. Bond-slip curves of the proposed analytical model and the experimental results of GG-15.9-5 d_b

the proposed model and the experimental results, starting from the linear portion until the peak of the curves. With this, it can be deduced that the derived equations can be used in performing numerical investigation on the interaction between geopolymer concrete and sand-coated GFRP bars. These analytical models can also be used in the specimens that failed because of concrete splitting because the bond-slip linear stiffness behavior of the specimens with the same diameter are the same. However, the obtained maximum bond stress between the GFRP bars and geopolymer concrete for specimens with longer embedment lengths maybe lower because of the splitting failure of concrete. Nevertheless, this is a conservative value that can be used in understanding the behavior of structures at the serviceability state level. The results of the study are also not sufficient to determine the maximum bond stress where the splitting of concrete will start to occur, i.e., the upper limit for its application for this type of failure. This needs further investigation and is beyond the scope of this paper.

Conclusions

This study evaluated the bond performance of sand-coated GFRP bars into geopolymer concrete under direct pullout tests. The influence of parameters such as bar diameter and embedment length to the bond between the GFRP bars and geopolymer concrete were investigated. Based on the results, the following conclusions are made:

- The average bond stress of sand-coated GFRP bars embedded into geopolymer concrete is around 23 MPa, which indicates that a sufficient bond exists between the GFRP bar and the geopolymer concrete;
- Generally, the specimens with a shorter embedment length ($5d_b$) failed because of bar pullout, whereas the specimens with a longer embedment length failed because of concrete splitting. As the bar diameter increased, concrete splitting type of failure became more dominant in specimens with longer embedment length;
- For specimens that failed because of bar pullout (specimens with $5d_b$), the increase in bar diameter causes the peak average bond stress to decrease. The increase of embedment length results in a lower average bond stress because of the different types of failure;
- The sand-coated GFRP bars have bond strength comparable to that of corrugated steel bars, suggesting that they can be an effective alternative as internal reinforcement for geopolymer concrete structures; and
- The bonding mechanism between the bar and the geopolymer can be accurately studied if a pullout type of failure is exhibited by all specimens. To achieve this, the use transverse confining materials such stirrups and FRP jackets are proposed.

Acknowledgments

The authors gratefully acknowledge V-Rod Australia for the materials and technical support they had given in the conduct of this research undertaking.

References

Achillides, A., and Pilakoutas, K. (2004). "Bond behaviour of fiber reinforced polymer bars under direct pullout conditions." *J. Compos. Constr.*, 10.1061/(ASCE)1090-0268(2004)8:2(173), 173–181.

Aldred, J., and Day, J. (2012). "Is geopolymer concrete a sustainable alternative to traditional concrete?" *37th Conf. on Our World in Concrete & Structures*, CI-Premier Pte, Singapore, 1–14.

American Concrete Institute (ACI). (2004). "Guide test methods for FRPs for reinforcing or strengthening concrete structures." *ACI 440.03R-04*, Farmington Hills, MI, 10–13.

American Concrete Institute (ACI). (2006). "Guide for the design and construction of concrete reinforced with FRP bars." *ACI 440.1R-06*, Farmington Hills, MI, 44.

Arias, J. P. M., Vasquez, A., and Escobar, M. M. (2012). "Use of sand coating to improve bonding between GFRP bars and concrete." *J. Compos. Mater.*, 46(18), 2271–2278.

Baena, M., Torres, L., Turon, A., and Barris, C. (2009). "Experimental study of bond behaviour between concrete and FRP bars using a pull-out test." *Compos. Part B*, 40(8), 784–797.

Bakis, C. E., Uppuluri, V. S., Nanni, A., and Boothby, T. E. (1998). "Analysis of bonding mechanisms of smooth and lugged FRP rods embedded in concrete." *Compos. Sci. Technol.*, 58(8), 1307–1319.

Canadian Standards Association (CSA). (2010). "Specification for fibre-reinforced polymers." *CAN/CSA S807–10*, Rexdale, ON, Canada.

Chaallal, O., and Benmokrane, B. (1993). "Pullout and bond of glass-fibre rods embedded in concrete and cement grout." *Mater. Struct.*, 26(3), 167–175.

Cosenza, E., Manfredi, G., and Realfonzo, R. (1997). "Behavior and modeling of bond of FRP rebars to concrete." *J. Compos. Constr.*, 10.1061/(ASCE)1090-0268(1997)1:2(40), 40–51.

Davidovits, J. (1988). "Geopolymer chemistry and applications." *Proc., Geopolymer '88, 1st European Conf. on Soft Mineralurgy*, The Geopolymer Institute, Compiegne, France, 25–48.

Duxson, P., Fernandez-Jimenez, A., Provis, L., Lukey, G. C., Palomo, A., and van Deventer, J. S. J. (2007). "Geolpolymer technology: The current state of the art." *J. Mater. Sci.*, 42(9), 2917–2933.

Fico, R. (2008). "Limit states design of concrete structures reinforced with FRP bars." Ph.D. thesis, Univ. of Naples Federico II, Naples, Italy.

Gangarao, H. V. S., Taly, N., and Vijay, P. V. (2007). *Reinforced concrete design with FRP composites*, CRC Press, Taylor & Francis Group, Boca Raton, FL.

Lloyd, N. A., and Rangan, B. V. (2010). "Geopolymer concrete: A review of development and opportunities." *35th Conf. on Our World in Concrete & Structures*, CI-Premier Pte, Singapore, 1–8.

Malvar, L. J. (1994). "Bond stress-slip characteristics of FRP rebars." *Technical Rep. 2013-SHR*, Naval Facilities Engineering Service Center, Port Hueneme, CA.

Mazaheripour, H., Barros, J. A. O., Sena-Cruz, J. M., Pepe, M., and Martinelli, E. (2013). "Experimental study on the bond performance of GFRP bars in self-compacting steel fiber reinforced concrete." *Compos. Struct.*, 95, 202–212.

McCaffrey, R. (2002). "Climate change and the cement industry." *Global Cem. Lime Mag.*, 15–19.

McLellan, B. C., Williams, R. P., Lay, J., Riessen, A., and Corder, G. D. (2011). "Costs and carbon emissions for geopolymer pastes in comparison to ordinary portland cement." *J. Cleaner Prod.*, 19(9–10), 1080–1090.

Okelo, R., and Yuan, R. L. (2005). "Bond strength of fiber reinforced polymer rebars in normal strength concrete." *J. Compos. Constr.*, 10.1061/(ASCE)1090-0268(2005)9:3(203), 203–213.

Sarker, P. K. (2011). "Bond strength of reinforcing steel embedded in fly ash-based geopolymer concrete." *Mater. Struct.*, 44(5), 1021–1030.

Selby, D. R. (2011). "An investigation into the bond of steel reinforcement in geopolymer and ordinary Portland cement concrete." Bachelor thesis, School of Civil Engineering, Univ. College, Univ. of New South Wales–ADFA, Canberra, Australia.

Sofi, M., van Deventer, J. S. J., and Mendis, P. A. (2007). "Bond performance of reinforcing bars in inorganic polymer concrete (IPC)." *J. Mater. Sci.*, 42(9), 3107–3116.

Tang, W. C., Lo, T. Y., and Balendran, R. V. (2008). "Bond performance of polystyrene aggregate concrete (PAC) reinforced with glass-fibre-reinforced polymer (GFRP) bars." *Build. Environ.*, 43(1), 98–107.

Tao, S., Ehsani, M. R., and Saadatmanesh, H. (1992). "Bond strength of straight GFRP rebars." *Material Performance and Prevention of Deficiencies and Failures, in Proc., Materials Engineering Congress*, ASCE, Reston, VA, 598–605.

Tastani, S. P., and Pantazopulou, S. J. (2006). "Bond of GFRP bars in concrete: Experimental study and analytical interpretation." *J. Compos. Constr.*, 10.1061/(ASCE)1090-0268(2006)10:5(381), 381–391.

Tastani, S. P., and Pantazopulou, S. J. (2010). "Direct tension pullout bond test: Experimental results." *J. Struct. Eng.*, 10.1061/(ASCE)ST.1943-541X.0000159, 731–743.

Tighiouart, B., Benmokrane, B., and Gao, D. (1998). "Investigation of bond in concrete members with fibre reinforced polymer (FRP) bars." *Constr. Build. Mater.*, 12(8), 453–462.

Zhang, B., and Benmokrane, B. (2002). "Pullout bond properties of fiber-reinforced polymer tendons to grout." *J. Mater. Civ. Eng.*, 10.1061/(ASCE)0899-1561(2002)14:5(399), 399–408.

3.2. Paper II: Pullout behaviour of GFRP bars with anchor head in geopolymer concrete

This paper evaluated the influence of anchor head on the pullout behaviour of glass fibre reinforced polymer (GFRP) bars in geopolymer concrete using the direct pullout test for straight FRP bars employed in **Paper I**. The effect of bar diameter and embedment length on the pullout resistance of headed GFRP bars in geopolymer concrete was evaluated thoroughly and was compared with the results of the previous researchers. Based on the experimental results, the provision of an anchor head enhanced the anchorage capacity of GFRP bars in geopolymer concrete. However, its contribution decreases as the embedment length increases. These observations showed that in some cases, the anchor heads produce an increase of the maximum pullout force and in some cases they do not, hence, a simple mechanical model (**Equation 4** of **Paper II**) that evaluates the pullout load resistance produced by the anchor heads only or by the anchor heads and sand-coating was developed. **Equation 2** of **Paper II** represents the pullout contribution of anchor heads. This equation was obtained by subtracting the tensile stresses developed in the pullout specimens with straight GFRP bars only (for example, SGG-15.9-5Ø) from the specimens with headed GFRP bars (for example, SGG-15.9-5Ø+l_{ah}). Then, based on regression analysis using MS Excel Software, an exponential relationship was found to be the best fit for the observed differences. In general, the equations formulated in **Paper II** would permit for evaluating the opportunity in adopting the proposed device in mainstream construction applications.

The results obtained from **Papers I** and **II** showed that there is an adequate bond between the sand-coated GFRP bars and geopolymer to secure a composite action. That is, the stress can be effectively transferred between the GFRP bars and geopolymer concrete. Hence, an investigation of the structural behaviour of geopolymer concrete beams and columns reinforced longitudinally and transversely with GFRP bars was conducted and the results are presented, analysed, and discussed in Papers III, IV and V.

Composite Structures 132 (2015) 1113–1121

Contents lists available at ScienceDirect

Composite Structures

journal homepage: www.elsevier.com/locate/compstruct

Pullout behaviour of GFRP bars with anchor head in geopolymer concrete

G.B. Maranan [a], A.C. Manalo [a,*], W. Karunasena [a], B. Benmokrane [b]

[a] Centre of Excellence in Engineered Fibre Composites (CEEFC), Faculty of Health, Engineering and Sciences (FoHES), University of Southern Queensland, Toowoomba 4350, Australia
[b] Department of Civil Engineering, University de Sherbrooke, Sherbrooke, Quebec J1K 2R1, Canada

ARTICLE INFO

Article history:
Available online 17 July 2015

Keywords:
Geopolymer concrete
Glass-fibre-reinforced polymer (GFRP)
Anchorage
Anchor head
Pullout behaviour
Headed GFRP bar

ABSTRACT

The geopolymer concrete internally reinforced with fibre-reinforced polymer (FRP) bars is anticipated to offer durable, sustainable, and cost-effective civil infrastructures. In this study, the effect of the anchor head on the pullout behaviour of the sand coated glass-fibre-reinforced polymer (GFRP) bars embedded in the geopolymer concrete was investigated using a direct pullout test. Straight and headed GFRP bars with different nominal diameters $\varnothing$ (12.7, 15.9, and 19.0 mm) and embedment lengths l_d ($0\varnothing + l_{ah}$, $5\varnothing + l_{ah}$, and $10\varnothing + l_{ah}$ for headed bars, where l_{ah} stands for the anchor head length, and $5\varnothing$ and $10\varnothing$ for straight bars) were considered. The results showed that the provision of anchor head is an efficient method to enhance the anchorage capacity of GFRP bars in geopolymer concrete. The anchor heads improved the anchorage of the sand coated GFRP bars by as much as 49–77%. Furthermore, the mechanical bearing resistance provided by the anchor head alone resulted in the development of approximately 45% of the GFRP bars' nominal tensile strength. A comparison of the experimental results with the published studies showed that a much higher load is required to pullout the GFRP bars in geopolymer concrete than in Ordinary Portland Cement-based concrete.

1. Introduction

The geopolymer concrete is currently attracting a widespread attention in Australia due to its lower embodied energy and carbon footprint, approximately 80% less CO_2 [1] compared to the Ordinary Portland Cement (OPC) concrete [2]. Geopolymer concrete has engineering properties that are suitable for structural applications, including rapid and good compressive strength development, highly durable, excellent chemical and fire resistance, and minimal thermal and drying shrinkage [3]. This type of concrete is produced from alkali-activated waste materials like fly ash and rice husk ash, that are rich in silica and alumina [4] resulting in 10–30% cheaper than the OPC concrete in terms of material costs [5,6]. While the geopolymer concrete reinforced with steel bars has been successfully trialled in a number of field applications, most of the researches being conducted focus only on mix design and durability [7]. It is necessary therefore to extend the understanding into the behaviour of structures made up of geopolymer concrete to increase its acceptance and utilisation in the mainstream construction application.

In Australia, the environments are severe to use steel as reinforcement to concrete structures from the viewpoint of corrosion damage. With the limited resource of the state and the federal government to maintain existing infrastructures, the Engineers Australia has been calling for a new approach and construction of more durable infrastructures promising results as long-term solutions [8]. Thus, the materials that are environmentally friendly, requires low energy consumption in production, light weight, and with good specific mechanical properties which require low maintenance are warranted. A promising solution is to combine fibre reinforced polymer (FRP) materials and geopolymer concrete to develop a structure with the best characteristics of each material. The use of FRP bars will have a major role in attaining a more sustainable and almost maintenance free infrastructure as the corrosion problem is eliminated. Also, there is more incentive for the construction industry to switch to the use of materials that can significantly reduce carbon dioxide emissions, which is one of the main causes of global warming. However, the use of FRP-reinforced concrete is still unfamiliar to many practising

* Corresponding author at: Civil Engineering (Structural), Centre of Excellence in Engineered Fibre Composites (CEEFC), Faculty of Health, Engineering and Sciences, University of Southern Queensland, Toowoomba, Queensland 4350, Australia. Tel.: +61 7 4631 2547; fax: +61 7 4631 2110.

E-mail addresses: ginghis.maranan@usq.edu.au (G.B. Maranan), allan.manalo@usq.edu.au (A.C. Manalo), karu.karunasena@usq.edu.au (W. Karunasena), bbenmokrane@andrew.sca.usherb.ca (B. Benmokrane).

http://dx.doi.org/10.1016/j.compstruct.2015.07.021
0263-8223/

Australian engineers, more so, with the use of FRP bars as internal reinforcement in geopolymer concrete structures.

In order to encourage the use of FRP-reinforced geopolymer concr ete, the anchorage of the FRP bars in this type of concrete must be investigated first as it is the key factor that influences the overall performance of structural elements in any reinforced concrete (RC) structures. Conventionally, the FRP bars are anchored to concrete through chemical adhesion, friction, and mechanical interlock through the provisions of sand coating and/or ribs on the surface of the bars. The other usual option to provide the required development is to use standard hooks such as 90 degrees- or 180 degrees-hook. However, unlike steel reinforcements, hooks should be pre-fabricated before installation because the bending of FRP bars on-site is almost impossible and the bent FRP bars are relatively weaker than the straight bars due to the redirection of the fibres in the bend [9]. Another approach is to use anchor heads to effectively utilise the strength of FRP bars, especially in a congested reinforcement area.

The use of FRP bars with anchor heads to internally reinforce the concrete is yet in its early stages with very limited studies. Hasaballa and El-Salakawy [10] investigated the seismic performance of beam-column joints reinforced with GFRP-headed bars. The results of their study showed that the straight-headed bars have excellent seismic performance than the bent ones. Johnson [11] reported that the straight double-headed GFRP bars can be effectively utilised as shear reinforcement for concrete beams. Mohamed and Benmokrane [12] studied the pullout capacity behaviour of FRP-headed bars. Their results showed that the FRP-headed bars can efficiently provide the necessary anchorage to develop the ultimate tensile strength of the bar. An in-depth investigation of the bond properties of anchorage systems for GFRP bars including straight, anchor heads, and bents were conducted by Vint [13]. It was concluded that the mechanical anchor heads greatly improved the bond capacity of the bars and are more effective for a smaller development length. Khederzadeh and Sennah [14] tested 114 pullout specimens and reported that the headed GFRP bars have a better anchorage capacity as compared with the hooked bars. However, these studies focused on the behaviour of the headed bars embedded in the OPC concrete only and not in the geopolymer concrete, which has been the key motivation of this undertaking.

This study evaluated the effects of the anchor head on the pullout behaviour of the sand coated GFRP bars in the geopolymer concrete using a direct pullout test. The results from this study will be used in developing some recommendations for the design of GFRP-reinforced geopolymer concrete (GFRP-RGC) structures, allowing their responsible introduction and wider use in civil infrastructure.

2. Experimental details

The properties of the component materials, the method of specimen preparation, and the direct pullout test employed in this study are presented in this section.

2.1. Properties of the GFRP bars and the geopolymer concrete

The GFRP bars used in this study were provided by V-Rod® Australia [15] and were manufactured by the pultrusion process of E-glass fibres impregnated with modified vinyl ester resin. Figs. 1 and 2 show the high modulus (HM) sand coated straight and headed GFRP bars (Grade III, CAN/CSA S807-10 [16]). Three types of bars having nominal diameters ∅ of 12.7 mm, 15.9 mm, and 19.0 m with fibre contents by weight of 84.1%, 83.9%, and 84%, respectively, were considered. The fibre content was determined in accordance with Method 1, Procedure G of ASTM D3171 [17]. Table 1 summarises the guaranteed properties as well as the nominal and actual (immersion) cross-sectional areas of the bars as reported by the manufacturer. The tensile strength and the elastic modulus were calculated using a nominal cross-sectional area.

On the other hand, one batch of geopolymer concrete was used to fabricate all the pullout specimens. The geopolymer binder was made from the alkali activation of fly ash and blast furnace slag (BFS). The concrete was composed of fine aggregates (fine and medium sand) and coarse aggregates (10 mm and 20 mm gravels). Plasticizers were added to improve the workability of the geopolymer concrete. Seven 100 × 200 mm cylinders were also cast from the same batch of geopolymer concrete. The cylinders were subjected to compression test following the ASTM C39/C39 M [18] standard using the SANS Testing Machine. Based on the test, the average compressive strength of the 32-day geopolymer concrete was 33.09 MPa.

2.2. Properties and configuration of the anchor head

Fig. 2 illustrates the anchor head configuration and the overview of the bar-head interface. The anchor heads were manufactured using the same type of resin as the GFRP bars. The bar ends bars were prepared with grooves/dents on the surface before attaching the head to the bars to enhance the bond and to increase the mechanical interlocking between the bar end and the head. The headed anchorages are cast onto the deformed ends of the straight bars and hardened at elevated temperatures.

The head lengths l_{ah} is approximately 92 mm. The maximum outer diameter D_{max} of the end heads is around three times the bar diameter. The surface geometry of the anchor head has a special configuration of ribs to enhance the bond with concrete interface. It begins with a wide wedge that helps to transfer a large portion of the load from the bar into the concrete and to develop the required uniform stress for equilibrium. Beyond this wedge, the head tapers in five steps to the outer diameter of the blank bar. This configuration is responsible to develop a stronger anchoring system, making it as a suitable alternative to bent bars in some applications, and to avoid the splitting action in the vicinity of the head.

2.3. Preparation of the pullout specimens

The loaded end of the GFRP bar was inserted into the steel tube tabs having a diameter and a wall thickness of 33 mm and 3 mm, respectively, using a commercially available epoxy adhesive as shown in Fig. 1. This was done to avoid the transverse failure of the bars caused by the gripping force of the machine clamps during testing. The desired embedment lengths were properly marked on the bars and were achieved by sleeving PVC pipes to disband the bars from the geopolymer concrete. Then, the bars were placed horizontally at the centre of each 150 × 150 × 300 mm rectangular plywood moulds to achieve a concentric alignment. The geopolymer concrete were poured into the moulds and were cast horizontally. A mechanical vibrator was used to compact the geopolymer concrete and to reduce the air voids present, especially near the bonded lengths. The specimens were carefully de-moulded seven days after casting to make sure that the concrete had cured properly to avoid damages upon their removal from formworks and during handling.

Embedment lengths of $0\varnothing + l_{ah}$, $5\varnothing + l_{ah}$, and $10\varnothing + l_{ah}$, were considered for the headed bars while embedment lengths of $5\varnothing$ and $10\varnothing$ were adopted for the straight bars. The $0\varnothing$, $5\varnothing$, and $10\varnothing$ represent the length of the straight sand coated portion of the bars. The embedment length $0\varnothing + l_{ah}$ was used to determine

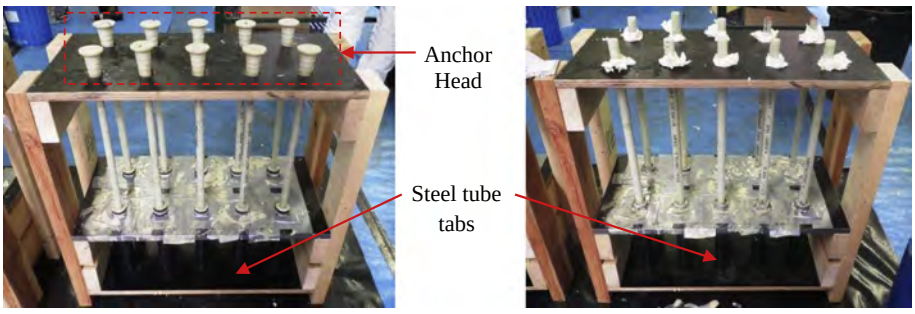

(a) With anchor head (b) Without anchor head

Fig. 1. High modulus GFRP bars coated with Grade 24 silica sand.

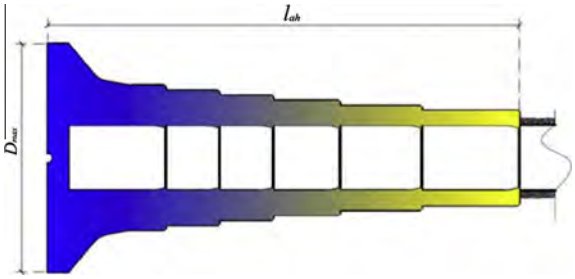

Fig. 2. Anchor head configuration and bar-head interface overview.

the pullout capacity of the anchor head. For each embedment length, three replicates were made yielding a total of 45 bond-slip specimens: 27 headed GFRP bars-geopolymer (HGG) and 18 straight GFRP bars-geopolymer (SGG) specimens. Each specimen was labelled and identified in a following manner: type of specimen-bar diameter-embedment length. For example, the specimen designated as HGG-12.7-5$\varnothing + l_{ah}$ means that it is a geopolymer concrete specimen with a 12.7 mm nominal diameter headed GFRP bar with a bonded a length of five times the bar diameter (straight portion) plus the anchor head length .

2.4. Direct pullout test

All the specimens were tested on their 32nd day using a direct pullout test in accordance with ACI 440.3R-04 [19] and CAN/CSA S806-02 [20] standards. Fig. 3 illustrates the schematic diagram and the actual test setup. During testing, the specimens were positioned in a reverse manner on top of a fixed circular base plate with a hole at the centre to accommodate the bars. The bars were pulled down at a constant displacement rate of 1.2 mm/min using a 500 kN AVERY testing machine, The absolute slip of the GFRP bar in the geopolymer concrete was measured using a Linear Variable Differential Transducer (LVDT) situated on top of the unloaded end of the bar. The support stand of the LVDT was isolated from the specimen so that the readings will not be affected by the movement and failure of the specimen. The load and displacement were recorded using a System5000 data logger.

Table 1
Mechanical properties of the GFRP bars.

Bar diameter*	Nominal cross sectional area (mm^2)	Guaranteed tensile strength, f_{ps}** (MPa)	Modulus of elasticity (GPa)***	Ultimate elongation (%)
12.7 mm (#4)	129	1312	65.6 ± 2.5	2.00
15.9 mm (#5)	199	1184	62.6 ± 2.5	1.89
19.0 mm (#6)	284	1105	63.7 ± 2.5	1.71

* Numbers in the () are the manufacturer's bar designation.
** Guaranteed tensile strength: Average value – 3x standard deviation (ACI 440.1R-06 [20]).
*** Numbers after "±" are the standard deviation of the modulus of elasticity.

3. Experimental results and discussion

This section summarises the experimental results such as the failure mode, the average bond stress (τ), the pullout load-slip relationship, and the tensile stress developed in the bar at failure (f_s). The effects of embedment length and bar diameter on the tensile strength development of the straight and headed GFRP bars were analysed. Empirical equations were derived to describe the relationship between the mentioned parameters and the tensile stress in the bars. Finally, the experimental outcomes were compared to verify the viability of the proposed technology for structural applications.

3.1. Mode of failure

Fig. 4 shows the failure mode of the SGG bond-slip specimens that were governed by either bar pullout from the geopolymer concrete or splitting of the geopolymer concrete. The pullout type of failure happened when the radial splitting stress, generated by the bond between the bar and the geopolymer concrete, was lower than the confining strength of the geopolymer concrete prism. On the other hand, the splitting type of failure happened when the hoop tension exceeded the tensile capacity of the geopolymer concrete, thereby creating wider longitudinal cracks that propagated to the external surface. Generally, the specimens with shorter anchorage length failed due to the bar pullout while those with longer embedment lengths failed due to the concrete splitting. The specimens with larger diameter and longer embedment length, generally, exhibited wider and more visible cracks that were confined along the bonded length of the GFRP bars. The geopolymer concrete failed in an explosive brittle manner. This was also observed by Sarker [21] and Sofi et al. [22] who studied the bond behaviour of steel bars in geopolymer concrete.

Fig. 5 illustrates the geopolymer concrete splitting failure of the HGG specimens. As depicted in Fig. 5a, a partial splitting failure was observed in the specimens with headed bars bonded 5$\varnothing + l_{ah}$ in geopolymer concrete. With the provision of anchor heads, the failure mode of straight bars embedded 5$\varnothing$ in the geopolymer concrete shifted from bar pullout to concrete splitting owing to the additional bearing resistance of the anchor head that yielded a significant amount of radial splitting stress in the geopolymer concrete. The specimens with embedment lengths of 0$\varnothing + l_{ah}$ and 10$\varnothing + l_{ah}$, on the other hand, exhibited full concrete

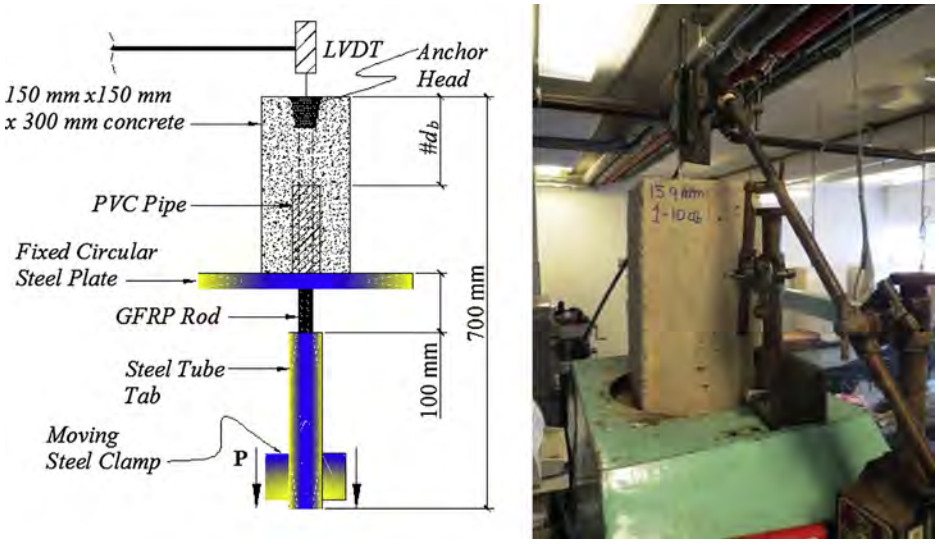

(a) Schematic diagram (b) Actual set-up

Fig. 3. Direct pullout test.

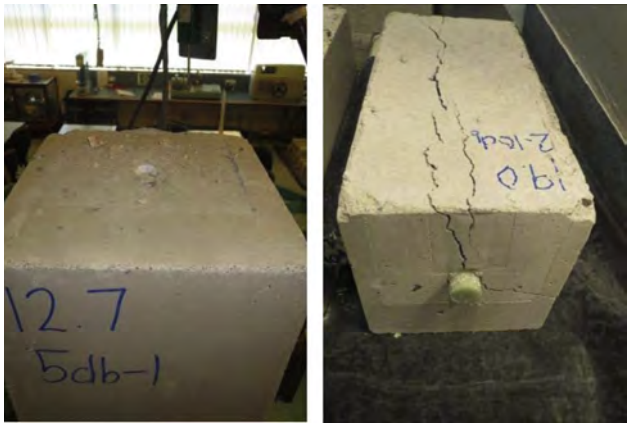

(a) Bar pullout (BP) (b) Concrete Splitting (CS)

Fig. 4. Typical failure of the SGG specimens.

splitting/breakout as shown in Fig. 5b and c, respectively. The splitting failure of the HGG specimens, however, was more severe than their SGG counterparts due to the high tensile splitting stress radiated by the anchor heads to the geopolymer concrete. More rigorous cracking and more explosive concrete breakout accompanied with huge sound were recorded as the bar diameter and embedment length increased.

The typical failure modes of the mechanical anchor heads were depicted in Fig. 6. Generally, the anchor heads failed by either the longitudinal crack formation (Fig. 6a) or the anchor head breakout (Fig. 6b).

3.2. Average bond stress

The average bond stress τ between the GFRP bars and the geopolymer was calculated from Eq. (1), assuming a uniform stress distribution along the bonded length of the bars,

$$\tau = \frac{P}{\pi \varnothing l_d} \tag{1}$$

where P is the pullout load at failure (N), $\varnothing$ is the nominal bar diameter (mm), and l_d is the embedment length (mm). Table 2 summarises the computed τ in the bars of the SGG specimens. The τ values in specimens with 12.7, 15.9, and 19.0 mm GFRP bars embedded 5$\varnothing$ and 10$\varnothing$ in the geopolymer concrete were 24 MPa and 22 MPa, 22 MPa and 18 MPa, and 20 MPa and 15 MPa, respectively. Generally, as the embedment length increases, the average bond stress between the bars and the geopolymer concrete decreases. Likewise, as the nominal bar diameter increases, the average bond stress also decreases. The bond stress between the headed bars and the geopolymer was not computed using Eq. (1) since the anchor head would also carry part of the applied pullout load. Thus, the comparison between the headed and the straight GFRP bars was done based on the pullout and/or tensile stress developed in each bar and was presented in the following sections.

3.3. Pullout load-slip relationship

Fig. 7 shows the typical relationship between the pullout load and the slip of the SGG and HGG specimens. The straight bars, represented by SGG-15.9-5$\varnothing$, that failed due to bar pullout from the geopolymer concrete showed a low stiffness characteristic during the early stage of the loading as depicted by the gradual increase of the load while the slip increases rapidly. This can be attributed to the settlement of the uneven face of the loaded end of the concrete. At this stage, the applied loads were simultaneously carried by the chemical bond between the bar and the geopolymer concrete and the mechanical interlock and friction forces provided by the sand coating. Once the specimen had stabilized, a linear behaviour occurred wherein the pullout load increased proportionally with the slip. Concurrently, longitudinal and interface cracks were developed that marked the breakdown of the chemical bond between the bars and the geopolymer concrete. The specimens, however, continued to carry additional loads owing to the mechanical interlock and friction resistance provided by the sand coating. A short non-linear behaviour was observed before reaching the maximum load that indicated the weakening of the sand coating's bond resistance due to wider cracks. The post-peak phase was characterised by a softening curve wherein only the sand friction forces sustained the remaining loads.

The initial and linear behaviour of the headed bars were generally comparable to the behaviour of the straight bars owing to the similar bond resistance mechanism provided by both bars at lower loads, the chemical bond and the friction and mechanical interlock

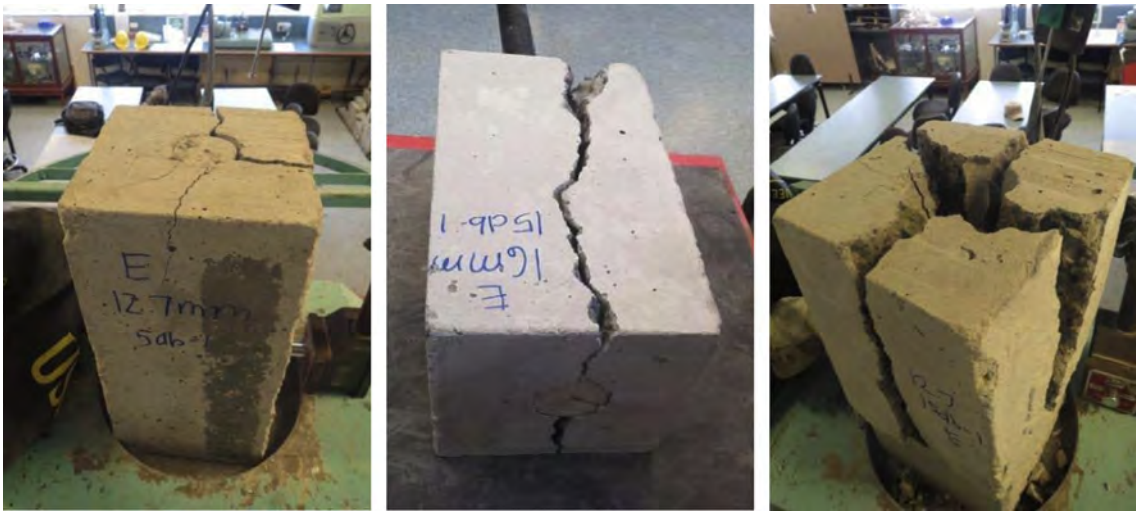

(a) Partial concrete splitting (PCS) (b) Full concrete splitting (FCS) (c) Concrete break out (CB)

Fig. 5. Typical failure of the HGG specimens.

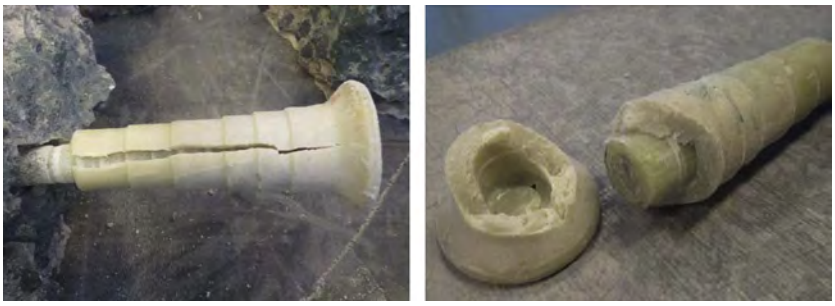

(a) Longitudinal cracking of the anchor head (HC) (b) Break out of the anchor head (HB)

Fig. 6. Typical failure of the anchor heads.

forces provided by the sand coating. As the applied load increases, wider interface cracks occurred that weakens the sand coating resistance. The applied loads, however, were predominantly carried by the anchor head yielding higher pullout load readings compared with the straight bars. Due to the high radial splitting stress induced by the anchor heads, the specimens failed without exhibiting the nonlinear and softening behaviour.

3.4. Tensile stress developed in the bars

Table 2 shows the ratio in percent between the tensile stress developed f_s and the nominal tensile strength f_{ps} of the GFRP bars. These values were calculated to determine the efficiency of each anchorage system in developing the GFRP bars' tensile strength. Initially, the tensile stress was calculated by dividing the pullout load with the bar's nominal area. As can be seen from Table 2, the anchor head alone can develop a tensile stress of 597 MPa in the bars, which is approximately 45% of their nominal tensile strength. The pullout resistance of HGG specimens with $5\varnothing + l_{ah}$ embedment length was predominantly sourced from the mechanical bearing of the anchor head, resulting in their higher pullout capacities compared with their SGG counterparts. The tensile stresses in the headed bars of the HGG-12.7-$5\varnothing + l_{ah}$ (834 MPa), HGG-15.9–$5\varnothing + l_{ah}$ (673 MPa), and HGG-19.0–$5\varnothing + l_{ah}$ (635 MPa) specimens were 64%, 57%, and 58%, respectively, of the strength of the bars and were 77%, 49%, and 54%, respectively, higher than that of the SGG-12.7-$5\varnothing$ (472 MPa), SGG-15.9-$5\varnothing$ (451 MPa), and SGG-19.0-$5\varnothing$ (411 MPa), respectively. The tensile stresses registered by the headed bars embedded $10\varnothing + l_{ah}$ in the geopolymer concrete were comparable to that of the straight bars, ranging from 91% to 109% of the stress developed in their counterparts. This can be expected because, as the embedment length increases, the pullout resistance of the headed bars was mainly provided by the mechanical interlock and friction forces of the sand coating. In addition, both types of specimens failed by concrete splitting failure that made the anchor heads inefficient. However, given that the concrete splitting failure is avoided, it can be anticipated that the pullout capacity of the headed bars with longer embedment lengths will be higher than the straight bars. This conclusion can be verified from the experimental results obtained by Khederzadeh and Sennah [14].

3.5. Influence of the bar diameter and the embedment length

Generally, the pullout behaviour of the tested specimens was dependent on the bar diameter and the embedment length. Fig. 8 shows the effect of the bar diameter ($\varnothing/cc$, cc = concrete cover) on the tensile stress developed in the GFRP bars (f_s/f_{ps}). The solid

Table 2
Pullout load, average bond stress, tensile stress, and failure mode of the bond-slip specimens.

Specimen	P[a] (kN)	τ (MPa)	f_s (MPa)	f_s/f_{ps} (%)	Failure mode[b]
SGG-12.7-5∅	60 (4)	24	472	36	BP
SGG-12.7-10∅	112 (10)	22	887	68	BP
SGG-15.9-5∅	90 (1)	22	451	38	BP
SGG-15.9-10∅	146 (1)	18	735	62	CS
SGG-19.0-5∅	117 (0)	20	411	37	BP
SGG-19.0-10∅	174 (1)	15	615	56	CS
HGG-12.7-0∅ + l_{ah}	76 (3)	–	597	45	PCS + IHB
HGG-12.7–5∅ + l_{ah}	106 (1)	–	834	64	CB + HC
HGG-12.7-10∅ + l_{ah}	110 (2)	–	870	66	CB + HC
HGG-15.9-0∅ + l_{ah}	115 (1)	–	577	49	CB + HB
HGG-15.9-5∅ + l_{ah}	134 (3)	–	673	57	PCS + IHB
HGG-15.9-10∅ + l_{ah}	159 (15)	–	799	67	FCS + HC
HGG-19.0–0∅ + l_{ah}	139 (5)	–	492	45	CB + HB
HGG-19.0-5∅ + l_{ah}	180 (3)	–	635	58	PCS + IHB
HGG-19.0-10∅ + l_{ah}	145 (5)	–	513	46	CB + HB

[a] The values inside the () are the standard deviation.
[b] BP = Bar pullout; CS = Concrete splitting; PCS + IHB = Partial concrete splitting and interface failure between the head and the bar; CB + HC = Break out of geopolymer concrete and longitudinal cracking of the anchor head; CB + HB = Breakout of geopolymer concrete and anchor head; FCS + IHB = Full concrete splitting and longitudinal cracking of the anchor head.

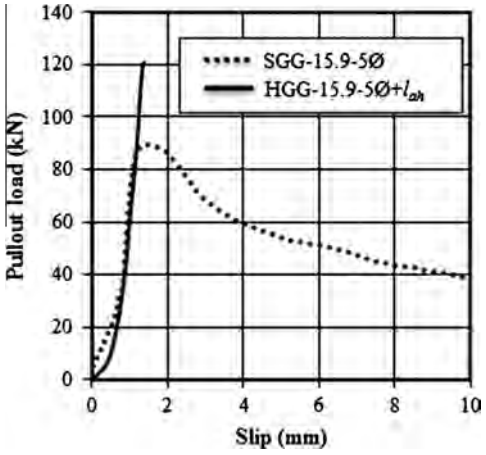

Fig. 7. Typical pullout load-slip curves of the SGG and HGG specimens.

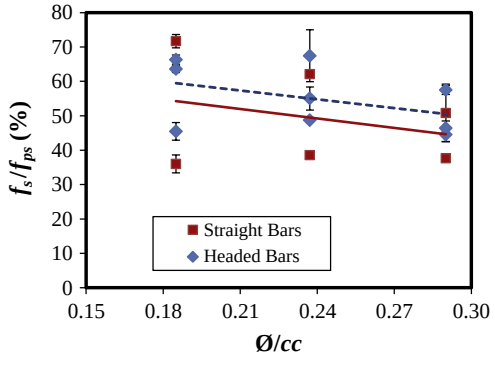

Fig. 8. Effect of bar diameter on the tensile stress developed in the GFRP bars.

and broken straight lines represent the general trend, not the actual correlation, between the parameters for the headed and straight GFRP bars, respectively. As can be seen from the figure, the tensile stress in the bars decreases as the bar diameter increases. This finding can be attributed to the shear lag and Poisson's ratio effects. The shear lag occurs when the bars are pulled in tension through its surface, yielding a differential movement between the surface fibre and the core of the bars. This movement results in a non-uniform distribution of the normal stress on the cross-section of the bar: maximum at the outer surface while minimum in the core. The surface stress is the one that governs the bond strength of the bar which is always higher than the calculated average tensile stress. The difference between the surface stress and the average stress increases as the bar diameter increases, yielding an inverse relationship between the tensile stress and the bar diameter. Furthermore, due to the low shear stiffness of the resin coupled with lower shear strength of the resin-fibre interface, shear lag is most likely to happen in GFRP bars. The Poisson's ratio effect, on the other hand, is characterised by a decrease of the bar diameter due to the pulling stress. This size reduction can weaken the connection between the bars and the concrete. The Poisson's ratio effect also increases as the bar diameter increases.

Fig. 9 illustrates the effect embedment length ($l_d/\varnothing$) on the tensile stress developed in the GFRP bars (f_s/f_{ps}). The enhancement of the HGG specimens' pullout capacity can be attributed to the mechanical bearing resistance provided by the anchor heads plus the higher mechanical interlock and friction forces coming from the longer bonded length that resulted in a stronger anchorage system of the HGG specimens. For SGG specimens, the increase in pullout load resistance was due to the increase in the amount of bar surface area that is bonded in geopolymer concrete, thereby producing higher mechanical interlock and friction forces to resist the applied load.

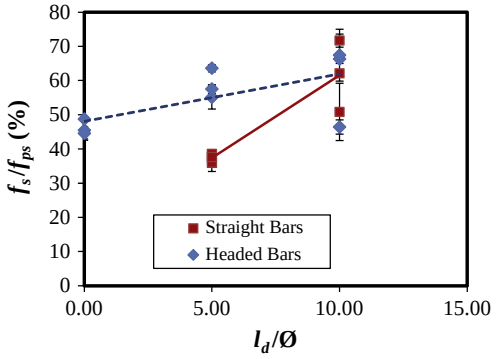

Fig. 9. Effect of embedment length on the tensile stress developed in the GFRP bars.

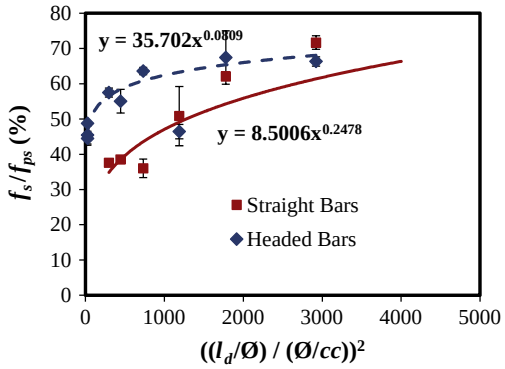

Fig. 10. Combined effects of bar diameter and embedment length on the tensile stress developed in the GFRP bars.

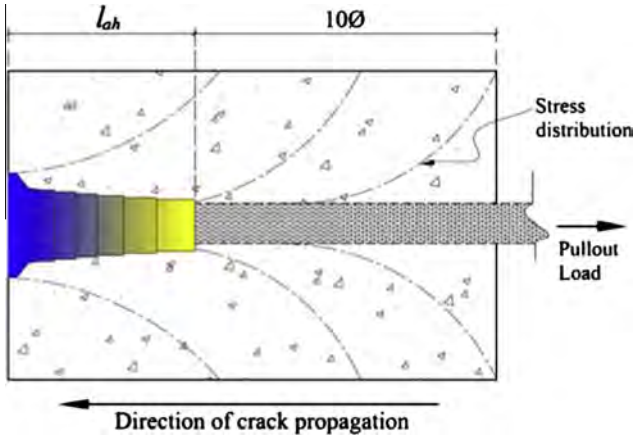

Fig. 11. Configuration of the HGG-19.0-10∅ + l_{ah}.

3.6. Prediction of the pullout load capacity

Fig. 10 shows the combined effects of the bar diameter and embedment length on the tensile stress developed in the straight and headed GFRP bars, including the two equations derived from the regression analysis of the experimental results. The contribution of the anchor heads (f_{sa}) can be obtained by subtracting the tensile stresses in the straight bars from that of the headed bars and can be expressed as

$$f_{sa} = 0.2944 f_{ps}\left(e^{-6\times10^{-4}\left(\frac{l_d\times cc}{\varnothing^2}\right)}\right) \quad \text{contribution of the anchor heads} \tag{2}$$

The tensile stress in the headed GFRP bars f_{sh}, therefore, can be calculated from Eq. (3), which is the sum of Eq. (2) and the tensile stress equation for straight GFRP bars (depicted in Fig. 10).

$$f_{sh} = f_{ps}\left(0.085\left(\frac{l_d\times cc}{\varnothing^2}\right)^{0.4916} + 0.2944\left(e^{-6\times10^{-4}\left(\frac{l_d\times cc}{\varnothing^2}\right)}\right)\right) \tag{3}$$

In terms of the pullout load capacity of the headed GFRP bars (P_{sh}), the equation can be expressed as

$$P_{sh} = P_{ps}\left(0.085\left(\frac{l_d\times cc}{\varnothing^2}\right)^{0.4916} + 0.2944\left(e^{-6\times10^{-4}\left(\frac{l_d\times cc}{\varnothing^2}\right)}\right)\right) \tag{4}$$

where P_{ps} is the nominal tensile load capacity of the GFRP bars. This equation, however, is applicable only to headed GFRP bars with embedment lengths ranging from 5∅ to l_{da}. The l_{da}, given by Eq. (5), was derived by equating the expressions, depicted in Fig. 10, for straight and headed GFRP bars.

$$l_{da} = 90.19\left(\frac{\varnothing^2}{cc}\right) \tag{5}$$

Table 3 summarised the predicted pullout load capacities using Eq. (4) and the corresponding estimation error in percent. It can be seen from the table that for the straight GFRP bars, the predicted values were relatively lower than the experimental values except the SGG-12.7-5∅ specimen. On the other hand, the pullout capacities of the headed bars were conservatively estimated by the proposed equation. It is notable from the table, however, that the pullout load capacity of the HGG-19.0-10∅ + l_{ah} was way higher than that of the experimental result. This is in line with the conclusion made previously wherein headed bars with longer embedment lengths would result into higher pullout capacity provided that concrete splitting can be prevented. Furthermore, the experimental capacity of this specimen is lower than that of the HGG-15.9-5∅ + l_{ah} because, unlike the HGG specimens with 5∅ + l_{ah} embedment length, this specimen does not have any unbonded geopolymer concrete in its loaded end that could prevent the early development of the longitudinal cracks, as shown in Fig. 11.

Table 3
The predicted pullout load capacity and corresponding percent error relative to the experimental results.

Specimen	Predicted pullout load capacity, P (kN)	% Error
SGG-12.7-5∅	71	18
SGG-12.7-10∅	100	−11
SGG-15.9-5∅	89	−1
SGG-15.9-10∅	126	−14
SGG-19.0-5∅	108	−8
SGG-19.0-10∅	152	−13
HGG-12.7-0∅ + l_{ah}	49	–
HGG-12.7-5∅ + l_{ah}	119	12
HGG-12.7-10∅ + l_{ah}	147	34
HGG-15.9-0∅ + l_{ah}	–	–
HGG-15.9-5∅ + l_{ah}	158	18
HGG-15.9-10∅ + l_{ah}	193	21
HGG-19.0-0∅ + l_{ah}	–	–
HGG-19.0-5∅ + l_{ah}	199	11
HGG-19.0-10∅ + l_{ah}	242	67

3.7. Comparison between the experimental and the published results

Fig. 12 shows the comparison between the experimental results and the published results on the pullout test of the straight and headed GFRP bars in normal concrete, denoted by SGN and HGN, respectively, and of the deformed steel bars in geopolymer concrete, symbolised by SG. For the specimens with headed bars, only the results of those with a portion of straight bars bonded in concrete were reflected in this figure. The results were presented in terms of the tensile stress normalised with a factor $\varnothing/(l_d\sqrt{(f'_c)})$. Fig. 13, on the other hand, displays the comparison between the experimental outputs and Mohammad and Benmokrane's [12] results for the specimens with only the anchor head embedded in concrete. These specimens, however, were evaluated in terms of their tensile stress normalised with the concrete compressive strength. For comparison purposes, only the specimens that failed due to bar pullout (for straight bars) and concrete splitting (for headed bars) were considered. Based on these figures, the following generalisations were made:

1. The tensile stresses developed in the bars of HGG specimens are higher than that of HGN specimens. This observation leads to concluded that the headed GFRP bars, used in this study, have

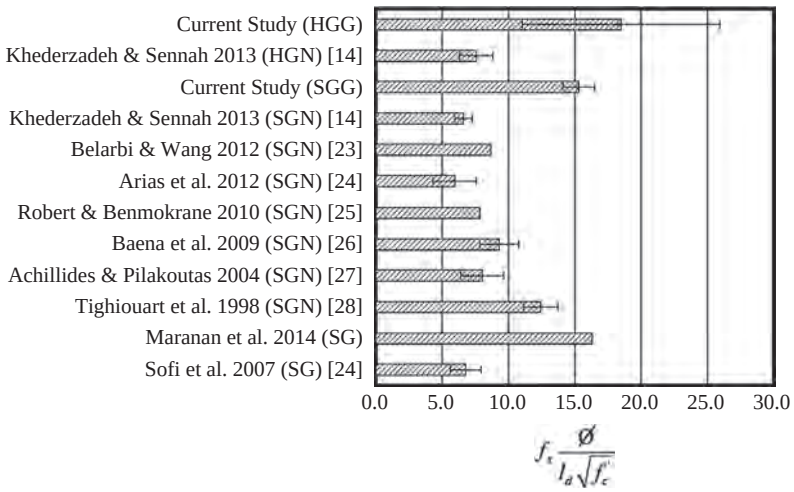

Fig. 12. Comparison between the experimental results (HGG and SGG) and the published results (SGN, HGN, & SG). (See above-mentioned references for further information.)

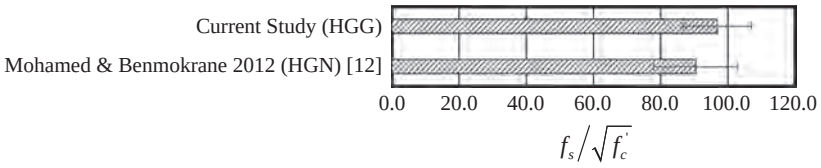

Fig. 13. Comparison between HGG and HGN specimens with only the anchor headembedded in concrete.

better pullout resistance compared with that of the previous studies and that the geopolymer concrete have superior tensile strength compared with cement-based concrete. Further experimental works, however, should be conducted to validate this conclusion.

2. The HGG specimens showed superior pullout capacity compared with SGG and SGN specimens, indicating that the use of anchor head is an efficient method to enhance the bonding of sand-coated GFRP bars in concrete.
3. The combination of anchor head and sand coating systems showed better bonding performance compared with the ridge system of deformed steel bars.
4. Generally, the HGG and SGG specimens showed better pullout resistance than SGN and HGN specimens, suggesting the potential of the GFRP-reinforced geopolymer concrete system for structural applications.

4. Conclusion

This study was conducted to investigate the effect of the anchor head on the pullout behaviour of sand coated GFRP bars in the geopolymer concrete using the direct pullout test. A total of 45 bond-slip specimens were tested following the ACI 440.3R-04 [19] and CAN/CSA S806-02 [20] standards. Based on the test, the following conclusions were made:

- Based on the experimental results, the headed GFRP bars can be an efficient method to enhance the anchorage capacity of the GFRP bars in the geopolymer concrete.
- The tensile stress developed in the headed GFRP bars with only the anchor head embedded in geopolymer concrete can reach up to approximately 597 MPa, which is 45% of the nominal tensile strength of the GFRP bars.
- With the provision of anchor heads, the tensile stresses in the 12.7, 15.9, and 19.0 mm straight sand coated GFRP bars embedded 5$\varnothing$ in geopolymer concrete increased by 362 MPa (77%), 222 MPa (49%), and 224 MPa (54%), respectively, and thereby shifting the failure mode of the specimens from bar pullout to geopolymer concrete splitting.
- The geopolymer concrete splitting failure of the specimens with the headed bars was more severe than that of the straight bars due to the high radial splitting stress induced by the anchor heads.
- The tensile stress in the headed GFRP bars embedded in geopolymer can be estimated from the derived empirical equation, however, with several limitations. Further experimental results, therefore, are needed to calibrate the equation.
- The pullout load resistance SGG and HGG were generally higher than that of the SGN and HGN, thereby showing the potential of the GFRP-reinforced geopolymer concrete system for structural applications.
- The use of anchor heads to achieve the required development is beneficial if bending of GFRP bars is impossible, especially in a congested reinforcement area, and if long lengths cannot be produced due to limited space available to anchor the bar in the concrete.

Acknowledgement

The authors gratefully acknowledge V-Rod® Australia for the materials and technical support they had given in the conduct of this research undertaking.

References

[1] Duxson P, Fernandez-Jimenez A, Palomo GC, vanDeventer JSJ. Geopolymer technology: the current state of the art. J Mater Sci 2007;42:2917.

[2] Aldred J, Day J. Is geopolymer concrete a suitable alternative to traditional concrete? 37th Conference on Our World in Concrete and Structures. Singapore 2012. p. 1–14.
[3] Sarker P. A Constitutive model for fly ash-based geopolymer concrete. ACEE J 2008;1:113–20.
[4] Davidovits J. Geopolymer properties and chemistry. Geopolymer '88, 1st European Conference on Soft Mineralurgy. Compiegne, France 1988. p. 25–8.
[5] Lloyd NA, Rangan BV. Geopolymer concrete: a review of development and opportunities. 3rd Conference on our world in concrete and structures. Singapore 2010.
[6] Anuradha R, Sreevidhaya V, Venkatasubramani R, Rangan VV. Modified guidelines for geopolymer concrete mix design using Indian Standard. Asian J Civil Eng 2012;13:353–64.
[7] Manalo A, Benmokrane B, Oark KT, Lutze D. Recent developments on FRP bars as internal reinforcement in concrete structures. Concr Aust 2014;40:45–56.
[8] Hardwicke L. Australian infrastructure report cards. Australia: Institution of Engineers, Australia; 2005.
[9] Ahmed EA, El-Sayed AK, El-Salakawy E, Benmokrane B. Bend strength of FRP stirrups: comparison and evaluation of testing methods. J Compos Constr 2010;14:3–10.
[10] Hasaballa MH, El-Salakawy E. Seismic performance of beam-column joints reinforced with GFRP headed bars. 3rd Asia-Pacific conference on FRP is structures (APFIS 2012). Hokkaido, Japan 2014.
[11] Johnson DTC. Investigation of glass fibre reinforced polymer (GFRP) bars as internal reinforcement for concrete structures. Toronto, Canada: University of Toronto; 2014.
[12] Mohamed HM, Benmokrane B. Pullout capacity behaviour of FRP-headed rebars. 6th International Conference on FRP Composites in Civil Engineering (CICE 2012). Rome, Italy 2012.
[13] Vint LM. Investigation of bond properties of glass fibre reinforced polymer (GFRP) bars in concrete under tension. Toronto, Canada: University of Toronto; 2012.
[14] Khederzadeh HR, Sennah K. Pullout strength of pre-installed GFRP bars in concrete. CSCE 2013 General Conference. Quebec, Canada 2013. p. 48-(1-9).
[15] V-Rod Australia; 2015.
[16] CAN/CSA. Specification for fibre-reinforced polymers. CAN/CSA S807-10. Toronto, Canada: Canadian Standards Association; 2010.
[17] ASTM. Standard test methods for constituent content for composite materials. ASTM D3171-11. Pennsylvania, USA: American Society for Testing and Materials; 2011.
[18] ASTM. Standard test method for compressive strength of cylindrical concrete specimens. ASTM C39/C39M-04. Pennsylvania, USA: American Society for Testing and Materials; 2004.
[19] ACI. Guide test methods for FRPs for reinforcing or strengthening concrete structures. ACI 4403 R-04. Michigan, USA: American Concrete Institute; 2004.
[20] CAN/CSA. Design and construction of building components with fibre reinforced polymers. CAN/CSA S806-02. Toronto, Canada: Canadian Standards Association; 2002.
[21] Sarker PK. Bond strength of reinforcing steel embedded in fly ash-based geopolymer concrete. Mater Struct 2011;44:1021–30.
[22] Sofi M, vanDeventer JSJ, Mendis PA. Bond performance of reinforcing bars in inorganic polymer concrete (IPC). J Mater Sci 2007;42:3107–16.
[23] Belarbi A, Wang H. Bond durability of FRP bars embedded in fiber-reinforced concrete. J Compos Constr 2012;4(1):370–80.
[24] Arias JPM, Vasquez A, Escobar MM. Use of sand coating to improve bonding between GFRP bars and concrete. SAGE J Compos Mater 2012:1–8.
[25] Robert M, Benmokrane B. Behavior of GFRP reinforcing bars subjected to extreme temperatures. J Compos Constr 2010;14(4):353–60.
[26] Baena M, Torres L, Turon A, Barris C. Experimental study of bond behaviour between concrete and FRP bars using a pull-out test. Compos Part B Eng 2009;40(8):784–97.
[27] Achillides A, Pilakoutas K. Bond behaviour of fiber reinforced polymer bars under direct pullout conditions. J Compos Constr 2004;8(2):173–81.
[28] Tighiouart B, Benmokrane B, Gao D. Investigation of bond in concrete members with fibre reinforced polymer (FRP) Bars. Constr Build Mater 1998;12:453–62.

3.3. Paper III: Evaluation of the flexural strength and serviceability of geopolymer concrete beams reinforced with glass-fibre-reinforced polymer (GFRP) bars

This paper evaluated the flexural behaviour of geopolymer concrete beams reinforced with glass fibre reinforced polymer (GFRP) bars using the four-point static bending test. The test parameters were the longitudinal reinforcement ratio, anchorage system, and nominal bar diameter. The beams were 3100 mm, 200 mm wide, and 300 mm deep (as shown in **Figure 3** of **Paper III**). For the beam with headed bars, the bars were arranged in a staggered manner to minimise the stress concentration at the ends of the beam. In addition to "2.1 Materials" section of **Paper III**, the comparison between the stress-strain curves of normal concrete and geopolymer concrete of the same grade and the properties of GFRP stirrups used in the paper were presented in **Figure B.3** and **Table B-2** of **Appendix B,** respectively, of the thesis. The test matrix was summarised in Table 3, wherein the footnote "b" corresponds to "Balanced steel reinforcement ratio (ρ_b) based on ACI 318-15" rather than "Balanced steel reinforcement (ρ_b)". Based on the experimental results, the beams with higher reinforcement ratio yielded better flexural performance (lower deflection, narrower crack, and higher strength at service condition) compared to the beams with lower reinforcement ratio. However, the beam with headed GFRP bars behaved similarly as the beams with straight GFRP bars. Noting that the bars were fully embedded in geopolymer concrete, this result tends to support the conclusion made for headed bars in **Paper II**, wherein the contribution of anchor heads diminishes as the embedment length increases. According to several studies (Bank 2006; Hollaway 2008), the short-term mechanical properties of FRP bars decrease with the increase in bar diameter. However, the bar size did not affect the performance of the beam at service and ultimate levels, mainly because the failure of the beams were governed by the crushing of geopolymer concrete in the compression zone rather than GFRP bar rupture. In general, GFRP-reinforced geopolymer concrete (GFRP-RGC) beams yielded higher flexural strength than GFRP-reinforced concrete beam (GFRP-RGC), which was shown in **Table 7** of **Paper III** and in **Table B-3** of **Appendix B** of the thesis.

The results presented in this paper demonstrated that GFRP bars is an effective longitudinal reinforcement to geopolymer concrete beams. Few studies, however, investigated the use of GFRP stirrups as transverse reinforcement in beams. Hence, an investigation of the shear behaviour of geopolymer concrete beams with GFRP stirrups was conducted and the results are presented, analysed, and discussed in **Paper IV**.

Engineering Structures 101 (2015) 529–541

Contents lists available at ScienceDirect

Engineering Structures

journal homepage: www.elsevier.com/locate/engstruct

Evaluation of the flexural strength and serviceability of geopolymer concrete beams reinforced with glass-fibre-reinforced polymer (GFRP) bars

G.B. Maranan [a], A.C. Manalo [a,*], B. Benmokrane [b], W. Karunasena [a], P. Mendis [c]

[a] Centre of Excellence in Engineered Fibre Composites (CEEFC), Faculty of Health, Engineering and Sciences (FoHES), University of Southern Queensland, Toowoomba 4350, Australia
[b] Department of Civil Engineering, University de Sherbrooke, Sherbrooke, Quebec J1K 2R1, Canada
[c] Department of Infrastructure Engineering, The University of Melbourne, Victoria 3010, Australia

ARTICLE INFO

Article history:
Received 16 December 2014
Revised 31 July 2015
Accepted 3 August 2015

Keywords:
Geopolymer concrete
Glass-fibre-reinforced polymer (GFRP) bars
Flexural strength
Serviceability
Effective bond
FRP-reinforced concrete

ABSTRACT

Geopolymer concrete reinforced with glass-fibre-reinforced polymer (GFRP) bars can provide a construction system with high durability, high sustainability, and adequate strength. Few studies deal with the combined use of these materials, and this has been the key motivation of this undertaking. In this study, the flexural strength and serviceability performance of the geopolymer concrete beams reinforced with GFRP bars were evaluated under a four-point static bending test. The parameters investigated were nominal bar diameter, reinforcement ratio, and anchorage system. Based on the experimental results, the bar diameter had no significant effect on the flexural performance of the beams. Generally, the serviceability performance of a beam is enhanced when the reinforcement ratio increases. The mechanical interlock and friction forces provided by the sand coating was adequate to secure an effective bond between the GFRP bars and the geopolymer concrete. Generally, the ACI 4401.R-06 and CSA S806-12 prediction equations underestimate the beam strength. The bending-moment capacity of the tested beams was higher than that of FRP-reinforced concrete beams from the previous studies.

1. Introduction

Reinforced concrete (RC) is one of the most commonly used composite materials in the construction of roads, bridges, buildings, and other civil infrastructures. The demand for this material is expected to increase in the future owing to the rise of infrastructure needs in many developing and industrialised countries. In fact, it is estimated that the total global infrastructure demand amounts to USD 4.0 trillion with a gap of at least USD 1.0 trillion per year [1]. Due to the serviceability and economic issues owing to the costly repair and rehabilitation of damaged RC structures caused by the corrosion of the steel bars and the sustainability issue owing to the extremely resource- and energy-intensive process of producing steel and cement materials, however, many engineers and researchers have sought viable alternatives. Among the solutions that are currently being employed are replacing cement-based concrete with geopolymer concrete and replacing steel bars with fibre-reinforced polymer (FRP) bars. Neither, however, can solve the issues altogether.

Geopolymer concrete is considered as a highly sustainable material since it can be manufactured from industrial waste materials that are rich in silica and alumina, like fly ash and blast-furnace slag. A number of studies have shown that geopolymer concrete has properties making it suitable as a construction material [2–5]. On the other hand, aside from being innately corrosion resistant, FRP bars are lightweight, electromechanically neutral, and fatigue- and chemical-resistant, as well as having high tensile-strength properties [6–8]. Given the advantages of these materials, their combined use should yield a durable, cost-effective, and sustainable construction system. As the demand for the rehabilitation of existing RC structures and the construction of new infrastructure increases, accompanied with the mounting fly-ash production mainly in China, India and Australia [9], there is an urgent need for a thorough investigation of the proposed system so as to increase its uptake in the construction industry.

* Corresponding author at: Centre of Excellence in Engineered Fibre Composites (CEEFC), Faculty of Health, Engineering and Sciences, University of Southern Queensland, Toowoomba, Queensland 4350, Australia. Tel.: +61 7 4631 2547; fax: +61 7 4631 2110.

E-mail addresses: ginghis.maranan@usq.edu.au (G.B. Maranan), allan.manalo@usq.edu.au (A.C. Manalo), Brahim.Benmokrane@USherbrooke.ca (B. Benmokrane), karu.karunasena@usq.edu.au (W. Karunasena), pamendis@unimelb.edu.au (P. Mendis).

http://dx.doi.org/10.1016/j.engstruct.2015.08.003
0141-0296/

Nomenclature

a	beam shear span
b	beam width
c	neutral axis depth from the top compression fibre
d	beam effective depth
E_c	modulus of elasticity of the geopolymer concrete
E_f	modulus of elasticity of the GFRP bars
E_s	modulus of elasticity of the steel bars
$f_{r\text{-}exp}$	experimental modulus of rupture of the geopolymer concrete
$f_{r\text{-}theo}$	theoretical modulus of rupture of the geopolymer concrete
f_{fu}	guaranteed tensile strength of the GFRP bars
f_f	tensile stress in the GFRP bars
f_y	yield strength of the steel bars
f'_c	compressive strength of the geopolymer concrete
h	beam total depth
I_{cr}	cracked moment of inertia
I_e	effective moment of inertia
I_g	gross moment of inertia
L	beam clear span
L_g	uncracked beam length
$M_{a.}$	actual bending-moment
$M_{cr.}$	cracking moment
$M_{cr\text{-}exp}$	experimental cracking moment
$M_{cr\text{-}theo}$	theoretical cracking moment
$M_{peak\text{-}exp}$	experimental peak bending-moment
$M_{s\text{-}exp}$	experimental bending-moment at service condition
$M_{u\text{-}exp}$	experimental bending-moment at geopolymer concrete crushing failure
$M_{u\text{-}theo}$	theoretical bending-moment at geopolymer concrete crushing failure
Y	neutral axis depth from the top compression fibre
P	applied load
α_1	constant variable
β_1	constant variable
Δ	midspan deflection
$\Delta_{peak\text{-}exp}$	experimental midspan deflection at peak
$\Delta_{s\text{-}exp}$	experimental midspan deflection at service load
$\Delta_{u\text{-}exp}$	experimental midspan deflection at concrete crushing failure
$\Delta_{u\text{-}theo}$	theoretical midspan deflection at concrete crushing failure
$\Delta_{unl\text{-}exp}$	experimental midspan deflection at the unloaded phase
ε'_{cu}	usable compressive strain of the geopolymer concrete
$\varepsilon'_{cu\text{-}exp}$	experimental compressive strain at geopolymer concrete crushing failure
ε'_c	peak strain, compressive strain at peak stress of the geopolymer concrete
ε_{fu}	ultimate usable tensile strain of the GFRP bars
η	constant variable
$Ø_f$	nominal diameter of the GFRP bars
$Ø_s$	diameter of the steel bars
ρ_b	balanced reinforcement ratio of the steel bars
ρ_f	reinforcement ratio of the GFRP bars
ρ_{fb}	balanced reinforcement ratio of the GFRP bars
ρ_s	reinforcement ratio of the steel bars

Generally, the behaviour of concrete beams reinforced with FRP bars (FRP-RC) is different from the traditional RC beams in many ways, mainly because of the differences between the physical and mechanical properties of FRP and steel reinforcements [10]. First, FRP-RC beams exhibit lower serviceability performance owing to the lower modulus of elasticity of FRP bars compared to steel bars [11–13]. Secondly, FRP-RC beams are usually designed as over-reinforced because concrete crushing failure is less brittle and less catastrophic compared to FRP rupture failure owing to the rigid and brittle behaviour of FRP bars. Lastly, since the surface geometries and mechanical features of FRP bars are different from steel bars, they bond differently to concrete than steel bars. Some researchers [14–16] predicted the structural behaviour of the FRP-RC system using the existing equations developed for the conventional RC with some modifications to account for these differences.

The flexural performance of steel-reinforced geopolymer concrete (S-RGC) beams is found to be superior even to traditional RC beams. Rangan et al. [17] stated that the behaviour and strength of fly-ash-based RGC beams are similar to those of beams made with Portland cement and suggested that the current design provisions can be used to design fly-ash geopolymer-concrete structural members. Some researchers [9,18,19] reported, however, that S-RGC beams have better load-carrying capacity, mainly because of the enhanced mechanical properties of geopolymer concrete compared to conventional concrete of the same grade. This enhancement can be attributed to the better bonding of geopolymer paste compared to cement paste [9]. Even though the strength is different, the load–deflection characteristics, crack patterns, and failure modes of RGC beams are analogous to RC beams [18,19].

While there are numerous references in the literature about the strength and serviceability performance of FRP-RC and S-RGC beams, few studies have investigated the behaviour of geopolymer concrete beams reinforced with FRP bars, which is the novelty of this research. The direct pullout test conducted by Maranan et al. [20] showed an adequate bond between glass-fibre-reinforced polymer (GFRP) bars and geopolymer concrete resulting from the mechanical interlock and friction force provided by the sand coating on the surface of the GFRP bars indicating their suitability as reinforcement to geopolymer concrete. In this study, the strength and serviceability performance of the geopolymer concrete beams reinforced with GFRP bars were evaluated with a four-point static bending test. The parameters investigated were the nominal bar diameter, the reinforcement ratio, and the anchorage system.

2. Experimental program

2.1. Materials

2.1.1. Geopolymer concrete

The geopolymer concrete used in this study was a commercially produced concrete with a proprietary mixture. The geopolymer concrete mix was composed of fine and medium sands, 10 mm and 20 mm coarse aggregates, design water, plasticizer, and a geopolymer paste produced from the chemical activation of two industrial by-products (Class F fly ash and blast furnace slag) using an alkaline liquid. Four 100 mm diameter by 200 mm high geopolymer concrete cylinders were subjected to compression test. Fig. 1 shows the compression stress–strain curves of the geopolymer concrete. The average compressive strength and modulus of elasticity of the 28-day geopolymer concrete were 38.2 MPa and 38.5 GPa, respectively. Furthermore, the modulus of rupture test of four geopolymer concrete prisms with a cross-sectional area of 75 mm by 75 mm and a length 250 mm yielded an average value of 3.86 MPa. This value was computed using Eq. (7) in Table 8.

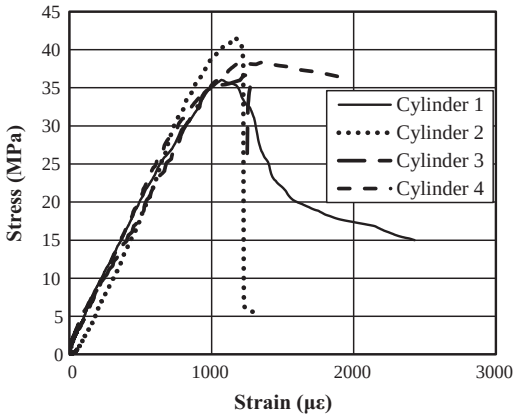

Fig. 1. Compression stress–strain curves of the geopolymer concrete.

2.1.2. GFRP bars

The GFRP bars used in this study were provided by V-ROD® Australia [8] and were manufactured by pultrusion process of E-glass fibres impregnated in modified vinyl ester resin. High modulus (HM) GFRP bars (Grade III, CSA S807-10) of varying nominal diameters were considered in this study (Fig. 2): 12.7 mm, 15.9 mm, and 19.0 mm nominal diameter sand-coated GFRP bars with fibre contents in percent by weight of 84.1, 83.9, and 84, respectively [21]. Straight (without anchor head) and headed (with anchor head) GFRP bars were used to investigate the influence of the anchorage system on the flexural behaviour of the specimens. The guaranteed properties of GFRP bars as reported by the manufacturer [21] are given in Table 1. The tensile strength and elastic modulus were calculated using nominal cross-sectional area. For the purpose of comparison, 16.0 mm deformed steel bars were utilised as longitudinal reinforcement in one of the tested beams. Table 2 presents the mechanical properties of the steel bar.

2.2. Test specimens

Five GFRP-reinforced and one steel-reinforced geopolymer concrete beams (the control specimen) were fabricated and tested. The beams had nominal dimensions of 200 mm wide, 400 mm deep, and 3100 mm long. Fig. 3 gives the cross-sectional geometry and reinforcement details of the beams. Two 12.7 mm diameter GFRP bars were used for compression-zone reinforcement. The beams were also provided with 9.53 mm diameter GFRP stirrups spaced at 100 mm on-centres. The test parameters were nominal bar diameter, longitudinal tensile reinforcement ratio, and anchorage system. Table 3 summarises the label and classification of the tested beams. The specimens were designated based on the type and amount of bottom longitudinal reinforcement. The first two letters indicate the reinforcement type such as SG for straight

Table 1
Guaranteed properties of GFRP reinforcing bars as reported by the manufacturer.

Bar diameter, $Ø_f$[a](mm)	Nominal cross-sectional area, A_f (mm^2)	Guaranteed tensile strength, f_{fu}[b] (MPa)	Modulus of elasticity, E_f (GPa)	Usable strain, ε_{fu} (με)
12.7 (#4)	129	1312	65.6 ± 2.5	2000
15.9 (#5)	199	1184	62.6 ± 2.5	1890
19.0 (#6)	284	1105	63.7 ± 2.5	1710

[a] Numbers in parentheses are the manufacturer's bar designation.
[b] Guaranteed tensile strength: Average value – 3× standard deviation (ACI 440.1R-06).

Table 2
Mechanical properties of the deformed steel bars.

Bar diameter, $Ø_s$ (mm)	Yield strength, f_y (MPa)	Modulus of elasticity, E_s (GPa)
16.0	529	200

GFRP bars (without anchor head), HG for headed GFRP bars (with anchor head), and DS for deformed steel bars. The abbreviation RGC stands for "reinforced geopolymer concrete" followed by a numeral that specifies the number of bottom bars. The last numeral represents the corresponding nominal bar diameter. For example, the specimen identified as SG-RGC-2-19.0 means that it is a geopolymer concrete beam reinforced with two 19.0 mm diameter straight GFRP bars. In this study, Eqs. 1 (3) and 2 (4), recommended by CSA-S806-12 [22] and ACI 440.1R-06 [23] (ACI 318-08 [24]), were used to calculate the actual reinforcement ratios ρ_f (ρ_s) and the balanced reinforcement ratios ρ_{fb} (ρ_b), respectively, of the geopolymer concrete beams reinforced with GFRP bars (steel bars). Table 8 provides these equations. The equivalent rectangular stress-block factors, α_1 and β_1, were calculated from Eq. (5) for CSA code and from Eq. (6) for ACI code, both equations can be found also in Table 8. SG-RGC and HG-RGC beams were designed as over-reinforced ($\rho_f/\rho_{fb} > 1.0$), while DS-RGC beam was designed as under-reinforced ($\rho_s/\rho_b < 1.0$). The ultimate strains were assumed equivalent to 0.0035 and 0.003, as per CSA and ACI, respectively.

2.3. Test setup and procedure

The four-point static bending test was employed to investigate the flexural performance of geopolymer concrete beams reinforced with GFRP and steel bars. Fig. 4 shows the test setup and schematic diagram. The load was gradually applied over a simply supported beam with a clear span and a shear span of 2900 mm and 1100 mm, respectively, through a spreader I-beam using a 2000 kN capacity hydraulic jack at a rate of approximately 3 mm/min. A laser-optical-displacement (LOD) device was placed at

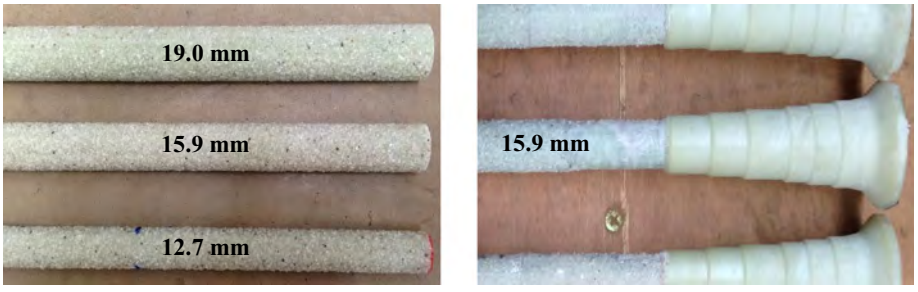

(a) Straight bars (without anchor head) (b) Headed bars (with anchor head)

Fig. 2. High-modulus GFRP bars coated with Grade 24 silica sand.

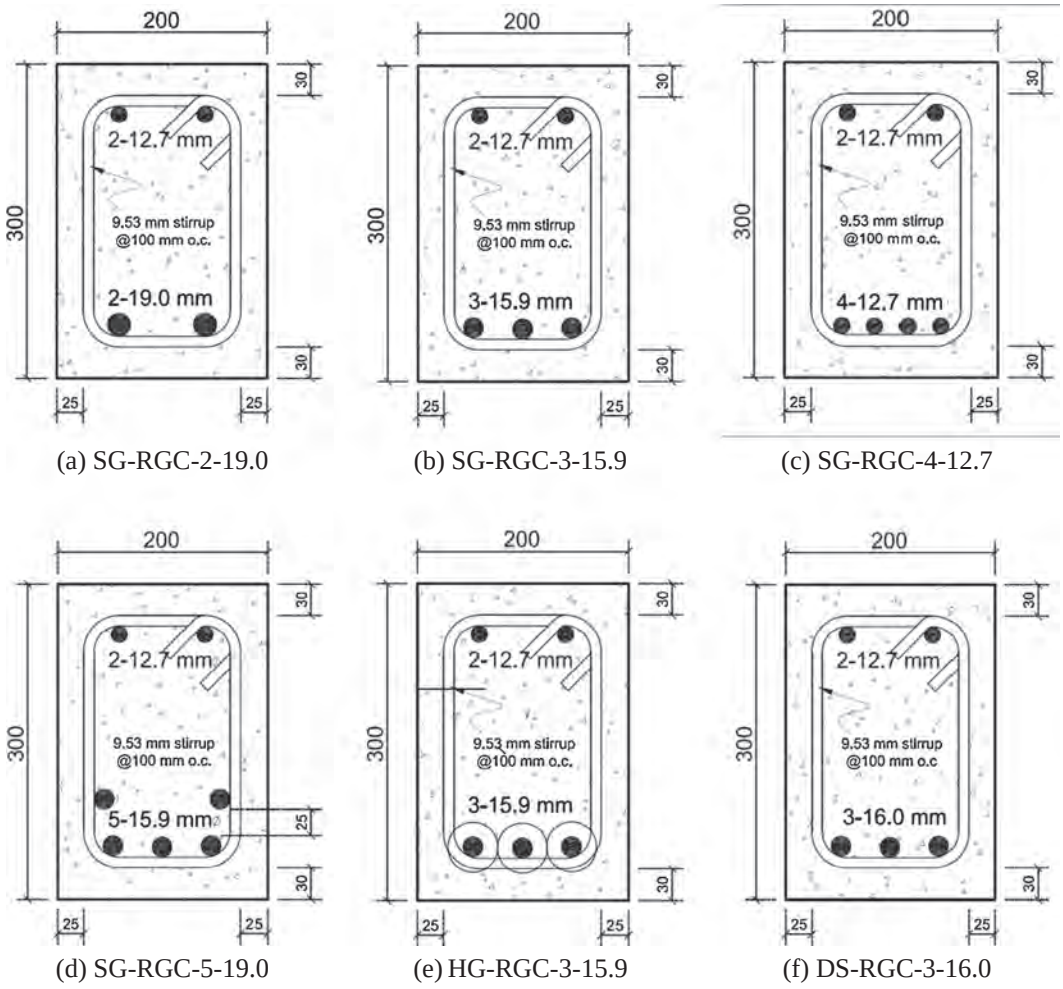

Fig. 3. Geometry and reinforcement details of the tested beams (dimensions are in mm).

Table 3
Label and classification of the tested specimens.

Beam	ρ_f (%)	ρ_{fb} (%)		Remarks
		CSA S806-12	ACI 440.1R-06	
SG-RGC-2-19.0	1.13	0.38	0.40	Over-reinforced
SG-RGC-3-15.9	1.18	0.33	0.35	Over-reinforced
SG-RGC-4-12.7	1.00	0.29	0.30	Over-reinforced
SG-RGC-5-15.9	2.12	0.33	0.35	Over-reinforced
HG-RGC-3-15.9	1.18	0.33	0.35	Over-reinforced
DS-RGC-3-16.0	1.19[a]	2.93[b]		Under-reinforced

[a] Steel reinforcement ratio (ρ_s).
[b] Balanced steel reinforcement ratio (ρ_b).

midspan to monitor the deflection. In addition, the beams were instrumented with electrical-resistance strain gauges at midspan—bonded to the top surface of the geopolymer concrete and on the top and bottom reinforcement—to measure the longitudinal strains during loading. The strain gauges and sensor were connected to a data-acquisition unit to record their readings continuously.

3. Test results and observations

This section summarises the experimental results, including the load–deflection relationship, mode of failure, flexural capacity, midspan deflection, strains in the bars and geopolymer concrete, and cracking behaviour of the tested beams.

3.1. Load–deflection relationship

Fig. 5 shows the relationships between the experimental bending load and the midspan deflection of SG-RGC and HG-RGC. Generally, the load–deflection curves of SG-RGC have three segments, differing from the typical two-segment curves observed in previous studies [25,26] for FRP-reinforced concrete, and an unloading curve segment. The first segment is a steep linear branch wherein the deflection increases linearly with the applied load. This phase represented the beam's uncracked condition and was identical for all the tested beams because, at this stage, the load-carrying capacity of the beam was governed predominantly by the geopolymer concrete properties. When the applied load exceeded the geopolymer concrete's tensile strength, vertical cracks appeared at the bottom within the constant moment zone, reducing the beam stiffness. This marked the beginning of the cracked condition of the beam, represented by the second and third segments of the curve. The second segment is composed of an almost linear response up to the peak compressive strain of the geopolymer concrete, followed by a nonlinear response up until the geopolymer concrete crushing failure in the compression zone. The observed nonlinearity was caused by either the extensive cracking at the bottom or the extensive crushing of the geopolymer concrete and not due to yielding of GFRP bars [27,28]. As the figure shows, the stiffness of the second segment is similar for beams with the same reinforcement ratio. The slope, however, increases as the amount of reinforcement increases. These findings seem to

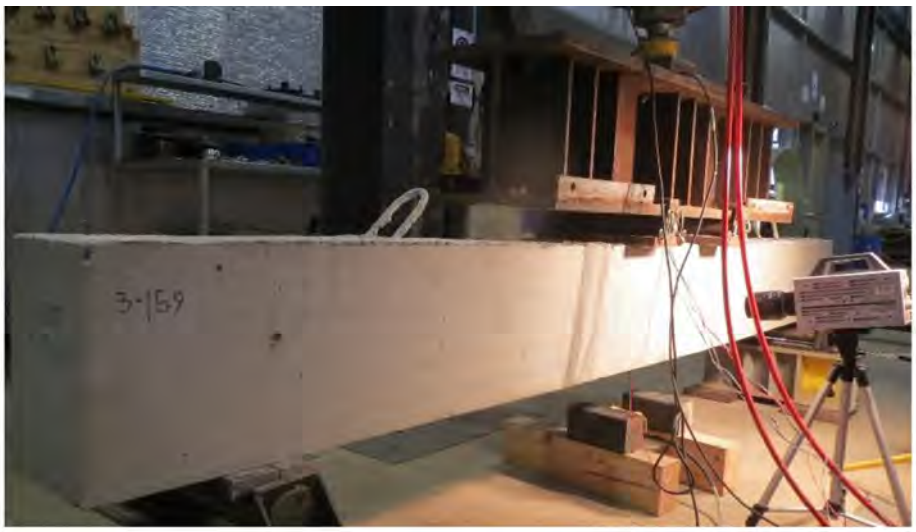

(a) Test setup

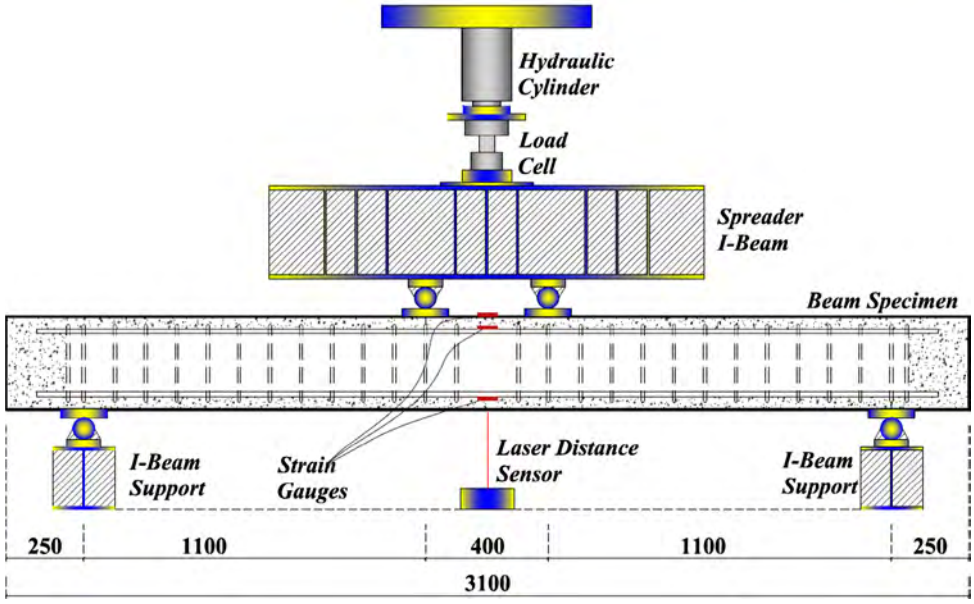

(b) Schematic diagram (dimensions are in mm)

Fig. 4. Four-point static bending test.

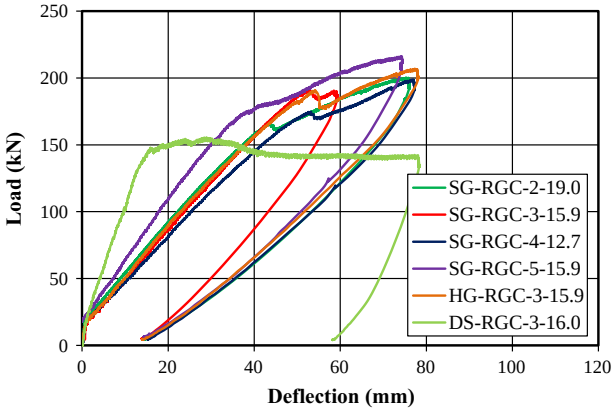

Fig. 5. Load–deflection relationship of the tested beams.

be consistent with the results obtained in FRP-reinforced concrete beams [26,29,30]. Afterwards, a sudden load drop occurred, indicating that concrete crushing failure had transpired. Interestingly, the beams did not readily lose their load-carrying capacity after this failure; instead, they continued to sustain additional loads. This behaviour can be attributed to the confinement effect provided by the GFRP stirrups that enhanced the beam ductility and strength. This section represents the third segment of the curve, which has a lower flexural stiffness owing to the initiation of failure in GFRP bars. To avoid any mishaps, the maximum applied load was limited to a magnitude marginally lower than the capacity of the load applicator. Similarly, the behaviour during load removal was recorded to create an unloading curve. This tends to show the elastic characteristic of the beams at higher loads, even after exhibiting nonlinear behaviour or even after the concrete crushing failure. On the other hand, the load–deflection relationship of HG-RGC is comparable to that of SG-RGC with similar amount of reinforcements. Noting that the bars are fully bonded

in geopolymer concrete, this result corroborates with the findings of Maranan et al. [31], which stated that, as the embedment length increases, the bond strength of the straight and headed GFRP bars become analogous to each other.

DS-RGC also yielded a three-segment load–deflection curve, with a different post-cracking nature, and an unloading curve. As can be anticipated, the second segment slope of this beam is steeper compared to those reinforced with GFRP bars owing to the higher modulus of elasticity of the steel bars. As the applied load exceeded the yield strength of the steel bar, a typical yielding plateau occurred: this designates the third segment of the curve. SG-RGC and HG-RGC did not exhibit this plastic behaviour. Upon the removal of the applied load, an unyielding curve occurred, but the residual deflection of this beam was much higher than that of SG-RGC and HG-RGC.

3.2. Mode of failure

Table 4 summarises the observed failure modes of the tested beams. As depicted in Fig. 6, the over-reinforced SG-RGC and HG-RGC failed in flexure due to geopolymer concrete crushing in the compression zone. The ACI 440.1R-06 and CSA S806-12 codes recommend this mode of failure for any concrete beams reinforced with FRP bars since this type of failure is more gradual, less brittle, and less catastrophic with higher deformability compared to the tensile rupture of FRP bars [32,33]. On the other hand, Fig. 7 shows that the under-reinforced DS-RGC also failed in flexure but steel yielding induced the failure. Since all the tested beams failed according to their intended failure, it can be deduced that the beams were designed satisfactorily.

3.3. Flexural capacity

3.3.1. Cracking moment

The loads at which the first crack appeared were recorded during the experiment and were verified from the load–deflection and moment–strain relationships. Table 4 presents the experimental cracking moment $M_{cr\text{-}exp}$ of the tested beams. Nearly similar $M_{cr\text{-}exp}$ values were obtained because this parameter mainly depends on the geopolymer concrete tensile strength. The average $M_{cr\text{-}exp}$ was 10.9 kN m that translates to a modulus of rupture f_r of 3.64 MPa, which is comparable to the f_r (3.86 MPa) of the geopolymer concrete prisms.

3.3.2. At service condition

In this study, two benchmarks were employed to determine the bending-moment capacity at service condition $M_{s\text{-}exp}$. The first criterion was based on ISIS-07 [34], which defines the $M_{s\text{-}exp}$ as the bending-moment that corresponds to a tensile-strain of 2000 με in the reinforcement. Using this principle, the $M_{s\text{-}exp}$ of SG-RGC and HG-RGC were relatively comparable with each other with an average value of 26.2 kN-m. The $M_{s\text{-}exp}$ of DS-RGC, however, was

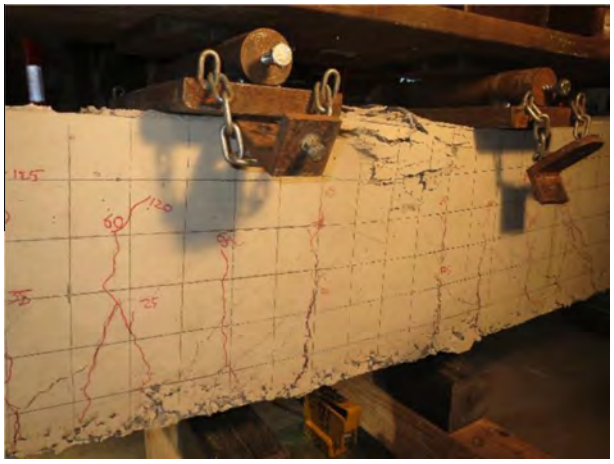

Fig. 6. Typical failure of SG-RGC and HG-RGC beams.

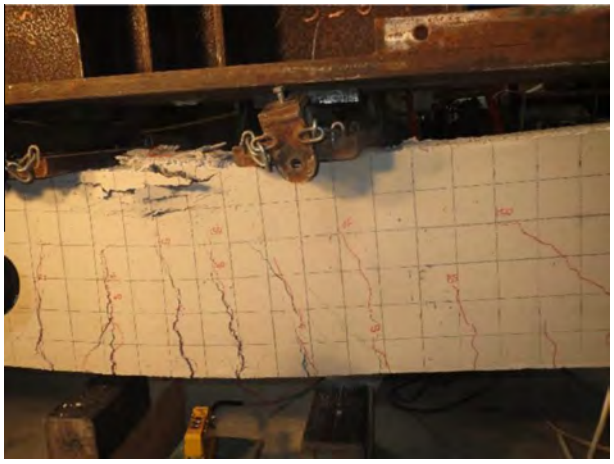

Fig. 7. Typical failure of DS-RGC beam.

1.85 times higher than that of SG-RGC and HG-RGC because of the higher elastic modulus of steel bars compared with GFRP bars. The second criterion was based on Bischoff et al.'s [35] recommendation wherein the $M_{s\text{-}exp}$ is approximated as 30% of the beam's bending-moment capacity at failure ($0.3M_{u\text{-}exp}$). All beams reinforced with GFRP bars, except SG-RGC-2-19.0, recorded comparable $M_{s\text{-}exp}$ values. Based on this criterion, however, DS-RGC yielded a lower $M_{s\text{-}exp}$ compared with SG-RGC and HG-RGC due to its lower $M_{u\text{-}exp}$.

3.3.3. At failure

Table 4 provides the experimental bending-moment capacity $M_{u\text{-}exp}$ of SG-RGC and HG-RGC at geopolymer concrete crushing

Table 4
Flexural capacity of the tested beams at cracking, at service condition, at failure, and at peak.

Specimen	M_{cr}[a] (kN m)	M_s (kN m)		M_u (kN m)	M_{peak} (kN m)	Failure mode[b]
		At 2000 με	At $0.3M_u$			
SG-RGC-2-19.0	11.9{11.1}[11.5]	27.0	27.4	91.4{78.0}[72.3]	110.1	CC
SG-RGC-3-15.9	11.5{11.1}[11.5]	21.3	31.4	104.8{79.7}[73.9]	104.7	CC
SG-RGC-4-12.7	10.4{11.1}[11.5]	27.2	28.8	96.1{77.2}[71.5]	109.3	CC
SG-RGC-5-15.9	10.4{11.1}[11.5]	27.7	29.8	99.3{84.3}[78.9]	118.9	CC
HG-RGC-3-15.9	10.5{11.1}[11.5]	27.8	31.5	105.0{79.7}[73.9]	113.8	CC
DS-RGC-3-16.0	10.8{11.1}[11.5]	48.6	25.6	85.4(72.7)	74.1	SY

[a] {} = Based on CSA-S806-12; [ ] = based ACI 440.1R-06; ( ) = based on ACI 318-08.
[b] CC = Failure due to concrete crushing, SY = failure due to steel yielding.

failure and of DS-RGC at steel yielding. The $M_{u\text{-}exp}$ of SG-RGC-2-19.0 (91.4 kN m), SG-RGC-3-15.9 (104.8 kN m), SG-RGC-4-12.7 (96.1 kN m), SG-RGC-5-15.9 (99.3 kN m), and HG-RGC-3-15.9 105.0 kN m were relatively equivalent to each other. The slight variation can be attributed to the intrinsic nonhomogeneous and anisotropic characteristic of the geopolymer concrete. On the other hand, the early yielding of steel bars prior to geopolymer concrete crushing failure resulted in a lower $M_{u\text{-}exp}$ for DS-RGC-3-16.0 (85.4 kN m) compared with SG-RGC and HG-RGC having similar ρ_f, thereby showing the superiority of the GFRP bars over the steel bars in terms of load-carrying capacity.

3.3.4. At peak

All the tested beams continued to carry additional loads after the concrete crushing failure, yielding another peak named as peak bending-moment capacity $M_{peak\text{-}exp}$ in this study. The $M_{peak\text{-}exp}$ of SG-RGC-2-19.0, SG-RGC-3-15.9, and SG-RGC-4-12.7 were 110.1 kN m, 104.7 kN m, and 109.3 kN m, respectively. The initial 25 mm gap between the beam and the load applicator yielded a relatively lower $M_{peak\text{-}exp}$ for SG-RGC-3-15.9 compared with the other beams. The 113.8 kN m and 118.9 kN m $M_{peak\text{-}exp}$ of HG-RGC-3-15.9 and SG-RGC-5-15.9 were slightly higher than that of SG-RGC-3-15.9. Nevertheless, the $M_{peak\text{-}exp}$ of the former beams could be much higher than that of the latter beam if the beams were taken to final failure. On the other hand, the $M_{peak\text{-}exp}$ achieved by DS-RGC-3-16.0 (74.2 kN m) was much lower compared to SG-RGC beams of similar ρ_f.

3.4. Midspan deflection

3.4.1. At service load

Table 5 summarises the immediate midspan deflection at service condition $\Delta_{s\text{-}exp}$ of the tested beams. The ISIS-07 criterion-based $\Delta_{s\text{-}exp}$ were 8.7 mm, 7.1 mm, and 10.6 mm for SG-RGC-2-19.0, SG-RGC-3-15.9, and SG-RGC-4-12.7, respectively, while the $\Delta_{s\text{-}exp}$ based from Bischoff's recommendation were 8.8 mm, 12.3 mm, and 11.5 mm, respectively. Generally, comparable results were obtained for each criterion. The $\Delta_{s\text{-}exp}$ (7.3 mm and 8.0 mm based on ISIS-07 and Bischoff, respectively) of SG-RGC-5-15.9 was generally lower than that of SG-RGC with lower ρ_f. HG-RGC-3-15.9, on the other hand, yielded similar $\Delta_{s\text{-}exp}$ as SG-RGC with comparable ρ_f, 10.0 mm based on ISIS-07 and 11.3 mm based on Bischoff's criterion. In general, the $\Delta_{s\text{-}exp}$ from Bischoff's recommendation were more conservative than that of ISIS-07 in terms of deflection limits set by ACI 440.1R-06 and CSA S806-12 (L/240 or 10.8 mm). Thus, the criterion set by Bischoff should be used as the basis for designing GFRP-reinforced geopolymer concrete beams. The $\Delta_{s\text{-}exp}$ of DS-RGC-3-16.0 was generally higher than that of its SG-RGC counterparts.

Table 5
Mid-span deflection of the tested beams at service condition, at failure, and at the unloaded phase.

Specimen	Δ_s[a] (mm)		Δ_u[a] (mm)	Δ_{res} (mm)
	At 2000 με	At 0.30M_u		
SG-RGC-2-19.0	8.7[6.6]	8.8[6.8]	43.4{34.7}[32.9]	14.4
SG-RGC-3-15.9	7.1[3.6]	12.3[8.3]	52.5{35.7}[36.3]	13.9
SG-RGC-4-12.7	10.6[7.4]	11.5[8.2]	53.2{35.3}[36.3]	15.2
SG-RGC-5-15.9	7.3[4.9]	8.0[5.6]	42.0{24.9}[26.0]	14.3
HG-RGC-3-15.9	10.0[7.2]	11.7[8.8]	54.1{35.9}[36.5]	14.0
DS-RGC-3-16.0	8.1(6.5)	3.7(3.55)	28.4(11.9)	58.2

[a] {} = Based on CSA-S806-12; [ ] = based ACI 440.1R-06; ( ) = based on ACI 318-08.

3.4.2. At failure

The measured $\Delta_{u\text{-}exp}$ of SG-RGC-2-19.0, SG-RGC-3-15.9, and SG-RGC-4-12.7 were 43.4 mm, 52.5 mm, and 53.2 mm, respectively. Except for SG-RGC-2-19.0, the recorded deflections were almost analogous with each other. SG-RGC-5-15.9 yielded a lower $\Delta_{u\text{-}exp}$ (42.0 mm) compared with the other beams due to its higher stiffness, owed to its higher amount of reinforcements. This finding was also observed by Yoo et al. [30]. The $\Delta_{u\text{-}exp}$ of HG-RGC-3-15.9 (54.1 mm) was nearly comparable to SG-RGC with similar reinforcement ratios. The $\Delta_{u\text{-}exp}$ (28.4 mm) of the DS-RGC beam is much lower than that of the SG-RGC.

3.4.3. At the unloading phase

After removing the applied load, all the beams reinforced with GFRP bars tended to return to their original position. The residual deflections, $\Delta_{res\text{-}exp}$, of SG-RGC were comparable to that of the HG-RGC beam, approximately equivalent to 14 mm. This finding proves the effective flexural bond of the sand-coated GFRP bars in the geopolymer concrete. Furthermore, it also shows the inherent elastic behaviour of the SG-RGC, mainly because of the partial development of the tensile strength of the GFRP bars. The $\Delta_{res\text{-}exp}$ of DS-RGC was approximately four times higher than that of SG-RGC owing to the inelastic yielding of the steel bars.

3.5. Strain distribution

Fig. 8 shows the relationship between the applied moment and the midspan strains at the top and bottom reinforcements, TB and BB, respectively, and on the top surface of the geopolymer concrete (GC). The analogous curvature of the moment–strain curves in TB, BB, and GC indicates the effectiveness of sand coating in anchoring the GFRP bars in the geopolymer concrete. Interestingly, the shape of the moment–strain curves of the reinforcement is similar to their load–deflection curves, including an initial linear segment with a steep slope, linear and nonlinear segments with reduced slope after cracking, and a nonlinear segment after the crushing failure of the geopolymer concrete. The moment–strain curves of the geopolymer concrete in compression zone consisted only of the first two segments since the strain gauges were damaged after the crushing failure. The top GFRP bars, however, continued to provide strain readings. This can be due to the confinement effect provided by the stirrups that protected the bars from buckling and/or kinking.

Table 6 summarises the bar and concrete strains at service condition as defined by Bischoff, at concrete crushing failure, and at peak load. SG-RGC with similar reinforcement ratios yielded nearly comparable strains at different load stages. The tabulated values make it clear, however, that increasing the reinforcement ratio would generally result in lower strains at the bottom GFRP bars. The strain readings at service condition of DS-RGC were generally lower than that of SG-RGC.

3.6. Cracking behaviour

For all the tested beams, a few fine vertical flexural cracks first developed within the pure bending-moment zone after the in-plane bending-moment exceeded the cracking moment of the beams. As the applied load increases, these cracks became wider and propagated upward, while new vertical cracks formed along the beams' shear span. The vertical cracks in SG-RGC and HG-RGC, at service condition, were generally wider than that of DS-RGC, owing to the lower elastic modulus of GFRP bars compared with steel bars. With further loading, the vertical cracks in the pure bending zone became even wider, while the inclined cracks, induced by shear stress, formed along the shear span and then propagated towards the points of load application. The rate

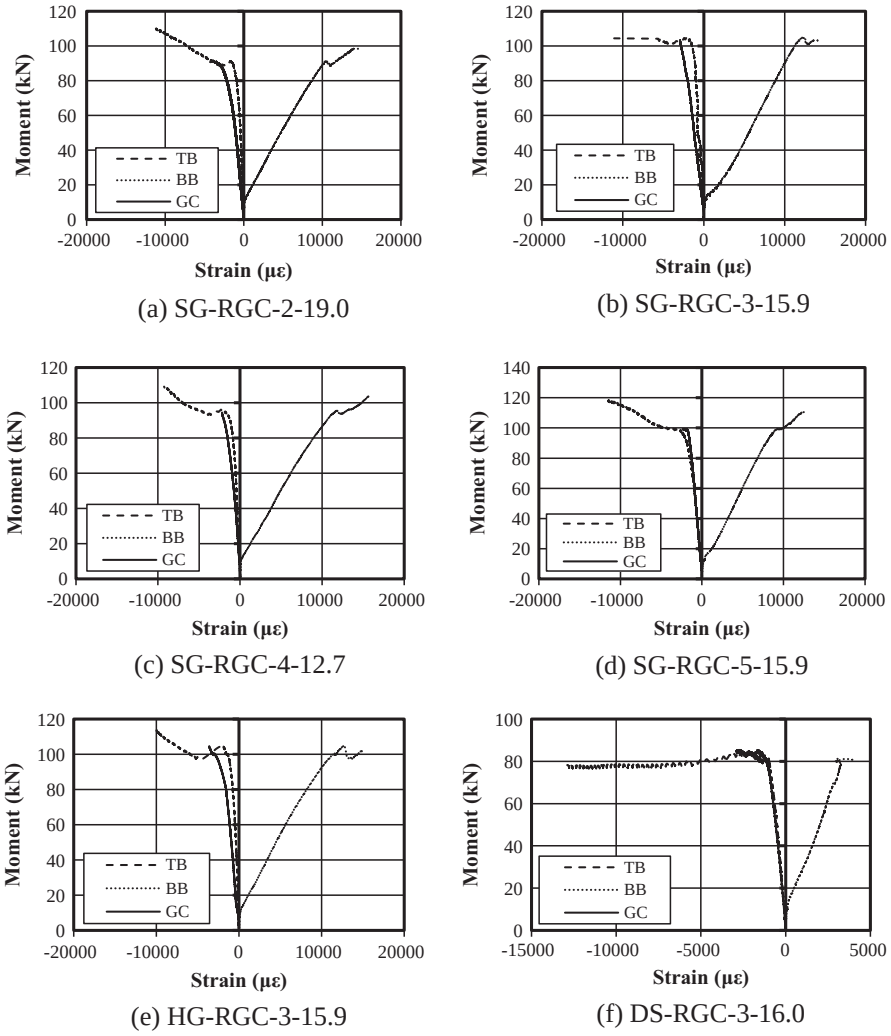

Fig. 8. Moment–strain relationships of the tested beams.

Table 6
Strain in the reinforcing bars and the geopolymer concrete (in με).

Specimen	At service condition ($0.3M_{u\text{-}exp.}$)			At failure			At peak	
	Concrete top surface	Top bar	Bottom bar	Concrete top surface	Top bar	Bottom bar	Top bar	Bottom bar
SG-2-19.0	502	203	2028	4226	2086	10,855	11,186	14,963
SG-3-15.9	698	156	3508	2934	2115	12,244	11,083	14,956
SG-4-12.7	348	247	2147	4831	2327	11,547	9271	15,746
SG-5-15.9	429	448	2146	2329	2924	9168	11,710	12,973
HG-3-15.9	401	401	2438	3603	2042	13,286	9989	15,757
DS-3-16.0	272	233	768	2915	1604	3936	12,983	6099

of progress of the inclined cracks, however, slowed down with the initiation of concrete crushing in the compression zone, thereby redistributing the stresses within the zone. At the final loading stage, a marginal number of inclined cracks reached the crushed zone of the geopolymer concrete. Furthermore, all the beams experienced significant flexural cracking before the inclined cracks joined the flexural cracks, thereby assuring that the beams failed in flexure and not in shear.

Fig. 9 depicts the crack pattern at peak of the tested beams. The number of cracks developed along the span of DS-RGC was smaller than that of SG-RGC and HG-RGC, but the cracks were wider and mostly concentrated at midspan, owing to yielding of the steel bars in this region. The figure clearly shows that the cracks were distributed uniformly along the span of SG-RGC, with a crack spacing of about 100 mm, similar to stirrup spacing. Ehsani et al. [36] and Faza and Gangarao [6] also reported this uniform crack distribution for concrete beams reinforced with sand-coated FRP bars. The tendency of the cracks to form at the stirrups location was due to the loss of bond between the GFRP bars and the geopolymer concrete. The stirrups caused the discontinuity of the mechanical interlock and friction force resistance of the sand coating, thereby yielding a spike in the concrete stresses. This could also explain the reason why there is no significant effect on the crack spacing upon doubling the amount of the GFRP reinforcement, as was also reported by Theriault et al. [29] and Masmoudi [37]. The absence of transverse reinforcements would increase the contact area

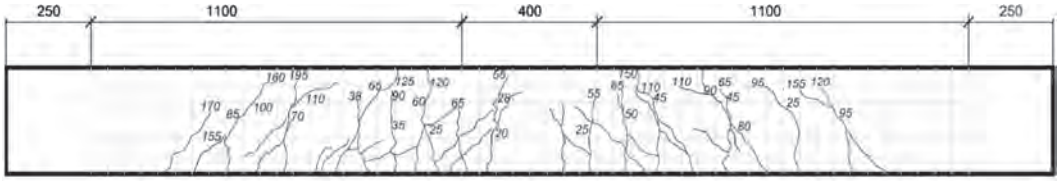

(a) SG-RGC-2-19.0

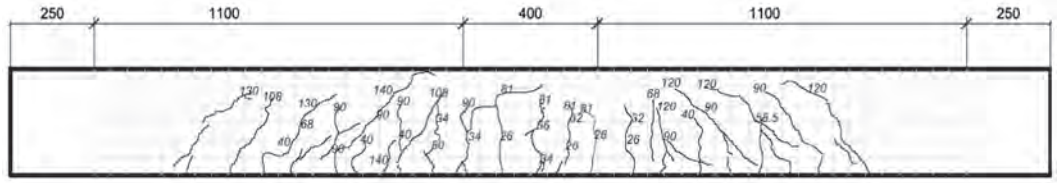

(b) SG-RGC-3-15.9

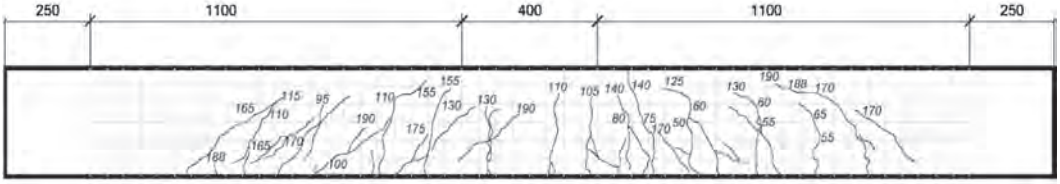

(c) SG-RGC-4-12.7

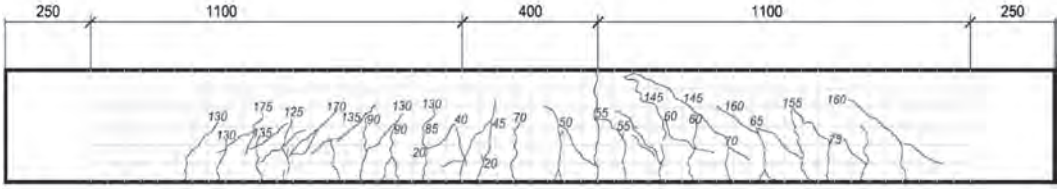

(d) SG-RGC-5-15.9

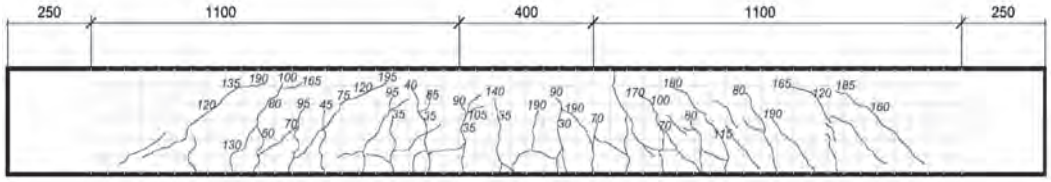

(e) HG-RGC-3-15.9

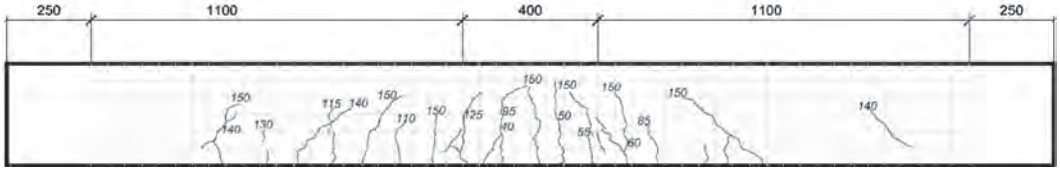

(f) DS-RGC-3-16.0

Fig. 9. Cracking patterns of the tested beams.

between the longitudinal GFRP reinforcements and the geopolymer concrete that would lead to an increase in the rate of stress transfer from the reinforcements to the geopolymer concrete, thereby reducing the crack spacing. The study conducted by Kassem et al. [26], on the other hand, showed that the beams with bundled sand-coated FRP bars developed fewer cracks with wider spacing than those with single bars owing to the better bond quality for single bars compared with bundled bars. This crack spacing mechanism described as a function of bond between the reinforcement and the concrete has been well researched and presented in the previous studies [38–43].

Comparable crack patterns were observed between SG-RGC and HG-RGC with similar ρ_f. The figure also demonstrates that the anchor heads have no significant influence on beam cracking behaviour and that an adequate bond can be secured with sand coating alone.

4. Discussion

This section summarises the influence of the nominal bar diameter, reinforcement ratio, and anchorage system on the flexural performance of the geopolymer concrete beams reinforced with GFRP bars. A comparison between the experimental and theoretical results was also presented in this section. The published results on FRP-reinforced concrete beams were compared with the experimental results.

4.1. Influence of the nominal bar diameter

This study utilised 12.7 mm, 15.9 mm, and 19.0 mm GFRP bars as longitudinal reinforcement for geopolymer concrete beams. Based on the experimental results, the nominal bar diameter had no significant effect on the flexural strength and serviceability performance of the geopolymer concrete beams reinforced with sand-coated GFRP bars. Generally, SG-RGC-2-19.0, SG-RGC-3-15.9, and SG-RGC-4-12.7 yielded similar flexural strengths, load–deflection characteristics, crack patterns, and deflections. The comparable behaviour of these beams can be expected, since these beams were designed as over-reinforced and consequently, their flexural behaviour would mainly depend on the properties of the geopolymer concrete and not on the diameter of the GFRP bars. Furthermore, noting that all the tested beams were manufactured with a single batch of geopolymer concrete, it can expected that beams with similar reinforcement ratios would yield similar flexural performance.

4.2. Influence of the reinforcement ratio

The flexural stiffness of the beams after cracking or the slope of the second segment of their load–deflection curves increases as the reinforcement ratio increases. Thus, it can be deduced from the experimental results that the serviceability performance of a GFRP-reinforced geopolymer concrete beam can be enhanced by increasing the amount of longitudinal reinforcement. This improvement can be clearly understood by imagining the bars as parallel springs. As the number of bars increased, the overall stiffness also increased, thereby lowering the deflection after cracking, limiting the crack width, and decreasing the strain in the reinforcement. Yoo et al. [30] reported that the flexural stiffness increased with increasing longitudinal rigidity (A_fE_f) and suggested that the reinforcement ratio should be increased in order to control crack width effectively.

The cracking moments of all the tested beams are similar, since this parameter mainly relied on the properties of the geopolymer concrete. The results also showed that doubling the reinforcement ratio would not significantly enhance the beam load-carrying capacity up to the point of geopolymer concrete crushing failure. This can be expected since all the tested beams were over-reinforced and their strength would be predominantly controlled by the properties of the geopolymer concrete. After the geopolymer concrete crushing failure, the GFRP bars began to sustain several damages and hence, at this stage, the beam strength was influenced by the amount longitudinal reinforcements. The load-carrying capacity of the beam with larger ρ_f was higher than that of beams with lower ρ_f, although the increase was just marginal. This result seems to corroborate with that of Kassem et al. [26] findings wherein they found out that increasing ρ_f by 50% and 100% will marginally increase the flexural capacity by just 4% and 16%, respectively. The study conducted by Kara et al. [44] showed that, for over-reinforced FRP-reinforced concrete beams, a large increase in FRP reinforcement produced a modest increase in normalised capacity. El-Nemr et al. [25], however, suggested that the influence of ρ_f on the strength of FRP-reinforced concrete beams could be fully realised when ρ_f is increased three to four times.

4.3. Influence of the anchorage system

The strength and serviceability performance of HG-RGC was nearly comparable to that of SG-RGC. This can be expected since the straight and headed bars were fully bonded in the geopolymer concrete, thereby yielding similar results. As reported by Maranan et al. [31], the bond strength of the straight and headed GFRP bars approached similar performances as the embedment length increased. Thus, it can be deduced that a composite action can be achieved between the straight bars and the geopolymer concrete by fully embedding the bars in the geopolymer concrete and that the friction and mechanical interlock resistance provided by the sand coating were sufficient to produce a composite action between the GFRP bars and the geopolymer concrete.

4.4. Comparison with current design provisions

In this study, the empirical equations recommended by the CSA S806-12 and ACI 440.R-06 were employed to assess the strength and serviceability performance of SG-RGC and HG-RGC, while the ACI 318-14 code was adapted for the DS-RGC beam. Using Eq. (7), the theoretical cracking moments, $M_{cr\text{-}theo}$, based on CSA and ACI are 11.1 kN m and 11.5 kN m, respectively. The f_r was calculated from Eq. (8) for the CSA code. Eq. (9), on the other hand, was used for the ACI codes with the assumption that λ is equivalent to 1.0. Generally, the predicted values were relatively close to the experimental results, with the ACI code providing a more conservative estimate.

The theoretical flexural capacity at concrete crushing failure, $M_{u\text{-}theo}$, of SG-RGC and HG-RGC were determined with Eq. (10). In CSA S806-12, the bar stress, f_f, was computed by solving first the neutral axis location, c, from Eq. (11) and then substituting this value to Eq. (12). For ACI 440.1R-06, the f_f was calculated with Eq. (13). On the other hand, Eq. (14), recommended by ACI 318-08, predicted the flexural capacity of DS-RGC at steel yielding failure. Table 4 summarises the $M_{u\text{-}theo}$ of the tested beams. The values estimated according to CSA S806-12 were higher than those predicted by ACI 440.1R-06, owing to the β_1 factor and the higher ε'_{cu} normally assumed in CSA (0.0035) compared to ACI (0.003). Generally, both prediction equations underestimated the flexural capacity of all the tested beams. The average theoretical strengths of the beams based on ACI 440.1R-06 and CSA S806-12 are 76% and 81%, respectively, of the experimental flexural strengths. Generally, this finding can be attributed to three major factors. First, the assumed concrete compressive strains (0.003–0.0035) used in the predictions are lower compared to the actual strain recorded during the flexural tests, which reached higher values ranging from 0.0042 to 0.0048. Second, the prediction equations did not include the contribution of the reinforcement in the compression zone. Finally, the confinement effect due to the lateral ties (stirrups) provided in the pure bending-moment zone were not considered.

Eqs. (18) and (19) show the deflection formula recommended by the CSA S806-12 and ACI 440.1R-06 codes, respectively. In CSA S806-12, the coefficient η was computed from Eq. (20). In the case of ACI 440.1R-06, the effective moment of inertia (I_e) formula, a concept that is used to describe presented in Eq. (21) was employed to calculate the midspan deflection. This formula, is Branson's formula for steel-reinforced concrete (Eq. (23)) modified with by incorporating a reduction factor β_d (Eq. (22)) to account for the reduced tension stiffening in the FRP-reinforced members [45]. Table 5 summarises the predicted midspan deflections at service condition $\Delta_{s\text{-}theo}$ of the tested beams based on ACI 4401.R-06. In

Table 7
Normalised bending-moment capacity of the tested beams and the GFRP-reinforced concrete (GFRP-RC) beams obtained from the previous studies.

Reference	Beam	ρ_f (%)	$M_u/f'_c bd^2$
Current Study	SG-RGC-2-19.0	1.13	47.7
	SG-RGC-3-15.9	1.18	54.3
	SG-RGC-4-12.7	1.00	49.6
	SG-RGC-5-15.9	2.12	51.5
	HG-RGC-3-15.9	1.18	54.5
[21]	G1-6	1.6	43.6
	G1-8	2.2	46.1
[35]	GB3-1	1.10	44.6
	GB3-2	1.10	47.3
[36]	ISO1	1.10	35.1
	ISO2	1.10	36.7
[37]	ISO30-2	1.01	35.9

general, the prediction equations underestimated the experimental results. The estimated values based on Bischoff's recommendations were more conservative than ISIS-07 in terms of deflection limit L/240. Table 5 also shows the predicted midspan deflection at failure $\Delta_{u\text{-}theo}$ of the tested beams. Again, both design equations did not conservatively estimate beam $\Delta_{u\text{-}theo}$. The degree of underestimation increased with an increase in the applied load, owing to the overestimation of the tension stiffening parameter. Furthermore, these equations were developed from a full-interaction analysis of transformed section wherein it is assumed that no slip between the concrete and the reinforcements, which is not the case in the actual condition. Visintin et al. [38] suggested the use of partial-interaction theory that allows the slip between the reinforcement and concrete. Thus, considering the mentioned factors and the concept of partial-interaction theory, an appropriate prediction equation is now being developed for the proposed system.

4.5. Comparison between the experimental results and the FRP-reinforced concrete beams

Table 7 presents a comparison between the normalised bending-moment capacity ($M_u/f'_c bd^2$) of the tested beams and the GFRP-reinforced concrete (GFRP-RC) beams obtained from the previous studies. The considered GFRP-RC beams had dimensions, concrete strengths, and reinforcement ratios nearly comparable to the tested beams. Furthermore, the GFRP bars were also sand-coated and all the beams were designed as over-reinforced, such that they failed due to crushing of concrete in the compression zone. Generally, the bending-moment capacity of the tested beams was higher than the bending-moment of the GFRP-RC beams, mainly due to the following factors. First, the geopolymer concrete had enhanced mechanical properties compared to the conventional concrete of the same grade (higher compressive strain capacity based on the flexural test of the beams and better tensile strength and improved modulus of elasticity according to the compression test of the cylinders). Second, all the tested beams had lateral ties within the pure bending-moment span, which provided confinement of the geopolymer concrete core, thereby increasing the beam strength and ductility. Lastly, the tensile strength (617–695 MPa) and modulus of elasticity (40–55 GPa) of the GFRP bars used in the previous studies were lower than the tensile strength and the modulus of elasticity of the bars used in this study. The high compressive strain capacity of geopolymer concrete was coupled with GFRP bars having a high tensile strength resulted in a beam with high flexural strength and ductility. Table 6 shows the amount of tensile strains in the bottom GFRP bars at geopolymer concrete crushing failure. These strains translate to a tensile stresses than can reach up to 892 MPa. If the beams were reinforced with GFRP bars of lower tensile strength, the beams will fail earlier due to bar rupture, yielding lower flexural strengths.

5. Conclusion

This paper presented an assessment of the strength and serviceability of geopolymer concrete beams reinforced with GFRP bars subjected to four-point static bending testing. Based on the experimental results and theoretical predictions, the following can be concluded:

- The load–deflection curves of the beams with GFRP bars consist primarily of three segments, including a steep linear branch that corresponds to cracked response of the beam; linear and nonlinear segments with reduced slope that represent the cracked response of the beam; and a nonlinear segment after the crushing failure of the geopolymer concrete.
- The beams reinforced with GFRP bars failed by concrete crushing failure, since they were designed as over-reinforced, while the under-reinforced beam with steel bars failed due to reinforcement yielding.

Table 8
CSA S806-12, ACI 440.1R-06, and ACI 318-08 prediction equations.

CSA S806-12	ACI 440.1R-06	ACI 318-08
$\rho_f = \frac{A_f}{bd}$ (1)		$\rho_s = \frac{A_s}{bd}$ (3)
$\rho_{fb} = \alpha_1\beta_1 \frac{f'_c}{f_{fu}} \frac{E_f\varepsilon'_{cu}}{E_f\varepsilon'_{cu}+f_{fu}}$ (2)		$\rho_b = \alpha_1\beta_1 \frac{f'_c}{f_y} \frac{E_s\varepsilon'_{cu}}{E_s\varepsilon'_{cu}+f_y}$ (4)
$\alpha_1 = 0.85 - 0.0015f'_c \geqslant 0.67$ (5a)	$\alpha_1 = 0.85$ (6a)	
$\beta_1 = 0.85 - 0.0025f'_c \geqslant 0.67$ (5b)	$\beta_1 = 0.85 - \frac{0.05(f'_c-27.6)}{6.9} > 0.65$ for $f'_c > 27.6$ MPa (6b)	
$f_r = \frac{M_{cr}y}{I_g}$ (7)		
$f_r = 0.6\lambda\sqrt{f'_c}$ (8)	$f_r = 0.62\lambda\sqrt{f'_c}$ (9)	
$M_u = \rho_f f_f bd^2\left(1 - \frac{\rho_f f_f}{2\alpha_1 f'_c}\right)$ (10)		$M_u = \rho_s f_s bd^2\left(1 - \frac{\rho_s f_s}{2\times\alpha_1 f'_c}\right)$ (14)
$\alpha_1\beta_1 f'_c bc - A_f \frac{\varepsilon'_{cu}(d-c)}{c}E_f = 0$ (11)	$f_f = \sqrt{\frac{(E_f\varepsilon_{cu})^2}{4} + \frac{0.85\beta_1 f'_c}{\rho_f}E_f\varepsilon_{cu}} - 0.5E_f\varepsilon_{cu} < f_{fu}$ (13)	If steel yields: $f_s = f_y$ (15)
$f_f = A_f \frac{\varepsilon'_{cu}(d-c)}{c}E_f < f_{fu}$ (12)		If steel does not yield: $\alpha_1\beta_1 f'_c bc - A_s \frac{\varepsilon'_{cu}(d-c)}{c}E_s = 0$ (16) $f_s = A_s \frac{\varepsilon'_{cu}(d-c)}{c}E_s < f_y$ (17)
$\Delta = \frac{(P/2)L^3}{24E_c I_{cr}}\left[3\frac{a}{L} - 4(\frac{a}{L})^3 - 8\eta\left(\frac{I_{cr}}{I_g}\right)^3\right]$ (18)	$\Delta = \frac{(Pa/2)(3L^2-4a^2)}{24E_c I_e}$ (19)	
$\eta = 1 - \frac{I_{cr}}{I_g}$ (20)	$I_e = \left(\frac{M_{cr}}{M_a}\right)^3\beta_d I_g + \left[1 - \left(\frac{M_{cr}}{M_a}\right)^3\right]I_{cr} \leqslant I_g$ (21)	$I_e = \left(\frac{M_{cr}}{M_a}\right)^3 I_g + \left[1 - \left(\frac{M_{cr}}{M_a}\right)^3\right]I_{cr} \leqslant I_g$ (23)
	$\beta_d = 0.2\left(\frac{\rho_f}{\rho_{fb}}\right) \leqslant 1.0$ (22)	

- The bending-moment capacities at concrete crushing failure of GFRP-reinforced geopolymer concrete beams were 1.2–1.5 times greater than that of steel-reinforced geopolymer concrete beam with similar reinforcement ratio.
- The uncracked response of all the tested beams was similar since, at this stage, the flexural performance of the beam was governed by the geopolymer concrete properties.
- For beams with similar reinforcement ratios, it appears that the GFRP bar nominal diameter had insignificant effect on their flexural behaviour.
- Increasing the reinforcement ratio would enhance the serviceability performance of the GFRP-reinforced geopolymer concrete beams. Doubling the reinforcement ratio, however, did not increase the beams load-carrying capacity at concrete crushing failure since the beams were designed as over-reinforced and therefore, their strength would be dependent on the geopolymer concrete strength and not by bar rupture.
- The mechanical interlock and friction force resistance provided by the sand coating, bonded on the surface of the GFRP bars, were found to be adequate to secure a composite action between the bars and the geopolymer concrete.
- Generally, both the ACI-440.1R-06 and CSA S806-12 prediction equations underestimated the flexural capacity of GFRP-reinforced geopolymer concrete beams. This may be due to the following factors: lower compressive strains used in the prediction (0.003 and 0.0035, respectively) compared to the actual strains (0.0042–0.0048); neglection of the compression strength contribution of top GFRP bars; and exclusion of the confinement effect of stirrups located in the pure bending-moment zone.
- The bending-moment capacity of GFRP-reinforced geopolymer concrete beams seems to be higher than that of GFRP-reinforced concrete beams mainly because of the enhanced mechanical properties of the geopolymer concrete compared to the conventional concrete of the same grade. Further investigations, however, are needed to support this generalisation.

Acknowledgements

The authors would like to express their special thanks to V-ROD® Australia for providing the materials, the Natural Science and Engineering Research Council of Canada (NSERC), and the technical staff of the structural lab at University of Southern Queensland.

References

[1] Ascione L, Razaqpur AG, Spadea S. Effectiveness of FRP stirrups in concrete beams subject to shear. In: El-Hacha R, editor. The 7th International Conference on FRP Composites in Civil Engineering (CICE 2014). Vancouver, Canada: International Institute for FRP in Construction (IIFC); 2014. p. 368–73.
[2] Hardjito D, Wallah SE, Sumajouw DMJ, Rangan BV. On the development of fly ash-based geopolymer concrete. ACI Mater J 2004;101:467–72.
[3] Sumajouw DMJ, Hardjito D, Wallah SE, Rangan BV. Fly-ash based geopolymer concrete: study of slender columns. J Mater Sci 2007;42:3124–30.
[4] Fernandez-Jimenez AM, Polomo A, Lopez-Hombrados C. Engineering properties of alkali-activated fly ash concrete. ACI Mater J 2006;103:251–7.
[5] Sofi M, Deventer JSJv, Mendis PA, Lukey GC. Engineering properties of inorganic polymer concretes (IPCs). Cem Concr Res 2007;42:3107–16.
[6] Faza SS, Gangarao HVS. Theoretical and experimental correlation of behaviour of concrete beams reinforced with fibre reinforced plastic rebars. Am Concr Inst 1993;SP138:599–614.
[7] Karbhari V, Seible F. Fiber-reinforced polymer composites for civil infrastructure in the USA. Struct Eng Int 1999;9:186–94.
[8] V-ROD. V-ROD® Australia: composite reinforcing rod. Inconmat Australia.
[9] Abraham R, Raj SD, Abraham V. Strength and behaviour of geopolymer concrete beams. Int J Innovative Res Sci Eng Technol 2013;2:159–66.
[10] Ribeiro SEC, Diniz SMC. Reliability-based design recommendations for FRP-reinforced concrete beams. Eng Struct 2013;52:273–83.
[11] Matos B, Correia JR, Castro LMS, Franca P. Structural response of hyperstatic concrete beams reinforced with GFRP bars: effect of increasing concrete confinement. Compos Struct 2012;94:1200–10.
[12] Mousavi SR, Esfahani MR. Effective moment of inertia prediction of FRP-reinforced concrete beams based on experimental results. ASCE J Compos Constr 2012;16.
[13] Nawy EG, Neuwerth GE, Philips CJ. Behaviour of fibre glass reinforced concrete beams. ASCE J Struct Div 1971;97:2203–15.
[14] Noel M, Soudki K. Estimation of the crack width and deformation of FRP-reinforced concrete flexural members with and without transverse shear reinforcement. Eng Struct 2014;59:393–8.
[15] Adam MA, Said M, Mahmoud AA, Shanour AS. Analytical and experimental flexural behavior of concrete beams reinforced with glass fiber reinforced polymer bars. Constr Build Mater 2015;84:354–66.
[16] Au FTK, Du JS. Deformability of concrete beams with unbonded FRP tendons. Eng Struct 2008;30:3764–70.
[17] Rangan BV, Sumajouw D, Wallah S, Hardjito D. Reinforced low-calcium fly ash-based geopolymer concrete beams and columns. Our world in concrete and structures. Singapore: CI-Premier PTE LTD; 2006.
[18] Dattatreya JK, Rajamane NP, Sabitha D, Ambily PS, Nataraja MC. Flexural behaviour of reinforced geopolymer concrete beams. Int J Civ Struct Eng 2011;2:138–59.
[19] Kumaravel S, Thirugnanasambandam S. Flexural behaviour of geopolymer concrete beams. Int J Adv Eng Res Stud 2013;3:4–6.
[20] Maranan GB, Manalo AC, Karunasena W, Benmokrane B. Bond stress-slip: case of GFRP bars in geopolymer concrete. ASCE J Mater Civ Eng 2014.
[21] Pultrall. V-ROD FRP reinforcing bars data sheet; 2012.
[22] CSA. Design and construction of building structures with fibre-reinforced polymers. CSA S806-12. Mississauga, Ontario, Canada: Canadian Standards Association; 2012.
[23] ACI. Guide for the design and construction of structural concrete reinforced with FRP bars. ACI 4401R-06. Farmington Hills, MI, USA: American Concrete Institute; 2006.
[24] ACI. Building code requirements for structural concrete. ACI 318-08. Farmington Hills, MI, USA: American Concrete Institute; 2008.
[25] El-Nemr A, Ahmed EA, Benmokrane B. Flexural behavior and serviceability of normal- and high-strength concrete beams reinforced with glass fiber-reinforced polymer bars. ACI Struct J 2013;110:1077–88.
[26] Kassem C, Farghaly AS, Benmokrane B. Evaluation of flexural behavior and serviceability performance of concrete beams reinforced with FRP bars. ASCE J Compos Constr 2011;15:682–95.
[27] Balendran RV, Tang WE, Leung HY, Nadeem A. Flexural behaviour of sand coated glass-fibre reinforced polymer (GFRP) bars in concrete. Our world in concrete and structures. Singapore; 2004. p. 203–12.
[28] Razaqpur AG, Svecova D, Cheung MS. Strength and deformations of FRP reinforced flat slab structures. In: Taerwe L, editor. Proceedings of the second international RILEM symposium (FRPRCS-2). E & FN Spon; 1995.
[29] Theriault M, Benmokrane B. Effects of FRP reinforcement ratio and concrete strength on flexural behaviour of concrete beams. ASCE J Compos Constr 1998;2:7–16.
[30] Yoo DY, Shin HO, Kwon KY, Yoon YS. Structural behavior of UHPFRC beams according to reinforcement ratio of internal GFRP bar. In: El-Haacha R, editor. The 7th international conference on FRP composites in civil engineering (CICE 2014). Vancouver, British Columbia, Canada: International Institute for FRP in Construction (IIFC); 2014.
[31] Maranan GB, Manalo AC, Karunasena W, Benmokrane B. Pullout behaviour of GFRP bars with anchor head in geopolymer concrete. Compos Struct 2015;132:1113–21.
[32] Gangarao HVS, Tally N, Vijay PV. Reinforced concrete design with FRP composites. CRC Press; 2007.
[33] Kakizawa T, Ohno S, Yonewa T. Flexural behavior and energy absorption of carbon FRP reinforced concrete beams. Am Concr Inst 1993;138:585–98.
[34] ISIS. Reinforcing concrete structures with fibre-reinforced polymers. ISIS Design Manual No 3. Winnipeg, Manitoba, Canada: Intelligent Sensing for Innovative Structures (ISIS) Canada; 2006.
[35] Bischoff PH, Gross S, Ospina CE. The story behind the proposed changes to the ACI 440 deflection requirements for FRP-reinforced concrete. In: Ospina C, Bischoff PH, Alkhrdaji T, editors. Serviceability of concrete members reinforced with internal/external FRP reinforcement. Farmington Hills, MI: American Concrete Institute; 2009. p. 53–76.
[36] Ehsani MR, Saadatmanesh H, Tao S. Bond behaviour of deformed GFRP rebars. J Compos Mater 1997;31:1413–30.
[37] Masmoudi R, Benmokrane B, Chaallal O. Cracking behaviour of concrete beams reinforced with FRP bars. Can J Civ Eng 1996;23:1172–9.
[38] Visintin P, Oehlers DJ, Muhamad R, Wu C. Partial-interaction short term serviceability deflection of RC beams. Eng Struct 2013;56:993–1006.
[39] Yankelevsky DZ, Jabareen M, Abutdul AD. One-dimensional analysis of tension stiffening in reinforce concrete with discrete cracks. Eng Struct 2008;30:206–17.
[40] Visintin P, Oehlers DJ, Wu C, Haskett M. A mechanics solution for hinges in RC beams with multiple cracks. Eng Struct 2012;36:61–9.
[41] Oehlers DJ, Ali MSM, Haskett M, Lucas W, Muhamad R, Visintin P. FRP-reinforced concrete beams: unified approach based on IC theory. J Compos Constr 2011;15. 3-293-303.

[42] Marti P, Alvarez M, Kaufmann W, Sigrist V. Tension chord model for structural concrete. Struct Eng Int 1998;8:287–98.
[43] Muhamad R, Ali MSM, Oehlers DJ, Sheikh AH. Load–slip relationship of tension reinforcement in reinforced concrete members. Eng Struct 2011;33:1098–106.
[44] Kara IF, Ashour AF. Flexural performance of FRP reinforced concrete beams. Compos Struct 2012;94:1616–25.
[45] Issa MS, Metwally IM, Elzeiny SM. Influence of fibers on flexural behavior and ductility of concrete beams reinforced with GFRP bars. Eng Struct 2011;33:1754–63.

3.4. Paper IV: Shear behavior of geopolymer concrete beams reinforced with GFRP bars

The shear behavior of geopolymer concrete beams reinforced with GFRP bars and stirrups was investigated in this paper. The test matrix was presented in **Table B-4** of **Appendix B** of the thesis. The properties of the 9.5 mm diameter GFRP stirrups were presented in **Table B-2** of thesis' **Appendix B**, wherein the measured actual bend radius was 38.1 mm (more than 4 times the bar diameter) while the total lap splice length at the corner was 150 mm. These stirrups represents those that were used in actual practice and were provided by the industry collaborator. In **Paper IV**, the influence of stirrup spacing and its contribution to shear strength were carefully evaluated. Stratford and Burgoyne (2003) stated that since FRP bars are brittle in nature, is not appropriate to assume that the stresses in the stirrups crossing an inclined crack are equal. Hence, to measure the strain, strain gauges were attached in one stirrup, which was positioned in the mid-shear span of the tested beams, with the assumption that this stirrup will be mostly stressed compared with the other stirrups within the shear span. Indeed, the diagonal shear cracks passed along the stirrups in which the strain gauges were attached. Based on the experimental results, the GFRP stirrups doubled both the shear strength and deflection capacity of the GFRP-RGC beams. The indicative strains measured from one stirrup were effectively utilised in investigating the influence of stirrup spacing and its contribution to shear strength of beam, which are presented in detail in sections "Crack Pattern and Propagation", "Cracking Load", "Failure Mode", and "Transverse-Reinforcement Strains". The comparison of test results with the existing literature verified the validity of the test results and findings of the study.

Aside from beams, columns are one of the most critical and important structural members. However, there are limited studies regarding the compression behaviour of concrete columns reinforced with GFRP bars. With the advent of FRP reinforcing technology, the new generation of GFRP bars have enhanced mechanical properties that can match that of steel. This was the key motivation for investigating the compression behaviour of circular geopolymer concrete columns reinforced longitudinally and transversely reinforced with GFRP bars and ties, which is presented, analysed, and discussed in Paper V.

SHEAR BEHAVIOR OF GEOPOLYMER CONCRETE BEAMS REINFORCED WITH GFRP BARS

Ginghis B. Maranan, Allan C. Manalo, Brahim Benmokrane, Warna Karunasena, and Priyan Mendis

Biography: **Ginghis B. Maranan** is a PhD Candidate at the School of Civil Engineering and Surveying in the University of Southern Queensland (USQ), Australia. He received his BS from the University of the Philippines Los Baños, Philippines and MEng from the University of Tokyo, Japan.

Allan C. Manalo is a Senior Lecturer at the School of Civil Engineering and Surveying, USQ. He received his BS from University of the Philippines Los Baños, Philippines; MEng at Saitama University, Japan; and PhD from USQ. He is a member of IIFC, Engineers Australia, and Concrete Institute of Australia. His research interests include engineered composite materials and structures, railway sleepers, and structural testing.

Brahim Benmokrane, FACI, is Professor of Civil Engineering and NSERC Research Chair in FRP Reinforcement for Concrete Infrastructure and Tier-1 Canada Research Chair in Advanced Composite Materials for Civil Structures in the Department of Civil Engineering at the University of Sherbrooke, QC, Canada. He is a member of ACI Committee 440 FRP Reinforcement and serves on Canadian Standard Association (CSA) committees on FRP structural reinforcing materials for buildings (CSA S806), bridges (CSA S6), and FRP specifications (CSA S807 and CSA S808).

Warna Karunasena is a Professor at the School of Civil Engineering and Surveying, USQ. He received his BS from University of Peradeniya, Sri Lanka; MS from Asian Institute of Technology; and PhD from University of Manitoba, Canada. He is a member of Engineers Australia, ASCE, and Structural Engineering Institute-USA. His research interests include composite materials, modelling and analysis of structures, and structural health monitoring.

Priyan Mendis is a Professor in the Department of Infrastructure Engineering and the Leader of the Advanced Protective Technology of Engineering Structures Group in the University of Melbourne, Australia. He received his BS from University of Moratuwa, Sri Lanka and PhD from Monash University, Australia. He is a member of ACI, Concrete Institute of Australia, and Engineers Australia. His research interests include fire behavior of structures, high-strength concrete, and modeling and durability of infrastructure.

ABSTRACT

The shear behavior of geopolymer concrete beams reinforced with GFRP bars and stirrups was investigated. Six short beams with a shear-span-to-effective-depth ratio (a/d) of 1.8 were cast: one with no stirrups, three with different stirrup spacing, one with less reinforcement, and one with steel stirrups. In addition, a slender beam (a/d=4.7) with the same cross-sectional area were built to investigate the influence of a/d. Experimental results showed that the GFRP stirrups enhanced both the shear strength and deflection capacity of the beams by approximately 200%. The shear crack initiated at a higher load and with a finer crack width in the beam with narrower stirrups spacing. The short beam yielded higher shear strength than the slender beam with a similar transverse reinforcement ratio. The beams with GFRP stirrups yielded a shear strength and deflection capacity—including an analogous load–deflection response—similar to that of the beam with steel stirrups.

INTRODUCTION

The corrosion of the internal reinforcing steel is the main factor shortening the life span of reinforced-concrete (RC) structures[1]. Many owners are faced with the problem of costly repairs and maintenance of RC structures that have been damaged and deteriorating due to steel corrosion. Likewise, there is a great demand for sustainable structures, which hints at the replacement of cement-based concrete with other types of environmentally friendly

concrete since cement production results in billions of tons of wastes and contributes to 5% to 8% of the world's greenhouse gases yearly[2]. According to 2008 estimates, Australia's cement industry accounts for approximately 1.3% of greenhouse-gas emissions[3]. A promising solution is to combine fiber-reinforced-polymer (FRP) bars and geopolymer concrete.

Several studies have shown that FRP bars can replace steel bars in building more durable structures, mainly because of its corrosion-resistant nature and the added benefits of being lightweight (approximately 20% to 25% the density of steel) and having high tensile strength (around twice steel's yield strength), and being electromechanically neutral[4]. Geopolymer concrete, on the other hand, is a viable substitute for cement-based concrete because it does not generate high volumes of greenhouse gases, and it can be manufactured using silica- and alumina-rich industrial-waste materials,[5] such as fly ash and slag. According to Duxson et al.,[6] geopolymer binders have a CO_2 footprint approximately 80% lower than that of ordinary portland cement (OPC) binder. Many studies have shown that geopolymer concrete has strength and durability comparable to or occasionally greater than that of normal concrete of the same grade[7]. Furthermore, it has better fire and chemical resistance, exhibits lower creep and shrinkage, and can develop high mechanical strength in a shorter period of time.[8] The high cost and lack of design guidelines, however, are some of the major disadvantages of geopolymer concrete.[9] Moreover, little research has gone into investigating the behavior of fiber-reinforced polymer-reinforced geopolymer-concrete (FRP-RGC) systems. Additional research, therefore, is required to enable engineers to understand the fundamental behavior and to identify the similarities or differences between the proposed system and conventional ones so that it can be generally adopted by the construction industry.

This study investigated the shear behavior of geopolymer concrete beams reinforced with GFRP bars and stirrups. The behavior of the beams was assessed based on crack pattern and propagation, failure mode, load–deflection response, cracking load, shear strength and

deflection capacity, and strain in the geopolymer concrete and reinforcement. The influence of stirrups, stirrup spacing, stirrup type, longitudinal-reinforcement ratio, and shear-span-to-effective-depth (a/d) ratio were analyzed and compared to the published results on FRP-reinforced normal-concrete (FRP-RC) and conventional RC beams. Different shear design provisions were employed to identify which of the existing codes could be used to predict the capacity of the tested beams, including the ACI 318-08[10] and CSA S806-12[11] strut-and-tie models, the JSCE 2007[12] shear formula for RC beams, and the kinematic model for deep beams developed by Mihaylov et al.[13].

RESEARCH SIGNIFICANCE

FRP bars are normally used to reinforce concrete beams and girders. Ample experimental and analytical research[14-16] on the flexural performance of FRP-reinforced concrete (FRP-RC) beams is available. While quite a few studies have investigated the concrete contribution to shear strength in FRP-RC beams, there are relatively few data that deal with the contribution of FRP stirrups[17-19] to shear strength, particularly in the case of FRP-RGC short beams. Short beams are commonly used as transfer girders, whose safety is often crucial for the whole structure's stability. The authors believe that the experimental outputs of this study would be beneficial for the development of design guidelines and specifications for the FRP-RGC systems that would facilitate their uptake in mainstream construction applications.

EXPERIMENTAL PROGRAM

Materials

GFRP stirrups (CSA S807-10[20]) of 9.5 mm (0.37 in.) nominal diameter (ϕ_f) and deformed steel stirrups of 10 mm (0.39 in.) diameter (ϕ_s) were used. The GFRP stirrups have a lap splice length of 150 mm at the corner. The transverse reinforcement was 150 mm (5.91 in.) wide and 240 mm (9.45 in.) deep with a bent corner radius of around 38.1 mm (0.98 in.).

High modulus GFRP bars[20] with 12.7 mm (0.5 in.) and 19.0 mm (0.75 in.) nominal diameter were used as longitudinal reinforcements at the top and bottom of the beam, respectively. **Table 1** provides the physical and mechanical properties of the reinforcement as reported by the manufacturers, including the nominal cross-sectional area (A_b), GFRP bars' guaranteed tensile strength (f_{fu}), guaranteed tensile strength of GFRP stirrup's straight leg (f_{fvu}) and bent (f_{bent}); steel bars' yield strength (f_y), modulus of elasticity of the GFRP bars (E_f), GFRP stirrups (E_{fv}), and steel bars (E_f).

Table 1 – Mechanical properties of the reinforcement

ϕ_f, mm (in.)	A_b, mm^2 (in.^{2})	f_{fu}^*, MPa (ksi)	f_{bend}, MPa (ksi)	E_f, GPa (ksi)
9.5 (0.38)	71.6 (0.11)	f_{fvu} = 1029 (149)	463 (67)	E_{fv} = 50 (7250)
12.7 (0.50)	127 (0.20)	1312 (190)	-	65.6 (9510) $\pm$ 2.5 (362)
15.9 (0.63)	199 (0.31)	1184 (172)	-	62.6 (9080) $\pm$ 2.5 (362)
19.0 (0.75)	284 (0.44)	1105 (160)	-	63.7 (9240) $\pm$ 2.5 (362)
ϕ_s = 10 (0.39)		f_y = 500 (73)		E_s = 200 (29000)

**Guaranteed tensile strength: average value – 3x standard deviation*

The geopolymer concrete used in this study is a proprietary mixture consisting of 10 mm (0.39 in.) and 20 mm (0.79 in.) coarse aggregates, fine and medium sands, and a geopolymer binder made from alkali-activated class F fly ash (FA) and ground granulated blast-furnace slag (GGBS). Water and superplasticizer were added to improve the workability of the concrete. The 28-day compressive strength f'_c and uniaxial tensile strength f'_{ct} of the geopolymer concrete, determined in accordance with ASTM C39/C39M-04a[21] and ASTM C496/C496M-11,[22] respectively, were 43 MPa (6.24 ksi) and 3.46 MPa (0.50 ksi). The flexural tensile strength (f_t), according to Maranan et al.,[23] was approximately 10% of the compressive strength of the geopolymer concrete or 4.3 MPa (0.62 ksi).

Test Specimens

Figure 1 shows the typical configuration of the tested beams. Five full-scale beams with a a/d of 1.8 and a total span L of 1500 mm (59.06 in.) were fabricated and tested up to failure. These beams were referred to as "short beams". The beams had a width b and total depth h of

200 mm (7.87 in.) and 300 mm (11.81 in.), respectively. The first beam was cast without stirrups to determine the shear capacity of the geopolymer concrete. The second, third, and fourth beams were reinforced with GFRP stirrups spaced at 75 mm (2.95 in.) or *h*/4, 100 mm (3.94 in.) or *h*/3, and 150 mm (5.91 in.) or *h*/2 on center, respectively, to investigate the effect of stirrup spacing. The fifth beam was transversely reinforced with steel stirrups spaced at 150 mm (5.91 in.) or *h*/2 on center for comparison purposes. These beams were designed to be over-reinforced (reinforcement ratio (ρ_f) = 1.66% and balanced reinforcement ratio (ρ_{fb}) = 0.36%) with three 19.0 mm (0.75 in.) bottom GFRP bars to induce shear failure prior to flexural failure. To investigate the influence of the amount of longitudinal reinforcement, a short beam longitudinally strengthened with two 19.0 mm and one 15.9 mm GFRP bars (ρ_f = 1.50% and ρ_{fb} = 0.36%) was cast with stirrups spaced at 125 mm (4.80 in.) or 5*h*/12. Another beam with the same cross-sectional area but with *a*/*d* and *L* of 4.7 and 3100 mm, respectively, was also built to determine the effect of *a*/*d*. The slender beam was transversely reinforced with GFRP stirrups spaced at 100 mm (3.94 in.) or *h*/3 on center and was also designed to be over-reinforced (ρ_f = 2.01% and ρ_{fb} = 0.29%) with five 19.0 mm bottom GFRP bars. All the beams were provided with two 12.7 mm (0.50 in.) top GFRP bars.

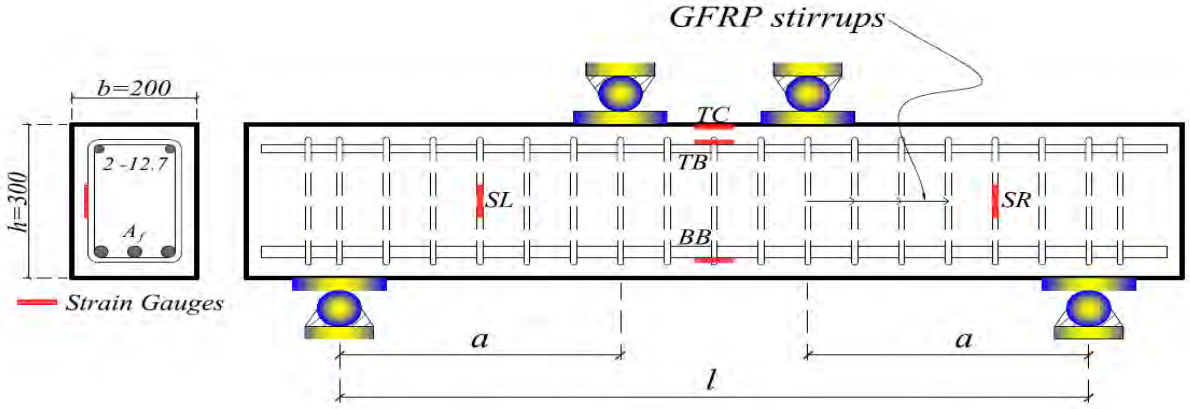

Fig. 1 – *The typical configuration and test set up of the beams.*

The specimens were labelled as follows: GG-*a*/*d*-G(S)-*s*. The first two letters (GG) stand for "GFRP-reinforced geopolymer-concrete beam" and *a*/*d* for their corresponding shear

span-to-effective depth ratio. The next letter represents the type of transverse reinforcement: G for GFRP stirrups and S for steel stirrups. The letter "*s*" represents the center-to-center spacing of the stirrups in millimeters. For example, the specimen identified as GG-1.8-G-75 is a GFRP-reinforced geopolymer-concrete beam with a *a*/*d* of 1.8 and transversely reinforced with 9.5 mm (0.37 in.) GFRP stirrups spaced at 75 mm (2.95 in.) or *h*/4 on center.

Test Program and Instrumentation

The four-point static-bending test shown in **Figure 1** was used to investigate the shear performance of the beams. The beams with clear spans *l* of 1200 mm (47.24 in.) and 3100 mm (122.05 in.) were loaded with two equally concentric loads 300 mm (11.81 in.) and 400 mm (15.74 in.) apart at midspan, respectively, yielding *a*/*d* of 1.8 and 4.7, respectively. To avoid bearing failure and premature crushing, loading and support plates measuring 250 mm (9.84 in.) by 150 mm (5.91 in.) by 20 mm (0.79 in.) and 250 mm (9.84 in.) by 75 mm (2.95 in.) by 20 mm (0.79 in.), respectively, were used to transfer the applied loads and reactions, respectively. **Figure 1** also shows the location of the electrical strain gauges. The *TC* strain gauge measured the strains on the geopolymer concrete top surface. *TB* and *BB* were used to measure the strains at the top and bottom longitudinal reinforcement, respectively. *SL* and *SR* were used to determine the strains at the mid-depth of the stirrup straight portion located on the left and right sides of the beam, respectively. These strain gauges were attached to the stirrups positioned at mid-shear spans, with the assumptions that these stirrups would receive more stress than the other stirrups within the shear span. The specimens were loaded to failure in displacement control mode with a hydraulic jack to allow for the observation of both the pre- and post-peak behavior. The applied load was measured with a 500 kN (112400 lbf) capacity load cell, while the corresponding midspan deflection was measured with a laser displacement sensor. The strain, load, and deflection readings were recorded with a data logger, while the crack pattern was documented visually during the test.

EXPERIMENTAL RESULTS

Crack Pattern and Propagation

Figure 2 shows the crack patterns and propagation just before the final failure. The numbers marked on the beam represent the magnitude of the applied load (in kN). As the tensile stress induced by the applied load exceeded the tensile capacity of the geopolymer concrete, some vertical cracks began to form within the constant bending-moment zone. With further loading, inclined cracks developed. Two types of shear cracks were observed in the experiment. The first type was the web-shear (WS) crack characterized by the formation of a diagonal crack that is independent of the flexural crack, and then propagated in both directions. This type of crack developed mainly in the tested short beams. As these cracks propagated toward the loading points, the geopolymer concrete strut simultaneously underwent crushing at the upper end region, just before the final failure. The other type of crack is the flexural–shear (FS) crack, which developed predominantly in the slender beam, wherein the initial vertical flexural crack in the shear span bent in diagonal direction and continued to grow in length and width, propagating toward the loading points and the supports. The vertical flexural crack spacing, in general, were the same as the stirrup spacing. This is expected since the mechanical bond between the bar and concrete was lost due to the presence of stirrups. Oehlers et al.[24] reported this crack-spacing mechanism, which is a function of bond between the reinforcement and concrete.

Based on **Figures. 2a-e** and through visual inspection, GG-1.8 yielded wider and fewer flexural and shear cracks compared to the GG-1.8-G beams, owing to the stirrups' clamping effect. This observation is consistent with Mohamed et al.'s[25] findings for FRP-RC deep beams, which showed that web reinforcement, specifically vertical stirrups, significantly controlled the width of diagonal cracks. The short beam with closer stirrup spacing (GG-1.8-G-75) yielded more shear cracks that were narrower and closely spaced than those in the

beams with wider stirrup spacing, which follows the well-known idea that crack-opening displacement or crack width increases as the spacing between shear cracks increases.[26] The reason for this behavior is that the smaller the stirrup spacing, the lower the effective concrete area needed to be controlled by a stirrup in terms of shear-crack-width development, thereby resulting in higher bond adhesion between the stirrup and the surrounding concrete. The major diagonal crack that developed in the short beams defined the inclination of the main concrete diagonal strut, as illustrated in the figures. The crack pattern in GG-1.8-S-150, as shown in **Figure 2f**, was nearly similar to that of GG-1.8-G-150. The former beam, however, had narrower and shorter shear cracks than the latter, owing to the lower elastic modulus of the GFRP compared to steel. GG-4.7-G-100, on the other hand, developed wider flexural cracks compared to GG-1.8-G-100 at comparable loads. No major shear cracks were developed along the shear span of the slender beam before its final failure, as shown in **Figure 2g**.

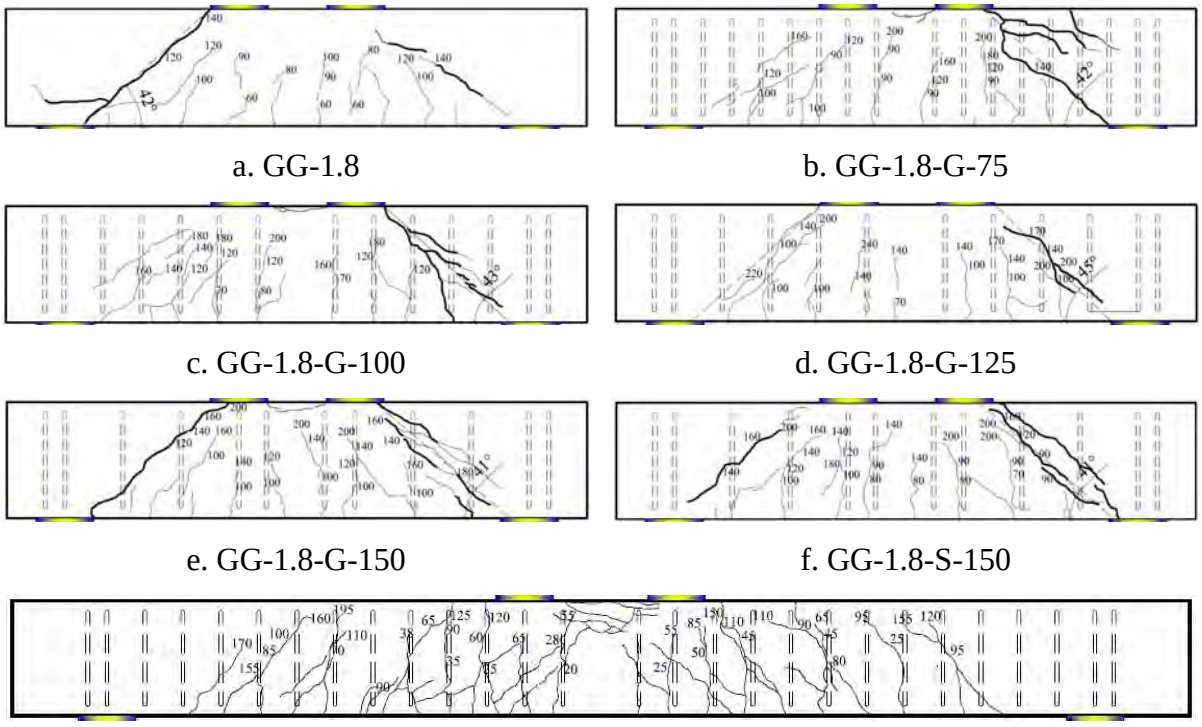

a. GG-1.8 b. GG-1.8-G-75

c. GG-1.8-G-100 d. GG-1.8-G-125

e. GG-1.8-G-150 f. GG-1.8-S-150

g. GG-4.7-G-100

Fig. 2 – *Crack pattern of the tested beams.*

Failure Mode

Figure 3 shows the failure mode of the tested beams. As can be expected, all the short beams exhibited brittle shear failure. That is, the shear capacity of the short beams was reached before the flexural capacity was attained. This outcome demonstrated the effectiveness of the design and testing procedures employed herein.

The failure of GG-1.8 can be classified as a diagonal-strut tension (DST) failure (**Figure 3a**) wherein the internal lateral spread of the compression force led to a transverse tension that split the concrete parallel to the strut axis. Secondary anchorage failure due to splitting action along the main reinforcement and minor concrete crushing at the top of the diagonal strut were also observed during the experiment. The failure of the GG-1.8-G beams, on the other hand, can be considered as a diagonal-strut compression (DSC) failure (**Figures 3b-e**). The stirrups' confining effect prevented longitudinal splitting and bond-splitting cracks and effectively distributed the stresses along the diagonal-strut length, thereby subjecting the strut to extreme compression stress. The lateral expansion of the compression field between the support and the point-load application, however, resulted in the rupture of the GFRP stirrups crossing the diagonal crack that subsequently led to the beams' failure. Interestingly, these failure modes were also observed by Mohamed et al.[25] in FRP-RC deep beams. The rupture of the stirrups' bent portion induced the failure of GG-1.8-G-75, GG-1.8-G-100, and GG-1.8-125, while the failure of GG-1.8-G-150 was initiated by the lap-splice failure located at the stirrup bent. These beams also exhibited secondary concrete crushing in the flexural compression zone. GG-1.8-G-75 experienced the most severe damage, followed by GG-1.8-G-100, GG-1.8-G-150, and GG-1.8-G-125, respectively. GG-1.8-S-150 also experienced a DSC mode of failure (**Figure 3f**). This beam, however, experienced a more ductile and a lesser degree of failure compared to GG-1.8-G-150 due to the steel stirrups yielding. In

contrast, the slender beam failed due to crushing of the geopolymer concrete in the flexural compression zone, as shown in **Figure 3g.**

a. GG-1.8

b. GG-1.8-G-75

c. GG-1.8-G-100

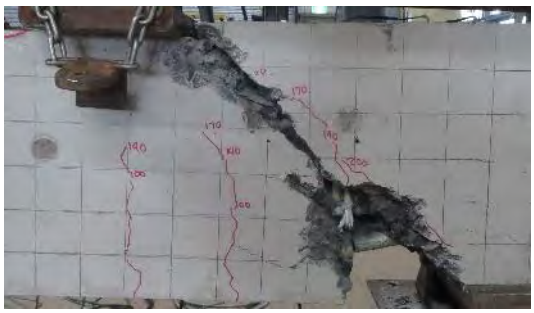

d. GG-1.8-G-125

e. GG-1.8-G-150

f. GG-1.8-S-150

g. GG-4.7-G-100

Fig. 3 – *Failure mode of the tested beams.*

Load–Deflection Response

Figure 4 (left) shows the relationships between the applied load and the mid-span deflection of all the tested beams. Generally, the beams exhibited a nearly bilinear load–deflection behavior. The first steep linear segment represents the uncracked response of the beam. As expected, the initial flexural stiffness was similar for all short beams since, at this stage, the gross moment of inertia of the geopolymer concrete section was fully utilized. The second linear segment with reduced stiffness, on the other hand, characterizes beam's cracked response. The stiffness reduction can be attributed to the successive flexural and shear cracking, which reduced the beam's moment of inertia. All GG-1.8-G beams with a reinforcement ratio of 1.66% yielded similar stiffness. Slight nonlinear behavior and stiffness degradation were observed in GG-1.8-G-150 and GG-1.8-S-150 before peak load due to the widening of shear cracks and geopolymer concrete crushing in the flexural compression zone. Interestingly, GG-1.8-S-150 evidenced a load–deflection response similar to GG-1.8-G-150.

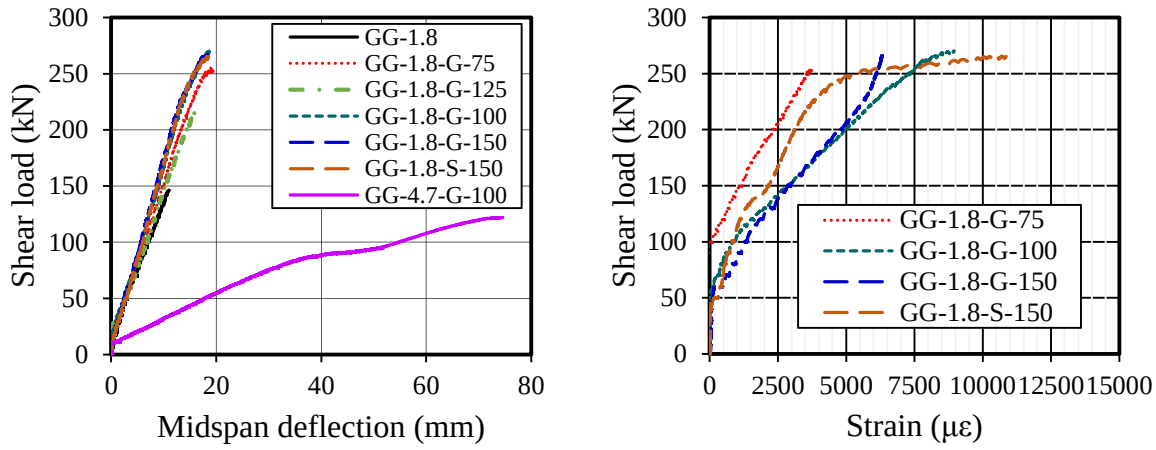

Fig. 4 – *Shear load–midspan deflection (left) and load–stirrup strain (right) relationships. (Note: 1 kN = 224.8 lbf, 1 mm = 0.039 in.)*

The post-cracking stiffness of GG-1.8-G-125 was comparable to that of the short beams with more reinforcement. El-Sayed et al.,[27] however, reported that, as the longitudinal reinforcement of FRP-RC deep beams increased, the cracked stiffness increased for the

reinforcement ratios tested (0.7%, 1.2%, and 1.7%). These findings suggest that, in order to enhance the cracked stiffness of the GFRP-RGC short beams, the reference reinforcement ratio should be increased by 40% or higher. Further studies, however, are needed to justify this statement. GG-4.7-G-100, on the other hand, yielded a cracked stiffness that was much lower than GG-1.8-G-100. This could be attributed to the decreasing influence of arch action with increasing *a*/*d*, indicating that the beam became less rigid. Interestingly, after the concrete crushing failure, the slender beam continued to carry additional loads, owing to the confined concrete core that provided the necessary compression contribution.

Cracking Load

Table 2 summarizes the applied shear loads when the vertical flexural cracks appeared in the beams ($V_{cr,f}$), which were verified from **Figure 4** (left). As can be anticipated, the tested short beams yielded comparable $V_{cr,f}$, with an average value of 24 kN (5170 lbf), since this parameter depends mainly on concrete tensile strength. GG-4.7-G-100, on the other hand, yielded a $V_{cr,f}$ (10 kN [2250 lbf]) that was around 43% that of GG-1.8-G-100.

Table 2 – Load capacity, deflection capacity, geopolymer concrete peak strain, top and bottom bars' peak strains, and failure mode of the tested beams

Beam	$V_{cr,f}$, kN (lbf)	$V_{cr,s}$, kN (lbf)	V_n kN (lbf)	V_s^*, kN (lbf)	Δ_n, mm (in.)	ε'_c, με	ε'_{frp}, με	ε_{frp}, με	Failure Mode**
GG-1.8	23 (5170)	50 (11240)	V_c=147 (33050)	-	11 (0.43)	1400	968	4677	DST
GG-1.8-G-75	23 (5170)	70 (15740)	256 (57550)	109 (24500)	20 (0.79)	1736	5220	10016	DSC
GG-1.8-G-100	25 (5620)	60 (13490)	273 (61370)	126 (28320)	19 (0.75)	3753	3929	11476	DSC
GG-1.8-G-125	23 (5170)	50 (11240)	218 (49010)	71 (16070)	16 (0.63)	1607	3626	7345	DSC
GG-1.8-G-150	25 (5620)	50 (11240)	267 (60020)	120 (26980)	19 (0.75)	2956	4264	10204	DSC
GG-1.8-S-150	25 (5620)	45 (10120)	266 (59800)	119 (26750)	19 (0.75)	4441	3824	9510	DSC
GG-4.7-G-100	10 (5620)	33 (7420)	122 (27430)	-	-	2329	11710	11710	12973

*$V_s=V_n-V_c$

**DST = diagonal-strut-tension failure; DSC = diagonal-strut-compression failure; GCC = geopolymer-concrete crushing failure

Table 2 also provides the shear cracking loads $V_{cr,s}$, which were verified from **Figures 2** and **4** (right). The $V_{cr,s}$ of GG-1.8 was approximately 50 kN (11240 lbf). Among the short beams with stirrups, GG-1.8-G-75 yielded the highest $V_{cr,s}$, approximately equivalent to 70 kN (15740 lbf), followed by GG-1.8-G-100 (60 kN [13490 lbf]), GG-1.8-G-125 (50 kN [11240 lbf]), and GG-1.8-G-150 (50 kN [11240 lbf]), respectively. This could be attributed to the enhancement of the geopolymer-concrete contribution and stirrup shear contribution in beams with closely spaced stirrups. On the other hand, the $V_{cr,s}$ of GG-1.8-G-150 was quite similar to that of GG-1.8-S-150 (45 kN [10120 lbf]). Lastly, the $V_{cr,s}$ (33 kN [7420 lbf]) of GG-4.7-G-100 was approximately half of GG-1.8-G-100's $V_{cr,s}$.

Shear Strength and Deflection Capacity

Table 2 also shows the shear-load capacity V_n and deflection capacity Δ_n of the tested beams. GG-1.8 yielded the lowest V_n (147 kN [33050 lbf]) and Δ_n (11 mm [0.43 in.]) among the short beams. This value of V_n represents the shear contribution of the geopolymer concrete V_c, which depends mainly on the diagonal strut's strength. The beams with similar reinforcement ratios and transversely reinforced with GFRP stirrups, however, had nearly double the V_n and Δ_n values of GG-1.8 (with average values of 265 kN (56930 lbf) and 19 mm (4346 in.), respectively). These findings corroborate Sagaseta and Vollum's[28] statement about short-span RC beams and the experimental results obtained by Nagasaka et al.[29] and Vijay et al.[30] for FRP-RC deep beams and Birrcher et al.'s[31] findings for RC beams with total depth-to-width ratios less than or equal to 2.0 ($h/b \leq 2.0$), wherein the use of stirrups enhanced the serviceability performance of the beams. Our results, however, contradicted Mohamed et al.'s[25] findings for the FRP-RC beams with h/b of 4.0, wherein they concluded that the web reinforcement had no significant impact on the ultimate load capacity. Based on the experimental and published results, it seems that stirrups are effective only

when the $h/b \leq 2.0$. Further research work, however, should be conducted to validate this premise and to determine the specific h/b limit that is applicable for the proposed system.

The short beams with similar reinforcement ratios (1.66%) and transversely reinforced with GFRP stirrups of varying spacing yielded nearly comparable V_n and Δ_n, suggesting that the stirrup spacing has no significant effect on the shear load and deflection capacities of the tested short beams. These findings seem to be consistent with Vijay et al.'s[30] and Birrcher's et al.'s[31] results obtained from FRP-RC (a/d =1.89) and conventional RC beams (a/d = 1.84), respectively, with stirrup spacing of 100 mm (3.94 in.) on centers or wider. The experimental results, however, contradict Nagasaka et al.'s[29] findings for FRP-RC beams having a a/d of 1.78 and stirrup spacing less than or equal to 80 mm, wherein they found out that, as the stirrup spacing decreased, the strength increased. It could be deduced, therefore, that, for the beams with a a/d of around 1.8, stirrups spaced at 75 mm (2.95 in.) on centers (the minimum spacing used in this study) or more have no significant effect on the shear strength of RC deep beams. Nevertheless, this conclusion needs further investigation. In addition, Birrcher et al.[31] concluded that the use of web reinforcement in excess of 0.2% or 0.3% in beams with a a/d of 1.2 or 1.85 would not enhance shear strength. The minimum amount of shear reinforcement used in this study was 0.48%. It would be logical, therefore, to investigate the minimum amount of web reinforcement that could be adopted for the proposed system. Furthermore, the V_n (266 kN [59800 lbf]) and Δ_n (19 mm [0.75 in.]) of GG-1.8-S-150 were comparable to that of GG-1.8-G-150. These results tend to show the suitability of GFRP stirrups, in lieu of steel stirrups, as web reinforcement for geopolymer-concrete beams.

GG-1.8-G-125's V_n (218 kN [49000 lbf]) and Δ_n (16 mm [0.63 in.]) were both 18% lower than that of the corresponding average values of the short beams with more reinforcement. This result corroborates Farghaly and Benmokrane's[32] findings for FRP-RC deep beams. They reported that increasing the reinforcement ratio enhanced the diagonal strut strength—

the governing failure—and, in return, increased the transferred shear forces through arch action. According to Yost et al.,[33] however, the amount of longitudinal reinforcement had no significant influence on the shear capacity of GFRP-reinforced beams. This could be attributed to the beam depth—less than 300 mm—they adopted in their study. The V_n (122 kN [27430 lbf]) and Δ_n (74 mm [2.91 in.]) of GG-4.7-G-100, on the other hand, were approximately 45% and 390%, respectively, of GG-1.8-G-100's V_n and Δ_n, respectively. As expected, the beam with low a/d yielded higher shear strength than those with high a/d. This is attributed to the strength enhancing effects of arching action in the short beams. According to Rebeiz,[34] a significant amount of additional loading can be resisted by the RC short beams beyond the formation of a first diagonal crack, owing to the redistribution of stresses in short beams due to the relatively short distance between the supports and applied loads.

According to Stratford and Burgoyne[35], the stresses in the stirrups crossing an inclined crack should not be assumed equal because of the brittle nature of FRP. Hence, in our study, the shear contribution of the transverse reinforcement V_s was determined by subtracting V_c, the V_n of GG-1.8, from the V_n of each beam specimen. As expected, the short beams with reinforcement ratio of 1.66% yielded comparable V_s with an average value of 119 kN [26750 lbf]). The short beam with lower reinforcement ratio (GG-1.8-G-125), on the other hand, yielded the lowest V_s, equivalent to 71 kN (16070 lbf).

Transverse-Reinforcement Strains

Figure 4 (right) shows the relationship between the applied shear load and the strain readings obtained from the straight portion of the stirrups located at the failure zone of all the short beams with a reinforcement ratio of 1.66%. Very low strain readings were recorded at lower shear loads in all the tested beams, suggesting that the full section of concrete carried most of the shear stresses. The stirrups then began to contribute to the beam's overall shear-resisting mechanism when diagonal cracking initiated. Among the GG-1.8-G beams, GG-1.8-G-75

recorded the lowest strains for the same magnitude of load, thereby incurring narrower shear cracks compared to GG-1.8-G-100 and GG-1.8-G-150. This could be attributed to the higher transverse-reinforcement ratio (ρ_{fv}) or reinforcement index ($\rho_{fv}E_{fv}/E_s$) of the GG-1.8-G-75 compared to GG-1.8-G-100 and GG-1.8-G-150 beams. GG-1.8-S150, on the other hand, yielded lower strains and consequently, experienced wider shear cracks compared to GG-1.8-G150 for similar applied loads, signifying the influence of the modulus of elasticity.

CSA S6-06[36] suggests a strain limit of 2500 με in FRP stirrups to limit diagonal-crack width. For the specified strain limit, GG-1.8-G-75 produced the highest shear-load capacity (205 kN [46080 lbf]), followed by GG-1.8-G-100 (142 kN [31920 lbf]) and GG-1.8-G-150 (138 kN [31020 lbf]), respectively. Both GG-1.8-G-100 and GG-1.8-G-150 exceeded the 4000 με limit recommended by ACI 440.1R-06[37] and CSA S6-14.[38] This indicates the applicability of the HM GFRP stirrups as web reinforcement for GFRP-RGC beam systems.

Geopolymer-Concrete and Longitudinal-Reinforcement Strains

Table 2 summarizes the measured peak strains in the geopolymer concrete (ε'_c) and in the top (ε'_{frp}) and bottom (ε_{frp}) longitudinal reinforcements. The maximum geopolymer-concrete strains for the GG-1.8-G beams with a reinforcement ratio of 1.66% ranged from 1,736 με to 3,753 με, whereas the strain at failure for GG-1.8 was just 1,400 με. The peak strains in the longitudinal compression bars of these beams ranged from 3,929 με to 5,220 με, approximately three to four times higher than that of GG-1.8 (968 με). Furthermore, the strains in the bottom longitudinal reinforcement in these beams (10,016 με to 11,746 με) were approximately 2.5 times higher than that of GG-1.8 (4,677 με). These tensile strain values were lower than the strain capacity of the bottom GFRP bars (17,300 με). Clearly, the provision of GFRP web reinforcement enhanced the strain resistance of each component material. GG-1.8-S-150 yielded strains relatively comparable to that of GG-1.8-G-150. These results seem to indicate that stirrup type and spacing have no significant effect on the peak

strains developed in the GG short beams. GG-1.8-G-125 also developed concrete (1,607 με), top-bar (3,636 με), and bottom-bar (7345 με) strains that were relatively lower compared to the beams with higher reinforcement ratios. In comparison to GG-1.8-G-100, GG-4.7-G-100 yielded relatively lower concrete strains (2,329 με), much higher top-bar strains (11,710 με), and slightly higher bottom-bar strains (12,973 με).

THEORETICAL PREDICTION AND ASSESSMENT

Strut-and-tie modelling (STM) is one of the most common methods used in analyzing disturbed regions or D-regions, wherein the strain does not vary linearly through the member's cross sections. In this study, two STM techniques were used to predict the shear capacity of the tested GFRP-reinforced geopolymer-short beams: the ACI 318-08[10] and CSA S806-12[11] STMs. The former model is normally adopted for steel-reinforced-concrete deep beams, while the latter is for FRP-reinforced-concrete deep beams. **Table 3** summarizes the STM stress limits for strut (f_{strut}), tie (f_{tie}), and node (f_{node}) for each design code. The ACI 318-08 STM technique depends mainly on concrete compressive strength and considers the transverse reinforcement effect through the factor β_s. It does not, however, specifically account for the influence of the orientation, type, and amount of the web reinforcement. The CSA S806-12 STM technique, on the other hand, is an MCFT-based approach that is predominantly influenced by the concrete strength and the axial stiffness of the longitudinal reinforcement. This model does not account for the influence of stirrups. For the models used in this study, ε_f was approximated as $0.5\varepsilon_{frp}$, since adopting a strain value of ε_f equivalent to ε_{frp} would lead to overly conservative estimates. **Figure 5** shows the single-panel STM adopted in the study: a pin-jointed truss consisting of the compression struts and tension tie. The variables h_a and h_b are depths of the bottom and top nodes, respectively, while l_a and l_b are the widths of the support and loading plates, respectively. This model, coupled with the iteration procedure suggested by Andermatt and Lubell,[39] was used to calculate the shear

capacities of the tested short beams. The parameter h_a was assumed to be twice the distance of the centroid of the reinforcement to the bottom of the beam. The inclination angle θ and the corresponding diagonal strut width w_{st} were computed from Equations 3 and 4, respectively. The equations in JSCE 2007[12] and the kinematic model proposed by Mihaylov et al.[13] for RC deep beams—shown in **Table 4**—were also used. Due to inherent differences in the properties of GFRP and steel bars, some parameters were modified so that these prediction equations could be applied in the proposed system. Furthermore, the shear contribution of dowel action was excluded in the prediction due to the relatively low shear strength of the GFRP bars.

Table 5 depicts the experimental-to-predicted shear capacity ratio (V_n/V_{n*}). Among these equations, the CSA S806-12 STM yielded the most conservative predictions (a value greater than 1.0 indicates a conservative estimation). Employing this technique, however, may yield largely uneconomical sections. Furthermore, this method assumes a tie strain of 0.002 for computing the CSA efficiency factor. If a higher strain value is assumed, however, the CSA model predictions are even more conservative. It should be noted that a strain of 0.002 is intended to represent strain in steel reinforcement. The strains in the FRP reinforcement were much higher than 0.002 due to the material's lower elastic modulus. The strain in FRP bars is typically higher than in steel reinforcement at similar stress levels, so the CSA S806-12 model does not appear suitable for the proposed system.[40] The ACI 318-08 STM, in general, gave the most accurate predictions, particularly in predicting the shear behavior of short beams with stirrups. Mihaylov's kinematic model also yielded nearly accurate predictions. The ACI 318-08 STM, which does not account for the variations in the type and spacing of transverse reinforcement, therefore seems to be the most appropriate method for predicting the strength of the tested short beams. The JSCE-07 model, on the other hand, yielded the most accurate prediction of the shear strength of the short beam without stirrups. As can be

expected, all the considered equations overestimated the shear capacity of the slender beam because these equations considered the strength enhancement due to arching action.

Table 3 – The ACI 318-08 and CSA S806-12 STM provisions

ACI 318-08[10]		CSA S806-12[11]	
$f_{strut} = 0.85\beta_s f_c^{'}$	(1-1)	$f_{strut} = \Phi_c f_c^{'} / \left(0.8 + 170\varepsilon_1\right) \le 0.85\Phi_c f_c^{'}$	(2-1)
		$\varepsilon_1 = \varepsilon_f + \left(\varepsilon_f + 0.002\right)\cot^2\theta$	(2-2)
		$\varepsilon_f = 0.5\varepsilon_{frp}$	(2-3)
$f_{node} = 0.85\beta_n f_c^{'}$	(1-2)	$f_{node} = \beta_n \Phi_c f_c^{'}$	(2-4)
		$f_{tie} = 0.65\Phi_f f_{fu}$	(2-5)

where: β_n = factor that accounts for the effect of anchorage ties on the effective compressive strength of the nodal zone; β_s = factor that accounts for the effect of cracking and confining reinforcement ratio within the strut; Φ_c and Φ_f = resistance factor for concrete and FRP reinforcement, respectively; ε_1 = principal tensile strain crossing the strut; and ε_f = tensile tie strain crossing the concrete strut centerline

Table 4 – The JSCE-07 and kinematic-model provisions for deep beams

JSCE-07[12]		Kinematic Model[13]	
$V_{n*} = V_c + V_{sf}$	(5-1)	$V_{n*} = V_{ci} + V_{CLZ} + V_s + V_d$	(6-1)
$V_c = \left(\beta_d + \beta_w\right)\beta_p\beta_a f_{dd} bd / \gamma_b$	(5-2)	$V_{ci} = 0.18\sqrt{f_c^{'}} \Big/ \left[0.31 + 24w / \left(a_{ge} + 16\right)\right]$	(6-2)
$\beta_d = \sqrt[4]{1000/d} \le 1.5$	(5-3)	$V_{CLZ} = k_1 f_{avg} b l_b \sin^2\alpha_1$	(6-3)
$\beta_w = 4.2\sqrt[3]{100\rho_{fv}}\left(a/d - 0.75\right) / \sqrt{f_c^{'}}$	(5-4)	$V_s = \rho_{fv} b\left(d\cot\alpha_1 - l_o - 1.5l_b\right) f_{fv}$	(6-4)
$\beta_p = \left(1 + \sqrt{100\rho_f}\right) / 2 \le 1.5$	(5-5)	$w = \Delta_c \cos\left(\alpha_o\right)$	(6-5)
$\beta_a = 5 / \left[1 + \left(a/d\right)^2\right]$	(5-6)	$\alpha_o = \tan^{-1}\left[d / \left(s_{\max} + 1.5l_b\right)\right]$	(6-6)
$f_{dd} = 0.19\sqrt{f_c^{'}}$	(5-7)	$\Delta_c = 0.0105 l_b \cot\alpha_1$	(6-7)
$V_s = \varphi V_d \quad (5-8)$	(5-8)	$s_{\max} = \left[0.28\phi_f / \rho_f\right]\left[2.5\left(h-d\right)/d\right]$	(6-8)
$\varphi = -0.17 + 0.3\left(a/d\right) + 0.33/\rho_{fv} \le 1.0$	(5-9)	$f_{avg} = 1.43 f_c^{'0.8}$	(6-9)
$V_d = \left[A_{fv} E_{fv} \varepsilon_{fv}\left(\sin\alpha + \cos\alpha\right)/s\right] z/\gamma_b$	(5-10)	$l_o = 1.5\left(h-d\right)\cot\alpha \ge s_{\max}$	(6-10)
		$\varepsilon_{fv} = 1.5\Delta_c / 0.9d$	(6-11)

where: a_{ge} = effective aggregate size that equals the coarse aggregate maximum size a_g for concrete strengths less than 60 MPa (8.70 ksi) and is zero for strengths greater than 70 MPa (10.15 kasi); A_{fv} = total area of the transverse steel or GFRP reinforcement (mm^2); d_v = effective shear depth (mm); f_{avg} = average compressive stress in the critical loading zone (MPa); f_{fv} = stress in the steel or GRRP stirrups (MPa); f_{ye} = effective yield strength of the bars and can be taken as the yield strength of the bars f_y and not more than 500 MPa (72.52 ksi) (MPa); k_1 = crack-shape coefficient; l_k = dowel length (mm); s_{max} = spacing of the radial cracks at the bottom section (mm); V_{ci} = shear contribution of the aggregate interlock; V_{CLZ} = shear contribution of the critical loading zone; V_d = shear contribution of the dowel action; w = crack width (mm); z = distance between points of action of the tensile and compressive resultant forces; equal to d/1.15 (mm); α = angle between the stirrups and the beam longitudinal axis; α_o = angle of the critical crack to the longitudinal axis of the beam at shear failure; α_1 = angle of line extending from the inner edge of support plate to the far edge of the loading plate's tributary area; Δ_c = vertical displacement of the critical loading zone (mm); ε_{fv} = strain in the transverse reinforcement; and γ_b = safety factor.

Table 5 – Experimental-shear-capacity-to-predicted-shear-capacity ratio (V_n/V_{n*})

Beam	Strut-and-Tie Model		JSCE-07	Kinematic Model
	ACI 318-08	CSA S806-12		
GG-1.8	0.667	1.176	0.997	0.711
GG-1.8-G-75	1.014	2.048	1.402	0.854
GG-1.8-G-100	1.082	2.184	1.567	0.988
GG-1.8-G-125	0.864	1.744	1.295	0.830
GG-1.8-G-150	1.058	2.136	1.629	1.055
GG-1.8-S-150	1.054	2.128	1.623	1.051
GG-4.7-G-100	0.483	0.976	0.700	0.482
Average (a/d=1.8)	0.957	1.903	1.419	0.915
STD (a/d=1.8)	0.162	0.390	0.246	0.151

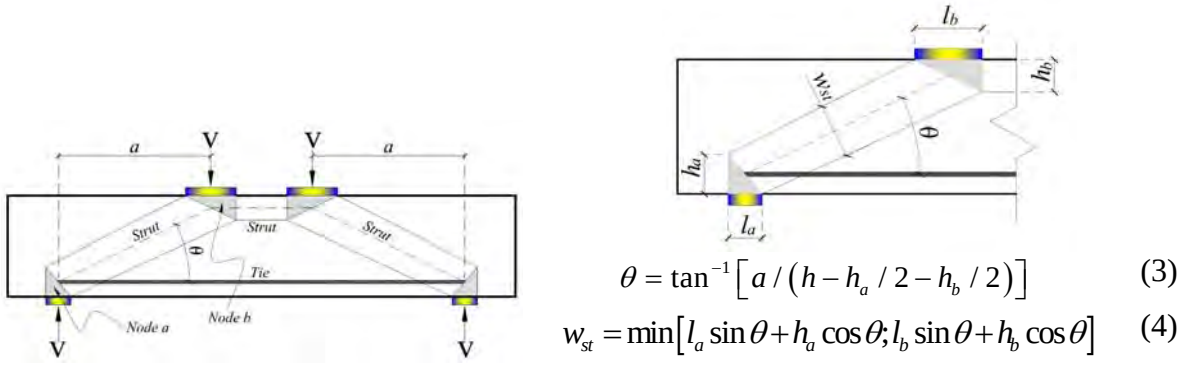

$$\theta = \tan^{-1}\left[a/\left(h - h_a/2 - h_b/2\right)\right] \quad (3)$$

$$w_{st} = \min\left[l_a \sin\theta + h_a \cos\theta; l_b \sin\theta + h_b \cos\theta\right] \quad (4)$$

a. truss model b. node and strut dimension

Fig. 5 – *Strut-and-tie model adopted in this study.*

COMPARISON WITH FRP-RC DEEP/SHORT BEAMS

Figure 6 shows the average normalized shear strength (v_n) of the tested GFRP-RGC short beams and the published results on FRP-RC deep/short beams with (right) and without (left) transverse reinforcement. The normalized value was obtained by dividing the ultimate shear load V_n (N) with the square root of f'_c (MPa), b (mm), and d (mm). The considered FRP-RC beams[17,29,30,41-49] had f'_c, b, d, ρ_f, ρ_{fv}, and a/d ranging from 22.9 MPa (3.32 ksi) to 74.2 MPa (10.76 ksi), 150 mm (5.91 in.) to 310 mm (12.20 in.), 225 mm (8.86 in.) to 891 mm (35.08 in.) 0.38% to 1.90%, 0.35% to 1.48%, and 1.44 to 2.50, respectively. Furthermore, all these beams exhibited a shear failure. From the figure, it is apparent that the tested short beams generally outperformed the FRP-RC deep beams with and without transverse reinforcement,

thereby suggesting the suitability of the proposed system for the fabrication of structural deep beams.

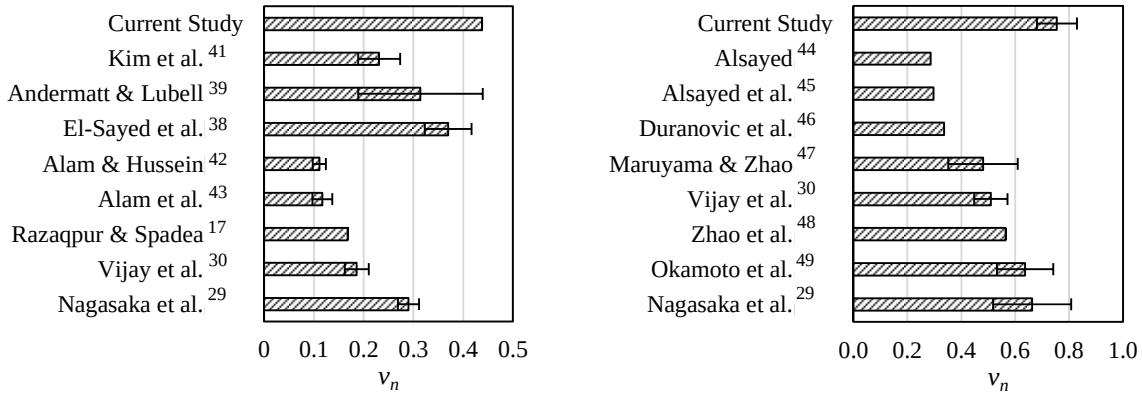

a. without stirrups b. with stirrups

Fig. 6 – *Normalized shear strength of GFRP-RGC and FRP-RC deep/short beams.*

CONCLUSIONS

This study investigated the shear performance of GFRP-reinforced geopolymer-concrete (GFRP-RGC) beams using the four-point static-bending test. From the experimental results, the following conclusions can be made:

1. The use of GFRP stirrups enhanced the shear strength of the GFRP-RGC beams with a *a*/*d* of 1.8 by approximately 200%, owing to the stirrups' contribution to vertical shear resistance and a clamping effect that enhanced the geopolymer-concrete's contribution to shear resistance. Furthermore, the shear-crack width also decreased with the use of web reinforcement.
2. The spacing of the GFRP stirrups had some effect on the initiation of shear cracking in the GFRP-RGC beams with a *a*/*d* of 1.8. The shear crack initiated at a higher load in beams with stirrups at narrower spacing. Similarly, lower strains were recorded in stirrups at narrower spacing at similar applied loads, suggesting the shear contribution of GFRP stirrups before final failure.

3. The shear-crack width decreased as the amount of web reinforcement increased. This could be due to the lower effective concrete area needed to be controlled by a stirrup in terms of the development of shear-crack width, thereby resulting in a higher bond adhesion between the stirrup and the surrounding geopolymer concrete.
4. The use of web reinforcement in excess of 0.48% did not enhance the shear strength of the GFRP-RGC beams with a a/d of 1.8. Similar phenomenon was also reported for the FRP-RC deep beams. Further studies, however, should be conducted to validate this generalization and to determine the possible range of a/d and the corresponding minimum amount of web reinforcement that could be adopted for the proposed system.
5. The shear-crack width of the short beams with GFRP stirrups was greater than that of the beam with steel stirrups, owing to the lower elastic modulus of GFRP bars compared to the steel bars.
6. The tested short and slender beams failed in a brittle manner, owing to the brittle nature of GFRP bars and geopolymer concrete. Hence, for future studies, it is recommended to use hybrid GFRP-steel longitudinal reinforcement to enhance beam ductility while, at the same time, maintaining beam durability properties.
7. Increasing the reinforcement ratio by 11% (from 1.50% to 1.66%) increased the load-carrying capacity by an average of 22%. This could be due to the enhancement of the diagonal strut strength—the governing failure—which increased the transferred shear forces through arch action.
8. The short beams yielded higher shear strength compared to the slender beam, owing to the strength enhancing effects of arching action in short beams.
9. Since the beam with GFRP stirrups yielded similar shear strength and deflection capacity, including an analogous load–deflection response, compared to the beam

with steel stirrups, the transverse reinforcement type was not a factor in an arch-action mechanism or, ultimately, in the shear strength of the GFRP-RGC short beams. Hence, it can be asserted that the GFRP stirrups could be a viable substitute for steel stirrups as web reinforcement for GFRP-RGC beams.

10. Among the design equations employed in the study, the CSA S806-12 STM gave the most conservative estimates of the shear capacity of the GFRP-RGC short beams, while the ACI 318-08 STM yielded the most accurate predictions.
11. The average normalized shear capacity of the tested GFRP-RGC short beams was higher than that of the FRP-RC deep beams, suggesting the suitability of the proposed system for the fabrication of structural deep/short beam members.

ACKNOWLEDGEMENTS

The authors would like to express their special thanks to V-ROD® Australia for providing the materials as well as to the Natural Science and Engineering Research Council of Canada (NSERC), and the technical staff of the Centre of Excellence in Engineered Fibre Composites (CEEFC) at University of Southern Queensland.

REFERENCES

1. Balendran RV, Rana TM, Maqsood T, Tang WC, "Application of FRP Bars as Reinforcement in Civil Engineering Structures," *Structural Survey*, V. 20, No. 2. 2002, pp. 62-72.

2. Malhotra VM, "Introduction: Sustainable Development and Concrete Technology," *ACI Concrete International*, V. 24, No. 7. 2002, pp. 22.

3. McLellan BC, Williams RP, Lay J, van-Riessen A, Corder GD, "Costs and Carbon Emissions for Geopolymer Pastes in Comparison to Ordinary Portland Cement," *Journal of Cleaner Production*, V. 19, No. 9-10. 2011, pp. 1080-90.

4. Gangarao HVS, Taly N, Vijay PV, "Reinforced Concrete Design with FRP Composites." Florida, USA: CRC Press; 2007.

5. Kong DLY, Sanjayan JG, "Effect of Elevated Temperatures on Geopolymer Paste, Mortar and Concrete," *Cement and Concrete Research*, V. 40, No. 2. 2010, pp. 334-9.

6. Duxson P, Provis JL, Lukey GC, Van Deventer JS, "The Role of Inorganic Polymer technology in the Development of 'Green Concrete'," *Cement and Concrete Research*, V. 37, No. 12. 2007, pp. 1590-7.

7. Diaz-Loya EI, Allouche EN, Vaidya S, "Mechanical Properties of Fly-Ash-Based Geopolymer Concrete," *ACI Materials Journal*, V. 108, No. 3. 2011, pp. 300-6.

8. Pacheco-Torgal F, Abdollahnejad Z, Camões A, Jamshidi M, Ding Y, "Durability of Alkali-Activated Binders: A Clear Advantage Over Portland Cement or an Unproven Issue?," *Construction and Building Materials*, V. 30. 2012, pp. 400-5.

9. Vasconcelos E, Fernandes S, de Aguiar JB, Pacheco-Torgal F, "Concrete Retrofitting Using Metakaolin Geopolymer Mortars and CFRP," *Construction and Building Materials*, V. 25, No. 8. 2011, pp. 3213-21.

10. ACI Committee 318, "Building Code Requirements for Structural Concrete (ACI 318-08) and Commentary," American Concrete Institute, Farmington Hills, MI, 2008, pp. 379-93.

11. CAN/CSA S806-12, "Design and Construction of Building Components with Fibre-Reinforced Polymers," *Canadian Standards Association*, Rexdale, ON, Canada, 2012, pp. 35-6.

12. JSCE 2007, "Standard Specifications for Concrete Structures," *Japan Society of Civil Engineers*, Tokyo, Japan, 2007.

13. Mihaylov BI, Bentz EC, Collins MP, "Two-Parameter Kinematic Theory for Shear Behavior of Deep Beams," *ACI Structural Journal*, V. 110, No. 3. 2013, pp. 447-55.

14. Benmokrane B, Chaallal O, Masmoudi R, "Glass Fibre Reinforced Plastic (GFRP) Rebars for Concrete Structures," *Construction and Building Materials*, V. 9, No. 6. 1995, pp. 353-64.

15. El-Nemr A, Ahmed EA, Benmokrane B, "Flexural Behavior and Serviceability of Normal- and High-Strength Concrete Beams Reinforced with Glass Fiber-Reinforced Polymer Bars," *ACI Structural Journal*, V. 110, No. 6. 2013, pp. 1077-88.

16. Kassem C, Farghaly AS, Benmokrane B, "Evaluation of Flexural Behavior and Serviceability Performance of Concrete Beams Reinforced with FRP Bars," *Journal of Composites for Construction*, V. 15, No. 5. 2011, pp. 682-95.

17. Razaqpur AG, Spadea S, "Shear Strength of FRP Reinforced Concrete Members with Stirrups," *Journal of Composites for Construction*, V. 19, No. 1, February 2015. 2015, pp. 04014025.

18. Ahmed EA, El-Salakawy EF, Benmokrane B, "Performance Evaluation of Glass Fiber-Reinforced Polymer Shear Reinforecment for Concrete Beams," *ACI Structural Journal*, V. 107, No. 1. 2010, pp. 53-61.

19. Oller E, Marí A, Bairán JM, Cladera A, "Shear Design of Reinforced Concrete Beams with FRP Longitudinal and Transverse Reinforcement," *Composites Part B: Engineering*, V. 74. 2015, pp. 104-22.

20. CAN/CSA S807-10, "Specification for Fibre-Reinforced Polymers," *Canadian Standards Association*, Rexdale, ON, Canada, 2010, pp. 44.

21. ASTM C39/C39M-04, "Standard Test Method for Compressive Strength of Cylindrical Concrete Specimens," *ASTM International*, West Conshohocken, PA, 2004.

22. ASTM C496/C496M-11, "Standard Test Method for Splitting Tensile Strength of Cylindrical Concrete Specimens," *ASTM International*, West Conshohocken, PA, 2011.

23. Maranan G, Manalo A, Benmokrane B, Karunasena W, Mendis P, "Evaluation of the Flexural Strength and Serviceability of Geopolymer Concrete Beams Reinforced with Glass-Fibre-Reinforced Polymer (GFRP) Bars," *Engineering Structures*, V. 101. 2015, pp. 529-41.

24. Oehlers DJ, Mohamed Ali M, Haskett M, Lucas W, Muhamad R, Visintin P, "FRP-Reinforced Concrete Beams: Unified Approach Based on IC Theory," *Journal of Composites for Construction*, V. 15, No. 3. 2010, pp. 293-303.

25. Mohamed K, Farghaly AS, Benmokrane B, "Effect of Web Reinforcement in FRP-Reinforced Deep beams," *Proceedings of the 7th International Conference on FRP Composites in Civil Engineering (CICE 2014)*, 20-22 August 2014, Vancouver, Canada, pp. 79.

26. Zakaria M, Ueda T, Wu Z, Meng L, "Experimental Investigation on Shear Cracking Behavior in Reinforced Concrete Beams with Shear Reinforcement," *Journal of Advanced Concrete Technology*, V. 7, No. 1. 2009, pp. 79-96.

27. El-Sayed AK, El-Salakawy EF, Benmokrane B, "Shear Strength of Fibre-Reinforced Polymer Reinforced Concrete Deep Beams Without Web Reinforcement," *Canadian Journal of Civil Engineering*, V. 39, No. 5. 2012, pp. 546-55.

28. Sagaseta J, Vollum RL, "Shear Design of Short-Span Beams," *Magazine of Concrete Research*, V. 62, No. 4. 2010, pp. 267-82.

29. Nagasaka T, Fukuyama H, Tanigaki M, "Shear Performance of Concrete Beams Reinforced with FRP Stirrups," *ACI Special Publication*, V. 138. 1993, pp. 789-812.

30. Vijay PV, Kumar SV, Gangarao HVS, "Shear and Ductility Behaviour of Concrete Beams Reinforced with GFRP Rebars," *Proceedings of the 2nd International Conference on Advanced Composite Materals in Bridges and Structures (ACMBS-2) Canadian Society of Civil Engineering (CSCE 2009) Annual General Conference*, 11-14 August 1996, Montreal, Quebec, Canada, pp. 217-26.

31. Birrcher DB, Tuchscherer RG, Huizinga M, Bayrak O, "Minimum Web Reinforcement in Deep Beams," *ACI Structural Journal*, V. 110, No. 2. 2013, pp. 297-306.

32. Farghaly AS, Benmokrane B, "Shear Behavior of FRP-Reinforced Concrete Deep Beams Without Web Reinforcement," *Journal of Composites for Construction*, V. 17, No. 6. 2013, pp. 04013015.

33. Yost JR, Gross SP, Dinehart DW, "Shear strength of normal strength concrete beams reinforced with deformed GFRP bars," *Journal of Composites for Construction*, V. 5, No. 4. 2001, pp. 268-75.

34. Rebeiz KS, "Shear Strength Prediction for Concrete Members," *Journal of Structural Engineering*, V. 125, No. 3. 1999, pp. 301-8.

35. Stratford T, Burgoyne C, "Shear Analysis of Concrete with Brittle Reinforcement," *Journal of Composites for Construction*, V. 7, No. 4. 2003, pp. 323-30.

36. CAN/CSA S6-06, "Canadian Highway Bridge Design Code," *Canadian Standards Association*, Rexdale, ON, Canada, 2006.

37. ACI Committee 2006, "Guide for the Design and Construction of Structural Concrete Reinforced with FRP Bars," *American Concrete Institute*, City, Farmington Hills, MI, 2006.

38. CAN/CSA S6-14, "Canadian Highway Bridge Design Code," *Canadian Standards Association*, Rexdale, ON, Canada, 2014.

39. Andermatt MF, Lubell AS, "Strength Modeling of Concrete Deep Beams Reinforced with Internal Fiber-Reinfored Polymer," *ACI Structural Journal*, V. 110, No. 4. 2013, pp. 595-605.

40. Nehdi M, Omeman Z, El-Chabib H, "Optimal Efficiency Factor in Strut-and-Tie Model for FRP-Reinforced Concrete Short Beams with (1.5<a/d<2.5)," *Materials and Structures*, V. 41. 2008, pp. 1713-27.

41. Kim D-J, Lee J, Lee YH, "Effectiveness Factor of Strut-and-Tie Model for Concrete Deep Beams Reinforced with FRP Rebars," *Composites Part B: Engineering*, V. 56. 2014, pp. 117-25.

42. Alam MS, Hussein A, "Effect of Member Depth on Shear Strength of High-Strength Fiber-Reinforced Polymer–Reinforced Concrete Beams," *Journal of Composites for Construction*, V. 16, No. 2. 2012, pp. 119-26.

43. Alam M, Hussein A, Ebrahim EAA, "Shear Strength of Concrete Beams Reinforced with Glass Fibre Reinforced Polymer (GFRP) Bars," *Proceedings of the Canadian Society of Civil Engineering (CSCE 2009) Annual General Conference*, 27-30 May 2009, St. John's, NL, Canada, V. 2, pp. 874-82.

44. Alsayed SH, "Flexural Behaviour of Concrete Beams Reinforced with GFRP Bars," Cement and Concrete Composites, V. 20, No. 1. 1998, pp. 1-11.

45. Alsayed SH, Al-Salloum YA, Almusallam TH, "Shear Design for Beams Reinforced by GFRP Bars," *Proceedings of the Third International Symposium on Non-Metallic (FRP) Reinforcement for the Concrete Structures (FRPRCS-3)*, 14-16 October 1997, Sapporo, Japan, V. 2, pp. 285-92.

46. Duranovic N, Pilakoutas K, Waldron P, "Tests on Concrete Beams Reinforced with Glass Fibre Reinforced Plastic Bars," *Proceedings of the Third International Symposium on Non-Metallic (FRP) Reinforcement for the Concrete Structures (FRPRCS-3)*, 14-16 October 1997, Sapporo, Japan, V. 2, pp. 479-86.

47. Maruyama K, Zhao W, "Size Effect in Shear Behavior of FRP Reinforced Concrete Beam," *Proceedings of the 2nd International Conference on Advanced Composite Materials in Bridges and Structures (ACMBS-2)*, 11-14 August 1996, Montreal, Quebec, Canada, pp. 227-34.

48. Zhao W, Maruyama K, Suzuki H, "Shear Behavior of Concrete Beams Reinforced by FRP rods as Longitudinal and Shear Reinforcement," *Proceedings of the Second International Symposium on Non-Metallic (FRP) Reinforcement for the Concrete Structures (FRPRCS-2)*, 23-25 August 1995, Ghent, Belgium, V. 29, pp. 352.

49. Okamoto T, Nagasaka T, Tanigaki M, "Shear Capacity of Concrete Beams Using FRP Reinforcement," *Journal of Structural and Construction Engineering*, No. 455. 1994, pp. 27-136.

3.5. Paper V: Behavior of concentrically loaded geopolymer concrete columns reinforced longitudinally and transversely with GFRP bars

This paper presents the investigation of the behaviour of concentrically loaded geopolymer-concrete circular columns reinforced longitudinally and transversely with GFRP bars. In addition to the materials properties specified in section "2.1 Materials" of **Paper V**, the typical stress-strain curve of the geopolymer concrete, labelled as **Figure 3** in section "2.1.2 Geopolymer Concrete" of **Paper V**, is provided in **Figure B.4** of **Appendix B** of the thesis. The columns tested in this study are large-scale specimens to simulate the behaviour of actual structure and fabricated based on maximum clearance and capacity limitations of the testing equipment. Nonetheless, testing these specimens allowed the thorough evaluation of several critical test parameters that affects the behaviour of concrete columns such as the contribution of stirrup, stirrup spacing, stirrup type, and slenderness ratio. Currently, there is no design guidelines that specify the minimum and maximum spacing of FRP ties for FRP-reinforced concrete (FRP-RC) columns. Hence, aside from 50 mm spacing, a spiral pitch of 100 mm was adopted in this paper for comparison purposes. This spacing was higher than the maximum clear spacing limit specified by ACI 318-08 in Section 7.10.4.3 for RC spiral column (clear spacing=76.2 mm (3 inches)), but, was more conservative compared to the ACI and AS limits for conventional RC tied column (e.g. 16 times bar diameter=254.4 mm (ACI 318) or 15 times bar diameter=238.5mm (AS 3600)), 48 times lateral tie diameter=456 mm, and the least column dimension=250 mm).

From the experimental results, the provision of closely spaced GFRP ties or spiral enhanced both the strength and ductility of the unconfined columns. The confinement effect of GFRP spirals, however, was more effective than that of the GFRP ties, owing to the continuous nature of spirals that evenly distributed the stresses along and around the concrete core. A notable observation from the paper is that the column with spiral pitch of 100 mm yielded almost similar compression capacity and stiffness as the column with spiral of 50 mm, suggesting the suitability of spiral pitch of 100 mm for adoption in the GFRP-RGC column. In addition, the longitudinal GFRP bars provided a notable compression contribution. However, these bars exhibited a plateau behaviour due to the local buckling after the spalling of the concrete cover. Finally, the results obtained from this paper suggested that the GFRP-RGC system could be adopted as compression members, particularly when corrosion resistance, material greenness, durability, and sustainability are sought.

Engineering Structures 117 (2016) 422–436

Contents lists available at ScienceDirect

Engineering Structures

journal homepage: www.elsevier.com/locate/engstruct

Behavior of concentrically loaded geopolymer-concrete circular columns reinforced longitudinally and transversely with GFRP bars

G.B. Maranan [a], A.C. Manalo [a,*], B. Benmokrane [b], W. Karunasena [a], P. Mendis [c]

[a] Centre of Excellence in Engineered Fibre Composites (CEEFC), Faculty of Health, Engineering and Sciences (FoHES), University of Southern Queensland, Toowoomba 4350, Australia
[b] Department of Civil Engineering, University de Sherbrooke, Sherbrooke, Quebec J1K 2R1, Canada
[c] Department of Infrastructure Engineering, The University of Melbourne, Victoria 3010, Australia

ARTICLE INFO

Article history:
Received 22 November 2015
Revised 11 March 2016
Accepted 14 March 2016

Keywords:
Geopolymer-concrete columns
Glass–fiber-reinforced polymer (GFRP) bars
Short columns
Slender columns
Hoops
Spirals

ABSTRACT

The behavior of concentrically loaded geopolymer-concrete circular columns reinforced longitudinally and transversely with glass–fiber-reinforced-polymer (GFRP) bars was investigated. Six full-scale short columns ($L/r = 8$) were cast: one column without transverse reinforcement; three columns with circular hoops spaced at 50 mm, 100 mm, and 200 mm on centers; and two columns with spirals spaced at 50 mm and 100 mm on centers. In addition, two slender columns ($L/r = 16$) transversely reinforced with hoops and spirals both spaced at 100 mm on centers were fabricated. Based on the experimental results, the GFRP bars contributed an average of 7.6% to the overall capacity of the tested columns. The hoop- and spiral-confined slender columns failed at a load equal to 66% and 82%, respectively, of the strength of their counterpart short columns. Irrespective of the tie configuration, the columns with higher volumetric ratios showed better compressive behavior than those with lower volumetric ratios. The ductility and confinement efficiency of the spiral-confined columns were higher than that of their counterpart hoop-confined columns. The tested columns yielded relatively superior compression performance compared to OPC-based concrete columns reinforced with GFRP bars and ties. Further studies dealing with the behavior and slenderness limit in GFRP-reinforced geopolymer concrete slender columns are recommended to increase its uptake in the construction industry.

1. Introduction

Fiber-reinforced-polymer (FRP) bars and geopolymer concrete have been increasingly used in the construction industry because of their many advantageous properties. Aside from being innately corrosion resistant, FRP bars are lightweight (20–25% of steel's density), have superior tensile strength (two to three times that of steel's yield strength), have high fatigue endurance, and are electromagnetically neutral [1–3], making them suitable as internal reinforcement for concrete structures. Geopolymer concrete, on the other hand, is a "green" material because it utilizes a geopolymer binder, rather than cement binder, that can be manufactured by the reaction of an alkaline liquid – normally a mixture of sodium silicate and sodium hydroxide solution – with industrial waste materials that are rich in silica and alumina, like fly ash (FA) and blast-furnace slag (BFS) [4,5]. Davidovits [6] coined the generic term "geopolymer" because the chemical reaction taking place is a geopolymerization process wherein a large amount of amorphous alumino-silicate oxides reacts with alkali polysilicates yielding a polymeric Si–O–Al bonds. Geopolymers are intrinsically fire and chemical resistant, have excellent thermal stability, and exhibit low shrinkage and creep, owing to their inorganic framework [7]. Furthermore, a number of studies have shown that geopolymer concrete has mechanical properties that are either comparable or superior to that of normal concrete of the same grade [8–10]. While there are significant studies on the flexural and shear behavior of FRP-reinforced concrete (FRP-RC) [11–19], steel-reinforced geopolymer-concrete (S-RGC) [20–25] systems, and FRP-reinforced geopolymer concrete (FRP-RGC) [26,27], relatively few studies are available that deal with the behavior of compression members comprised of these systems [28]. In fact, among the current design guidelines and codes of practice for FRP-RC systems, only the Japan Society of Civil Engineers (JSCE) has established a design procedure for FRP-RC columns [29]. The ACI 440.1R-06 [30] does not recommend the use of FRP bars in columns while the CSA S806-12 [31] ignores the compression contribution of FRP bars, owing to their low compression contribution.

* Corresponding author. Tel.: +61 7 4631 2547; fax: +61 7 4631 2110.
E-mail addresses: ginghis.maranan@usq.edu.au (G.B. Maranan), allan.manalo@usq.edu.au (A.C. Manalo), Brahim.Benmokrane@USherbrooke.ca (B. Benmokrane), karu.karunasena@usq.edu.au (W. Karunasena), pamendis@unimelb.edu.au (P. Mendis).

http://dx.doi.org/10.1016/j.engstruct.2016.03.036
0141-0296/

Nomenclature

A_b	nominal area of the GFRP bars (mm^2)
A_f	total area of the longitudinal GFRP reinforcement (mm^2)
A_g	gross cross-sectional area of the column (mm^2)
A_{ft}	cross-sectional area of the transverse reinforcement (mm^2)
D	column diameter (mm)
D_c	concrete-core diameter delineated by the outside diameter of hoops or spirals (mm)
E_c	modulus of elasticity of the concrete (MPa)
E_f	tension modulus of the GFRP bars (MPa)
E_f'	compression modulus of the GFRP bars (MPa)
E_{sec}	tangent modulus of elasticity of the concrete (MPa)
EI	flexural stiffness of the reinforced-concrete column
f_{fu}	tensile strength of the GFRP bars (MPa)
f_{fu}'	ultimate compressive stress in the GFRP bars (MPa)
f_c'	concrete compressive strength (MPa)
f_{cc}'	confined-column compressive strength (MPa)
f_{co}'	unconfined-column in-place compressive strength, $0.9f_c'$ (MPa)
f_{lGFRP}'	maximum confinement pressure
I_{se}	moment of inertia of reinforcement about members' centroidal axis (mm^4)
k	effective length factor
k_a	efficiency factor that accounts for the geometry of the section, taken as 1.0 for circular sections
k_e	efficiency factor that accounts for the premature failure of the FRP system
L	column height (mm)
L/r	slenderness ratio
L_{uf}	unsupported length of GFRP bars (mm)
m	parameter that controls the initial slope and curvature of the ascending branch
n	number of longitudinal bars
P_c	concrete core capacity (N, kN)
P_{fc}	compression contribution of GFRP bars at P_c load level (N, kN)
P_{fg}	compression contribution of GFRP bars at P_g load level (N, kN)
P_g	gross capacity of the column (N, kN)
P_o	nominal capacity of the column (N, kN)
P_{peak}	peak capacity of the column (N, kN)
r	radius of gyration (mm)
r_f	radius of gyration of GFRP bars (mm)
s	circular hoop spacing or spiral pitch on-center (mm)
α_g	compressive-strength reduction of the GFRP bar as a function of its tensile strength
β_d	concrete creep factor (assumed equivalent to 1.0 in this study)
Δ_c	deformation at P_c load level (mm)
Δ_g	deformation at P_g load level (mm)
Δ_1	displacement that corresponds to the limit of the elastic behavior (mm)
Δ_{85}	displacement that corresponds to 85% of maximum load (mm)
ε_c	axial strain in geopolymer concrete (με)
ε_{cc}	axial strain in confined geopolymer concrete at f_{cc}' (με)
$\varepsilon_{0.50cc}$	axial strain in confined geopolymer concrete at $0.50f_{cc}'$ (με) in the descending branch of the stress–strain model
$\varepsilon_{0.85cc}$	axial strain in confined geopolymer concrete at $0.85f_{cc}'$ (με) in the descending branch of the stress–strain model
ε_{cg}	average axial concrete strain at P_g load level (με)
$\varepsilon_{cg\text{-}ave}$	average of ε_{cg} (με)
ε_{co}	axial strain in unconfined geopolymer concrete corresponding to f_{co}' (με)
ε_f	ultimate tensile strain of the GFRP bars
ε_{fc}	average strain in the longitudinal GFRP bars at P_c load level (με)
ε_{fg}	average strain in the longitudinal GFRP bars at P_g load level (με)
$\varepsilon_{fg\text{-}ave}$	average of ε_{fg} (με)
ε_{ftg}	average tie strain at P_g load level (με)
ε_{ftc}	average tie strain at P_c load level (με)
ε_{ftcc}	tie strain at f_{cc}' (με)
ε_{ft}	ultimate tensile strain of the transverse reinforcement (με)
γ_b	safety factor
μ	ductility index
ϕ_f	nominal diameter of the GFRP bars (mm)
ρ_f	longitudinal reinforcement ratio
ρ_{ft}	transverse reinforcement volumetric ratio

Moreover, design guidelines for S-RGC systems have yet to be established.

The strength and stiffness of glass-FRP (GFRP) bars in compression, based on earlier research [32–35], ranged from 30% to 70% and from 77% to 100%, respectively, of the tension values. Paramanantham [36] tested fourteen 200 × 200 × 1800 mm GFRP-reinforced beam columns and stated that the GFRP bar was stressed to up to 20–30% of its ultimate strength when subjected to pure compression. Based on fifteen 450 × 250 × 1200 mm columns, Alsayed et al. [37] reported that, irrespective of the tie type (steel or GFRP), replacing the longitudinal steel bars with an equal amount of GFRP bars reduced column capacity by 13%. The results of the experimental investigation conducted by De Luca et al. [29] and Tobbi et al. [38] on a number of square columns reinforced with GRFP bars and ties revealed that the longitudinal GFRP bars contributed 5–10% of column capacity. The series of studies conducted by Tobbi et al. [38–40] on a number of 350 × 350 mm concrete columns with GFRP bars and ties showed that (1) the GFRP bars could be used in compression members provided that there is sufficient confinement to eliminate bar buckling; (2) GFRP ties are effective in increasing the strength, toughness, and ductility of the confined concrete core; and (3) the strength-reduction factor of 0.85 and the equations used for conventional RC columns can be adopted for GFRP-RC columns with some modifications to account for the different mechanical properties of GFRP bars compared to steel bars. Pantelides et al. [28] tested two circular columns with internal GFRP spirals and vertical reinforcement under axial compressive loading to failure. The test results indicated that these columns achieved 84% of the axial load capacity of the all-steel control column. Afifi et al. [41] and Mohamed et al. [42] investigated the axial capacity of circular columns reinforced with GFRP bars and ties. Their study indicated that concrete columns reinforced with GFRP and steel bars behaved similarly, although the axial capacities of the GFRP-RC columns were, on the average, 7.0% lower than their counterpart steel-RC columns. Moreover, the experimental findings showed that GFRP hoops and spirals enhanced the ductility and effectively confined the concrete core in the post-peak stages. In conclusion, the research work cited indicates the suitability of concrete columns longitudinally and transversely reinforced with GFRP bars.

Some researchers have investigated the applicability of geopolymer concrete for reinforced columns. Sumajouw et al. [43,44] tested 12 slender fly-ash-based, geopolymer-concrete columns reinforced with steel bars. Their results showed that the column capacity increased when the longitudinal reinforcement and concrete compressive strength increased. Furthermore, they stated that the current design provisions for conventional concrete could be adopted for geopolymer concrete. Sarker [45] analyzed the behavior of geopolymer-concrete columns reinforced with steel bars. He recommended that the analytical method for conventional concrete columns could be used for geopolymer-concrete columns with the appropriate stress–strain relationship of geopolymer concrete. Sujatha et al. [46] tested a total of 12 slender geopolymer-concrete column specimens reinforced with M30 and M60 grade bars. The results showed that the geopolymer-concrete columns behaved similarly to OPC columns regardless of the concrete grade, with the geopolymer concrete yielding higher load and deflection capacities and more ductile behavior than OPC.

The studies cited above demonstrate that FRP bars and geopolymer concrete are suitable materials for compression members. Moreover, combining them would yield a more durable and more sustainable structural member with adequate strength and structural integrity. As of this writing, however, there have been only two studies that dealt with the bond behavior of FRP bars in geopolymer concrete [47,48], two research works about the structural behavior of FRP-RGC beams [26,27], and none about compression members. Thus, gaining an understanding of their structural performance is very important. This study investigated the compression behavior of geopolymer-concrete columns longitudinally and transversely reinforced with GFRP bars. The parameters considered were tie configuration (hoops and spirals), tie spacing, and slenderness ratio.

2. Experimental program

2.1. Materials

2.1.1. Longitudinal and transverse reinforcement

No. 5 high-modulus (HM) GFRP bars (CSA S807-10 [49]) with a nominal diameter of 15.9 mm (Fig. 1) were used to reinforce the circular column specimens in the longitudinal direction. No. 3 HM GFRP spirals and circular hoops with a nominal diameter of 9.5 mm (Fig. 2) were used to reinforce the corresponding columns transversely. These two types of lateral reinforcement are most commonly adopted for circular columns, and are the only currently available types of lateral FRP reinforcement in the market. The transverse reinforcement had an inner diameter of 180 mm. The hoops had an overlap length of 80 mm. The GFRP reinforcement was manufactured by pultruding E-glass fibers impregnated with modified vinyl-ester resin and had a sand-coated surface to enhance the bond and force transfer between the bars and the geopolymer concrete. Table 1 provides the mechanical properties of the reinforcement as reported by the manufacturer. The tensile properties of the bars were determined in accordance with the B.2 test method in ACI 440.3R-12 [50]. The tensile strength f_{fu} and elastic modulus E_f were calculated using the nominal cross-sectional area A_b. Currently, there is no standard method for determining the compressive strength of FRP bars since it is complicated due to the occurrence of fiber micro-buckling. Nevertheless, this study utilized five 15.9 mm GFRP bars, with a length of 50 mm, that were cut as flat as possible and were subjected to axial loads. Based on the test, the average compressive strength of the GFRP bars was 612.5 MPa, which was 51.7% of the bars' tensile strength. This strength ratio was comparable to that proposed by Deitz et al. [33] (50%), but was higher than that stated by Kobayashi and Fujisaki [34] (30–40%) for GFRP bars. In addition, this study assumed that the GFRP bars' elastic modulus in compression was similar to its elastic modulus in tension and that the tension and compression behavior of GFRP bars was linearly elastic up to failure. These assumptions were also reported by the previous researchers.

Fig. 1. 15.9 mm GFRP bars.

2.1.2. Geopolymer concrete

A commercially produced geopolymer concrete with a proprietary mixture consisting of fine and medium sands, 10 and 20 mm coarse aggregates, plasticizer, water, and a geopolymer binder resulting from the alkali activation of two industrial waste materials – class F fly ash (FA) and ground granulated blast-furnace slag (BFS) – were used to fabricate the column specimens. All the geopolymer concrete cylinders and column specimens were cured in an ambient condition. Fig. 3 shows the typical stress–strain curve of the geopolymer concrete with a 28-day compressive strength f_c' and modulus of elasticity E_c of 38 MPa and 33 GPa, respectively, as determined in accordance with ASTM C39/C39M-15a [51]. The average slump and setting time of the geopolymer concrete, following the ASTM C143/C143M-15 [52] and ASTM C807-13 [53], respectively, were 150 mm and 90 min, respectively. The unique feature of this geopolymer concrete is that the entire constituent materials can be mixed in a truck bowl and remain completely dormant until the activator chemicals are added [54]. The other mechanical properties of the geopolymer concrete were reported by Maranan et al. [26] and Aldred and Day [54].

2.2. Test specimens

Eight full-scale GFRP-RGC columns were cast and tested. One short column was fabricated without transverse reinforcement in the test region, which served as the control specimen. Three short columns reinforced with circular hoops uniformly spaced at 50, 100, and 200 mm on centers and two short columns reinforced with spirals spaced at 50 and 100 mm on centers were fabricated to investigate the influence of tie spacing and configuration. The specimen with spirals at 200 mm on centers was not considered in this study because this spacing caused the GFRP bars to buckle inward, yielding an almost hourglass-shaped reinforcement cage. In addition, two slender columns reinforced with circular hoops and spirals spaced at 100 mm on centers were produced to examine the slenderness effect. The short and slender columns had total heights (L) of 1.0 m and 2.0 m, respectively, yielding slenderness ratios (L/r) of 8 and 16, respectively. The L/r of 16 was practically equivalent to the slenderness limit of 17.2 suggested by Mirmiran [55], Mirmiran et al. [56], and Zadeh and Nanni [57]

(a) Circular hoops (b) Spirals

Fig. 2. 9.5 mm GFRP ties.

Table 1
Mechanical properties of the reinforcement.

Bar	ϕ_f (mm)	A_b (mm^2)	f_{fu}[a] (MPa)	E_f (GPa)	ε_f (%)
No. 3	9.5	71.3	1372	65.1 ± 2.5	2.11
No. 5	15.9	197.9	1184	62.6 ± 2.5	1.89

[a] Guaranteed tensile strength: average value – 3× standard deviation (ACI 440.3R-12 [42]).

for GFRP-reinforced concrete columns. Fig. 3 presents the specific details and configurations of the tested GFRP-RGC columns. All of the columns had a diameter of 250 mm and were reinforced with similar amounts of longitudinal reinforcement, consisting of six 15.9 mm GFRP bars, equivalent to 2.43% of the column's gross cross-sectional area (A_g). The column height was divided into a middle test region of 2L/3 and two end regions of L/6. The columns' end regions were strengthened with ties spaced at 50 mm on centers to make sure that failure occurred in the test region. Fig. 4 shows the actual configuration of the GFRP reinforcement cages. Fig. 5, on the other hand, shows the wooden framework and the plastic-tube formwork with cast column specimens.

Table 2 depicts the column specimen identification and the test matrix. The columns were labelled as follows: GGC-L/r-H(S)##. The first three letters (GGC) stand for "GFRP-reinforced geopolymer-concrete column" followed by the corresponding L/r. The next letter represents the type of transverse reinforcement: H for circular hoops and S for spirals. The ## sign represents the hoop center-to-center spacing or the spiral pitch in millimeters. For example, the specimen identified as GGC-8-H50 is a GFRP-reinforced geopolymer-concrete column with a L/r of 8 and transversely reinforced with 9.5 mm circular GFRP hoops spaced at 50 mm on centers. The specimen labelled as GGC-8-S50, on the other hand, is a GFRP-reinforced geopolymer-concrete column with a L/r of 8 and transversely reinforced with 9.5 mm GFRP spirals with a pitch of 50 mm on centers.

2.3. Test program and instrumentation

Fig. 6 shows the test setup and instrumentation employed to investigate the compression behavior of the GFRP-RGC column specimens. The columns were supported at both ends with two pairs of 10 mm thick steel collars/clamps, with an inner radius of 127 mm, to confine the top and bottom of the columns to prevent end crushing, thereby ensuring failure at the test region. Three-millimeter-thick neoprene rubber were also provided to fill the gaps between the clamps and specimens, thereby ensuring that the end regions were properly confined. The top and bottom ends were smoothened and levelled evenly during the casting process and were provided with 3 mm thick neoprene rubber during testing to ensure uniform distribution of the applied load across the cross section. Furthermore, chicken wire was placed around the column specimens for safety purposes.

Fig. 3 provides the location of the electrical strain gauges. Three strain gauges were mounted onto three longitudinal bars to

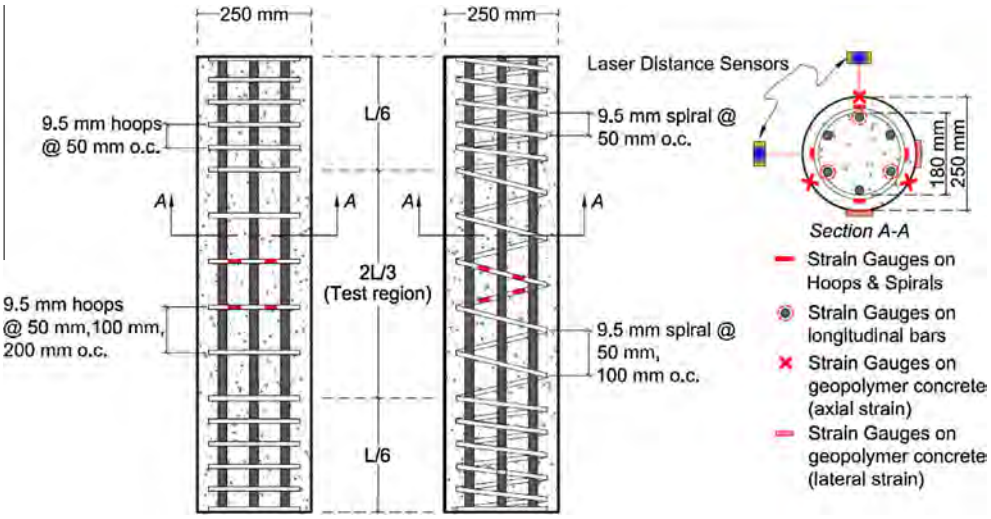

Fig. 3. Details and configuration of the column specimens.

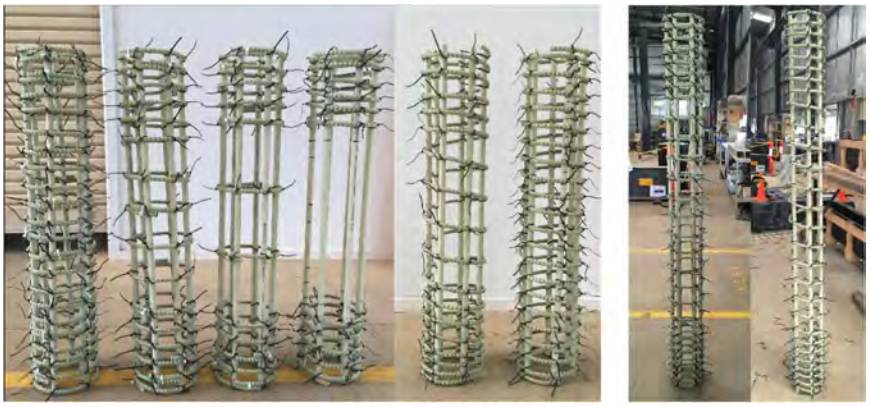

(a) for short columns (b) for slender columns

Fig. 4. Configuration of the GFRP reinforcement cages.

Fig. 5. Wooden framework and plastic formworks with cast column specimens.

capture their compression contribution. Another three strain gauges were attached to the geopolymer concrete to measure the concrete strain; the strain gauges were positioned/aligned with the strain gauges on the bars. Four strain gauges set 90° apart were also used to capture the strains in the transverse reinforcement. All the strain gauges were positioned at mid-height of the test region. Two laser displacement sensors (LDSs) set 90° apart were used to record the columns' lateral deformations and/or lateral deflections. The columns were subjected to monotonically increasing axial concentric loads and were loaded to failure in displacement control with a hydraulic jack to allow for the observation of both the pre- and post-peak behavior. The magnitude of the applied loads was measured with a 3000 kN capacity load cell, whereas the corresponding deformations were measured with a string pot. The strain, load, and deflection readings were recorded with a data logger attached to the machine, while the failure modes were documented with a video recorder.

3. Experimental results

3.1. Load–deformation response

Fig. 7 shows the relationships between the axial load and the deformation of the tested columns. The load–deformation of the unconfined short column (GGC-8-00) consisted only of a relatively linear ascending segment, with a stiffness of 301 kN/mm, up until the peak load level, denoted as P_g in this study. P_g represents the gross capacity of the geopolymer-concrete column or the column's capacity before concrete cover spalling. After exceeding P_g, the column failed suddenly and did not show any post-peak behavior.

The load–deformation responses of GGC-8-H50, GGC-8-H100, GGC-8-S50, and GGC-8-S100 can be divided into three phases. The first phase was comparable to that of GGC-8-00, a relatively linear load–deformation relationship with an average stiffness of 318 kN/mm. This can be expected since, at this stage, the columns' behavior was governed predominantly by the geopolymer concrete's compressive properties with little or no significant contribution from the GFRP ties. Furthermore, to activate the passive

Table 2
Specimen identification and test matrix.

Column	D (mm)	D_c (mm)	ρ_f (%)	s (mm)	ρ_{ft} (%)	L/r	Type
GGC-8-00	250	200	2.43	–	–	8	–
GGC-8-H50	250	200	2.43	50	3.13	8	Hoops
GGC-8-H100	250	200	2.43	100	1.57	8	Hoops
GGC-8-H200	250	200	2.43	200	0.78	8	Hoops
GGC-8-S50	250	200	2.43	50	3.13	8	Spirals
GGC-8-S100	250	200	2.43	100	1.57	8	Spirals
GGC-16-H100	250	200	2.43	100	1.57	16	Hoops
GGC-16-S100	250	200	2.43	100	1.57	16	Spirals

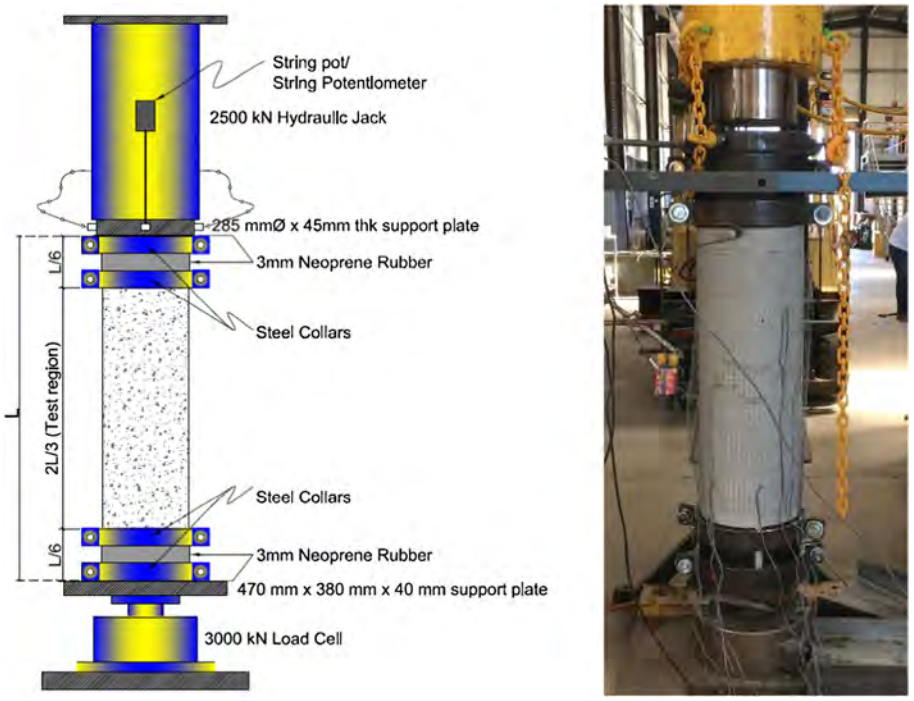

(a) Schematic Diagram (b) Actual

Fig. 6. Test set-up.

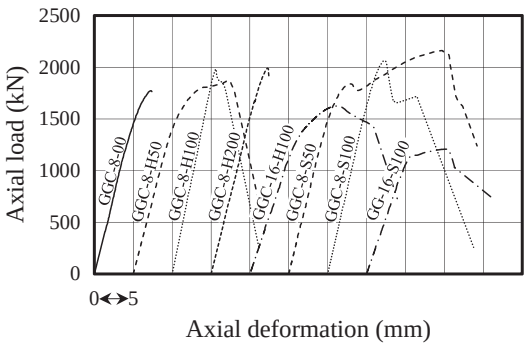

Fig. 7. Load–deformation response of the specimens.

confinement of the GFRP ties, a higher magnitude of applied loads was needed due to the low elastic-modulus characteristics of these ties. Upon exceeding a load level approximately equivalent to GGC-8-00's P_g, micro-cracks were formed causing the lateral expansion of the geopolymer concrete that subsequently yielded vertical hairline cracks on the concrete surface. At this stage, the passive confinement of the lateral reinforcement was marginally activated. A short nonlinear segment with reduced slope occurred prior to P_g owing to simultaneous crushing and cracking of the geopolymer concrete. Right after exceeding P_g, the concrete cover began to spall, producing a short descending branch that represents the second phase response of the columns. These columns, except GGC-8-H200, continued to sustain additional loads owing to the still-intact concrete core confined by lateral ties as represented by ascending or descending lines, depending on the amount of transverse reinforcement. This behavior represents the third phase response. A second peak load P_c was recorded that corresponds to the maximum load capacity of the confined geopolymer-concrete core. This load level also marks the initiation of geopolymer-concrete core crushing failure. The load–deformation response of GGC-8-H200, on the other hand, consisted only of two phases: a linear load–deformation response and a short descending branch.

GGC-16-H100 and GGC-16-S100 columns yielded similar initial linear load–deformation curves, although their initial stiffness (221 kN/mm) was lower compared to the GGC-8 columns. This is expected since the axial stiffness is inversely proportional to the height of the column. These columns also showed more noticeable nonlinear behavior and stiffness degradation before reaching their P_g compared to their counterpart GGC-8 columns.

3.2. Failure mode

Fig. 8 shows the post-failure overview of the tested columns, while Fig. 9 displays the specific failure of each material. As can be expected, the specimens failed by either crushing failure or buckling failure depending upon the slenderness ratio, suggesting the effectiveness of the design and construction procedure employed in the study. Right after reaching P_g, GGC-8-00 failed suddenly through the simultaneous crushing of the geopolymer concrete and global buckling of the GFRP bars (Fig. 9a). The columns failed in a brittle manner accompanied with an explosive sound. A well-formed cone on both ends (Fig. 8a) characterized GGC-8-00's post-failure configuration.

The failure of GGC-8-H200 commenced with the formation of vertical hairline cracks at an applied load approximately equivalent to GGC-8-00's P_g. Since the columns had poor confinement, the longitudinal bars started to deflect laterally that contributed further to the splitting of the geopolymer-concrete cover. Upon reaching its P_g, simultaneous crushing of the geopolymer-concrete core and buckling of the longitudinal bars occurred. Concrete-cover spalling and concrete shearing outward along the inclined plane (Fig. 8d) typified GGC-8-H200's failure, with relatively more intact geopolymer-concrete core compared to GGC-8-00, owing to the presence of circular ties.

(a) GGC-8-00 (b) GGC-8-H50 (c) GGC-8-H100 (d) GGC-8-H200 (e) GGC-8-S50 (f) GGC-8-S100 (g) GGC-8-H100 (h) GGC-8-S100

Fig. 8. Overview of the column specimens after failure.

(a) GFRP bars' global buckling

(b) Vertical cracks formation and geopolymer concrete cover spalling

(c) GFRP bars' kinking and delamination, geopolymer concrete core crushing, and circular hoops' lap splice joint failure

(d) GFRP bars' kinking and delamination, geopolymer concrete core crushing, and spiral rupture

Fig. 9. Different failure mode configurations of the column specimens.

GGC-8-H50 (Fig. 8b), GGC-8-H100 (Fig. 8c), GGC-8-S50 (Fig. 8e), and GGC-8-S100 (Fig. 8f), on the other hand, failed in a relatively ductile and more complex manner compared to the other columns. The failure can be described, generally, as the sequential occurrence of the following mechanism. The concentric compression load induced longitudinal strains that yielded transverse tensile strains due to Poisson's effect. At higher load levels, the axial strains and Poisson's effect increased, thereby increasing the geopolymer concrete's lateral strain, which consequently induced the formation of vertical columnar hairline cracks on the concrete surface. These cracks progressively widened and increased in number prior to P_g, as shown in Fig. 8b. More but narrower cracks were formed with increasing amounts of transverse reinforcement. After the concrete cover spalled, the geopolymer-concrete core underwent significant cracking, followed by the lateral expansion of the core, again, due to Poisson's effect. The longitudinal GFRP bars, on the other hand, started to kink and to delaminate due to the closely spaced ties preventing the bar lateral movement (Fig. 9c). These events were subsequently followed by GFRP-bar rupture, geopolymer-concrete core crushing, and lap-splice joint failure of the GFRP hoops (Fig. 9c) or rupture of the GFRP spirals (Fig. 9d), specifically at the intersection of the longitudinal and transverse reinforcement.

GGC-16-H50 (Fig. 8g) and GGC-16-S50 (Fig. 8f) underwent cracking and crushing mechanisms similar to that of their counterpart short columns before reaching ultimate failure. The failure of these columns, however, was governed by column buckling and not by the crushing or shear failure of the concrete, as shown by post-failure curvature/shape of the specimens.

3.3. Strength and deformation capacity

Table 3 summarizes the gross concrete and concrete-core load capacities (P_g and P_c, respectively) of the tested columns. The P_g

Table 3
Peak loads and the corresponding deformations.

Column	P_g (kN)	P_c (kN)	Δ_g (mm)	Δ_c (mm)	P_{fg} (kN)	P_{fc} (kN)
GGC-8-00	1772	–	7.2	–	123	–
GGC-8-H50	1791	1872	8.6	12.1	188	451
GGC-8-H100	1981	1763	5.6	6.9	133	444
GGC-8-H200	1988	–	7.3	–	134	–
GGC-8-S50	1838	2160	8.0	19.7	158	645
GGC-8-S100	2063	1717	7.2	11.4	147	587
GGC-16-H100	1624	–	11.1	–	107	–
GGC-16-S100	1208	–	10.4	–	143	–

of GGC-8-00 was 1772 kN. The geopolymer concrete's strength was calculated by subtracting the compression contribution of the GFRP bars from this load and then dividing the remaining load by the difference between the geopolymer concrete's gross area and total bar area ($(P_g–P_{fg})/(A_g–A_f)$). The resulting strength was equivalent to 34.42 MPa, which was approximately 90% of the average compressive strength of the standard geopolymer-concrete cylinders used in the study. Interestingly, this ratio was higher than the commonly used value of 85% for estimating the theoretical capacity of ordinary-concrete column sections, which tends to support Maranan et al.'s [26] conclusion that geopolymer concrete has better mechanical properties than ordinary Portland-cement concrete of the same grade such as higher elastic modulus (leading to its better compatibility with GFRP bars compared to normal concrete), greater ultimate compressive strain (approximately 4500 με), and larger tensile strength. The use of lateral ties, however, increased the P_g of GGC-8-00. GGC-8-H50, GGC-8-H100, and GGC-8-H200 yielded P_g values of 1791 kN, 1981 kN, and 1988 kN, respectively, which translated into strength increases of 1%, 12%, and 12%, respectively. Similarly, the P_g of GGC-8-S50 (1838 kN) and GGC-8-S100 (2063 kN) increased by 4% and 16%, respectively. As mentioned earlier, this enhancement could be attributed to the activation of the lateral confining pressures of the circular hoops or spirals right after a load level approximately equivalent to GGC-8-00's P_g had been achieved. The P_g of GGC-8-H50 and GGC-8-S50 were relatively low compared to the columns with lower volumetric ratios. Given that the P_g was mainly dependent on the geopolymer concrete, this result could be due to the presence of closely spaced ties that caused discontinuity of the geopolymer concrete between the cover and core, making the column more susceptible to early concrete-cover spalling. Only GGC-8-H50, GGC-8-H100, GGC-8-S50, and GGC-8-S100, however, yielded P_c of 1872 kN, 1763 kN, 2160 kN, and 1691 kN, respectively, which were 105%, 89%, 118% and 82% of their respective P_g. As can be expected, the well-confined columns (GGC-8-H50 and GGC-8-H100) yielded P_c that were higher than their P_g. The columns with spiral reinforcement, in general, produced higher P_g and P_c compared to their counterpart circular-tie-reinforced columns. GGC-16-H100 and GGC-16-S100, on the other hand, reached P_g of 1624 kN and 1208 kN, respectively, which were just 90% and 64%, respectively, of that of GGC-8-H100 and GGC-8-S100, respectively. This result could be expected since these columns failed due to buckling, a geometric type of failure, and not by compressive or shear failure.

Table 3 summarizes the GFRP bars' compression contribution at P_g load level (P_{fg}), which was determined by multiplying the measured average longitudinal bar strain (ε_{fg}) with the total nominal area (A_f) and elastic modulus (E_f) of the GFRP bars. P_{fg} represents the maximum compression contribution of the GFRP bars since the bars yielded an almost plateau behavior right after reaching this load level. The control specimen GGC-8-00 yielded the lowest P_{fg} of 123 kN, while those with lateral ties obtained P_{fg} ranging from 133 kN to 188 kN. The columns with widely spaced lateral ties (GGC-8-H100, GGC-8-H200, and GGC-8-S100) yielded an average P_{fg}/P_g of 6.9%, which was similar to GGC-8-00, whereas those with closely spaced lateral ties (GGC-8-H50 and GGC-8-S50) produced higher P_{fg}/P_g than GGC-8-00, with an average of 9.5%. The P_{fg} of GGC-16-H100 and GGC-16-S100 were 107 kN and 143 kN, respectively, which is generally lower than their counterpart GGC-8 columns. Nevertheless, it can be generalized from these results that the longitudinal GFRP bars made a notable compression contribution and that it could be enhanced through the provision of adequate lateral confinement. This generalization contradicts De Luca et al.'s [29] findings that the compression contribution of GFRP bars was less than 5% of column capacity. Hence, they concluded that the bar contribution could be ignored when evaluating the nominal capacity of an axially loaded square RC column. This could be related to the lower longitudinal reinforcement ratio (1.0%) they used and the better mechanical properties of the GFRP bars used in this study compared to the bars they used for their research work.

Table 3 also provides the axial deformation at P_g and P_c load levels (Δ_g and Δ_c, respectively). Except for GGC-8-H100 (5.6 mm), all the transversely reinforced GGC-8 columns produced Δ_g values that were higher than that of GGC-8-00 (7.2 mm). GGC-8-H100 yielded a lower axial deformation than GGC-8-00 because the former column exhibited less severe cracking, prior to reaching its peak capacity, compared to the latter column, owing to the circular hoops that restrained the expansion of concrete core and delayed the formation of cracks. The Δ_g of the hoop-confined columns were in the following increasing order: GGC-8-H100 (5.6 mm), GGC-8-H200 (7.3 mm), and GGC-8-H50 (8.6 mm), respectively. The axial deformation of GGC-H-100 was lower than GGC-8-H200 because the former column had higher volumetric ratio, resulting to a larger volume of effectively confined geopolymer concrete; hence, the premature dilation of the core was prevented and the formation of cracks was delayed. The well confined column (GGC-8-H50), on the other hand, had denser arrangement of the steel cage that produced planes of weakness between the cover and core, and hence, this column yielded a larger axial deformation than GGC-8-H100. This was also the reason why the axial deformation of GGC-8-S50 (8.0 mm) was greater than that of GGC-8-S100 (7.2 mm). GGC-16-H100 and GGC-16-S100, on other hand, achieved Δ_g of 14.1 mm and 12.9 mm, respectively, which are higher than that of GGC-8-H100 and GGC-8-S100, respectively. The Δ_c of GGC-8-H50 (12.1 mm), GGC-8-H100 (6.9 mm), GGC-8-S50 (19.7 mm), and GGC-8-S100 (11.4) were approximately 1.41, 1.23, 2.46, and 1.57 times that of their corresponding Δ_g, respectively. Obviously, the column with higher volumetric ratio or lower tie spacing, irrespective of the tie configuration, demonstrated better deformability performance compared to those with lower volumetric ratios. Furthermore, the column with spiral reinforcement showed higher deformability compared to that with circular ties. The Δ_g of GGC-16-H100 (11.09 mm) and GGC-16-S100 (10.39 mm) were greater than their counterpart short columns.

3.4. Geopolymer concrete and GFRP reinforcement strains

Fig. 10 shows the relationships between the axial load and the average axial strains in the geopolymer concrete. These strains were similar for all the tested columns up until an applied load approximately equivalent to 81% of GGC-8-00's P_g. Table 4, on the other hand, shows the maximum average strains in the geopolymer concrete at the P_g load level or the average concrete strain when the cover began to spall (ε_{cg}). Right after reaching its

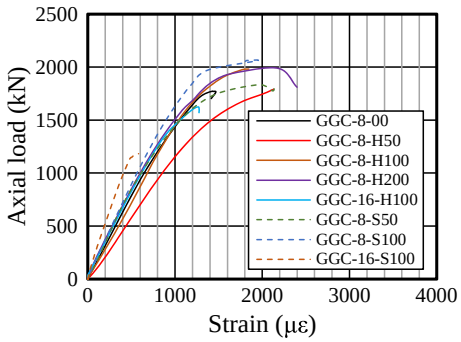

Fig. 10. Axial load versus geopolymer concrete strain curves.

Table 4
Geopolymer concrete and GFRP reinforcement strains.

Column	ε_{cg} (με)	ε_{fg} (με)	ε_{fc} (με)	ε_{ftg} (με)	ε_{ftc} (με)
GGC-8-00	1424	1647	–	–	–
GGC-8-H50	2129	2518	6047	1729	3302
GGC-8-H100	1845	1779	5955	664	5569
GGC-8-H200	2183	1803	–	853	–
GGC-8-S50	2183	2116	8680	968	7765
GGC-8-S100	1821	1967	7866	730	13,131
GGC-16-H100	1266	1436	–	552	–
GGC-16-S100	637	1922	–	700	–

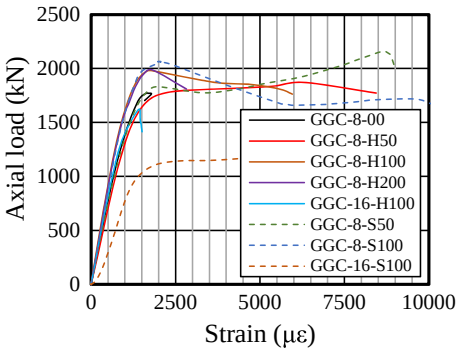

Fig. 11. Axial load versus longitudinal bar strain curves.

P_g, GGC-8-00 failed suddenly at a ε_{cg} of 1424 με. The ε_{cg} of the GGC-8 columns, however, varied from 1776 με to 2183 με. These strain values were larger than GGC-8-00's ε_{cg}, owing to the transverse reinforcement that prevented the premature cracking within the specimen and prevented the early buckling of the GFRP bars. Interestingly, the average ε_{cg} of the tested short columns $\varepsilon_{cg\text{-}ave}$, equivalent to 2032 με, was comparable to that of the normal concrete (2000 με) suggested by Afifi [58] and Saatcioglu and Razvi [59]. The ε_{cg} of GGC-16-H100 and GGC-16-S100 were 1266 με and 637 με, respectively, which is generally lower than their counterpart short columns.

Fig. 11 displays the relationships between the axial load and the axial compression strains in the longitudinal bars. As with the geopolymer concrete's strains, at the same load levels, relatively comparable strain readings were obtained from all specimens up until 81% of GGC-8-00's P_g. The figure clearly shows that the GFRP bars maintained their integrity and load resistance until after the surrounding concrete was crushed and spalled off after the peak load. Table 4 summarizes the strains in the longitudinal GFRP bars at P_g load level (ε_{fg}). The ε_{fg} of GGC-8-00 was 1647 με, which is equivalent to 8.7% of the GFRP bars' ultimate tensile strain ε_f. Generally, the GFRP ties enhanced the ε_{fg} of the short columns. The ε_{fg} of GGC-8-H100 and GGC-8-H200 were 1779 με and 1803 με, respectively, yielding $\varepsilon_{fg}/\varepsilon_f$ ratios of 9.4% and 9.5%, respectively. The well-confined GGC-8-H50, on the other hand, yielded the highest ε_{fg} among the columns with circular hoops, equivalent to 3070 με or 13.3% of ε_f. GGC-8-S50 and GGC-8-S100 developed ε_{fg} of 2116 με and 1967 με, respectively, translating to strain development of 11.2% and 10.4% of ε_f, respectively. The strains in the bars at P_c load level were also summarized in Table 4. The ε_{fc} were 6047 με, 5955 με, 8648 με, and 7866 με for GGC-8-H50, GGC-8-H100, GGC-8-S50, and GGC-8-S100, respectively, translating to $\varepsilon_{fc}/\varepsilon_f$ ratios of 32.0%, 31.5%, 45.8%, and 41.6%, respectively. These values were lower than the strain ratio capacity (51.7%) reported earlier. GGC-16-H100 (1436 με) and GGC-16-S100 (1922 με) produced $\varepsilon_{fg}/\varepsilon_f$ ratios of 7.6% and 10.2%, respectively. These results showed that the GFRP bars had a compression contribution that

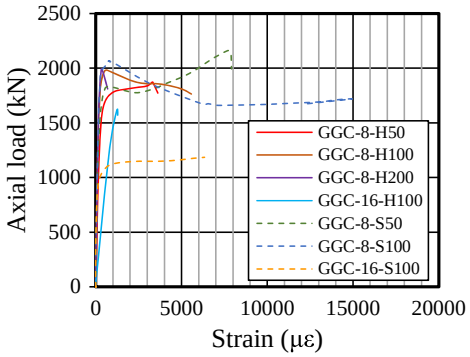

Fig. 12. Axial load versus lateral-tie strain curves.

cannot be neglected. Interestingly, the average ε_{fg} of the short columns $\varepsilon_{fg\text{-}av}$ (2036 με) was relatively comparable to $\varepsilon_{cg\text{-}ave}$, suggesting the compatibility between the bars and the geopolymer concrete and that equivalency between these materials could be assumed for design and analysis purposes. Furthermore, this strain value was higher than the design strain limit of 1000 με proposed by Zadeh and Nanni [57] to avoid exaggerated deflections.

Fig. 12 shows the relationships between the axial load and the lateral-tie strain. Marginal strains (ε_{ftg}) were recorded at lower loads. After exceeding the load equivalent to GGC-8-H100's P_g, however, relatively higher strains were obtained from GGC-8-H50 and GGC-8-S50 because of the early spalling of their concrete covers compared to the columns with wider tie spacing. The ε_{ftg} of GGC-8-H50 (1729 με) was higher than that of GGC-8-H100 (664 με) and GGC-8-H200 (853 με). A similar trend was also observed in the spiral-confined columns with GGC-8-S50 (968 με) yielding a higher ε_{ftg} than GGC-8-S100 (730 με). The trend reversed, however, right after the P_g load level was reached. The ε_{ftc}, the transverse reinforcement strain at P_c load level, were 5569 με and 13,131 με for GGC-8-H100 and GGC-8-S100, respectively. These strains were higher than that of GGC-8-H100 (3302 με) and GGC-8-S100 (7765 με), respectively. On the other hand, the columns with spiral reinforcement generally yielded higher ε_{ftc} compared to their counterpart columns with circular hoops. GGC-16-H100 and GGC-16-S100 recorded ε_{ftg} values of 552 με and 700 με, respectively, which were lower than their counterpart short columns.

3.5. Confinement efficiency and ductility index

In this study, the column ductility index (D.I.) was defined as the ratio of the displacement that corresponds to 85% of P_{peak} to the displacement that corresponds to the elastic behavior limit (Δ_{85}/Δ_1), as shown in Fig. 13. The procedure for determining these

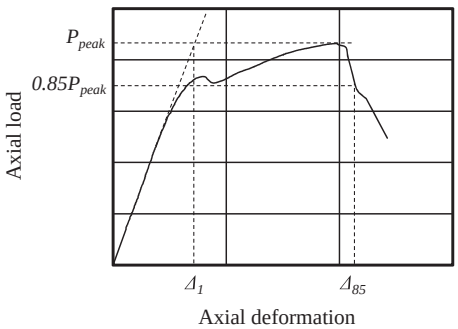

Fig. 13. Definition of Δ_{85} and Δ_1.

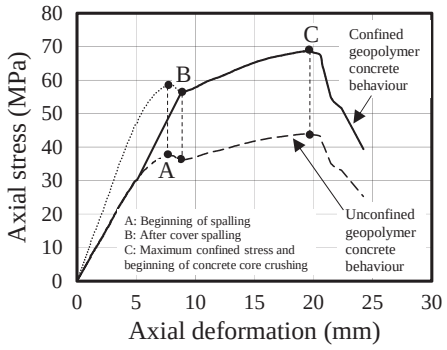

Fig. 14. Confined stress–deformation curve of GGC-8-S50.

Table 5
Normalised strength, ductility index (D.I.) and confinement efficiency (C.E.) of GFRP-RGC and GFRP-RC circular columns.

Author	Specimen	Type	ρ_{ft} (%)	$\frac{P_g - P_t}{f'_c A_g}$	D.I.	C.E.
Current study	GGC-8-H50	Hoop	3.13	85.9	2.08	1.84
	GGC-8-H100	Hoop	1.57	99.1	1.32	1.74
	GGC-8-S50	Spiral	3.13	90.1	2.99	2.13
	GGC-8-S100	Spiral	1.57	102.7	1.79	1.67
Afifi et al. [41]	G4V-3H80	Spiral	1.48	89.0	1.13	1.37
	G8V-3H40	Spiral	2.95	89.4	4.75	1.89
	G8V-3H80	Spiral	1.48	89.2	2.00	1.69
	G8V-3H120	Spiral	0.98	85.9	1.54	1.32
	G12V-3H80	Spiral	1.48	89.4	2.45	1.78
Mohamed et al. [42]	G3H200	Hoop	1.48	88.8	1.83	1.57
	G3H400	Hoop	1.48	84.8	1.88	1.60
	G3H600	Hoop	1.48	87.7	1.91	1.63
Pantelides et al. [28]	13GLCTL	Spiral	1.91	–	1.70	1.76
	14GLCTL	Spiral	1.91	–	3.60	1.59

displacements was based on Pantelides et al.'s [28] recommendations. The confinement efficiency (C.E.), on the other hand, was computed as the ratio of the compressive strength of the confined column to the compressive strength of the unconfined column (f_{cc}'/f_{co}'). The f_{cc}' was calculated as the peak load divided by the area of the confined geopolymer concrete, which is represented by point C in Fig. 14. The f_{co}', on the other hand, was equivalent to $0.90f_c'$. Table 5 summarizes the D.I. and C.E. values of the tested columns. Based on the experimental results, the ductility index and confinement efficiency increased when the amount of transverse reinforcement increased. These results are consistent with Afifi et al.'s [41] findings on circular concrete columns reinforced with GFRP bars and spirals. Sharma et al. [60] also reported a similar trend regarding the ductility of the confined columns for

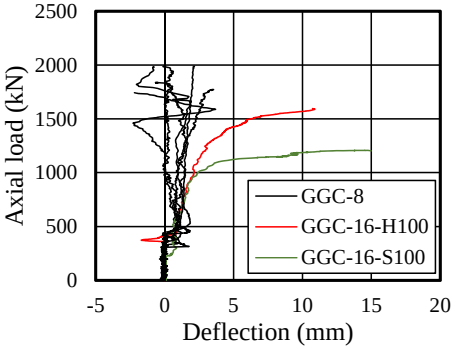

Fig. 15. Axial load versus lateral deflection.

conventional RC columns. The geopolymer concrete columns with spiral reinforcement, in general, showed higher ductility and confinement efficiency than those with circular hoops. These findings are not consistent with those of Mohamed et al. [42] wherein they concluded that the FRP circular hoops have similar confining efficiency as the FRP spirals. This could be expected since they utilized hoops with longer lap or splice lengths, approximately 2.5–5 times longer than that of the hoops employed in this study. The ductility and confinement efficiency of the slender geopolymer concrete columns were not considered in this study, mainly because of the nature of failure of these specimens.

3.6. Lateral deflection

Fig. 15 shows the typical lateral deflection readings, just before the initiation of concrete-cover spalling, obtained from the horizontally positioned laser displacement sensors. The black lines represent that of the short columns while the red and green lines correspond to that of GGC-16-H100 and GGC-16-S100. At lower applied loads, the deflection was approximately equivalent to zero for both column types. At higher loads, however, the GGC-8 columns yielded relatively random readings owing to the geopolymer-concrete crushing and cracking. The slender columns, on the other hand, yielded deflections that increased hyperbolically with increasing loads, clearly indicating that the columns were undergoing lateral buckling.

4. Discussion

4.1. Influence of the transverse reinforcement

The provision of transverse reinforcement generally enhanced the compression performance of the tested GFRP-RGC columns. The compression failure of the confined columns was less brittle compared to the unconfined control specimen. At P_g load level, the average strength and deformation capacity of the confined columns were 10% and 1%, respectively, higher than that of the corresponding values for the unconfined column. Furthermore, the average geopolymer concrete and longitudinal GFRP bar strains of confined columns were 24% and 43% higher, respectively, than that of the unconfined column, suggesting the ties' effectiveness in enhancing the strain development in each component material of the column.

4.2. Influence of the transverse-reinforcement spacing

The effect of the amount of transverse reinforcement on the performance of confined concrete has been well studied. As can be expected, the closer the tie spacing or the larger the volumetric ratio, the less brittle the compression failure of the tested columns, showing a slower rate of strength decay after the peak. After the geopolymer-concrete cover spalled, the well-confined columns (GGC-8-H50 and GGC-8-S50) showed relatively higher strength and deformation capacities than the less-confined columns (GGC-8-H100 and GGC-8-S100). These observations tend to support Paultre and Légeron's [61] generalization for confined columns, which states that the effectiveness of confinement reinforcement in restraining concrete varies from "one" for a continuous tube to "zero" when the ties are spaced more than half the minimum core cross section. This conclusion may also explain why the poorly confined GGC-8-200 evidenced load–deformation behavior and failure mode similar to GGC-8-00, since the hoop spacing was too wide to provide any lateral confinement. Interestingly, the columns with a volumetric ratio of 3.13% or a transverse-reinforcement spacing of 50 mm on centers yielded another peak

and deformation capacities that were higher than their initial capacities. This can be related to the high confinement that enhanced the geopolymer-concrete core and prevented vertical GFRP bar buckling, owing to reduced the unbraced length of the bars, which enhanced the compression contribution of the GFRP bars.

The amount of transverse reinforcement, expressed in terms of ρ_{ft}, played a major role after the concrete cover spalled. An adequate amount of lateral reinforcement with respect to the unsupported length of longitudinal reinforcement ensured the stability of the longitudinal reinforcement between the ties. Furthermore, after the concrete spalled, the well-confined geopolymer-concrete columns yielded an ascending load–deformation relationship, while the poorly confined geopolymer-concrete columns produced a descending response.

4.3. Influence of the transverse-reinforcement configuration

The geopolymer-concrete columns confined by spirals exhibited relatively higher ductility and confinement efficiency compared to their counterpart columns confined with circular hoops, owing to the continuous nature of the spirals, which effectively confined the whole geopolymer-concrete core by distributing the lateral confining pressures uniformly around the perimeter and along the height of the geopolymer-concrete core. This observation corroborates Yong et al.'s [62] and Mohamed et al.'s [42] findings for conventional RC and FRP-RC columns, respectively. Furthermore, the difference between the two types of lateral ties can be clearly seen after the spalling of the concrete cover of the well-confined columns. The P_c-to-P_g ratio of GGC-8-S50 was 1.18, whereas, for GGC-8-H50, the ratio was just 1.04. This result tends to suggest that the strength enhancement in hoop-confined columns due to transverse reinforcement could be ignored. Interestingly, this finding corroborates those of Kent and Park [63] for rectangular conventional RC columns transversely reinforced with rectilinear ties, in which the concrete core delineated by the outer tie diameter was not fully confined due to the non-uniform lateral pressure that resulted in poor strength enhancement. This could be attributed to the discontinuous nature of the circular hoops, since the column failure was governed by lap-splice failure at the joint and not by the GFRP ties rupturing. It can be deduced, therefore, with the same amount of strength and ductility improvement, hoop-confined columns should be much more confined than spiral-confined columns.

4.4. Influence of the slenderness ratio (L/r)

Generally, the columns with higher slenderness ratios and confined with hoops and spirals yielded strength capacities (P_g) that were 66% and 82% of the strength of their short-column counterparts. The hoop-confined slender column yielded ε_{cg}, ε_{fg}, and ε_{ftg} that were just 35%, 80%, and 83%, respectively, of the strains of their counterpart hoop-confined short columns. The spiral-confined slender column, on the other hand, recorded strains that were 68%, 97%, and 95%, respectively, of the corresponding values for spiral-confined short columns. Furthermore, the confinement efficiency of the hoop- and spiral-confined slender columns was just 59% and 46%, respectively, of their counterpart short columns. These results could be attributed to the buckling failure of the slender columns—a geometric type of failure not related to the strength of the material—which lowered their strength capacities and did not allow the efficient use of each component material. The higher deformation values could be attributed to column lateral movement. Clearly, these results indicate the influence of slenderness in the tested columns with $L/r = 16$, thereby suggesting that the previously proposed slenderness limit for GFRP-RC columns (17.2) must be lowered for the proposed system. The critical buckling load P_c—estimated from Eq. (1)—was equivalent to 1898 kN. This is higher than the P_g of the tested slender columns, indicating that a lower P_c limit must be adopted for the proposed system. Further research is needed, however, to support these generalizations.

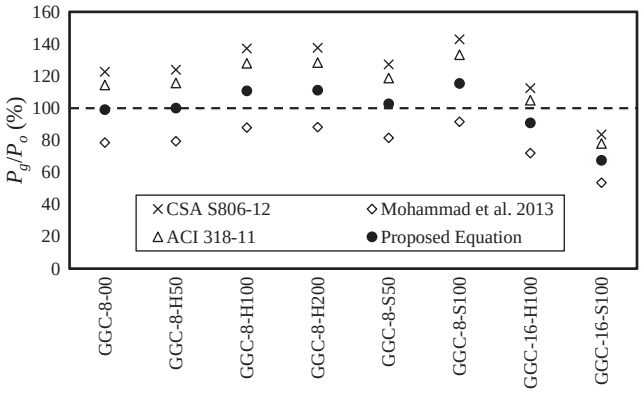

Fig. 16. P_g-to-P_o ratios.

$$P_c = \frac{\pi^2 EI}{(kL_u)^2} \tag{1a}$$

$$EI = \frac{0.2E_c I_g + E_f I_{se}}{(1+\beta_d)} \tag{1b}$$

4.5. Theoretical prediction

The nominal capacities of the tested GFRP-RGC columns were determined using the equations below. These formulas were used to estimate column strength at P_g load levels. Fig. 16 shows the comparison of the experimental-to-predicted (P_g-to-P_o) ratios using these equations.

$$P_o = \alpha_1 f'_c(A_g - A_f); \quad \alpha_1 = 0.85 - 0.0015f'_c \geqslant 0.67 \tag{2}$$

$$P_o = 0.85f'_c(A_g - A_f) \tag{3}$$

$$P_o = 0.85f'_c(A_g - A_f) + \alpha_g f_{fu} A_f \tag{4}$$

$$P_o = 0.90f'_c(A_g - A_f) + \varepsilon_{fg} E_f A_f \tag{5}$$

Of the current North American standards for FRP-RC systems, only CSA S806-12 has established a prediction equation for FRP-RC columns, as depicted by Eq. (2). This equation, however, ignores the compression contribution of the FRP bars. Using this equation, the ratios of the peak experimental load-to-predicted nominal capacity (P_g/P_o) varied from 113% to 143%, with an average value of 129%. Eq. (3) was based on the equation in ACI 318-11 [64] recommended for conventional RC columns. It neglects, however, the compression contribution of GFRP bars. Based on this formula, the P_g/P_o ratios ranged from 105% to 129% with an average value of 121%, yielding less conservative estimates compared to Eq. (1).

Eq. (4) depicts the equation recommended by Afifi et al. [41]. The compression contribution of the GFRP bars was considered by introducing a factor α_g that accounts for the reduced compressive strength of the GFRP bars as a function of their tensile strength. Currently, no standard test is available to determine the compressive strength of FRP bars. Hence, in order to determine the factor α_g in this study, five 15.9 mm GFRP bars 40 mm in length were used and were subjected to compressive testing. The test yielded an average α_g approximately equivalent to 0.5. From Eq. (4), the P_g/P_o ratios ranged from 72% to 92% and an average of 83%. This equation generally yielded unconservative estimates, indicating its inapplicability for the proposed system. Eq. (5) was

based on Mohamed et al.'s [42] recommendations, although we used a reduction factor of 0.90 obtained from the experiment instead of the commonly used value of 0.85. Adoption of higher strength-reduction factor seems to be logical for the proposed system owing to the higher elastic modulus of the geopolymer concrete (33 GPa) compared to a normal concrete (29 GPa, calculated using the ACI 318-11 formula) of the same grade (38 MPa). This would result in better compatibility in the GFRP-RGC system, as evidenced by the recorded average strains in the GFRP bars and geopolymer concrete that, subsequently, would yield more area under the stress–strain curve compared to a GFRP-RC system. Further studies, however, are recommended to validate these conclusions. The longitudinal reinforcement's contribution was calculated based on the actual strains in the bars, represented by $\varepsilon_{fg\text{-}ave}$. This strain corresponds to the average compression strain in GFRP bars at the P_g load level or the strain at which the plastic deformation of the geopolymer concrete initiated. Based on the column compression test, the $\varepsilon_{fg\text{-}ave}$ was equivalent to 0.002. The P_g/P_o ratios varied from 68% to 111%, with an average value of 100%. Interestingly, among the equations considered herein, this equation yielded the relatively most accurate prediction of the nominal capacity of the column specimens. In addition, this equation produced conservative estimates, except for the slender columns, thereby suggesting the equation's suitability in predicting the capacity of short GFRP-RGC columns. A new equation must, therefore, be proposed to consider the slenderness effect on the capacity of GFRP-RGC columns.

4.6. Comparison with the GFRP-RC circular columns

The performance of the tested GFRP-RGC circular columns was compared to that of Afifi et al.'s [41], Mohamed et al.'s [42], and Pantelides et al.'s [28] GFRP-RC circular columns in terms of normalized strength, ductility index, and confinement efficiency. These values were summarized in Table 5. The normalized strength was calculated as the difference between P_g and P_f divided by the concrete strength (f_c') and the gross area (A_g) of the column. From the table, it can be seen that the strength of the GFRP-RGC columns were higher than that of the GFRP-RC columns. Interestingly, this finding tends to support the authors' earlier claim that GFRP bars have better compatibility with geopolymer concrete compared with OPC concrete, owing to the higher elastic modulus of the former concrete compared to the latter concrete. Comparing the ductility and confinement efficiency of GFRP-RGC columns to that of GFRP-RC columns with comparable amounts and types of transverse reinforcement, the two systems showed relatively comparable performance. From these findings, it can be inferred that GFRP bars can be used as reinforcement for geopolymer-concrete columns, particularly when structural columns that are corrosion resistant and electromagnetic transparent are targeted. This conclusion corroborates Zadeh and Nanni's [57] generalization based on past experimental research, stating that GFRP bars can be used to strengthen conventional RC columns.

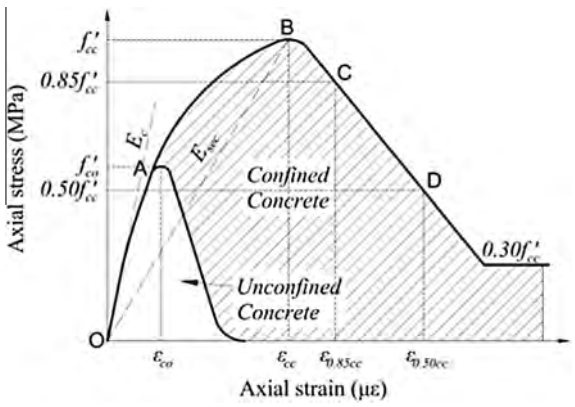

Fig. 17. Adopted stress–strain curve for the confined geopolymer concrete.

4.7. Proposed stress–strain model for confined GFRP-RGC circular columns

Fig. 17 shows the stress–strain curve adopted in this study. The first segment (O–A) represents the unconfined behavior because, at this stage, the transverse strain were not high enough to activate the lateral confinement pressure of the stirrups. This seems to be to logical to adopt because according to Ozbakkaloglu et al. [65] the confinement action by the FRP shell (GFRP ties in this study) on the concrete core is of the passive type, wherein the pressure arises as a result of lateral expansion of concrete under axial compression. Since GFRP ties have low elastic modulus, it would require high transverse strain to activate its passive confining pressure. The remaining segment (A–B–C–D), on the other hand, embodies that of the confined behavior, upon the activation of the GFRP ties' passive confinement. Eqs. (6a)–(6e), proposed by Popovics [66], was employed to model the ascending branch (O–A–B) while Eqs. (7a)–(7c), which was proposed by Han et al. [67] for high strength reinforced concrete tied columns, was used to model the descending part (B–C–D). Eqs. (6d) and (6e) were also adopted by Afifi et al. [68] to predict the peak stress and corresponding strain in the circular concrete columns confined by GFRP spirals and hoops. The maximum confining pressure (f_{lGFRP}) was computed from Eqs. (8a) and (8b). The constants a, b, c, d, e, f, g, h, i, and j were determined through the regression analysis of short columns' experimental results, as implemented by Han et al. [67], such as the confined compressive strength (f_{cc}'); the axial strains, derived from longitudinal reinforcement strains, at f_{cc}', $0.85f_{cc}'$, and $0.50f_{cc}'$ (ε_{cc}, $\varepsilon_{0.85cc}$, and $\varepsilon_{0.50cc}$, respectively); and transverse reinforcement strain at f_{cc}' (ε_{ftcc}). These constants were tabulated in Table 6. Fig. 18 shows a good correlation between the predicted and the experimental stress–strain curves for the tested GFRP-RGC column specimens. The proposed equations, however, are applicable only for the specimens considered in this study. Further research works are needed to further calibrate the proposed equations.

$$f_c = \frac{f'_{cc}(\varepsilon_c/\varepsilon_{cc})^m}{m-1+(\varepsilon_c/\varepsilon_{cc})^m}, \quad \varepsilon_c \leqslant \varepsilon_{cc} \tag{6a}$$

$$m = \frac{E_c}{E_c - E_{sec}} \tag{6b}$$

$$E_{sec} = f'_{cc}/\varepsilon_{cc} \tag{6c}$$

$$f'_{cc} = f'_{co} + a(\rho_{ft} f_{lGFRP})^b \tag{6d}$$

$$\varepsilon_{cc} = \varepsilon_{co}\left[1 + c\left(\frac{\rho_{ft} f_{lGFRP}}{f'_{co}}\right)^d\right] \tag{6e}$$

$$f_c = f'_{cc}\left[0.85 - 0.5\frac{\varepsilon_c - \varepsilon_{0.85cc}}{\varepsilon_{0.50cc} - \varepsilon_{cc}}\right] \geqslant 0.3f'_{cc} \tag{7a}$$

$$\varepsilon_{0.85cc} = \varepsilon_{co}\left[1 + e\left(\frac{\rho_{ft} f_{lGFRP}}{f'_{co}}\right)^f\right] \tag{7b}$$

$$\varepsilon_{0.85cc} = \varepsilon_{co}\left[1 + g\left(\frac{\rho_{ft} f_{lGFRP}}{f'_{co}}\right)^h\right] \tag{7c}$$

$$f_{lGFRP} = \frac{\rho_{ft}}{2} E_f \varepsilon_{ftcc} \tag{8a}$$

$$\varepsilon_{ftcc} = i \times \exp[j(\varepsilon_{ft}/s)] \tag{8b}$$

Table 6
Constants *a*, *b*, *c*, *d*, *e*, *f*, *g*, *h*, *i*, and *j*.

Column	*a*	*b*	*c*	*d*	*e*	*f*	*g*	*h*	*i*	*j*
Hoop-confined column	22.01	−0.03	72.23	0.54	102.40	0.40	210.54	0.36	790.1	0.003
Spiral-confined column	34.88	0.05	132.88	0.64	35.39	0.36	7.25	0.02	196.1	0.009

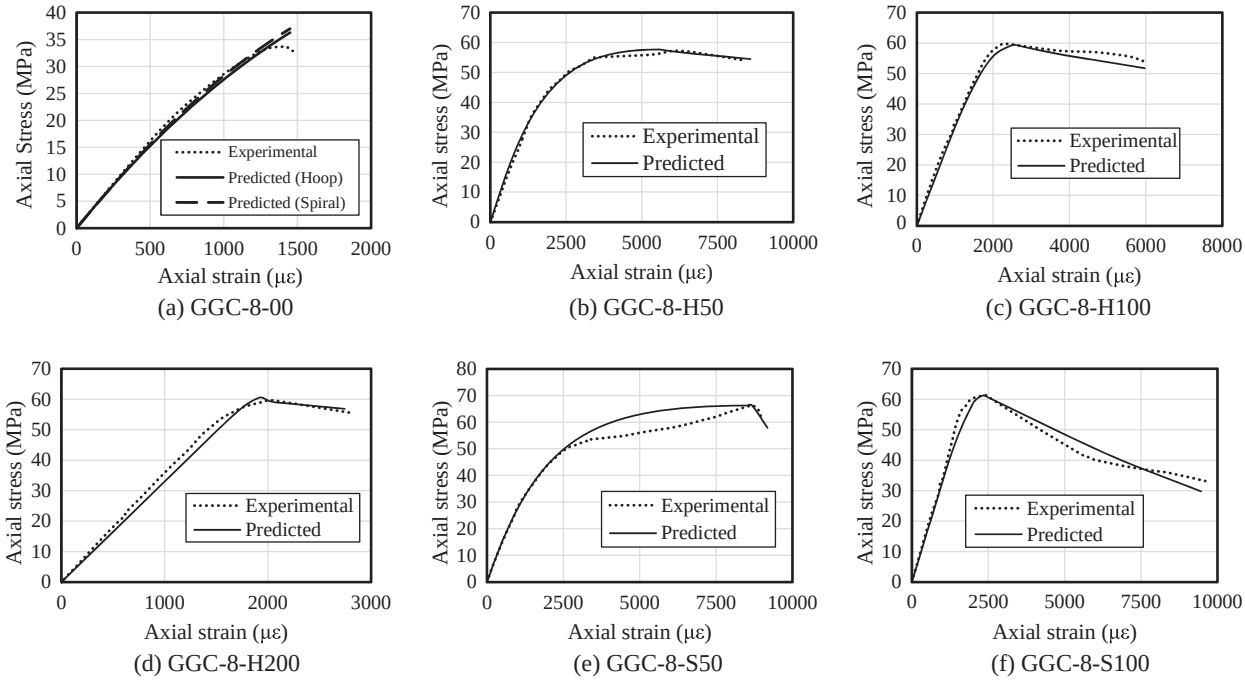

Fig. 18. Experimental and predicted stress–strain curves of the GFRP-RGC columns.

4.8. Proposed compression relationship for GFRP bars

It was evident from the experiment that the GFRP bars in the columns with ties spaced at 50–200 mm exhibited local combined crushing and buckling failure while the control specimen undergone buckling failure; hence, two equations were proposed. Eq. (9a) shows the proposed relationship for predicting the ultimate compression stress in the GFRP bars (f_{fu}') that undergone local combined crushing and buckling failure. The maximum value of 612.5 MPa was adopted from the compression test of GFRP bars. This equation was basically derived from the regression analysis of the experimental results acquired from the actual column test. To calculate the experimental f_{fu}', the load P_{fg} was divided by the total area and number of longitudinal bars. The compression behavior of GFRP bars encased in geopolymer concrete and confined by a closely spaced ties can intuitively be expected to be different from that of buckling test of the bars. The buckling test resulted in a fixed-fixed end condition while in the column test, the end conditions are not as simply defined. Furthermore, buckling behavior of GFRP bars is not only influenced by the lateral bracing distance (or tie spacing) but also by the geopolymer concrete core condition [69]. Eq. (9b), on the other hand, predicts that of GFRP bars that undergone global buckling failure, the bars in the control specimen. Interestingly, the obtained effective length factor k (0.926) was approximately equivalent to 1.0, which is typically adopted for pinned-end specimen. Table 7 shows that the predictions by the proposed models show a good agreement with the experimental results for the aforesaid specimens. Further research works, however, are needed to enhance the accuracy of the proposed equations.

$$f_{fu}' = 612.5 - 53.564 \times s \times \left(\frac{L_{uf}}{r_f}\right)^{-0.946} \quad \text{For}: \ 50\ \text{mm} < L_{uf} < 200\ \text{mm} \tag{9a}$$

$$f_{fu}' = \frac{\pi^2 E_{fc}}{(kL_{uf}/r_f)^2}; \quad k = 0.926 \quad \text{For}: L_{uf} > 200\ \text{mm} \tag{9b}$$

Table 7
Compressive stress in GFRP bars.

Column	L_{uf} (mm)	Experimental (MPa)	Predicted (MPa)
GGC-8-00	667	102	101.5
GGC-8-H50	50	158	142.2
GGC-8-H100	100	112	124.3
GGC-8-H200	200	112	105.7
GGC-8-S50	50	133	142.2
GGC-8-S100	100	123	124.3

5. Conclusion

This study investigated the behavior of geopolymer-concrete columns reinforced longitudinally and transversely with GFRP bars. From the experimental results, the following conclusions were drawn:

- The compression contribution of the GFRP bars (2.43% reinforcement ratio) with respect to column capacity prior to concrete spalling varied from 6.6% to 10.5%, with an average value of 7.6%.
- Irrespective of tie configuration, the columns with closely spaced lateral ties or higher volumetric ratios failed in a more ductile manner and showed higher confinement efficiency compared

to the columns with relatively lower volumetric ratios. The hoop- and spiral-confined columns with ties spaced at 50 mm on centers yielded ductility indices [confinement efficiency] that were 58% [7%] and 67% [28%], respectively, higher than their counterpart columns with ties spaced 100 mm on centers.

- The spiral-confined columns exhibited a more ductile behavior and higher post-concrete-cover spalling strength compared to their hoop-confined counterparts, as proven by the higher average ductility index and average confinement efficiency (2.39 and 1.90, respectively) of the spiral-confined columns compared to the hoop-confined ones (1.79 and 1.70, respectively). These findings could be attributed to the uniform lateral confining pressure of the spirals.
- The short columns failed due to crushing and/or shear failure, while the slender columns failed due to buckling. Hence, irrespective of the type and amount of transverse reinforcement, the short columns yielded higher compression capacities than the slender columns. The hoop- and spiral-confined short columns with ties spaced at 100 mm on centers yielded strength capacities that were 22% and 71%, respectively, higher than their counterpart slender columns.
- The GFRP-RGC circular columns yielded a relatively higher normalized strength (97.3%) compared to GFRP-RC circular columns (88.3%). This could be attributed to the higher elastic modulus of geopolymer concrete (33 GPa) compared to normal concrete (29 GPa) of the same grade (38 MPa), resulting in better compatibility in the GFRP-RGC system than in a GFRP-RC system. Further studies, however, are needed to validate this generalization.
- The slender columns failed at a load 66% and 82% of the strength of their short-column counterparts. They exhibited higher deformation compared to the short columns due to the lateral movement and they failed due to buckling.
- The nominal capacity of the tested columns could be estimated accurately using the proposed equation because it considers the actual geopolymer-concrete strength-reduction factor (0.90) and the actual compression contribution of the GFRP bars (using the average bar strain as being equivalent to 2000 με).
- The proposed confined stress–strain equations show good correlation with the experimentally established stress–strain relationship for the GFRP-RGC columns. Further research works, however, are needed to further calibrate these equations.
- It can be inferred, therefore, that a GFRP-RGC system could be adopted as compression members, particularly when corrosion resistance, electromagnetic transparency, material greenness, durability, and sustainability are sought.

Acknowledgements

The authors would like to express their special thanks to V-ROD® Australia for providing the materials as well as to the Natural Science and Engineering Research Council of Canada (NSERC) and the technical staff of the structural lab at University of Southern Queensland.

References

[1] Rizkalla S, Hassan T, Hassan N. Design recommendations for the use of FRP for reinforcement and strengthening of concrete structures. Prog Struct Mater Eng 2003;5:16–28.
[2] Benmokrane B, El-Salakawy E, El-Ragaby A, Lackey T. Designing and testing of concrete bridge decks reinforced with glass FRP bars. J Bridge Eng 2006;11(2):217–29.
[3] Gangarao HVS, Tally N, Vijay PV. Reinforced concrete design with FRP composites. CRC Press; 2007.
[4] Kong DLY, Sanjayan JG. Effect of elevated temperatures on geopolymer paste, mortar and concrete. Cem Concr Res 2010;40:334–9.
[5] Neupane K, Bajewa D, Shrestha R, Chalmers D, Sleep P. Mechanical properties of geopolymer concrete: applicability of relationship defined by AS 3600. Concr Australia 2014;40:50–6.
[6] Davidovits J. Geopolymers: inorganic polymeric new materials. J Therm Anal 1991;37:1633–56.
[7] Duxson P, Provis JL, Lukey GC, Van Deventer JS. The role of inorganic polymer technology in the development of 'green concrete'. Cem Concr Res 2007;37:1590–7.
[8] Sofi M, van Deventer JSJ, Mendis PA, Lukey GC. Engineering properties of inorganic polymer concretes (IPCs). Cem Concr Res 2007;37:251–7.
[9] Sarker PK. A constitutive model for fly ash-based geopolymer concrete. Arch Civ Eng Environ (Silesian Univ Technol) 2008;1:113–20.
[10] Olivia M, Nikraz H. Properties of fly ash geopolymer concrete designed by Taguchi method. Mater Des 2012;36:191–8.
[11] Adam MA, Said M, Mahmoud AA, Shanour AS. Analytical and experimental flexural behavior of concrete beams reinforced with glass fiber reinforced polymer bars. Constr Build Mater 2015;84:354–66.
[12] El-Nemr A, Ahmed EA, Benmokrane B. Flexural behavior and serviceability of normal- and high-strength concrete beams reinforced with glass fiber-reinforced polymer bars. ACI Struct J 2013;110:1077–88.
[13] Kassem C, Farghaly AS, Benmokrane B. Evaluation of flexural behavior and serviceability performance of concrete beams reinforced with FRP bars. ASCE J Compos Constr 2011;15:682–95.
[14] Benmokrane B, Chaallal O, Masmoudi R. Flexural response of concrete beams reinforced with FRP bars. ACI Struct J 1996;91:46–55.
[15] Mohamed K, Farghaly AS, Benmokrane B. Effect of web reinforcement in FRP-reinforced deep beams. In: Proceedings of the 7th international conference on FRP composites in civil engineering (CICE 2014). Vancouver, Canada. p. 79.
[16] Razaqpur AG, Spadea S. Shear strength of FRP reinforced concrete members with stirrups. J Compos Constr 2015;19:04014025.
[17] Oller E, Marí A, Bairán JM, Cladera A. Shear design of reinforced concrete beams with FRP longitudinal and transverse reinforcement. Compos B Eng 2015;74:104–22.
[18] Shahnewaz M, Machial R, Alam MS, Rteil A. Optimized shear design equation for slender concrete beams reinforced with FRP bars and stirrups using genetic algorithm and reliability analysis. Eng Struct 2016;107:151–65.
[19] Goldston M, Remennikov A, Sheikh MN. Experimental investigation of the behaviour of concrete beams reinforced with GFRP bars under static and impact loading. Eng Struct 2016;113:220–32.
[20] Kumaravel S, Thirugnanasambandam S. Flexural behaviour of geopolymer concrete beams. Int J Adv Eng Res Stud 2013;3:4–6.
[21] Abraham R, Raj SD, Abraham V. Strength and behaviour of geopolymer concrete beams. Int J Innov Res Sci, Eng Technol 2013;2:159–66.
[22] Dattatreya JK, Rajamane NP, Sabitha D, Ambily PS, Nataraja MC. Flexural behaviour of reinforced geopolymer concrete beams. Int J Civ Struct Eng 2011;2:138–59.
[23] Chang EH. Shear and bond behaviour of reinforced fly ash-based geopolymer concrete beams [PhD thesis]. Perth, Australia: Curtin University of Technology; 2009.
[24] Ambily P, Madheswaran C, Lakhsmanan N, Dattatreya J, Sathik S. Experimental studies on shear behaviour of reinforced geopolymer concrete thin webbed T-beams with and without fibres. Int J Civ Struct Eng 2012;3:128–40.
[25] Ng TS, Foster SJ. Shear strength of lightweight fibre reinforced geopolymer concrete composite beam. In: Fragomeni S, Venkatesan S, Lam NTK, Setunge S, editors. 21st Australasian conference on the mechanics and structures of materials. Victoria University, Melbourne, Australia: Taylor & Francis Group; 2010. p. 77–82.
[26] Maranan G, Manalo A, Benmokrane B, Karunasena W, Mendis P. Evaluation of the flexural strength and serviceability of geopolymer concrete beams reinforced with glass-fibre-reinforced polymer (GFRP) bars. Eng Struct 2015;101:529–41.
[27] Maranan G, Manalo A, Karunasena W, Benmokrane B, Mendis P. Comparison of the shear behaviour of geopolymer concrete beams with GFRP and steel transverse reinforcements. In: Wu Z, Wu G, Wang X, editors. The 12th international symposium on fiber reinforced polymers for reinforced concrete structures (FRPRCS-12) & the 5th Asia-Pacific conference on fiber reinforced polymer in structures (APFIS-2015). Nanjing, China. p. 169.
[28] Pantelides CP, Gibbons ME, Reaveley LD. Axial load behavior of concrete columns confined with GFRP spirals. J Compos Constr 2013;17:305–13.
[29] De Luca A, Matta F, Nanni A. Behavior of full-scale glass fiber-reinforced polymer reinforced concrete columns under axial load. ACI Struct J 2010;107.
[30] ACI 440.1R-06. Guide for the design and construction of structural concrete reinforced with FRP bars. Farmington Hills (Michigan, USA): American Concrete Institute; 2006.
[31] CSA S806-12. Design and construction of building components with fibre-reinforced polymers. Toronto, Canada: Canadian Standards Association; 2012.
[32] Chaallal O, Benmokrane B. Physical and mechanical performance of an innovative glass–fiber-reinforced plastic rod for concrete and grouted anchorages. Can J Civ Eng 1993;20:254–68.
[33] Deitz D, Harik I, Gesund H. Physical properties of glass fiber reinforced polymer rebars in compression. J Compos Constr 2003;7:363–6.
[34] Kobayashi K, Fujisaki T. Compressive behavior of FRP reinforcement in non-prestressed concrete members. In: Taerwe L, editor. Proceedings of the 2nd international RILEM symposium (FRPRCS 2): non-metallic (FRP) reinforcement for concrete structures. CRC Press; 1995. p. 267–74.

[35] Wu W-P. Thermomechanical properties of fiber reinforced plastic (FRP) bars. Dissert Abstr Int (USA) 1992;52:292.
[36] Paramanantham NS. Investigation of the behavior of concrete columns reinforced with fiber reinforced plastic rebars [MS thesis]. Texas, USA: Lamar University; 1993.
[37] Alsayed S, Al-Salloum Y, Almusallam T, Amjad M. Concrete columns reinforced by glass fiber reinforced polymer rods. ACI Special Publ 1999;188.
[38] Tobbi H, Farghaly AS, Benmokrane B. Concrete columns reinforced longitudinally and transversally with glass fiber-reinforced polymer bars. ACI Struct J 2012;109.
[39] Tobbi H, Farghaly AS, Benmokrane B. Behavior of concentrically loaded fiber-reinforced polymer reinforced concrete columns with varying reinforcement types and ratios. ACI Struct J 2014;111.
[40] Tobbi H, Farghaly AS, Benmokrane B. Strength model for concrete columns reinforced with fiber-reinforced polymer bars and ties. ACI Struct J 2014;111.
[41] Afifi MZ, Mohamed HM, Benmokrane B. Axial capacity of circular concrete columns reinforced with GFRP bars and spirals. J Compos Constr 2013.
[42] Mohamed HM, Afifi MZ, Benmokrane B. Performance evaluation of concrete columns reinforced longitudinally with FRP Bars and confined with FRP hoops and spirals under axial load. J Bridge Eng 2014;19:04014020.
[43] Sumajouw D, Hardjito D, Wallah S, Rangan B. Fly ash-based geopolymer concrete: study of slender reinforced columns. J Mater Sci 2007;42:3124–30.
[44] Sumajouw D, Hardjito D, Wallah S, Rangan B. Behavior of geopolymer concrete columns under equal load eccentricities. ACI Special Publ 2005;228:577–94.
[45] Sarker PK. Analysis of geopolymer concrete columns. Mater Struct 2009;42:715–24.
[46] Sujatha T, Kannapiran K, Nagan S. Strength assessment of heat cured geopolymer concrete slender column. Asian J Civ Eng 2012;13:635–46.
[47] Maranan G, Manalo A, Karunasena K, Benmokrane B. Bond stress-slip behavior: case of GFRP bars in geopolymer concrete. J Mater Civ Eng 2014;27:04014116.
[48] Maranan G, Manalo A, Karunasena W, Benmokrane B. Pullout behaviour of GFRP bars with anchor head in geopolymer concrete. Compos Struct 2015;132:1113–21.
[49] CSA S807-10. Specification for fibre-reinforced polymers. Toronto, Canada: Canadian Standards Association; 2010. p. 44.
[50] ACI 440.3R-12. Guide test methods for fiber-reinforced polymers (FRPs) for reinforcing or strengthening concrete structures. B2-Test method for longitudinal tensile properties of FRP bars. Farmington Hills (MI, USA): American Concrete Institute; 2012.
[51] ASTM C39/C39M-15a. Standard test method for compressive strength of cylindrical concrete specimens. West Conshohocken (Pennsylvania, USA): ASTM International; 2015.
[52] ASTM C143/C143M-15. Standard test method for slump of hydraulic-cement concrete. West Conshohocken (Pennsylvania, USA): ASTM International; 2015.
[53] ASTM C807-13. Standard test method for time of setting of hydraulic cement mortar by modified Vicat needle. West Conshohocken (Pennsylvania, USA): ASTM International; 2013.
[54] Aldred J, Day J. Is geopolymer concrete a suitable alternative to traditional concrete. In: 37th conference on our world in concrete and structures. Singapore.
[55] Mirmiran A. Length effects on FRP-reinforced concrete columns. In: Saadatmanesh H, Ehsani MR, editors. The 2nd international conference on composites in infrastructure (ICCI 1996). Tucson (AZ, USA): ICCI; 1998.
[56] Mirmiran A, Yuan W, Chen X. Design for slenderness in concrete columns internally reinforced with fiber-reinforced polymer bars. ACI Struct J 2001;98.
[57] Zadeh HJ, Nanni A. Design of RC columns using glass FRP reinforcement. J Compos Constr 2013;17:294–304.
[58] Afifi MZ. Behavior of circular concrete columns reinforced with FRP bars and stirrups [PhD thesis]. Quebec, Canada: University of Sherbrooke; 2013.
[59] Saatcioglu M, Razvi SR. Strength and ductility of confined concrete. J Struct Eng 1992;118:1590–607.
[60] Sharma UK, Bhargava P, Kaushik S. Behavior of confined high strength concrete columns under axial compression. J Adv Concr Technol 2005;3:267–81.
[61] Paultre P, Légeron F. Confinement reinforcement design for reinforced concrete columns. J Struct Eng 2008;134:738–49.
[62] Yong Y-K, Nour MG, Nawy EG. Behavior of laterally confined high-strength concrete under axial loads. J Struct Eng 1988;114:332–51.
[63] Kent DC, Park R. Flexural members with confined concrete. J Struct Divis 1971;97:1969–90.
[64] ACI 318-11. Building code requirements for structural concrete and commentary. Farmington Hills (MI, USA): American Concrete Institute; 2011.
[65] Ozbakkaloglu T, Lim JC, Vincent T. FRP-confined concrete in circular sections: review and assessment of stress–strain models. Eng Struct 2013;49:1068–88.
[66] Popovics S. A numerical approach to the complete stress–strain curve of concrete. Cem Concr Res 1973;3:583–99.
[67] Han B-S, Shin S-W, Bahn B-Y. A model of confined concrete in high-strength reinforced concrete tied columns. Mag Concr Res 2003;55:203–14.
[68] Afifi MZ, Mohamed HM, Benmokrane B. Theoretical stress–strain model for circular concrete columns confined by GFRP spirals and hoops. Eng Struct 2015;102:202–13.
[69] Tavassoli A. Behaviour of GFRP-reinforced concrete columns under combined axial load and flexure [Master's thesis]. Toronto, Canada: University of Toronto; 2013.

4. CONCLUSIONS

Glass fibre reinforced polymer (GFRP) bar has gained considerable acceptance as internal reinforcement for concrete structures mainly to enhance the durability and to prolong the serviceability of these structures while geopolymer concrete is considered as a viable alternative to the traditional cement-based concrete for the development of environmentally friendly and more sustainable structures. To date, numerous research works on GFRP-reinforced concrete (GFRP-RC) and relatively less studies on steel-reinforced geopolymer concrete (S-RGC) systems are available in the literature. The use of GFRP-reinforced geopolymer concrete (GFRP-RGC) system, however, had not been studied before and this had been the key motivation of this undertaking. In this study, the structural behaviour of geopolymer concrete beams and columns internally reinforced with GFRP bars was experimentally and analytically investigated. The study was conducted in five phases:

1. Determination of the influence of the bar diameter and embedment length on the bond performance of straight GFRP bars in geopolymer concrete using the direct pullout test.
2. Assessment of the effects anchor head on the pullout behaviour of GFRP bars in geopolymer concrete, including the influences of the bar diameter and embedment length.
3. Evaluation of the flexural strength and serviceability of geopolymer concrete beams reinforced with GFRP bars and stirrups with different bar diameters, reinforcement ratios, and anchorage systems using the four-point static bending test.
4. Investigation of the influence of stirrups, stirrup spacing, stirrup type, longitudinal reinforcement ratio, and shear-span-to-effective depth ratio on the shear behaviour of geopolymer concrete beams reinforced with GFRP bars and stirrups using the four-point static bending test.
5. Examination of the influence of ties, tie spacing, tie configuration, and slenderness ratio on the behaviour of concentrically loaded geopolymer concrete columns reinforced with GFRP bars and ties.

4.1. Bond behaviour of GFRP bars in geopolymer concrete

The bond-slip response of high modulus straight and headed GFRP bars in geopolymer concrete was determined following the direct pullout test. The effects of bar diameter, embedment length, and anchorage system were evaluated. For comparison purposes, bond-slip

specimens with steel embedded in geopolymer concrete were also cast and tested. Based on the test results, the following conclusions were derived:

- There is a sufficient bond between the sand-coated straight GFRP bars and geopolymer concrete to secure a composite action, owing to the mechanical interlock and friction forces coming from the sand particles. In fact, the maximum average bond stress of the sand-coated straight GFRP bars in geopolymer concrete reached as much as 23 MPa.
- The bond development of GFRP bars can be enhanced further through the mechanical bearing resistance provided by the anchor heads. This was proven by an increase of tensile stress developed in the bars, approximately 45% of the bar's tensile strength, and the failure mode of the specimens, wherein the use of anchor head shifted the failure from bar pullout to concrete splitting. The strength-enhancing effect of anchor head, however, diminishes as the embedment length increases.
- For both straight and headed bars, an increase in the bonded length was accompanied by a decrease in the average bond strength, owing to the nonlinear stress distribution along the effectively bonded length of the bar. Similarly, as the bar diameter increases, the average bond strength decreases, which could be attributed to Poisson's and shear lag effects.
- Bar pullout failure occurred in the specimens with shorter embedment length while concrete splitting failure happened in the specimens with longer embedment lengths.
- No significant difference was found between the bond strengths developed by the sand-coated GFRP and deformed steel bars, suggesting that the provision of sand particles was an effective means to anchor the GFRP bars in geopolymer concrete properly.
- The bond strengths obtained from straight and headed GFRP bars embedded in geopolymer concrete were higher than those embedded in OPC concrete of similar grade, indicating that the geopolymer concrete have superior tensile strength compared to the OPC concrete.
- The developed bond stress-slip models, based on CMR models, yielded outcomes that were practically similar to the experimental results. The proposed equation for predicting the pullout capacity of GFRP bars, on the other hand, yielded lower estimates for straight GFRP bars while it produced conservative estimates for headed GFRP bars.
- Sufficient bond exist between the GFRP bar and geopolymer concrete to effectively transfer the stresses from one to the other and secure a composite action, which

validated the acceptability of GFRP bars as alternative reinforcement to geopolymer concrete structures such as beams and columns.

4.2. GFRP-reinforced geopolymer concrete beams

Five full-scale slender GFRP-RGC beams and one full-scale slender S-RGC beam with nominal dimensions of 200 mm wide, 300 mm deep, and 3100 mm long were subjected to a four-point static bending test to investigate the flexural strength and serviceability performance of the proposed system. The test parameters were the nominal bar diameter, longitudinal tensile reinforcement ratio, and anchorage system. On the other hand, six beams with the same cross-sectional area as the beams in flexure but with a length of 1500 mm were tested to examine the shear behaviour of the GFRP-RGC system. The influence of stirrups, stirrup spacing, stirrup type, and longitudinal reinforcement ratio were analysed. From the test results, the following generalisations were made:

- The failure of the beams in flexure was due to concrete crushing failure, and yielded a three-segment load-deflection. The first part was a stiff linear segment that characterises the uncracked response while the second part was an almost linear segment with reduced slope that represents the cracked response of the beams. The third segment, a nonlinear segment with much reduced slope, signifies the post-crushing behaviour of the beams, owing to the still intact geopolymer concrete core confined by stirrups that provide the compression resistance.
- The serviceability performance of the beams was enhanced by doubling the longitudinal reinforcement ratio, such as lower deflection and narrower crack widths; however, it did not improve the load-carrying capacity of the beam, specifically at the concrete crushing stage. This outcome suggests that a much higher amount of longitudinal reinforcement must be used in beams to enhance both its flexural strength and serviceability performance.
- The diameter of the bars have no significant effect on the flexural strength and stiffness of the beams.
- The beam reinforced with headed GFRP bars yielded similar flexural performance as the beam reinforced with straight GFRP bars with similar reinforcement ratio. Noting that the bars are fully bonded in geopolymer concrete, this observation tends to support the earlier conclusion that the influence of anchor heads diminishes as the embedment length increases.

- The bending-moment capacities at concrete crushing failure of GFRP-RGC beams were 1.2 to 1.5 times greater than that of S-RGC beam with similar reinforcement ratio.
- The bending-moment capacity of GFRP-RGC beams seems to be higher than that of GFRP-RC beams, owing to the enhanced mechanical properties of the geopolymer concrete compared to the conventional concrete of the same grade. Further investigations, however, are needed to support this generalisation.
- Two methods were proposed to predict the flexural strength of the tested beams. For the first method, using the rectangular stress block, accurate results were obtained when a concrete strength reduction factor of 0.90 and a usable concrete strain of 0.0048 were adopted and by incorporating the compression contribution of GFRP bars. The second method adopted Popovics stress-strain model and linear equation to model the ascending and descending branches, respectively, of the parabolic stress block. Accurate predictions were obtained when the same amount of concrete strain was adopted and when the compression contribution of top GFRP bars were included.
- The mid-span deflection of the tested beams were accurately estimated by modifying Branson's effective moment of inertia formula through the factors β_a and β_b, both functions of actual and balanced reinforcement ratios.
- The shear failure of the beams was governed by either diagonal strut tension failure or diagonal strut compression failure. Furthermore, these beams produced a two-segment load-deflection response: the cracked and uncracked responses of the beams.
- The provision of GFRP stirrups enhanced both the shear strength and deflection capacity of the GFRP-RGC beams by approximately 200%, owing to the stirrups' contribution to vertical shear resistance and a clamping effect that enhanced the geopolymer-concrete's contribution to shear resistance.
- A small increase of longitudinal reinforcement, around 11%, enhanced both the shear strength and deflection capacities of the beams with average of 22% and 16%, respectively.
- At the same strain level in the GFRP stirrups, the beam with closely spaced stirrups, 75 mm on center in this study, yielded the highest shear-load capacity. Similarly, the shear crack initiated at a higher load in the beam with stirrups with narrower spacing. These observations could be attributed higher reinforcement index $\rho_{fv}E_{fv}/E_s$ of the beam with closer stirrup spacing compared to the other tested beams. Furthermore, the shear crack width decreases with the stirrup spacing because, the smaller the stirrup spacing, the

lower the effective concrete area needed to be controlled by a stirrup in terms of shear-crack-width development, thereby resulting in higher bond adhesion between the stirrup and the surrounding concrete.

- The short beam with a shear-span to effective depth ratio (a/d) of 1.8 yielded higher shear strength compared to the slender beam with a a/d of 4.4 with similar amount of transverse reinforcement, owing to the strength enhancing effects of arching action in short beams.
- The shear capacity of the tested GFRP-RGC beams were higher than that of their counterpart GFRP-RC beams with similar configurations
- The ACI 318-14 yielded the most accurate estimates among the equations considered in this study in predicting the shear strength of the tested beams.
- These results suggest that the GFRP-RGC system can be as effective as GFRP-RC and S-RGC systems for the fabrication of structural beams; however, some considerations should be considered in their design. To validate further the adoptability of the proposed system in the construction sector, the behaviour of GFRP-RGC columns subjected to compressive loading was then investigated.

4.3. GFRP-reinforced geopolymer concrete columns

The compression behaviour of 250 mm diameter circular geopolymer concrete columns reinforced longitudinally with GFRP bars (2.43%) and confined by either GFRP spirals or hoops with different spacing was investigated by subjecting the column specimens to axial loads. Six (6) short and two (2) slender columns with slenderness ratios (L/r) of 8 and 16, respectively, were considered in this study. From the experimental and analytical results, the following conclusions were drawn:

- The GFRP bars contributed an average of 7.6% to the overall capacity of the tested columns, suggesting that these bars have compression contribution that cannot be ignored in the design calculations.
- The provision of transverse reinforcement generally enhanced the both the strength and deformation capacity of the tested GFRP-RGC columns by 10% and 1%, respectively.
- Irrespective of the tie configuration, the columns with ties spaced at 50 mm on-centre yielded higher strength and deformation capacities than the columns with ties spaced at 100 mm and 200 mm on-centres, because the former columns have closely spaced ties that enhanced the compression properties of the geopolymer-concrete core and prevented the buckling of GFRP bars. Furthermore, the closer the tie spacing or the

larger the volumetric ratio, the less brittle the compression failure of the tested columns, showing a slower rate of strength decay after the peak.

- The ductility and confinement efficiency of the spiral-confined columns were higher than their counterpart hoop-confined columns because the spirals effectively confined the whole geopolymer-concrete core by distributing the lateral confining pressures uniformly around the perimeter and along the height of the geopolymer-concrete core.
- The slender columns yielded lower failed at a load 66% and 82% of the strength of their short-column counterparts. They exhibited higher deformation compared to the short columns due to the lateral movement and they failed due to buckling.
- Geopolymer concrete columns reinforced with GFRP bars yielded relatively superior compression strength than OPC-based concrete columns reinforced with GFRP bars and ties because the GFRP bars have better compatibility with geopolymer concrete compared with OPC concrete, owing to the higher elastic modulus of the former concrete compared to the latter concrete.
- The proposed confined stress-strain equations show good correlation with the experimentally established stress-strain relationship for the GFRP-RGC columns.

4.4. Contributions of the study

The results obtained from this study showed that the GFRP-RGC system is a promising application. The outcomes of this thesis provide the research community and the construction industry with a more in-depth understanding on the structural behaviour of GFRP-RGC beams and columns, thus filling the knowledge gap that currently exists in civil infrastructure. The experimental data, proposed design parameters, and analytical models developed in this study can be important tools for design engineers permitting the safe design and development of GFRP-RGC system, enabling their increased acceptance and utilisation in the mainstream construction application. Upon the widespread acceptance of GFRP-RGC system, it is expected that CO_2 emissions from the cement and concrete sectors can be minimised, the virgin resource materials for manufacturing cement can be preserved, the energy can be saved, the costly repair and rehabilitation can be avoided, and the landfill needed for fly ash disposal can be reduced.

Further, the results obtained from the study could create a platform whereupon designers and engineers could begin to employ GFRP materials and systems in their design solutions. It is believed that by understanding the behaviour of geopolymer concrete structures

reinforced with GFRP bars, new and innovative structural forms would emerge to incorporate GFRP and geopolymer concrete materials in a more functional and economically viable manner.

4.5. Areas for further study

The study of GFRP-RGC system is at an early stage and requires further experimental and analytical works to increase its adoptability in the mainstream construction applications. Based on the findings of this study, the following recommendations for future investigations are drawn:

1. A higher bond performance of straight and headed GFRP bars embedded in geopolymer concrete can be achieved if the geopolymer concrete will exhibit a pullout type of failure. It is suggested, therefore, to use transverse confining materials, like stirrups and FRP wraps, to achieve this mode of failure.
2. Since the design of GFRP-RGC beams is governed by serviceability requirements, a detailed experimental and analytical investigation on the crack width and on the long-term deflections of GFRP-RGC beams and columns should be carried out. Furthermore, the use of headed GFRP bars as the main flexural reinforcement for geopolymer concrete deep beams should also be investigated.
3. Further experimental works incorporating the effects of other parameters, such as geopolymer concrete strength, transverse reinforcement ratio, GFRP bar types, size effects, and type of loads, should be done to be able to calibrate accurately the proposed prediction equations. In addition, finite element models should be developed so that parametric investigations could be done easily.
4. Additional investigations, using a wide variety of geopolymer concrete mixes and FRP bars, is recommended to be able to establish design codes for geopolymer concrete structures reinforced with FRP bars.
5. Given that the GFRP-RGC system is a doable technology, the investigation should be extended to the evaluation of the structural performance of other structural elements like slabs, footings, retaining walls, hollow beams and columns, and even precast elements.
6. Finally, the durability performance of GFRP bars under a high-alkali condition must be evaluated since the geopolymer binders have a higher pH than OPC binders.

List of References

Abraham, R., Raj, S. D., & Abraham, V. (2013). Strength and behaviour of geopolymer concrete beams. International Journal of Innovative Research in Science, Engineering and Technology, 2(1), 159-166.

Achillides, Z., & Pilakoutas, K. (2004). Bond behavior of fiber reinforced polymer bars under direct pullout conditions. Journal of Composites for Construction, 8(2), 173-181.

Achillides, Z., Pilakoutas, K., & Waldron, P. (1997, 14-10 October 1997). Modelling of FRP rebar bond behaviour. Paper presented at the 3rd International Symposium on Non-Metallic (FRP) Reinforcement for Concrete Structures (FRPRCS 3), Sapporo, Japan.

ACI 318-02. (2002). Building code requirements for structural concrete and commentary. Farmington Hills, MI, USA: American Concrete Institute.

ACI 318-14. (2014). Building code requirements for structural concrete and commentary. Farmington Hills, MI, USA: American Concrete Institute.

ACI 440.1R-15. (2015). Guide for the design and construction of structural concrete reinforced with FRP bars. Farmington Hills, Michigan, USA: American Concrete Institute.

Adam, M. A., Said, M., Mahmoud, A. A., & Shanour, A. S. (2015). Analytical and experimental flexural behavior of concrete beams reinforced with glass fiber reinforced polymer bars. Construction and Building Materials, 84, 354-366.

Afifi, M. (2013). Behaviour of circular concrete columns reinforced with FRP bars and stirrups. PhD in Civil Engineering, University de Sherbrooke, Quebec, Canada.

Afifi, M. Z., Mohamed, H. M., & Benmokrane, B. (2013). Axial capacity of circular concrete columns reinforced with GFRP bars and spirals. Journal of Composites for Construction, 18(1), 04013017.

Ahmad, S. (2003). Reinforcement corrosion in concrete structures, its monitoring and service life prediction—a review. Cement and Concrete Composites, 25(4), 459-471.

Ahmed, E. A., & Benmokrane, B. (2009). Characterization and strength evaluation of the headed GFRP Bars. University of Sherbrooke, Technical report submitted to Pultrall Inc, 1-21.

Ahmed, E. A., El-Salakawy, E. F., & Benmokrane, B. (2010a). Performance evaluation of glass fiber-reinforced polymer shear reinforcement for concrete beams. ACI Structural Journal, 107(1), 53.

Ahmed, E. A., El-Salakawy, E. F., & Benmokrane, B. (2010b). Shear performance of RC bridge girders reinforced with carbon FRP stirrups. Journal of Bridge Engineering, 15(1), 44-54.

Aiello, M. A., & Ombres, L. (2000). Load-deflection analysis of FRP reinforced concrete flexural members. Journal of Composites for Construction, 4(4), 164-171.

Al-Zahrani, M. M., Al-Dulaijan, S. U., Nanni, A., Bakis, C. E., & Boothby, T. E. (1999). Evaluation of bond using FRP rods with axisymmetric deformations. Construction and Building Materials, 13(6), 299-309.

Aldred, J., & Day, J. (2012). Is geopolymer concrete a suitable alternative to traditional concrete. Paper presented at the 37th Conference on our World In Concrete and Structures (OWICs 2012), Singapore.

Aleem, M. A., & Arumairaj, P. (2012). Geoolymer concrete - a review. International journal of engineering sciences & emerging technologies, 1(2), 118-122.

Alsayed, S. H. (1998). Flexural behaviour of concrete beams reinforced with GFRP bars. Cement and Concrete Composites, 20(1), 1-11.

Alsayed, S. H., Al-Salloum, Y. A., & Almusallam, T. H. (2000). Performance of glass fiber reinforced plastic bars as a reinforcing material for concrete structures. Composites Part B: Engineering, 31(6), 555-567.

Alsayed, S. H., Al-Salloum, Y. A., Almusallam, T. H., & Amjad, M. A. (1999). Concrete columns reinforced by glass fiber reinforced polymer rods. ACI Special Publication, 188.

Ambily, P. S., Madheswaran, C. K., Lakhsmanan, N., Dattatreya, J. K., & Sathik, S. A. (2012). Experimental studies on shear behaviour of reinforced geopolymer concrete thin webbed T-beams with and without fibres. International Journal of Civil & Structural Engineering, 3(1), 128-140.

Arias, J. P. M., Vazquez, A., & Escobar, M. M. (2012). Use of sand coating to improve bonding between GFRP bars and concrete. Journal of Composite Materials, 0021998311431994.

AS 3600-01. (2001). Concrete structures. Sydney, Australia: Standards Australia.

AS 3600-05. (2005). Concrete structures. Sydney, Australia: Standards Australia.

Ascione, L., Razaqpur, A. G., & Spadea, S. (2014, 20-22 August 2014). Effectiveness of FRP stirrups in concrete beams subject to shear. Paper presented at the 7th International Conference on FRP Composites in Civil Engineering–CICE 2014, Vancouver, Canada.

Australia, V.-R. (2012). V-Rod product guide specification. Retrieved 25 February, 2016, from http://www.vrodaustralia.com.au/

Baena, M., Torres, L. l., Turon, A., & Barris, C. (2009). Experimental study of bond behaviour between concrete and FRP bars using a pull-out test. Composites Part B: Engineering, 40(8), 784-797.

Bakis, C., Uppuluri, V., Nanni, A., & Boothby, T. (1998). Analysis of bonding mechanisms of smooth and lugged FRP rods embedded in concrete. Composites science and technology, 58(8), 1307-1319.

Bank, L. C. (2006). Composites for construction: structural design with FRP materials: John Wiley & Sons.

Barris, C., Torres, L. l., Turon, A., Baena, M., & Catalan, A. (2009). An experimental study of the flexural behaviour of GFRP RC beams and comparison with prediction models. Composite Structures, 91(3), 286-295.

Beeby, A. W., & Narayanan, R. S. (1995). Designers' handbook to Eurocode 2: Design of concrete structures. London, UK: Thomas Telford.

Benhelal, E., Zahedi, G., Shamsaei, E., & Bahadori, A. (2013). Global strategies and potentials to curb CO2 emissions in cement industry. Journal of Cleaner Production, 51, 142-161.

Benmokrane, B., Chaallal, O., & Masmoudi, R. (1995). Glass fibre reinforced plastic (GFRP) rebars for concrete structures. Construction and Building Materials, 9(6), 353-364.

Benmokrane, B., Elgabbas, F., Ahmed, E. A., & Cousin, P. (2015). Characterization and comparative durability study of glass/vinylester, basalt/vinylester, and basalt/epoxy FRP bars. Journal of Composites for Construction, 19(6), 04015008.

Benmokrane, B., & Tighiouart, B. (1996). Bond strength and load distribution of composite GFRP reinforcing bars in concrete. ACI Materials Journal, 93(3), 254-259.

Bentz, E. C., Massam, L., & Collins, M. P. (2010). Shear strength of large concrete members with FRP reinforcement. Journal of Composites for Construction, 14(6), 637-646.

Bertolini, L. (2008). Steel corrosion and service life of reinforced concrete structures. Structure and Infrastructure Engineering, 4(2), 123-137.

Branson, D. E. (1968). Design procedures for computing deflections. ACI journal, 65(9), 730-742.

Bruun, E. (2014). GFRP bars in structural design: Determining the compressive strength versus unbraced length interaction curve. Canadian Young Scientist Journal, 2014(1), 22-29.

Cabrera, J. G. (1996). Deterioration of concrete due to reinforcement steel corrosion. Cement and Concrete Composites, 18(1), 47-59.

CAN/CSA A23.3-04. (2004). Design of concrete structures. Toronto, Canada: Canadian Standards Association.

CAN/CSA S6-14. (2014). Canadian highway bridge design code. Toronto, Canada: Canadian Standards Association.

CAN/CSA S806-12. (2012). Design and construction of building components with fibre-reinforced polymers. Toronto, Canada: Canadian Standards Association.

CAN/CSA S807-10. (2010). Specification for fibre-reinforced polymers (pp. 44). Toronto, Canada: Canadian Standards Association.

Capozucca, R. (1995). Damage to reinforced concrete due to reinforcement corrosion. Construction and Building Materials, 9(5), 295-303.

Castro, P. F., & Carino, N. J. (1998). Tensile and nondestructive testing of FRP bars. Journal of Composites for Construction, 2(1), 17-27.

Chaallal, O., & Benmokrane, B. (1993). Physical and mechanical performance of an innovative glass-fiber-reinforced plastic rod for concrete and grouted anchorages. Canadian Journal of Civil Engineering, 20(2), 254-268.

Chen-Tan, N. W., Van Riessen, A., Ly, C. V., & Southam, D. C. (2009). Determining the reactivity of a fly ash for production of geopolymer. Journal of the American Ceramic Society, 92(4), 881-887.

CNR DT-203/2006. (2007). Guide for the design and construction of concrete structures reinforced with fiber-reinforced polymer bars CNR DT-203/2006. Rome, Italy: Italian Research Council.

Cosenza, E., Manfredi, G., & Realfonzo, R. (1995). Analytical modelling of bond between FRP reinforcing bars and concrete. Paper presented at the 2nd International RILEM Symposium: Non-Metallic (FRP) Reinforcement for Concrete Structures (FRPRCS 2).

Cosenza, E., Manfredi, G., & Realfonzo, R. (1996). Bond characteristics and anchorage length of FRP rebars. Paper presented at the 2nd International Conference on Advanced Composite Materials in Bridges and Structures, Montreal, Canada.

Cosenza, E., Manfredi, G., & Realfonzo, R. (1997). Behavior and modeling of bond of FRP rebars to concrete. Journal of Composites for Construction, 1(2), 40-51.

Criado, M., Fernández-Jiménez, A., De La Torre, A. G., Aranda, M. A. G., & Palomo, A. (2007). An XRD study of the effect of the SiO2 / Na2O ratio on the alkali activation of fly ash. Cement and Concrete Research, 37(5), 671-679.

Dattatreya, J. K., Rajamane, N. P., Sabitha, D., Ambily, P. S., & Nataraja, M. C. (2011). Flexural behaviour of reinforced geopolymer concrete beams. International Journal of Civil and Structural Engineering, 2(1), 138-159.

Davalos, J. F., Chen, Y., & Ray, I. (2008). Numerical modeling for the interface bond of concrete and FRP bar. Earth & Space, 3-5.

Davidovits, J. (1991). Geopolymers: Inorganic polymeric new materials. Journal of Thermal Analysis, 37(8), 1633-1656.

de Almeida Filho, F. M., Mounir, K., & El Debs, A. L. H. (2008). Bond-slip behavior of self-compacting concrete and vibrated concrete using pull-out and beam tests. Materials and structures, 41(6), 1073-1089.

De Luca, A., Matta, F., & Nanni, A. (2010). Behavior of full-scale glass fiber-reinforced polymer reinforced concrete columns under axial load. ACI Structural Journal, 107(05), 589-596.

Deb, P. S., Sarker, P. K., & Barbhuiya, S. (2015). Effects of nano-silica on the strength development of geopolymer cured at room temperature. Construction and Building Materials, 101, 675-683.

Dhake, P. D., Patil, H. S., & Patil, Y. D. (2015). Anchorage behaviour and development length of headed bars in exterior beam–column joints. Magazine of concrete research, 67(2), 53-62.

Diaz, E. I., Allouche, E. N., & Eklund, S. (2010). Factors affecting the suitability of fly ash as source material for geopolymers. Fuel, 89(5), 992-996.

Duxson, P., Provis, J. L., Lukey, G. C., & Van Deventer, J. S. J. (2007). The role of inorganic polymer technology in the development of ‘green concrete’. Cement and Concrete Research, 37(12), 1590-1597.

El-Gamal, S., Abdulrahman, B., & Benmokrane, B. (2011). Deflection behaviour of concrete beams reinforced with different types of GFRP bars Advances in FRP Composites in Civil Engineering (pp. 279-282): Springer.

El-Mogy, M., El-Ragaby, A., & El-Salakawy, E. (2010). Flexural behavior of continuous FRP-reinforced concrete beams. Journal of Composites for Construction, 14(6), 669-680.

El-Sayed, A. K., El-Salakawy, E. F., & Benmokrane, B. (2012). Shear strength of fibre-reinforced polymer reinforced concrete deep beams without web reinforcement. Canadian Journal of Civil Engineering, 39(5), 546-555.

El-Sayed, A. K., & Soudki, K. (2011). Evaluation of shear design equations of concrete beams with FRP reinforcement. Journal of Composites for Construction, 15(1), 9-20.

Eligehausen, R., Popov, E. P., & Bertero, V. V. (1982). Local bond stress-slip relationships of deformed bars under generalized excitations.

Farghaly, A. S., & Benmokrane, B. (2013). Shear behavior of FRP-reinforced concrete deep beams without web reinforcement. Journal of Composites for Construction, 17(6), 04013015.

Fernández-Jiménez, A., & Palomo, A. (2003). Characterisation of fly ashes. Potential reactivity as alkaline cements☆. Fuel, 82(18), 2259-2265.

fib Bulletin 40. (2007). FRP reinforcement in RC structures. Lausanne, Switzerland: The Internationa Federation for Structural Concrete.

Foster, S. J., Kilpatrick, A. E., & Warner, R. F. (2010). Reinforced concrete basics 2E: Analysis and design of reinforced concrete structures. Frenchs Forest, NSW, Australia: Pearson Education Australia.

Ganesan, N., Indira, P. V., & Santhakumar, A. (2015). Bond behaviour of reinforcing bars embedded in steel fibre reinforced geopolymer concrete. Magazine of concrete research, 67(1), 9-16.

Gangarao, H. V. S., Tally, N., & Vijay, P. V. (2007). Reinforced concrete design with FRP composites: CRC Press.

Guo, X., Shi, H., & Dick, W. A. (2010). Compressive strength and microstructural characteristics of class C fly ash geopolymer. Cement and Concrete Composites, 32(2), 142-147.

Han, B. S., Shin, S. W., & Bahn, B. Y. (2003). A model of confined concrete in high-strength reinforced concrete tied columns. Magazine of concrete research, 55(3), 203-214.

Hardjito, D., & Rangan, B. V. (2005). Development and properties of low-calcium fly as- based geopolymer concrete. Perth, Australia: Faculty of Engineering, Curtin University of Technology.

Hardjito, D., Wallah, S. E., Sumajouw, D. M. J., & Rangan, B. V. (2004). On the development of fly ash-based geopolymer concrete. ACI Materials Journal-American Concrete Institute, 101(6), 467-472.

Hollaway, L. (2008). Advanced fibre polymer composite structural systems used in bridge engineering. ICE manual of bridge engineering, 34525.

Isgor, O. B., & Razaqpur, A. G. (2006). Modelling steel corrosion in concrete structures. Materials and structures, 39(3), 291-302.

ISIS 3(2)-01. (2006). Reinforcing concrete structures with fibre-reinforced polymers ISIS Design Manual No. 3. Winnipeg, Manitoba, Canada: Intelligent Sensing for Innovative Structures (ISIS) Canada.

JSCE. (2007). Standard specifications for concrete structures JSCE 2007. Tokyo, Japan: Japan Society of Civil Engineers.

Kambic, M., & Hammaker, J. (2012). Geopolymer concrete: The future of green building materials. Retrieved 03 July 2016 from http://136.142.82.187/eng12/Author/data/2099.docx.

Kang, T. H.-K., & Mitra, N. (2012). Prediction of performance of exterior beam-column connections with headed bars subject to load reversal. Engineering Structures, 41, 209-217.

Kassem, C., Farghaly, A. S., & Benmokrane, B. (2011). Evaluation of flexural behavior and serviceability performance of concrete beams reinforced with FRP bars. ASCE Journal of Composites for Construction, 15(5), 682-695.

Khale, D., & Chaudhary, R. (2007). Mechanism of geopolymerization and factors influencing its development: a review. Journal of Materials Science, 42(3), 729-746.

Kim, J. S., & Park, J. (2014). An Experimental Evaluation of Development Length of Reinforcements Embedded in Geopolymer Concrete. Paper presented at the Applied Mechanics and Materials.

Krall, M. D., & Polak, M. A. (2014, 20-22 August 2014). Tests on concrete beams with GFRP flexural and shear reinforcements. Paper presented at the 7th International Conference on FRP Composites in Civil Engineering (CICE 2014), Vancouver, Canada.

Kumaravel, S., & Thirugnanasambandam, S. (2013). Flexural behaviour of geopolymer concrete beams. International Journal of Advanced Engineering Research and Studies, 3(1), 4-6.

Lloyd, N. A., & Rangan, B. V. (2010). Geopolymer concrete: A review of development and opportunities. Paper presented at the 35th Conference on Our World in Concrete and Structures (OWICs 2010), Singapore.

Luca, A. D., Matta, F., & Nanni, A. (2009). Structural response of full-scale reinforced concrete columns with internal FRP reinforcement under compressive load. Paper presented at the Proceedings of the 9th International Symposium of the Fiber-Reinforced Polymer Reinforcement for Reinforced Concrete Structures (FRPRCS-9), Sydney, Australia.

MacGinley, T. J., & Choo, B. S. (1990). Reinforced concrete: Design theory and examples (2nd Edition ed.): SPON Press.

Machida, A., & Uomoto, T. (1997). Recommendation for design and construction of concrete structures using continuous fiber reinforcing materials (Vol. 23): Research Committee on Continuous Fiber Reinforcing Materials, Japan Society of Civil Engineers.

Madlool, N. A., Saidur, R., Hossain, M. S., & Rahim, N. A. (2011). A critical review on energy use and savings in the cement industries. Renewable and Sustainable Energy Reviews, 15(4), 2042-2060.

Mahasenan, N., Smith, S., Humphreys, K., & Kaya, Y. (2003). The cement industry and global climate change: current and potential future cement industry CO2 emissions. Paper presented at the 6th International Conference on Greenhouse Gas Control Technologies.

Mahmoud, K., & El-Salakawy, E. (2014, 20-22 August 2014). Shear strength of GFRP-reinforced concrete continuous beams. Paper presented at the 7th International Conference on FRP Composites in Civil Engineering (CICE 2014), Vancouver, Canada.

Mallick, P. K. (2007). Fiber-reinforced composites: materials, manufacturing, and design: CRC press.

Malvar, L. J. (1994). Bond stress-slip characteristics of FRP rebars: DTIC Document.

Masmoudi, A., Ouezdou, M. B., & Bouaziz, J. (2012). New parameter design of GFRP RC beams. Construction and Building Materials, 29, 627-632.

Matos, B., Correia, J. R., Castro, L. M. S., & Franca, P. (2012). Structural response of hyperstatic concrete beams reinforced with GFRP bars: Effect of increasing concrete confinement. Composite Structures, 94(3), 1200-1210.

Mehta, P. K. (1997). Durability - critical issues for the future. ACI Concrete International, 19(7), 27-33.

Mehta, P. K. (2001). Reducing the environmental impact of concrete. Concrete International, 23(10), 61-66.

Mehta, P. K. (2002). Greening of the concrete industry for sustainable development. Concrete International, 24(7), 23-28.

Mehta, P. K. (2010). Sustainable cements and concrete for the climate change era – a review. Paper presented at the 2nd International Conference on Sustainable Construction Materials and Technologies (ICCI 1996), Universita Politecnica delle Marche, Ancona, Italy.

Mejeoumov, G. G. (2007). Improved cement quality and grinding efficiency by means of closed mill circuit modeling. Doctor of Philosophy, Texas A&M University, Texas, USA.

Mihaylov, B. I., Bentz, E. C., & Collins, M. P. (2013). Two-parameter kinematic theory for shear behavior of deep beams. ACI Structural Journal, 110(3), 447-455.

Mohamed, H. M., Afifi, M. Z., & Benmokrane, B. (2014). Performance evaluation of concrete columns reinforced longitudinally with FRP bars and confined with FRP hoops and spirals under axial Load. Journal of Bridge Engineering, 19(7), 04014020.

Mohamed, H. M., & Benmokrane, B. (2009). Pullout capacity behaviour of FRP-headed rebars. Paper presented at the 5th International Conference on Composites in Civil Engineering Rome, Italy.

Mohamed, K., Farghaly, A. S., & Benmokrane, B. (2014, 20-22 August 2014). Effect of web reinforcement in FRP-reinforced deep beams. Paper presented at the 7th International Conference on FRP Composites in Civil Engineering (CICE 2014), Vancouver, Canada; .

Mousavi, S. R., & Esfahani, M. R. (2012). Effective moment of inertia prediction of FRP-reinforced concrete beams based on experimental results. Journal of Composites for Construction, 16(5), 490-498.

Mufti, A. A., Banthia, N., Benmokrane, B., Boulfiza, M., & Newhook, J. P. (2007). Durability of GFRP composite rods. Concrete International, 29(02), 37-42.

Murugavel, P., & Mala, C. (2014). Experimental study on reinforced geopolymer concrete wih high volume fly ash. International Journal of Engineerig Research and Advanced Technology, 2(3), 97-135.

Nagasaka, T., Fukuyama, H., & Tanigaki, M. (1993). Shear performance of concrete beams reinforced with FRP stirrups. ACI Special Publication, 138, 789-812.

Najm, M. M. S. (2012). Investigating the use of fiber-reinforced polymer bars in concrete. Master of Engineering, Massachusetts Institute of Technology.

Nanni, A., Al-Zaharani, M. M., Al-Dulaijan, S. U., Bakis, C. E., & Boothby, I. E. (1995). Bond of FRP reinforcement to concrete-experimental results. Paper presented at the 2nd International RILEM Symposium: Non-Metallic (FRP) Reinforcement for Concrete Structures (FRPRCS 2).

Nilson, A., Darwin, D., & Dolan, C. W. (2003). Design of concrete structures. New York, USA: McGraw-Hill.

Nkurunziza, G., Benmokrane, B., Debaiky, A., & Masmoudi, R. (2005). Effect of sustained load and environment on long-term tensile properties of glass fiber-reinforced polymer reinforcing bars. ACI Structural Journal, 102(4), 615.

Okelo, R., & Yuan, R. L. (2005). Bond strength of fiber reinforced polymer rebars in normal strength concrete. Journal of Composites for Construction, 9(3), 203-213.

Olivier, J. G. J., Janssens, M. G., Muntean, M., & Peters, J. A. H. W. (2015). Trends in global CO2 emissions: 2015 Report (pp. 1-80). Hague, Netherlands.

Oller, E., Marí, A., Bairán, J. M., & Cladera, A. (2015). Shear design of reinforced concrete beams with FRP longitudinal and transverse reinforcement. Composites Part B: Engineering, 74, 104-122.

Otieno, M., Beushausen, H., & Alexander, M. (2016). Chloride-induced corrosion of steel in cracked concrete – Part I: Experimental studies under accelerated and natural marine environments. Cement and Concrete Research, 79, 373-385.

Palomo, A., & Glasser, F. P. (1992). Chemically-bonded cementitious materials based on metakaolin. British ceramic. Transactions and journal, 91(4), 107-112.

Pantazopoulou, S. J., & Papoulia, K. D. (2001). Modeling cover-cracking due to reinforcement corrosion in RC structures. Journal of Engineering Mechanics, 127(4), 342-351.

PCA. (2002). Types and cause of concrete deterioration. Retrieved 16 February 2016 from http://www.cement.org/docs/default-source/th-paving-pdfs/concrete/types-and-causes-of-concrete-deterioration-is536.pdf?sfvrsn=4.

PCA. (2015). Global cement consumption on the rise. Retireved 20 February 2016 from http://www.cement.org/news/2015/06/03/global-cement-consumption-on-the-rise.

Pecce, M., Manfredi, G., & Cosenza, E. (2000). Experimental response and code models of GFRP RC beams in bending. Journal of Composites for Construction, 4(4), 182-190.

Popovics, S. (1973). A numerical approach to the complete stress-strain curve of concrete. Cement and Concrete Research, 3(5), 583-599.

Rangan, B. V. (2008). Fly ash based geopolymer concrete Research Report GC4. Perth Australia: Curtin University of Rechnology.

Ratcliff, S. (2009). Research shows corrosion costs the local economy. Retrieved 03 March 2016 from http://news.curtin.edu.au/media-releases/research-shows-corrosion-costs-the-local-economy/.

RILEM 7-II-128. (1994). RC6: Bond test for reinforcing steel. 1. Pull-out Test (pp. 102-105). Oxfordshire, UK: E & FN Spon.

Robert, M., & Benmokrane, B. (2009). Behavior of GFRP reinforcing bars subjected to extreme temperatures. Journal of Composites for Construction, 14(4), 353-360.

Robert, M., & Benmokrane, B. (2010). Effect of aging on bond of GFRP bars embedded in concrete. Cement and Concrete Composites, 32(6), 461-467.

Robert, M., Cousin, P., & Benmokrane, B. (2009). Durability of GFRP reinforcing bars embedded in moist concrete. Journal of Composites for Construction, 13(2), 66-73.

Rodriguez, J., Ortega, L. M., & Casal, J. (1997). Load carrying capacity of concrete structures with corroded reinforcement. Construction and Building Materials, 11(4), 239-248.

Sakulich, A. R. (2011). Reinforced geopolymer composites for enhanced material greenness and durability. Sustainable Cities and Society, 1(4), 195-210.

Sarker, P. K. (2008). A constitutive model for fly ash-based geopolymer concrete. Architecture Civil Engineering Environment (The Silesian University of Technology), 1(4), 113-120.

Sarker, P. K. (2009). Analysis of geopolymer concrete columns. Materials and structures, 42(6), 715-724.

Sarker, P. K. (2011). Bond strength of reinforcing steel embedded in fly ash-based geopolymer concrete. Materials and structures, 44(5), 1021-1030.

Sayed-Ahmed, M., & Sennah, K. (2014). Pullout strength of sand-coated GFRP Bars embedded in ultra-high performance fiber reinforced concrete. Paper presented at the 4th International Structural Specialty Conference, Halifax, NS.

Selby, D. R. (2011). An investigation into the bond of steel reinforcement in geopolymer and ordinary portland cement concrete. Bachelor of Engineering Degree in Civil Engineering, The University of New South Wales, Canberra, Australia.

Shehata, E., Morphy, R., & Rizkalla, S. (2000). Fibre reinforced polymer shear reinforcement for concrete members: behaviour and design guidelines. Canadian Journal of Civil Engineering, 27(5), 859-872.

Sofi, M., van Deventer, J. S. J., Mendis, P. A., & Lukey, G. C. (2007). Engineering properties of inorganic polymer concretes (IPCs). Cement and Concrete Research, 37(2), 251-257.

Sonobe, Y., Fukuyama, H., Okamoto, T., Kani, N., Kimura, K., Kobayashi, K., . . . Nagasaka, T. (1997). Design guidelines of FRP reinforced concrete building structures. Journal of Composites for Construction, 1(3), 90-115.

Soong, W. H., Raghavan, J., & Rizkalla, S. H. (2011). Fundamental mechanisms of bonding of glass fiber reinforced polymer reinforcement to concrete. Construction and Building Materials, 25(6), 2813-2821.

Stratford, T., & Burgoyne, C. (2003). Shear analysis of concrete with brittle reinforcement. Journal of Composites for Construction, 7(4), 323-330.

Sujatha, T., Kannapiran, K., & Nagan, S. (2012). Strength assessment of heat cured geopolymer concrete slender column. Asian Journal of Civil Engineering, 13(5), 635-646.

Sumajouw, D. M. J., Hardjito, D., Wallah, S. E., & Rangan, B. V. (2007). Fly ash-based geopolymer concrete: study of slender reinforced columns. Journal of Materials Science, 42(9), 3124-3130.

Sumajouw, D. M. J., & Rangan, B. V. (2006). Low-calcium fly ash-based geopolymer concrete: reinforced beams and columns. In R. R. GC3 (Ed.). Perth, Australia: Faculty of Engineering, Curtin University of Technology.

Sung-Gul, H., Sung-Chul, C., Sung-Ho, L., & Oh, B. (2007). Strut-and-tie model for development of headed bars in exterior beam-column joint. ACI Structural Journal, 104(5), 590.

Sung-Ho, T., & Rak-Hyun, K. (2011). A study on improvement of durability of reinforced concrete structures mixed with Natural Inorganic Minerals. Construction and Building Materials, 25(11), 4263-4270.

Tang, W. C., Lo, T. Y., & Balendran, R. V. (2008). Bond performance of polystyrene aggregate concrete (PAC) reinforced with glass-fibre-reinforced polymer (GFRP) bars. Building and environment, 43(1), 98-107.

Tao, S., Ehsani, M. R., & Saadatmanesh, H. (1992). Bond strength of straight GFRP rebars. Paper presented at the Materials Performance and Prevention of Deficiencies and Failures, Atlanta, Georgia, USA.

Theriault, M., & Benmokrane, B. (1998). Effects of FRP reinforcement ratio and concrete strength on flexural behavior of concrete beams. Journal of Composites for Construction, 2(1), 7-16.

Tighiouart, B., Benmokrane, B., & Gao, D. (1998). Investigation of bond in concrete member with fibre reinforced polymer (FRP) bars. Construction and Building Materials, 12(8), 453-462.

Tobbi, H., Farghaly, A. S., & Benmokrane, B. (2012). Concrete columns reinforced longitudinally and transversally with glass fiber-reinforced polymer bars. ACI Structural Journal, 109(4), 551-558.

Torres-Acosta, A. A., Navarro-Gutierrez, S., & Teran-Guillen, J. (2007). Residual flexure capacity of corroded reinforced concrete beams. Engineering Structures, 29(6), 1145-1152.

van Oss, H. G. (1996-2016). Mineral commodity summaries 1996-2016. Retrieved 20 February, 2016, from http://minerals.usgs.gov/minerals/pubs/commodity/cement/index.html#mcs

Vasconcelos, E., Fernandes, S., de Aguiar, J. B., & Pacheco-Torgal, F. (2011). Concrete retrofitting using metakaolin geopolymer mortars and CFRP. Construction and Building Materials, 25(8), 3213-3221.

Vijay, P. V., Kumar, S. V., & Gangarao, H. V. S. (1996). Shear and ductility behaviour of concrete beams reinforced with GFRP rebars. Paper presented at the 2nd International Conference on Advanced Composite Materials in Bridges and Structures (ACMBS-II), Montreal, Canada.

Wallah, S. E., Hardjito, D., Sumajouw, D. M. J., & Rangan, B. V. (2003). Sulfate resistance of fly ash-based geopolymer concrete. Concrete in The Third Millenium, 205-212.

Wang, J., Dai, Y., & Gao, L. (2009). Exergy analyses and parametric optimizations for different cogeneration power plants in cement industry. Applied Energy, 86(6), 941-948.

Wasti, S. T., & Ersoy, U. (2006). The seismic well-being of buildings: Diagnostic and remedies. In S. T. Wasti & G. Ozcebe (Eds.), Advances in Earthquake Engineering for Urban Risk Reduction (Vol. 66, pp. 521-534): Springer.

Wight, J. K., & MacGreggor, J. G. (2009). Reinforced concrete mechanics and design. (5th Edition), 1130.

Xu, H., & van Deventer, J. S. J. (2000). The geopolymerisation of alumino-silicate minerals. International Journal of Mineral Processing, 59(3), 247-266.

Xu, H., & van Deventer, J. S. J. (2002). Geopolymerisation of multiple minerals. Minerals Engineering, 15(12), 1131-1139.

Zhou, J., Chen, X., & Chen, S. (2011). Durability and service life prediction of GFRP bars embedded in concrete under acid environment. Nuclear Engineering and Design, 241(10), 4095-4102. doi: http://dx.doi.org/10.1016/j.nucengdes.2011.08.038

Appendix A

A.1. Flexural strength prediction

The following is the summary of the basic assumptions adopted to determine the theoretical bending-moment capacity at concrete crushing failure ($M_{u\text{-}theo}$) of the tested beams:

i. Plane sections normal to the axis remain plane after bending;
ii. There is a perfect bond between the GFRP bars and geopolymer concrete; and
iii. The tensile strength of the geopolymer concrete is ignored.

In this study, two methods were adopted to calculate the $M_{u\text{-}theo}$. The first method adopted the equivalent rectangular stress block to estimate the geopolymer concrete compression force (C_c), represented by the first term of the equation. The neutral axis depth c is iteratively obtained when equilibrium of forces from Equation A-1, **Table A-1** is satisfied. The second term represents the compression forces provided by the top GFRP bars (C_f) while the last term embodies the tensile force of the bottom GFRP bars (T_f). Then, the corresponding bending moment capacity is computed using Equation A-2, **Table A-1**. The effect of varying the geopolymer concrete strain ε_{cu} (0.003, normally adopted for ordinary concrete, or 0.0048, determined from the flexural test of GFRP-RGC beams) was investigated, including the influence of adding the compression GFRP bars. **Table A-2** summarises the different scenarios considered.

The second method, on the other hand, utilised a parabolic stress block to determine C_c. The ascending part of the block is represented by Popovics (1973) stress-strain model (Equation A-3,) while the descending segment is modelled using Equation A-4, **Table A-1**. The value of c is iteratively determined using the fibre model analysis (FMA) and the procedure is repeated until the equilibrium of forces in Equation A-3, **Table A-1** is satisfied. Finally, the bending moment capacity is calculated from Equation A-4, **Table A-1**. Different scenarios were also considered, as shown in **Table A-2**.

For both predictions, the results obtained from the compression tests of 200 mm high by 100 mm diameter geopolymer concrete cylinders presented in **Paper V** were merged with the outputs in Paper III, since both batches of geopolymer concrete were manufactured using similar materials and compositions. The results yielded average compressive strength (f'_c), strain at f'_c (ε'_c), and elastic modulus (E_c) of 38 MPa, 1600 με, and 33 GPa, respectively. The

properties of the GFRP bars, on the other hand, were adopted from the manufacturer's specifications.

Table A-3 shows the experimental-to-predicted flexural strength ratio of the tested beams obtained from the first method. A value greater than 1.0 means that the strength was conservatively estimated. Among the scenarios considered, Scenario 3 yielded the most accurate predictions with an average experimental-to-predicted ratio of 1.05. It also provided conservative estimates. This result, interestingly, tends to support the generalisations made from the experimental works such as the ε_{cu} could reach as much as 0.0048 (**Paper III**), and the GFRP bars have compression contribution that should not be ignored (**Papers III**). **Table A-3** also shows the computed experimental-to-predicted flexural strength ratio of the tested beams using the second method. The scenario that adopts ε_{cu} equivalent to 0.0048 and that did not consider the top GFRP bars (Scenario *8*) yielded the most accurate predictions with an average experimental-to-predicted ratio of 0.98. Furthermore, it can be generalised from the results that, for more conservative estimates, the current flexural design provision for FRP-RC system could be adopted for the proposed system. Further research works, however, are needed to validate these claims.

Table A-1 Summary of equations used to determine the theoretical bending moment capacity of GFRP-RGC beams

First Method		Second Method	
$0.85 f_c^{'} \beta_1 cb + \varepsilon_f^{'} E_f^{'} A_f^{'} = \varepsilon_f E_f A_f$	(A-1a)	$\sum_{i=1}^{n} C_{ci} + \varepsilon_f^{'} E_f^{'} A_f^{'} = \varepsilon_f E_f A_f ; C_{ci} = f_{ci} t_i b$	(A-3a)
$\varepsilon_f^{'} = \varepsilon_{cu}\left(\frac{c-d^{'}}{c}\right)$	(A-1b)	$f_{ci} = \frac{f_c^{'}\left(\varepsilon_{ci}/\varepsilon_c^{'}\right)m}{m-1+\left(\varepsilon_{ci}/\varepsilon_c^{'}\right)^m}; \varepsilon_{ci} \le \varepsilon_c^{'}$	(A-3b)
$\varepsilon_f = \varepsilon_{cu}\left(\frac{d-c}{c}\right)$	(A-1c)	$f_{ci} = f_c^{'}\left[0.85 - 0.5\frac{\varepsilon_{ci}-\varepsilon_{0.85c}}{\varepsilon_{0.50c}-\varepsilon_c^{'}}\right]; \varepsilon_{ci} \ge \varepsilon_c^{'}$	(A-3c)
$\beta_1 = 0.85 - \frac{0.05\left(f_c^{'}-27.6\right)}{7}$	(A-1d)	$\varepsilon_{ci} = \varepsilon_{cu}\left(\frac{c-y_i}{c}\right)$	(A-3d)
$M_{u-theo} = C_c\left(d - \frac{\beta_1 c}{2}\right) + C_f\left(d-d^{'}\right)$	(A-2)	$m = \frac{E_c}{E_c - E_{sec}}; E_{sec} = f_c^{'}/\varepsilon_c^{'}$	(A-3e)
		$M_{u-theo} = \sum_{i=1}^{n} C_{ci}\left(c-y_i\right) + C_f\left(c-d^{'}\right) + T_f\left(c-d\right)$	(A-4)

Table A-2 Summary of the scenarios considered in the ultimate strength design (USD) method

Method	Scenario	ε_{cu}	Top bars
Based on equivalent rectangular stress block	*1*	0.0030	With
	2	0.0030	Without
	3	0.0048	With
	4	0.0048	Without
Parabolic stress block	*5*	0.0030	With
	6	0.0030	Without
	7	0.0048	With
	8	0.0048	Without

Table A-3 The experimental-to-predicted flexural strength ratio using the first method (rectangular stress block) and second method (parabolic stress block)

Specimen	*1*	*2*	*3*	*4*	*5*	*6*	*7*	*8*
SG-RGC-2-19.0	1.22	1.25	1.00	1.05	1.10	1.11	0.89	0.92
SG-RGC-3-15.9	1.37	1.40	1.13	1.18	1.23	1.25	1.00	1.03
HG-RGC-3-15.9	1.37	1.40	1.13	1.18	1.23	1.25	1.00	1.04
SG-RGC-4-12.7	1.30	1.33	1.07	1.11	1.17	1.14	0.95	0.98
SG-RGC-5-15.9	1.13	1.16	0.94	0.99	1.07	1.09	0.88	0.92
Average	1.28	1.31	1.05	1.10	1.16	1.18	0.94	0.98
SD	0.10	0.10	0.08	0.08	0.08	0.08	0.06	0.06

A.2. Midspan deflection prediction

The midspan flexural deflection at any given loads of the tested slender GFRP-reinforced geopolymer concrete (GFRP-RGC) beams (**Paper III**) subjected in a four-point load system were theoretically determined from Equation A-5. The deflections at the uncracked stage were calculated using the gross moment of inertia I_g while those at the cracked stage were computed using the proposed effective moment of inertia I_e for GFRP-RGC beam (Equation A-6a) since the current prediction equations suggested by the ACI 440.1R-15 (2015) and CSA S806-12 (2012) for FRP-RC beams underestimated the deflections of GFRP-RGC beams. Equation A-6a was basically derived from the ACI 318-14 (2014) , the I_e formula proposed by Branson (Branson 1968) for steel-reinforced concrete beam, and was modified by incorporating the effects of the actual and balanced reinforcement ratios through the reduction coefficients β_a (Equation A-6b) and β_b (Equation A-6c). This method of modifying I_e, using the actual and balanced reinforcement ratios, was also adopted by the ACI 440.1R-15. In this study, the coefficients β_a and β_b were determined using the following steps:

1. For each pair of experimental bending moment (starting from the experimental cracking moment, $M_{cr\text{-}exp}$, up until the bending moment at geopolymer concrete crushing failure,

$M_{u\text{-}exp}$) and midspan deflection, the corresponding experimental effective moment of inertia $I_{e\text{-}exp}$ were determined using Equation A-5.

2. The corresponding theoretical effective moment of inertia $I_{e\text{-}theo}$, on the other hand, was determined from Equation A-6a, given preset values of β_a and β_b.
3. Then, with β_a and β_b as the changing variables, the sum of the square of the difference between $I_{e\text{-}exp}$ and $I_{e\text{-}theo}$ was minimised, using the option Generalised Reduced Gradient (GRG) nonlinear engine of the Excel solver, to determine the true β_a and β_b.
4. Finally, the relationship between these constants and the actual and balanced reinforcement ratios was established, which are depicted in Equations A-6a and A-6b.

Figure 1.1 shows the relationship between the bending moment and midspan deflection. It was evident from the figure that there is a good agreement between the experimental and predicted moment-deflection curves. At service level, the predicted deflection was relatively higher than the experimental deflection, suggesting that the proposed equations yielded conservative estimates. **Figure A.2(a)** shows the experimental moment-deflection curves of all the tested beams. Based on the figure, as the reinforcement ratio increases, the stiffness of the beams also increases. The proposed prediction equations also yielded the same behaviour as shown in **Figure A.2(b)**. Additional experimental works, however, are needed to enhance further the accuracy of the proposed equations.

$$\Delta = \frac{M_a}{24E_cI_e}\left(3L^2 - 4a^2\right) \tag{A-5}$$

$$I_e = \beta_a\left(\frac{M_{cr}}{M_a}\right)^3 I_g + \beta_b\left[1-\left(\frac{M_{cr}}{M_a}\right)^3\right]I_{cr} \tag{A-6a}$$

$$\beta_a = \frac{\rho_f}{10\rho_{fb}} \tag{A-6b}$$

$$\beta_b = \frac{1}{\sqrt[5]{\rho_f/\rho_{fb}}} \tag{A-6c}$$

$$I_{cr} = \frac{bd^3}{12}k^3 + n_f A_f d^2\left(1-k^2\right) \tag{A-6d}$$

$$k = \sqrt{2\rho_f n_f + \left(\rho_f n_f\right)^2} - \rho_f n_f \tag{A-6e}$$

$$M_{cr} = \frac{f_r I_g}{c} \tag{A-7}$$

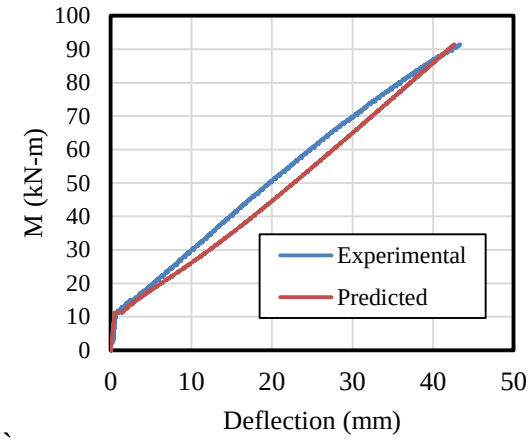

(a) SG-RGC-2-19.0

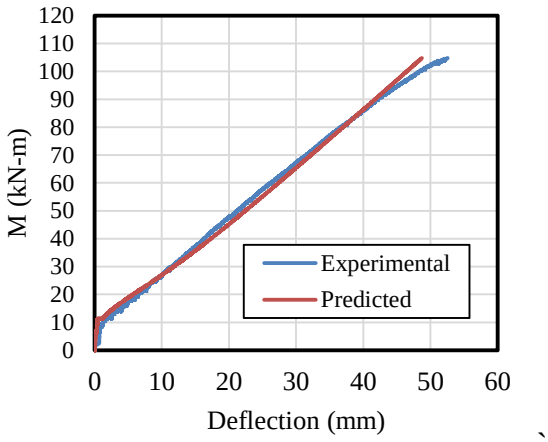

(b) SG-RGC-3-15.9

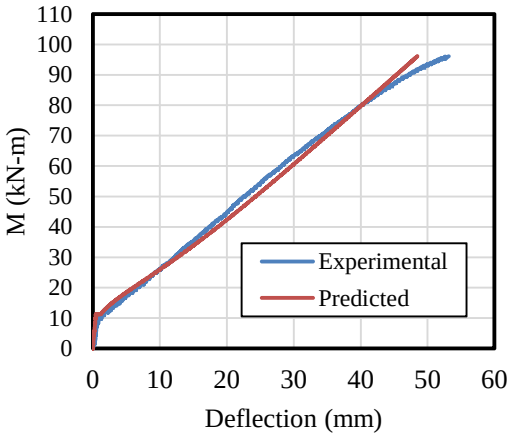

(c) SG-RGC-4-12.7

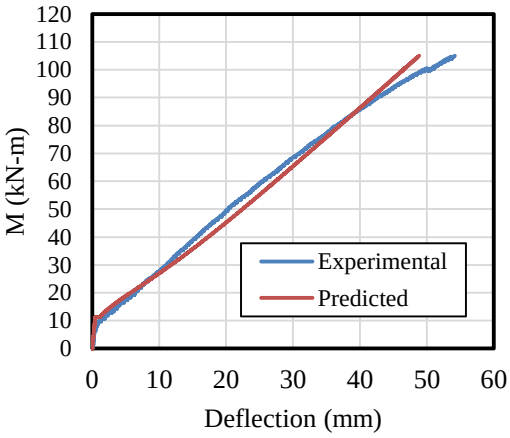

(d) HG-RGC-3-15.9

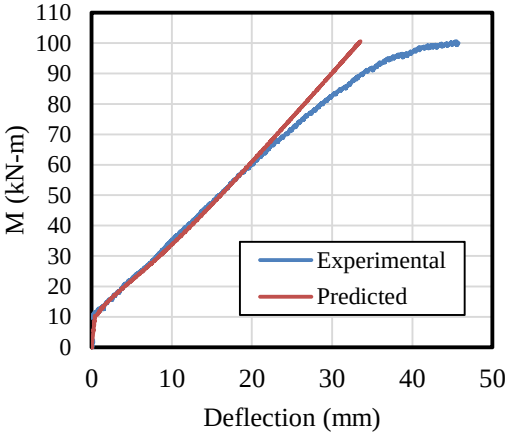

(e) HG-RGC-3-15.9

Figure A.1 Comparison between the experimental and predicted moment-deflection relationship of the tested beams

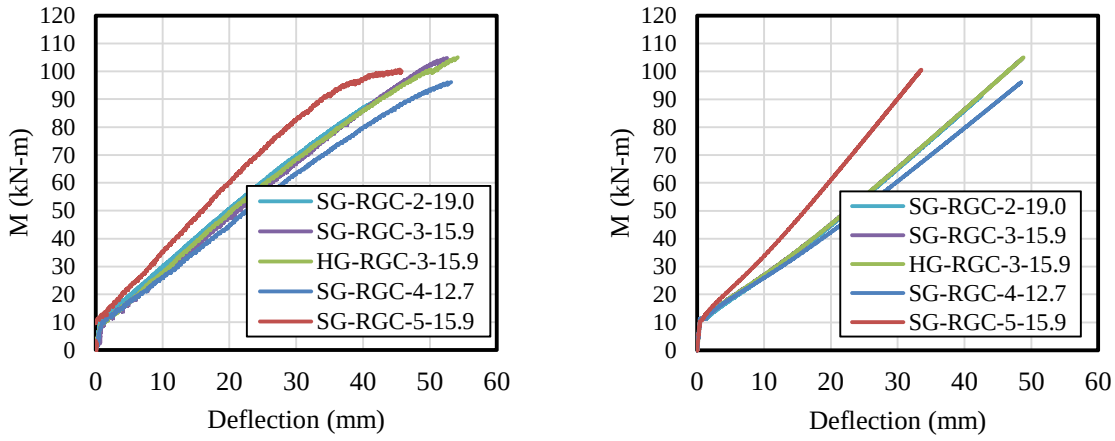

(a) Experimental (b) Theoretical

Figure A.2 Summary of the experimental and predicted moment-deflection curves

Nomenclature:

a = shear span of the beam (mm)

A_f = total area of the bottom longitudinal GFRP bars (mm^2)

A'_f = total area of the top longitudinal GFRP bars (mm^2)

b = beam width (mm)

c = neutral axis depth (mm)

C_c = compressive force provided by the geopolymer concrete (N or kN)

C_{ci} = compressive force provided by the i^{th} strip geopolymer concrete (N or kN)

C_f = total compressive force provided by the GFRP bars (N or kN)

d = effective depth of the beam (mm)

d' = distance of the centroid of compression bars from the top-most compression fibres (mm)

E_c = elastic compressive modulus of the geopolymer concrete (MPa)

E_f = tensile modulus of the GFRP bars (MPa)

E_{sec} = secant modulus of the geopolymer concrete (MPa)

E'_f = compression modulus of the GFRP bars (MPa)

f_{ci} = concrete compressive or tensile stress at the centroid of the i^{th} strip (MPa)

f_r = modulus of rupture of the geopolymer concrete (MPa)

f'_c = geopolymer concrete compressive strength (MPa)

I_{cr} = cracked moment of inertia (mm^4)

I_g = gross moment of inertia (mm^4)

I_e = effective moment of inertia (mm^4)

$I_{e\text{-}exp}$ = experimental effective moment of inertia (mm^4)

$I_{e\text{-}theo}$ = theoretical effective moment of inertia (mm^4)

L = clear span of the beam (mm)

m = constant that describe the initial curvature of Popovics stress-strain model

M_a = actual bending moment in the beam (Nmm or kNm)

M_{cr} = cracking moment of the beam (Nmm or kNm)

$M_{u\text{-}theo}$ = theoretical bending moment capacity of the beam (Nmm or kNm)

T_f = total tensile force provided by the GFRP bars (N or kN)

y_i = distance of the centroid of the i^{th} segment from the top-most compression fibres (mm)

α = parameter use to calculate the average uniform stress of the equivalent rectangular stress block

β_1 = parameter that determine the depth of the equivalent rectangular stress block

β_a = constant that modify the first term of the proposed I_e equation

β_b = constant that modify the second term of the proposed I_e equation

Δ = midspan deflection (mm)

$\varepsilon_{0.85c}$ = post-peak strain at $0.85f'_c$ of the geopolymer concrete

$\varepsilon_{0.50c}$ = post-peak strain at $0.50f'_c$ of the geopolymer concrete

ε_{ci} = concrete compressive or tensile strain at the centroid of the i^{th} strip

ε_{cu} = usable compressive strain of the geopolymer concrete

ε_f = ultimate tensile strain of the GFRP bars

ε'_c = strain at f'_c of the geopolymer concrete

ε'_f = compressive strain of the GFRP bars

ρ_f = longitudinal reinforcement ratio

ρ_{fb} = balanced reinforcement ratio

Appendix B

B.1 Paper I: Bond stress-slip behaviour: Case of GFRP bars in geopolymer concrete

Figure B.1 shows the schematic of pullout specimens showing the locations of bonded and debonded lengths. The desired embedment lengths were achieved by sleeving PVC pipes to disband the bars from the geopolymer concrete. On the other hand, the bond stress-slip curves of all the tested pullout specimens in **Paper I** are shown in **Figure B.2**. From the figure, it can be observed that peak stress at failure and the pre- and post-peak behaviour varies per specimen. In this study, the average bond stress at failure was determined from the average of the three specimens. The bond stress-slip curves presented in **Figures 6**, **7**, and **8** of **Paper I**, used to represent the bond-stress slip behaviour of the specimen's group, were based on the average value of the test results. The average bond stiffness of the pullout specimens are summarised in **Table B-1**. This stiffness was obtained from Region I of the bond stress-slip curve of the tested specimens. From the table, it can be generalised that as the bar diameter and embedment length increase, the bond stiffness also decrease. This could be expected since the specimens with larger bar diameter and longer embedment have larger contact area between the reinforcement and the geopolymer concrete that resulted in better chemical adhesion and mechanical interlocking, the main pullout resistance mechanism in Region I, between the two materials. However, the GG-15.9-15d_b and GG-19.0-15d_b specimens, yielded lower stiffness compared to their counterpart specimens with shorter embedment length, because these specimens have little or no unbonded geopolymer concrete in its loaded end that could prevent the early development of longitudinal cracks.

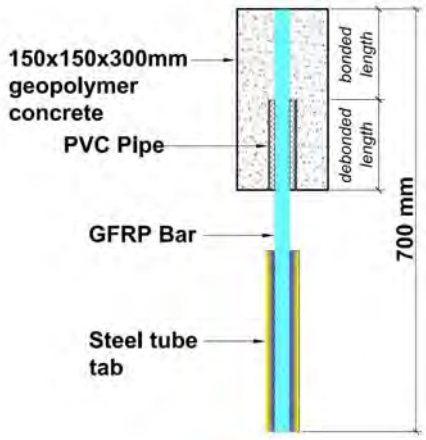

Figure B.1 The schematic diagram of pullout specimen showing the bonded and debonded lengths

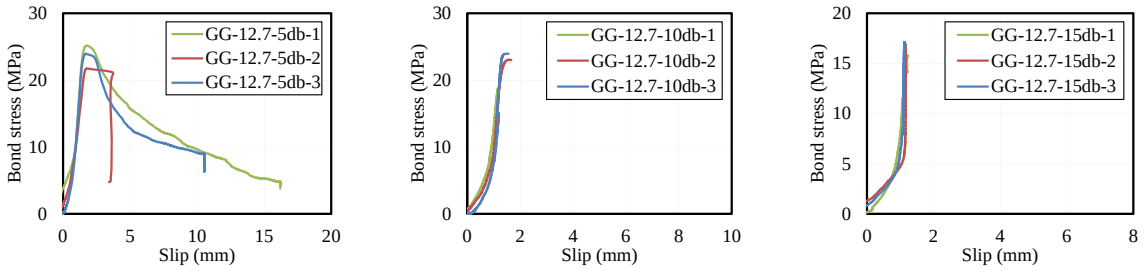

(a) GG-12.7-5d_b (b) GG-12.7-10d_b (c) GG-12.7-15d_b

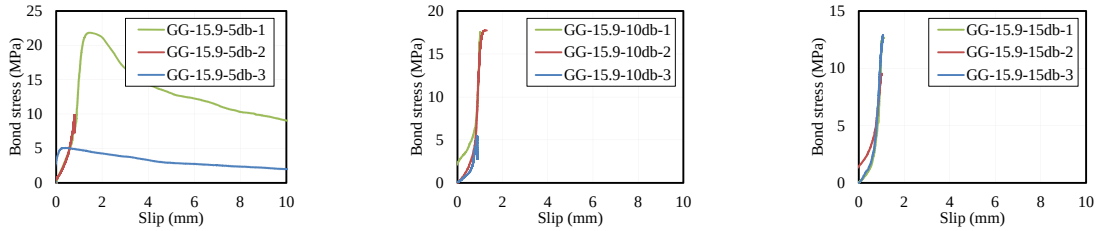

(d) GG-15.9-5d_b (e) GG-15.9-10d_b (f) GG-15.9-15d_b

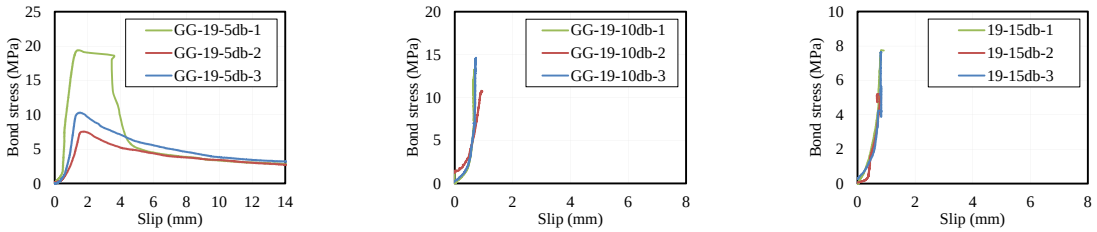

(d) GG-19.0-5d_b (e) GG-19.0-10d_b (f) GG-19.0-15d_b

Figure B.2 Bond-stress slip curves of pullout specimens

Table B-1 Bond stiffness of the pullout specimen

Specimen	Bond stiffness (N/mm)
GG-12.7-5d_b	67
GG-12.7-10d_b	206
GG-12.7-15d_b	345
GG-15.9-5d_b	145
GG-15.9-10d_b	474
GG-15.9-15d_b	381
GG-19.0-5d_b	305
GG-19.0-10d_b	879
GG-19.0-15d_b	641

B.2 Paper III: Evaluation of the flexural strength and serviceability of geopolymer concrete beams reinforced with glass-fibre-reinforced polymer (GFRP) bars

Figure B.3 shows the comparison between the stress-strain curves of geopolymer concrete and ordinary portland cement (OPC) concrete with average compressive strength of 38 MPa and

41 MPa, respectively. Generally, the shape of the stress-strain curves of geopolymer concrete was similar to that of OPC concrete. However, the average modulus of elasticity of geopolymer concrete (38 GPa) was higher than that of the normal concrete (32.9 GPa) while the strain at peak of geopolymer concrete (1200 microstrain) was lower than that of normal concrete (1600 microstrain). **Table B-2** shows the mechanical properties of the GFRP stirrups, which were the results of the numerous actual tests conducted by Pultrall Inc. (the bar manufacturer) and by the researchers in the University of Sherbrooke, Canada.

The comparison between the strength of the GFRP-RGC beams and GFRP-RC beams with stirrups in the constant bending moment zone are presented in **Table B-3**. These beams have width, height, and concrete compressive strength ranging from 149 mm to 203 mm, 152 mm to 400 mm, and 27.6 MPa to 73.4 MPa, respectively. Furthermore, all the beams failed due to crushing of concrete in the compression zone. The comparison showed that the tested beams in this study (GFRP-RGC beams) have higher strength compared to the GFRP-RC beams.

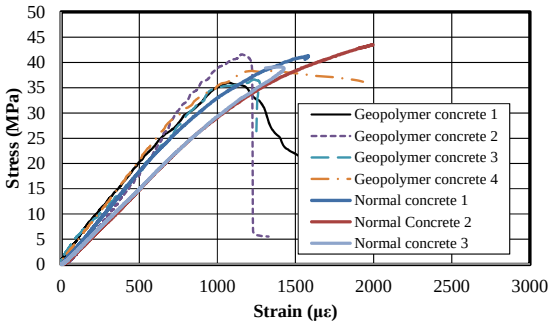

Figure B.3 Comparison between the stress-strain curves of geopolymer concrete and normal concrete

Table B-2 Mechanical properties of GFRP stirrups

Properties	Values
Nominal Diameter	9.5 mm
Nominal Area	71.6 mm^2
Bend radius	38.1 mm
Lap splice	150 mm
Tensile strength*	1029 MPa
Strength at bend	463 MPa
Tensile modulus	50 GPa

**Guaranteed tensile strength: average value – 3x standard deviation*

Table B-3 Comparison between GFRP-RGC and GFRP-RC beams with stirrups in the constant bending moment zone

Beam Type	$M_u / \left(f_c' bd^2 \right)$, %
GFRP-RGC	20.38
El-Nemr et al. 2013 (GFRP-RC)	11.44
Kassem et al. 2011 (GFRP-RC)	12.62
Lau and Pam 2010 (GFRP-RC)	19.69
Saikia et al. 2007(GFRP-RC)	9.13
Yost et al. 2001(GFRP-RC)	19.25
Alsayed et al. 2000 (GFRP-RC)	17.02

B.3 Paper IV: Shear behavior of geopolymer concrete beams reinforced with GFRP bars.

Table B-4 shows the test matrix and test parameters considered in **Paper IV**. The beam specimens were labelled as follows: GG-1.8-G(S)-#. The first two letters (GG) stand for "GFRP-reinforced geopolymer-concrete beam" while the numbers 1.8 and 4.7 corresponds to their shear-span-to-effective depth ratio *a*/*d*. The next letter represents the type of transverse reinforcement: G for GFRP stirrups and S for steel stirrups. The # sign represents the center-to-center spacing of the stirrups in millimeters. For example, the specimen identified as GG-1.8-G-75 is a GFRP-reinforced geopolymer-concrete beam with a *a*/*d* of 1.8 and transversely reinforced with 9.5 mm (0.37 in.) GFRP stirrups spaced at 75 mm (2.95) in. or *h*/4 on-centre. The symbols *b, h, l,* f'_c*, s,* ρ_f*,* ρ_{fb}*, and* ρ_{fv} stand for the width, total depth, total length, compressive strength of geopolymer concrete, stirrup spacing, longitudinal reinforcement ratio, balanced reinforcement ratio, and transverse reinforcement ratio.

Table B-4 Test matrix and test parameters

Beam	*b* (mm)	*h* (mm)	*l* (mm)	*a*/*d*	f'_c (MPa)	*s* (mm)	ρ_f (%)	ρ_{fb} (%)	ρ_{fv} (%)
GG-1.8	200	300	1500	1.8	43	*n*/*a*	1.69	0.56	*n*/*a*
GG-1.8-G-75	200	300	1500	1.8	43	75	1.69	0.56	0.95
GG-1.8-G-100	200	300	1500	1.8	43	100	1.69	0.56	0.71
GG-1.8-G-150	200	300	1500	1.8	43	150	1.69	0.56	0.48
GG-1.8-S-150	200	300	1500	1.8	43	100	1.69	0.56	0.48
GG-4.7-G-100	200	300	2900	4.4	38	100	2.01	0.33	0.71

B.5 Paper V: Behavior of concentrically loaded geopolymer-concrete circular columns reinforced longitudinally and transversely with GFRP bars

Figure B.4 shows the typical stress-strain curves (mentioned as **Figure 3** in section "2.1.2 Geopolymer Concrete" of **Paper V)** of the geopolymer concrete obtained from the compression test of four 100 mm diameter by 200 mm high geopolymer concrete cylinder.

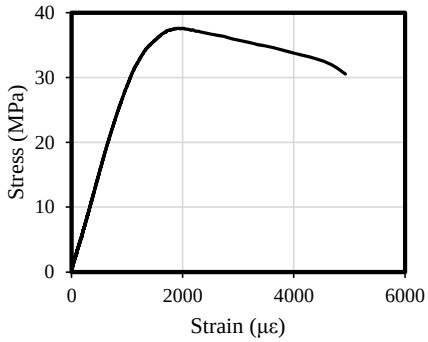

Figure B.4 Typical stress-strain curve of the 100 mm diameter by 200 mm high geopolymer concrete cylinder

Appendix C

C.1. Conference Paper I: Bond stress–slip behaviour: Case of GFRP bars in geopolymer concrete

Maranan GB, Manalo AC, Karunasena W, and Benmokrane B (2014). Bond-slip behaviour of GFRP bars into geopolymer concrete. *Proceedings of the 7th International Conference on FRP Composites in Civil Engineering (CICE 2014)*, 20-22 August, Vancouver, Canada, pp. 106 (full paper in USB).

Abstract: Geopolymer concrete reinforced with glass fibre reinforced polymer (GFRP) bars is a new and emerging technology that is suitable for the construction of corrosion resistant, durable, and highly sustainable civil infrastructures. To encourage its utilisation in the construction industry, a better understanding on its bond mechanism should be gained since it is the critical factor that controls the structural performance of reinforced concrete members. In this study, the bond-slip behaviour of 15.9 mm nominal diameter sand-coated GFRP bars with and without anchor head into geopolymer concrete, with a compressive strength of 33 MPa, was evaluated using direct pullout test. Three embedment lengths (5Ø, 10Ø, and 15Ø) were adopted to assess the interface bond between the GFRP bars and the geopolymer concrete. The results were compared to that of the pullout test of 16 mm diameter deformed steel bars embedded into geopolymer concrete. The results showed that as the embedment length increases, the pullout capacity of bond-slip specimen also increases. In addition, the GFRP bars have comparable bonding capacity to that of the deformed steel bars. Finally, the provision of anchor head increased the pullout capacity of the GFRP bar by as much as 31%.

C.2. Conference Paper II: Flexural behavior of GFRP bars subjected to elevated temperature

Maranan GB, Manalo AC, Karunasena W, Benmokrane B, and Lutze D (2014). Flexural behavior of GFRP bars subjected to elevated temperature. *Proceedings of the 23rd Australasian Conference on the Mechanics of Structures and Materials (ACMSM23)*, 9-12 December, Byron Bay, Australia, pp.187-192.

Abstract: The FRP reinforced concrete structures may be exposed to high temperatures that may reduce the structural integrity of the bars, and eventually of the entire structure. Therefore, the thermal stability of the FRP bars must be thoroughly investigated before they can be fully utilized in the construction industry. The flexural strength testing has long been a staple technique for measuring the uniaxial tensile strength of the brittle materials because it is inexpensive and convenient to run rather than the direct tension test. Although the results obtained were not the absolute tensile data, they can provide an indication about the relative tensile performance of the FRP bars. In this study, the flexural behaviour of the GFRP bars of varying nominal diameters (12.7 mm, 14.0 mm, 15.9 mm, 17.0 mm, and 20.5 mm) subjected to elevated temperatures (up to 150 °C) was investigated. The results showed that as the temperature increases, the flexural strength and stiffness of the GFRP bars decreases. As the temperature approaches the glass transition temperature (T_g) of the bars, a drastic strength and stiffness reduction was observed. These findings were also observed in the pure tension testing of the FRP bars done by other researchers. The bars with a larger nominal diameter showed a better flexural strength decay resistance than those with a smaller nominal diameter at elevated temperatures. However, a comparable flexural stiffness deterioration was observed at an increasing temperature.

23rd Australasian Conference on the Mechanics of Structures and Materials (ACMSM23)
Byron Bay, Australia, 9-12 December 2014, S.T. Smith (Ed.)

FLEXURAL BEHAVIOUR OF GLASS FIBRE REINFORCED POLYMER (GFRP) BARS SUBJECTED TO ELEVATED TEMPERATURE

G.B. Maranan*
Centre of Excellence in Engineered Fibre Composites (CEEFC),
School of Civil Engineering and Surveying, University of Southern Queensland,
Toowoomba, QLD, 4350, Australia. ginghis.maranan@usq.edu.au (Corresponding Author)

A.C. Manalo
Centre of Excellence in Engineered Fibre Composites (CEEFC),
School of Civil Engineering and Surveying, University of Southern Queensland,
Toowoomba, QLD, 4350, Australia. allan.manalo@usq.edu.au

W. Karunasena
Centre of Excellence in Engineered Fibre Composites (CEEFC),
School of Civil Engineering and Surveying, University of Southern Queensland,
Toowoomba, QLD, 4350, Australia. karu.karunasena@usq.edu.au

B. Benmokrane
Department of Civil Engineering, Faculty of Engineering, University of Sherbrooke,
Sherbrooke, Quebec, Canada JIK 2R1. Brahim.Benmokrane@USherbrooke.ca

D. Lutze
Inconmat Australia, 240 Victoria Rd, Largs Bay, SA 5016. daren.lutze@inconmat.com.au

ABSTRACT

The FRP reinforced concrete structures may be exposed to high temperatures that may reduce the structural integrity of the bars, and eventually of the entire structure. Therefore, the thermal stability of the FRP bars must be thoroughly investigated before they can be fully utilized in the construction industry. The flexural strength testing has long been a staple technique for measuring the uniaxial tensile strength of the brittle materials because it is inexpensive and convenient to run rather than the direct tension test. Although the results obtained were not the absolute tensile data, they can provide an indication about the relative tensile performance of the FRP bars. In this study, the flexural behaviour of the GFRP bars of varying nominal diameters (12.7 mm, 14.0 mm, 15.9 mm, 17.0 mm, and 20.5 mm) subjected to elevated temperatures (up to 150 °C) was investigated. The results showed that as the temperature increases, the flexural strength and stiffness of the GFRP bars decreases. As the temperature approaches the glass transition temperature (T_g) of the bars, a drastic strength and stiffness reduction was observed. These findings were also observed in the pure tension testing of the FRP bars done by other researchers. The bars with a larger nominal diameter showed a better flexural strength decay resistance than those with a smaller nominal diameter at elevated temperatures. However, a comparable flexural stiffness deterioration was observed at an increasing temperature.

KEYWORDS

FRP bar, thermal stability, flexural strength, tensile strength, glass transition temperature.

INTRODUCTION

The corrosion of the steel bars is the prime factor that causes the premature failure and/or shorter service life of reinforced concrete (RC) structures, especially those that are located in harsh environments, such as in marine and mining areas. One of the promising solutions is to utilize a corrosion resistant material called the fibre reinforced polymer (FRP) bars. Aside from being corrosion resistant, the FRP bars have high durability, high strength-to-weight ratio, and electromagnetic resistant (Gangarao *et al.* 2007). The FRP bars have been successfully used as internal reinforcement for concrete in the construction of roads and bridges. Many engineers and researchers are now extending the application of FRP reinforced concrete (FRP-RC) for the construction of multi-storey and industrial buildings. However, data regarding the fire resistance performance of FRP-RC structures (e.g. the time duration the structures can withstand high temperatures as well as fire exposures; the temperature at which the strength, stiffness, and bond between the materials decreased) must be gained for their wider acceptance and application in the construction industry.

The fire resistance of FRP-RC structures are dependent on its constituent materials, the concrete and the FRP bars. Between these two materials, the latter is more susceptible to degradation at higher temperatures. The strength and stiffness of the polymer are known to decrease significantly as the temperature approaches its glass transition temperature (T_g) (Fried 1995). The composite action between the fibres and the polymer diminishes and this would result into wider crack width in the concrete and consequently larger deflection of the structural element. The tensile behaviour of the FRP bar at elevated temperatures, therefore, must be thoroughly investigated. Many researchers (e.g. Kumahara *et al.* 1993; Abbasi and Hogg 2005; Wang *et al.* 2007; and Kashwani and Al-Tamimi 2014) studied the tensile performance of FRP bars at varying temperatures using a pure tension test. However, this test has several disadvantages such as the requirement for a longer test specimen, longer time duration and high costs of specimen fabrication and testing, and the difficulties of gripping. With the stated limitations, the bending test can be employed to roughly investigate the tensile performance of the FRP bars. The flexural strength testing has long been a staple technique for measuring the uniaxial tensile strength of the brittle materials such as ceramics and glasses (Quinn et al. 2009) and is relatively easy to run and inexpensive rather than direct tension test (Whitney and Knight 1980). Generally, the tensile stress obtained from the flexure test of the GFRP bars are higher than that obtained from the pure tension test (Whitney and Knight 1980; Tripathi 2003). In the present work, three-point bending tests were performed to investigate the tensile performance of the sand-coated GFRP bars subjected to elevated temperatures. The experimental results obtained from this study can provide an approximate interpretation of the tensile behaviour of the bars at elevated temperatures. Furthermore, the results can be used in the future for establishing a relationship between the tensile strength and the flexural strength of the GFRP bars at elevated temperatures such that the tensile response can be back-calculated from the bending behaviour. In this way, a large statistical-database can be obtained in a far more convenient and low cost approach.

EXPERIMENTAL PROGRAM

GFRP Bars

Five sand-coated GFRP bars with nominal diameters of 12.7 mm, 14.0 mm, 15.9 mm, 17.0 mm, and 20.7 mm were considered as shown in Figure 1. Three specimens were prepared for each bar diameter. The bars were provided by V-Rod® Australia (www.vrodaustralia.com.au) and were made by embedding E-glass fibres in a modified vinyl ester resin using a pultrusion process. The glass fibre content of the GFRP bars, determined by Burn-out test according to ISO 1172:1996(E), is 84.05 %.

Differential Scanning Calorimetry (DSC) Analysis

The average glass transition temperature (T_g) of the bars was obtained using a TA Instruments Q100 DSC machine following the ASTM D3418-12 standard. Approximately, 30-mg unconditioned samples were cut from the reference bars. After the samples were cleaned and dried, they were placed

in aluminium pans and sealed, as shown in Figure 2, using forceps. The samples were heated from 10 °C to 150 °C at a ramp rate of 3 °C/min for one hour duration. Based on the test, the mean T_g of the bars (117 °C) was found to be within the range of the T_g of a vinyl ester matrix system (110 °C to 120 °C) reported by Robert *et al.* (2009).

Flexural Test

The three-point bending test of the GFRP bars was presented in Figure 3. The test was conducted following the ASTM D4476 standard using full bars, instead of half bars. The simply supported specimens, with clear span of 180 mm, were loaded at midspan at the rate of 10 mm/min using the 100 kN capacity MTS testing machine. The test was conducted using a steady-state temperature (heat then load) regime. The temperature in the oven chamber was raised to the desired temperature. Then, the bars were placed inside the chamber for 15 minutes prior to testing to be sure that the temperature at the core of the bars reached the required temperature. The bars were subjected to temperatures ranging from room temperature (21°C) to 150 °C. The load and displacement were recorded using a data logger. Each specimen was identified in the following manner: nominal bar diameter (12.7mm, 14.0 mm, 15.9mm, 17.0 mm, and 20.5 mm) - temperature it was subjected to (21°C to 150 °C).

Figure 1. GFRP bars

Figure 2. Sample T_g specimen

Figure 3. Three-point bending test

RESULTS AND DISCUSSION

Table 1 summarizes the experimental results such as the flexural load (F) and the corresponding standard deviation (SD), the flexural strength (f_b), and the flexural stiffness (E_b). The flexural strength and stiffness were calculated using Eq. 1 and Eq. 2, respectively, where L, d_b, and Δ are the clear span, the nominal diameter, and the midspan deflection, respectively. The ratio (F/Δ) was obtained from the slope of the linear portion of the load-deflection curves presented in Figure 4. In general, the strength and stiffness of the GFRP bars decrease as the bar diameter increases.

$$f_b = \frac{8FL}{\pi d_b^{\,3}} \qquad (1)$$

$$E_b = \frac{F}{\Delta}\frac{4L^3}{3\pi d_b^4} \qquad (2)$$

Load and Midspan Deflection Relationship at Elevated Temperatures

The typical relationship between the load and the midspan deflection of the GFRP bars (represented by 12.7 mm GFRP bars) subjected to elevated temperatures is shown in Figure 4. As can be seen from the figure, the load increases linearly with deflection up to failure for all subjected to temperatures ranging from 21 °C to 80 °C. The load drops observed, before reaching the peak load, were attributed to the debonding of the sand coating just beneath the point of load application. Generally, the bars failed in a brittle manner. The failure of the GFRP bars is dominated by the simultaneous crushing of the resin and fibre in the compression zone as depicted in Figure 5. In addition, the bars with larger diameters exhibited interlaminar shear failure in the tension zone as shown in Figure 6. On the other hand, it can be seen from Figure 7 that the mode of failure of the 12.7 mm and 15.9 mm GFRP bars was dominated by the fibre rupture and interlaminar shear failure at the tension zone of the bar that leads to the debonding of the sand coating.

The bars subjected to temperatures ranging from 100 °C to 150 °C exhibited a non-linear behaviour and stiffness degradation before reaching the maximum load because the T_g of the bars falls within this temperature range. The polymer behaves like a rubbery material and this has resulted in a ductile behaviour of the bars. Figure 8 shows the typical crushing failure of the GFRP bars exposed at these temperatures. White powder resins were formed. At a temperature of 150 °C, interlaminar shear failure was also observed in the tension zone of the bars with larger diameter. The bars with larger diameter exhibited more severe failure than those with smaller diameter.

Table 1. Flexural load, strength, and stiffness of the GFRP bars at elevated temperatures

Specimen	F (kN)	SD (kN)	f_b (MPa)	E_b (GPa)	Specimen	F (kN)	SD (kN)	f_b (MPa)	E_b (GPa)
12.7-21	7.6	0.1	999.8	77.3	15.9-21	7.6	0.1	869.7	41.9
12.7-35	3.6	0.2	815.0	77.1	15.9-35	7.1	0.1	811.6	41.4
12.7-50	2.2	0.3	495.1	74.1	15.9-50	5.2	0.3	598.1	41.7
12.7-65	2.2	0.5	495.4	72.0	15.9-65	5.3	0.4	603.3	38.5
12.7-80	2.4	0.5	534.6	68.3	15.9-80	4.6	0.6	520.8	36.8
12.7-100	2.1	0.1	473.8	53.9	15.9-100	3.2	0.2	370.4	31.6
12.7-120	0.9	0.1	191.5	28.5	15.9-120	1.6	0.2	184.9	15.8
12.7-150	0.3	0.1	60.5	24.5	15.9-150	0.9	0.1	102.0	11.4
14.0-21	6.6	0.4	1468.0	77.3	17.0-21	10.5	0.4	1201.3	63.1
14.0-35	5.6	0.0	1263.6	77.1	17.0-35	9.0	0.1	1031.7	62.2
14.0-50	3.7	0.3	820.0	74.1	17.0-50	7.3	0.4	828.0	58.1
14.0-65	3.6	0.3	815.8	72.0	17.0-65	7.0	0.4	796.0	57.4
14.0-80	3.5	0.4	792.9	68.3	17.0-80	4.5	0.3	510.1	53.2
14.0-100	1.7	0.1	385.3	53.9	17.0-100	3.5	0.1	396.9	40.9
14.0-120	1.0	0.1	222.6	28.5	17.0-120	2.3	0.3	261.5	29.6
14.0-150	0.5	0.1	122.6	24.5	17.0-150	1.0	0.0	118.3	15.4
20.5-21	15.5	0.2	1034.1	52.1	20.5-80	9.9	0.7	664.3	47.2
20.5-35	15.1	0.5	1012.1	52.2	20.5-100	7.5	1.5	501.2	39.4
20.5-50	12.6	0.8	838.9	50.9	20.5-120	3.8	1.3	254.6	23.2
20.5-65	12.1	0.6	811.8	50.1	20.5-150	2.0	0.2	132.1	10.8

Effect of Temperature on the Flexural Strength of the GFRP Bars

The relationship between the normalized flexural strength and the temperature is shown in Figure 9. The normalized values were calculated by finding the quotient between the flexural stress at t temperature, f_{bt}, and the flexural stress at room temperature (21 ^{o}C), f_{RT}. Generally, the flexural strength of the GFRP bars decreases as the temperature increases due to the decomposition of the resin. This trend was also observed in the pure tension test of FRP bars, conducted by Wang (2007), Abbasi (2005), and Robert and Benmokrane (2010). Furthermore, as the temperature approaches the T_g of the bars, a significant decreased of the flexural strength occurred because the polymer becomes soft and consequently looses its ability to hold the glass fibres together and to transfer stresses from one fibre to another. It can be seen that the bars with a larger nominal diameter experienced better flexural performance at higher temperature as compared to those with smaller diameter, which indicates that size effect (specifically the variation in the nominal diameters) should be considered in the investigation of the thermal stability of FRP bars.

Effect of Temperature on the Flexural Stiffness of the GFRP Bars

Figure 10 shows the correlation between the normalized flexural stiffness and the temperature. The normalized values were obtained by dividing the flexural stiffness at t temperature, E_{bt}, to the flexural

stiffness at room temperature (21 °C), E_{RT}. The same as the flexural strength, the flexural stiffness of the GFRP bars decrease as the temperature increases. However, the rate of deterioration of the flexural strength is faster than the flexural stiffness at temperature ranging from 21 °C to 100 °C. The same as the flexural strength, a drastic decrease in the flexural stiffness was also observed as the temperature approaches the T_g of the bars for the same reason. The composite action between the fibres and the polymer diminishes and this resulted in lower flexural stiffness (and strength) of the GFRP bars. On the other hand, a comparable rate of degradation of the flexural stiffness of the GFRP bars with varying diameter was observed at increasing temperatures.

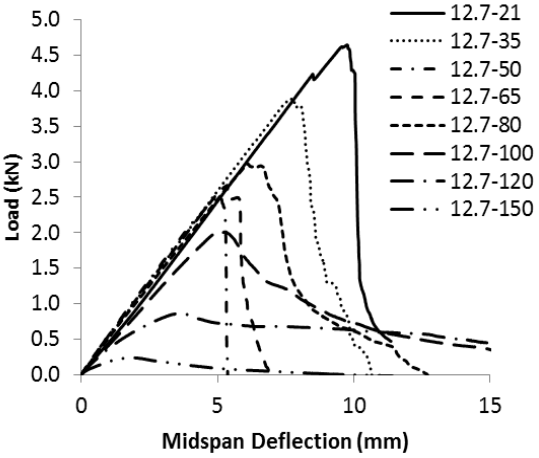

Figure 4. Typical load and midspan deflection relationships of the GFRP bars at elevated temperatures

Figure 5. Crushing of the resin and fibre of GFRP bars (21 °C to 80 °C)

Figure 6. Interlaminar shear failure of GFRP bars (21 °C to 80 °C)

Figure 7. Interlaminar shear failure of the 12.7 mm and 15. 9mm GFRP bars (21 °C to 80 °C)

Figure 8. Crushing of the resin and fibres of GFRP bars (100°C to 150°C)

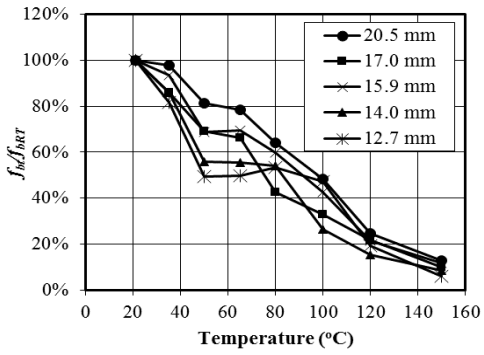

Figure 9. Flexural strength of the GFRP bars at elevated temperatures

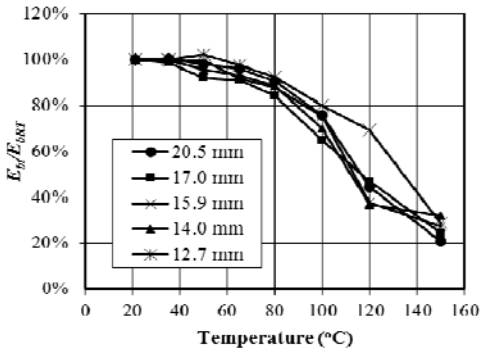

Figure 10. Flexural stiffness of the GFRP bars at elevated temperatures

CONCLUSIONS

The three-point bending test of the GFRP bars subjected to elevated temperatures was conducted. Based on the experimental results, the following conclusions were made:

- Generally, as the temperature increases, the flexural strength and stiffness of the GFRP bars decreases.
- A drastic decrease of the flexural strength and stiffness of the GFRP bars was observed as the temperature approaches the T_g of the bars because the polymer transition from a glassy (hard) material to a rubbery (soft) material, thereby losing its ability to hold the fibres together and to transfer stresses from one fibre to the other.

- The bars with a larger nominal diameter showed better flexural strength decay resistance than those with a smaller nominal diameter at elevated temperatures.
- The rate of degradation of the flexural stiffness of the GFRP bars with varying diameter was comparable with each other at increasing temperatures.
- Additional studies should be carried out to provide further information that can be used to establish a relationship that can predict the tensile response of the GFRP bars from the bending response at elevated temperatures.

ACKNOWLEDGMENTS

The authors gratefully acknowledge V-Rod® Australia for the materials and technical support they had given in the conduct of this research undertaking.

REFERENCES

Abbasi, A. and Hogg, P. (2005). "Temperature and environmental effects on glass fibre rebar: modulus, strength and interfacial bond strength", *Composites Part B: Engineering*, Vol. 36, No. 5, pp. 394-404.

ASTM D3418-12 (2012). "Standard test method for transition temperatures and enthalpies fusion and crystallization of polymers by differential scanning calorimetry." *ASTM International*, West Conshohocken, PA, United States.

ASTM D4476-14 (2014). "Standard test method for flexural properties of fiber reinforced pultruded plastic rods." *ASTM International*, West Conshohocken, PA, United States.

Fried J.R. (1995). Polymer Science and Technology. Prentice-Hall, Englewood Cliffs, New Jersey, pp 167-169.

Gangarao, H.V.S., Taly, N., and Vijay, P.V. (2007). "Reinforced Concrete Design with FRPcomposites", CRC Press, Taylor & Francis Group, Florida, USA.

ISO 1172:1996 (E) (1996). "Textile-glass-reinforced plastics – Preregs, moulding, compounds and laminates – Determination of the textile-glass and mineral-filler content – Calcination Methods", *International Organization for Standard*.

Kumahara, S., Masuda, Y., and Tanano, Y. (1993). "Tensile strength of continuous fiber reinforcing bar under high temperature." *ACI Special Publication*, 138, 731-742.

Nkurunziza, G., Benmokrane, B., Debaiky, A.S., and Masmoudi, R. (2005). "Effect of sustained load and environment on long-term tensile properties of glass fiber-reinforced polymer reinforcing bars", *ACI Structural Journal*, 102 (4), 615-621.

Quinn, G.D, Sparenberg, B.T., Koshy P., Ives, L.K., Jahanmir S., and Arola D.D. (2009). "Flexural strength of ceramic and glass rods." *Journal of Testing and Evaluation*, 37 (3), 1-23.

Robert, M., Cousin, P., and Benmokrane, B. (2009). "Durability of GFRP reinforcing bars embedded in moist concrete", *Journal of Composites for Construction*, Vol. 13, No. 2, pp. 66-73.

Robert, M. and Benmokrane, B. (2010). "Behavior of GFRP reinforcing bars subjected to extreme temperatures", *Journal of Composites for Construction*, Vol. 14, No. 1, pp. 353-360.

Tripathi, V.K. (2003). "Standardization of test methods for property evaluation of FRP bars." *Master Thesis*, Department of Civil and Environmental Engineering, West Virginia Unviversity, USA.

Wang, Y.C., Wong, P.M.H., and Kodur, V. (2007). "An experimental study of the mechanical properties of fibre reinforced polymer (FRP) and steel reinforcing bars at elevated temperature", *Composite Structures*, 80, 131-140.

Whitney, J.M., and Knight, M. (1980). "The relationship between tensile strength and flexure strength in fiber-reinforced composites." *Experimental Mechanics*, 20 (6), 211-216.

V-Rod® Australia, <www.vrodaustralia.com.au>.

C.3. Conference Paper III: An overview of the use of composite rebars as reinforcement in geopolymer concrete structures

Maranan GB, Manalo AC, Karunasena W, Benmokrane B, Mendis P, and Darren Lutze (2015). An overview of the use of composite rebars as reinforcement in geopolymer concrete structures. *The 2015 Composites Australia CRC-ACS Conference (2015 Composites Conference)*, 21-23 April, Gold Coast, Australia, 11 p. (http://www.compositesconference.com.au/2015-composites-conference/)

Abstract: Fibre reinforced polymer (FRP) bar has gained considerable acceptance as internal reinforcement for concrete structures because of its non-corrosive, lightweight, nonmagnetic, and high tensile strength properties while geopolymer concrete, normally manufactured using industrial waste materials like fly ash and blast furnace slags, has been successfully used in the construction of pavement, retaining walls, and bridges. To date, numerous research works on FRP-reinforced concrete and steel-reinforced geopolymer concrete are available. However, the use of FRP bar as internal reinforcement to geopolymer concrete had not been studied extensively and this has been the key motivation of this undertaking. This paper presents an overview on the research and development of the proposed system, the glass fibre reinforced polymer-reinforced geopolymer concrete (GFRP-RGC). Firstly, the issues and challenges on the use of the traditional steel-reinforced concrete were presented. Secondly, the existing solutions to address these problems were discussed. Then, the current research gap in the present solutions were identified. Finally, the results of the on-going research and development works on understanding the behaviour of the geopolymer concrete reinforced with FRP bars were presented. It is anticipated that the proposed system would yield more durable, greener, and cost-effective construction system compared to the conventional ones.

C.4. Conference Paper IV: Flexural response of GFRP-reinforced geopolymer concrete beams

Maranan GB, Manalo AC, Karunasena WM, Benmokrane B, and Mendis P (2015). Flexural response of GFRP-reinforced geopolymer concrete beams. *Proceedings of the 27th Biennial National Conference of the Concrete Institute of Australia (Concrete 2015),* 30 August-2 September, Melbourne, Australia, pp. 287-296 (full paper in USB).

Abstract: This study investigated the flexural response of glass fibre reinforced polymer-reinforced geopolymer concrete (GFRP-RGC) beams using a four-point static bending test. Three full-scale beams were cast and reinforced with nearly same amount of longitudinal GFRP reinforcements but of varying diameters at the bottom (4-12.7 mm, 3-15.9 mm, and 2-19.0 mm), two 12.7 mm GFRP bars at the top, and 9.5 mm GFRP stirrups spaced at 100 mm on-centre. The average compressive strength of the geopolymer concrete was 38.2 MPa. Based on the experimental results, all the tested beams showed nearly similar crack pattern, load-deflection response, bending-moment and deflection capacities, and strain readings, suggesting that the flexural response of a GFRP-RGC beam was not significantly influenced by the bar diameter; instead, by the properties of the geopolymer concrete. The $0.3M_u$ criterion suggested by Bischoff must be adapted in the serviceability design of a GFRP-RGC beam. The flexural capacities of the tested beams were generally higher than the predicted values from ACI 440.1R-15 and CSA S806-12 standards. Furthermore, the GFRP-RGC beams have higher strength compared with their GFRP-reinforced concrete counterparts. Thus, it can be concluded that the GFRP-RGC beams have structural properties that are suitable for civil infrastructure applications.

C.5. Conference Paper V: Comparison of the shear behaviour of geopolymer concrete beams with GFRP and steel transverse reinforcements

Maranan GB, Manalo AC, Karunasena W, Benmokrane B, and Mendis P (2015). Comparison of the shear behaviour of geopolymer concrete beams with GFRP and steel transverse reinforcements. *Proceedings of the 12th International Symposium on Fiber Reinforced Polymers for Reinforced Concrete Structures (FRPRCS-12) & The 5th Asia-Pacific Conference on Fiber Reinforced Polymers in Structures (APFIS-2015),* 14-16 December, Nanjing, China, pp. 169 (full paper in USB).

Abstract: This study presents a comparison of the shear behaviour of geopolymer concrete beams transversely reinforced with glass fiber-reinforced polymer (GFRP) and steel bars. Two full-scale beams with GFRP and steel stirrups spaced at 150 mm on-center were fabricated and tested up to failure using the four-point static bending test. Another beam without web reinforcements was also cast to determine the shear contribution of the geopolymer concrete. All the beams were provided with the same amount of flexural reinforcements. The beams were supported over a 1200 mm clear span with 450 mm shear span on each side. The shear span-to-depth ratio of the beams was 1.8. Based on the test results, the provision of GFRP stirrups almost doubled the shear capacity of the beam without web reinforcements. Comparable load-deflection response, shear strength, deflection capacity, and strain readings were observed between the beams with GFRP and steel stirrups. The two beams yielded similar crack pattern; however, wider cracks were developed in the former beam owing to the lower elastic modulus of GFRP bar compared with steel bar. Furthermore, both beams failed in shear, classified as a diagonal strut compression failure; however, the failure of the beam with GFRP stirrups was induced by the stirrup's lap splice failure while steel yielding caused the failure of beam with steel stirrups. This had led to a more brittle final failure of the former beam compared with the latter beam.

Appendix D

D.1. Paper I Copyright Information: Bond stress–slip behavior: Case of GFRP bars in geopolymer concrete

Maranan, G. B., Manalo, A. C., Karunasena W. M., and Benmokrane, B. (2015). Bond stress–slip behavior: Case of GFRP bars in geopolymer concrete. Journal of Materials in Civil Engineering, Vol. 27, Issue 1, pp. 04014116-1-9. (IF: 1.296, SNIP: 1.668)

ASCE AMERICAN SOCIETY OF CIVIL ENGINEERS

Title:	Bond Stress-Slip Behavior: Case of GFRP Bars in Geopolymer Concrete
Author:	Ginghis Maranan, Allan Manalo, Karu Karunasena, et al
Publication:	Journal of Materials in Civil Engineering
Publisher:	American Society of Civil Engineers
Date:	01/01/2015

Permissions Request

As an ASCE author, you are permitted to reuse you own content for another ASCE or non-ASCE publication.

Please add the full credit line "With permission from ASCE" to your source citation. Please print this page for your records.

Type of use: Dissertation/Thesis

Portion: full article

Format: electronic

Author of this ASCE work or ASCE will publish the new work: yes

D.2. Paper II Copyright Information: Pullout behaviour of GFRP bars with anchor head in geopolymer concrete

Maranan, G. B., Manalo, A. C., Karunasena W. M., and Benmokrane, B. (2015). Pullout behaviour of GFRP bars with anchor head in geopolymer concrete. Composite Structures, Vol. 132, pp. 1113-1121. (IF: 3.318, SNIP: 2.486)

ELSEVIER LICENSE
TERMS AND CONDITIONS

Mar 08, 2016

This is a License Agreement between Ginghis B Maranan ("You") and Elsevier ("Elsevier") provided by Copyright Clearance Center ("CCC"). The license consists of your order details, the terms and conditions provided by Elsevier, and the payment terms and conditions.

All payments must be made in full to CCC. For payment instructions, please see information listed at the bottom of this form.

Supplier	Elsevier Limited The Boulevard,Langford Lane Kidlington,Oxford,OX5 1GB,UK
Registered Company Number	1982084
Customer name	Ginghis B Maranan
Customer address	537-561 West Street Darling Heights Toowoomba, Queensland 4350
License number	3824000844227
License date	Mar 08, 2016
Licensed content publisher	Elsevier
Licensed content publication	Composite Structures
Licensed content title	Pullout behaviour of GFRP bars with anchor head in geopolymer concrete
Licensed content author	G.B. Maranan,A.C. Manalo,W. Karunasena,B. Benmokrane
Licensed content date	15 November 2015
Licensed content volume number	132
Licensed content issue number	n/a
Number of pages	9
Start Page	1113
End Page	1121
Type of Use	reuse in a thesis/dissertation
Portion	full article
Format	electronic
Are you the author of this Elsevier article?	Yes
Will you be translating?	No
Title of your thesis/dissertation	Structural behaviour of geopolymer concrete beams and columns reinforced with glass fibre reinforced polymer (GFRP) bars
Expected completion date	Mar 2016
Estimated size (number of pages)	200
Elsevier VAT number	GB 494 6272 12

Permissions price	0.00 AUD
VAT/Local Sales Tax	0.00 AUD / 0.00 GBP
Total	0.00 AUD

Terms and Conditions

INTRODUCTION

1. The publisher for this copyrighted material is Elsevier. By clicking "accept" in connection with completing this licensing transaction, you agree that the following terms and conditions apply to this transaction (along with the Billing and Payment terms and conditions established by Copyright Clearance Center, Inc. ("CCC"), at the time that you opened your Rightslink account and that are available at any time at http://myaccount.copyright.com).

GENERAL TERMS

2. Elsevier hereby grants you permission to reproduce the aforementioned material subject to the terms and conditions indicated.
3. Acknowledgement: If any part of the material to be used (for example, figures) has appeared in our publication with credit or acknowledgement to another source, permission must also be sought from that source. If such permission is not obtained then that material may not be included in your publication/copies. Suitable acknowledgement to the source must be made, either as a footnote or in a reference list at the end of your publication, as follows:
"Reprinted from Publication title, Vol /edition number, Author(s), Title of article / title of chapter, Pages No., Copyright (Year), with permission from Elsevier [OR APPLICABLE SOCIETY COPYRIGHT OWNER]." Also Lancet special credit - "Reprinted from The Lancet, Vol. number, Author(s), Title of article, Pages No., Copyright (Year), with permission from Elsevier."
4. Reproduction of this material is confined to the purpose and/or media for which permission is hereby given.
5. Altering/Modifying Material: Not Permitted. However figures and illustrations may be altered/adapted minimally to serve your work. Any other abbreviations, additions, deletions and/or any other alterations shall be made only with prior written authorization of Elsevier Ltd. (Please contact Elsevier at permissions@elsevier.com)
6. If the permission fee for the requested use of our material is waived in this instance, please be advised that your future requests for Elsevier materials may attract a fee.
7. Reservation of Rights: Publisher reserves all rights not specifically granted in the combination of (i) the license details provided by you and accepted in the course of this licensing transaction, (ii) these terms and conditions and (iii) CCC's Billing and Payment terms and conditions.
8. License Contingent Upon Payment: While you may exercise the rights licensed immediately upon issuance of the license at the end of the licensing process for the transaction, provided that you have disclosed complete and accurate details of your proposed use, no license is finally effective unless and until full payment is received from you (either by publisher or by CCC) as provided in CCC's Billing and Payment terms and conditions. If full payment is not received on a timely basis, then any license preliminarily granted shall be deemed automatically revoked and shall be void as if never granted. Further, in the event that you breach any of these terms and conditions or any of CCC's Billing and Payment terms and conditions, the license is automatically revoked and shall be void as if never granted. Use of materials as described in a revoked license, as well as any use of the materials beyond the scope of an unrevoked license, may constitute copyright infringement and publisher reserves the right to take any and all action to protect its copyright in the materials.
9. Warranties: Publisher makes no representations or warranties with respect to the licensed material.
10. Indemnity: You hereby indemnify and agree to hold harmless publisher and CCC, and

their respective officers, directors, employees and agents, from and against any and all claims arising out of your use of the licensed material other than as specifically authorized pursuant to this license.
11. No Transfer of License: This license is personal to you and may not be sublicensed, assigned, or transferred by you to any other person without publisher's written permission.
12. No Amendment Except in Writing: This license may not be amended except in a writing signed by both parties (or, in the case of publisher, by CCC on publisher's behalf).
13. Objection to Contrary Terms: Publisher hereby objects to any terms contained in any purchase order, acknowledgment, check endorsement or other writing prepared by you, which terms are inconsistent with these terms and conditions or CCC's Billing and Payment terms and conditions. These terms and conditions, together with CCC's Billing and Payment terms and conditions (which are incorporated herein), comprise the entire agreement between you and publisher (and CCC) concerning this licensing transaction. In the event of any conflict between your obligations established by these terms and conditions and those established by CCC's Billing and Payment terms and conditions, these terms and conditions shall control.
14. Revocation: Elsevier or Copyright Clearance Center may deny the permissions described in this License at their sole discretion, for any reason or no reason, with a full refund payable to you. Notice of such denial will be made using the contact information provided by you. Failure to receive such notice will not alter or invalidate the denial. In no event will Elsevier or Copyright Clearance Center be responsible or liable for any costs, expenses or damage incurred by you as a result of a denial of your permission request, other than a refund of the amount(s) paid by you to Elsevier and/or Copyright Clearance Center for denied permissions.

LIMITED LICENSE

The following terms and conditions apply only to specific license types:
15. **Translation**: This permission is granted for non-exclusive world **English** rights only unless your license was granted for translation rights. If you licensed translation rights you may only translate this content into the languages you requested. A professional translator must perform all translations and reproduce the content word for word preserving the integrity of the article.
16. **Posting licensed content on any Website**: The following terms and conditions apply as follows: Licensing material from an Elsevier journal: All content posted to the web site must maintain the copyright information line on the bottom of each image; A hyper-text must be included to the Homepage of the journal from which you are licensing at http://www.sciencedirect.com/science/journal/xxxxx or the Elsevier homepage for books at http://www.elsevier.com; Central Storage: This license does not include permission for a scanned version of the material to be stored in a central repository such as that provided by Heron/XanEdu.
Licensing material from an Elsevier book: A hyper-text link must be included to the Elsevier homepage at http://www.elsevier.com . All content posted to the web site must maintain the copyright information line on the bottom of each image.

Posting licensed content on Electronic reserve: In addition to the above the following clauses are applicable: The web site must be password-protected and made available only to bona fide students registered on a relevant course. This permission is granted for 1 year only. You may obtain a new license for future website posting.
17. **For journal authors:** the following clauses are applicable in addition to the above:
Preprints:
A preprint is an author's own write-up of research results and analysis, it has not been peer-reviewed, nor has it had any other value added to it by a publisher (such as formatting, copyright, technical enhancement etc.).
Authors can share their preprints anywhere at any time. Preprints should not be added to or enhanced in any way in order to appear more like, or to substitute for, the final versions of

articles however authors can update their preprints on arXiv or RePEc with their Accepted Author Manuscript (see below).
If accepted for publication, we encourage authors to link from the preprint to their formal publication via its DOI. Millions of researchers have access to the formal publications on ScienceDirect, and so links will help users to find, access, cite and use the best available version. Please note that Cell Press, The Lancet and some society-owned have different preprint policies. Information on these policies is available on the journal homepage.
Accepted Author Manuscripts: An accepted author manuscript is the manuscript of an article that has been accepted for publication and which typically includes author-incorporated changes suggested during submission, peer review and editor-author communications.
Authors can share their accepted author manuscript:

- immediately
  - via their non-commercial person homepage or blog
  - by updating a preprint in arXiv or RePEc with the accepted manuscript
  - via their research institute or institutional repository for internal institutional uses or as part of an invitation-only research collaboration work-group
  - directly by providing copies to their students or to research collaborators for their personal use
  - for private scholarly sharing as part of an invitation-only work group on commercial sites with which Elsevier has an agreement
- after the embargo period
  - via non-commercial hosting platforms such as their institutional repository
  - via commercial sites with which Elsevier has an agreement

In all cases accepted manuscripts should:

- link to the formal publication via its DOI
- bear a CC-BY-NC-ND license - this is easy to do
- if aggregated with other manuscripts, for example in a repository or other site, be shared in alignment with our hosting policy not be added to or enhanced in any way to appear more like, or to substitute for, the published journal article.

Published journal article (JPA): A published journal article (PJA) is the definitive final record of published research that appears or will appear in the journal and embodies all value-adding publishing activities including peer review co-ordination, copy-editing, formatting, (if relevant) pagination and online enrichment.
Policies for sharing publishing journal articles differ for subscription and gold open access articles:
Subscription Articles: If you are an author, please share a link to your article rather than the full-text. Millions of researchers have access to the formal publications on ScienceDirect, and so links will help your users to find, access, cite, and use the best available version.
Theses and dissertations which contain embedded PJAs as part of the formal submission can be posted publicly by the awarding institution with DOI links back to the formal publications on ScienceDirect.
If you are affiliated with a library that subscribes to ScienceDirect you have additional private sharing rights for others' research accessed under that agreement. This includes use for classroom teaching and internal training at the institution (including use in course packs and courseware programs), and inclusion of the article for grant funding purposes.
Gold Open Access Articles: May be shared according to the author-selected end-user license and should contain a CrossMark logo, the end user license, and a DOI link to the formal publication on ScienceDirect.
Please refer to Elsevier's posting policy for further information.

18. **For book authors** the following clauses are applicable in addition to the above: Authors are permitted to place a brief summary of their work online only. You are not allowed to download and post the published electronic version of your chapter, nor may you scan the printed edition to create an electronic version. **Posting to a repository:** Authors are permitted to post a summary of their chapter only in their institution's repository.
19. **Thesis/Dissertation**: If your license is for use in a thesis/dissertation your thesis may be submitted to your institution in either print or electronic form. Should your thesis be published commercially, please reapply for permission. These requirements include permission for the Library and Archives of Canada to supply single copies, on demand, of the complete thesis and include permission for Proquest/UMI to supply single copies, on demand, of the complete thesis. Should your thesis be published commercially, please reapply for permission. Theses and dissertations which contain embedded PJAs as part of the formal submission can be posted publicly by the awarding institution with DOI links back to the formal publications on ScienceDirect.

Elsevier Open Access Terms and Conditions
You can publish open access with Elsevier in hundreds of open access journals or in nearly 2000 established subscription journals that support open access publishing. Permitted third party re-use of these open access articles is defined by the author's choice of Creative Commons user license. See our open access license policy for more information.
Terms & Conditions applicable to all Open Access articles published with Elsevier:
Any reuse of the article must not represent the author as endorsing the adaptation of the article nor should the article be modified in such a way as to damage the author's honour or reputation. If any changes have been made, such changes must be clearly indicated.
The author(s) must be appropriately credited and we ask that you include the end user license and a DOI link to the formal publication on ScienceDirect.
If any part of the material to be used (for example, figures) has appeared in our publication with credit or acknowledgement to another source it is the responsibility of the user to ensure their reuse complies with the terms and conditions determined by the rights holder.
Additional Terms & Conditions applicable to each Creative Commons user license:
CC BY: The CC-BY license allows users to copy, to create extracts, abstracts and new works from the Article, to alter and revise the Article and to make commercial use of the Article (including reuse and/or resale of the Article by commercial entities), provided the user gives appropriate credit (with a link to the formal publication through the relevant DOI), provides a link to the license, indicates if changes were made and the licensor is not represented as endorsing the use made of the work. The full details of the license are available at http://creativecommons.org/licenses/by/4.0.
CC BY NC SA: The CC BY-NC-SA license allows users to copy, to create extracts, abstracts and new works from the Article, to alter and revise the Article, provided this is not done for commercial purposes, and that the user gives appropriate credit (with a link to the formal publication through the relevant DOI), provides a link to the license, indicates if changes were made and the licensor is not represented as endorsing the use made of the work. Further, any new works must be made available on the same conditions. The full details of the license are available at http://creativecommons.org/licenses/by-nc-sa/4.0.
CC BY NC ND: The CC BY-NC-ND license allows users to copy and distribute the Article, provided this is not done for commercial purposes and further does not permit distribution of the Article if it is changed or edited in any way, and provided the user gives appropriate credit (with a link to the formal publication through the relevant DOI), provides a link to the license, and that the licensor is not represented as endorsing the use made of the work. The full details of the license are available at http://creativecommons.org/licenses/by-nc-nd/4.0.
Any commercial reuse of Open Access articles published with a CC BY NC SA or CC BY NC ND license requires permission from Elsevier and will be subject to a fee.
Commercial reuse includes:

- Associating advertising with the full text of the Article
- Charging fees for document delivery or access
- Article aggregation
- Systematic distribution via e-mail lists or share buttons

Posting or linking by commercial companies for use by customers of those companies.

20. **Other Conditions**:

v1.8

Questions? customercare@copyright.com or +1-855-239-3415 (toll free in the US) or +1-978-646-2777.

D.3. Paper III Copyright Information: Evaluation of the flexural strength and serviceability of geopolymer concrete beams reinforced with glass-fibre-reinforced polymer (GFRP) bars

Paper III: Maranan, G. B., Manalo, A. C., Benmokrane, B., Karunasena W. M., and Mendis, P. (2015). Evaluation of the flexural strength and serviceability of geopolymer concrete beams reinforced with glass-fibre-reinforced polymer (GFRP) bars. Engineering Structures, Vol. 101, pp. 529-541. (IF: 1.838, SNIP: 2.396)

ELSEVIER LICENSE
TERMS AND CONDITIONS

Mar 08, 2016

This is a License Agreement between Ginghis B Maranan ("You") and Elsevier ("Elsevier") provided by Copyright Clearance Center ("CCC"). The license consists of your order details, the terms and conditions provided by Elsevier, and the payment terms and conditions.

All payments must be made in full to CCC. For payment instructions, please see information listed at the bottom of this form.

Supplier	Elsevier Limited The Boulevard,Langford Lane Kidlington,Oxford,OX5 1GB,UK
Registered Company Number	1982084
Customer name	Ginghis B Maranan
Customer address	537-561 West Street Darling Heights Toowoomba, Queensland 4350
License number	3824001451204
License date	Mar 08, 2016
Licensed content publisher	Elsevier
Licensed content publication	Engineering Structures
Licensed content title	Evaluation of the flexural strength and serviceability of geopolymer concrete beams reinforced with glass-fibre-reinforced polymer (GFRP) bars
Licensed content author	G.B. Maranan,A.C. Manalo,B. Benmokrane,W. Karunasena,P. Mendis
Licensed content date	15 October 2015
Licensed content volume number	101
Licensed content issue number	n/a
Number of pages	13
Start Page	529
End Page	541
Type of Use	reuse in a thesis/dissertation
Intended publisher of new work	other
Portion	full article
Format	electronic
Are you the author of this Elsevier article?	Yes
Will you be translating?	No
Title of your thesis/dissertation	Structural behaviour of geopolymer concrete beams and columns reinforced with glass fibre reinforced polymer (GFRP) bars
Expected completion date	Mar 2016
Estimated size (number of	200

pages)	
Elsevier VAT number	GB 494 6272 12
Permissions price	0.00 USD
VAT/Local Sales Tax	0.00 USD / 0.00 GBP
Total	0.00 USD

Terms and Conditions

INTRODUCTION

1. The publisher for this copyrighted material is Elsevier. By clicking "accept" in connection with completing this licensing transaction, you agree that the following terms and conditions apply to this transaction (along with the Billing and Payment terms and conditions established by Copyright Clearance Center, Inc. ("CCC"), at the time that you opened your Rightslink account and that are available at any time at http://myaccount.copyright.com).

GENERAL TERMS

2. Elsevier hereby grants you permission to reproduce the aforementioned material subject to the terms and conditions indicated.
3. Acknowledgement: If any part of the material to be used (for example, figures) has appeared in our publication with credit or acknowledgement to another source, permission must also be sought from that source. If such permission is not obtained then that material may not be included in your publication/copies. Suitable acknowledgement to the source must be made, either as a footnote or in a reference list at the end of your publication, as follows:
"Reprinted from Publication title, Vol /edition number, Author(s), Title of article / title of chapter, Pages No., Copyright (Year), with permission from Elsevier [OR APPLICABLE SOCIETY COPYRIGHT OWNER]." Also Lancet special credit - "Reprinted from The Lancet, Vol. number, Author(s), Title of article, Pages No., Copyright (Year), with permission from Elsevier."
4. Reproduction of this material is confined to the purpose and/or media for which permission is hereby given.
5. Altering/Modifying Material: Not Permitted. However figures and illustrations may be altered/adapted minimally to serve your work. Any other abbreviations, additions, deletions and/or any other alterations shall be made only with prior written authorization of Elsevier Ltd. (Please contact Elsevier at permissions@elsevier.com)
6. If the permission fee for the requested use of our material is waived in this instance, please be advised that your future requests for Elsevier materials may attract a fee.
7. Reservation of Rights: Publisher reserves all rights not specifically granted in the combination of (i) the license details provided by you and accepted in the course of this licensing transaction, (ii) these terms and conditions and (iii) CCC's Billing and Payment terms and conditions.
8. License Contingent Upon Payment: While you may exercise the rights licensed immediately upon issuance of the license at the end of the licensing process for the transaction, provided that you have disclosed complete and accurate details of your proposed use, no license is finally effective unless and until full payment is received from you (either by publisher or by CCC) as provided in CCC's Billing and Payment terms and conditions. If full payment is not received on a timely basis, then any license preliminarily granted shall be deemed automatically revoked and shall be void as if never granted. Further, in the event that you breach any of these terms and conditions or any of CCC's Billing and Payment terms and conditions, the license is automatically revoked and shall be void as if never granted. Use of materials as described in a revoked license, as well as any use of the materials beyond the scope of an unrevoked license, may constitute copyright infringement and publisher reserves the right to take any and all action to protect its copyright in the materials.

9. Warranties: Publisher makes no representations or warranties with respect to the licensed material.
10. Indemnity: You hereby indemnify and agree to hold harmless publisher and CCC, and their respective officers, directors, employees and agents, from and against any and all claims arising out of your use of the licensed material other than as specifically authorized pursuant to this license.
11. No Transfer of License: This license is personal to you and may not be sublicensed, assigned, or transferred by you to any other person without publisher's written permission.
12. No Amendment Except in Writing: This license may not be amended except in a writing signed by both parties (or, in the case of publisher, by CCC on publisher's behalf).
13. Objection to Contrary Terms: Publisher hereby objects to any terms contained in any purchase order, acknowledgment, check endorsement or other writing prepared by you, which terms are inconsistent with these terms and conditions or CCC's Billing and Payment terms and conditions. These terms and conditions, together with CCC's Billing and Payment terms and conditions (which are incorporated herein), comprise the entire agreement between you and publisher (and CCC) concerning this licensing transaction. In the event of any conflict between your obligations established by these terms and conditions and those established by CCC's Billing and Payment terms and conditions, these terms and conditions shall control.
14. Revocation: Elsevier or Copyright Clearance Center may deny the permissions described in this License at their sole discretion, for any reason or no reason, with a full refund payable to you. Notice of such denial will be made using the contact information provided by you. Failure to receive such notice will not alter or invalidate the denial. In no event will Elsevier or Copyright Clearance Center be responsible or liable for any costs, expenses or damage incurred by you as a result of a denial of your permission request, other than a refund of the amount(s) paid by you to Elsevier and/or Copyright Clearance Center for denied permissions.

LIMITED LICENSE

The following terms and conditions apply only to specific license types:
15. **Translation**: This permission is granted for non-exclusive world **English** rights only unless your license was granted for translation rights. If you licensed translation rights you may only translate this content into the languages you requested. A professional translator must perform all translations and reproduce the content word for word preserving the integrity of the article.
16. **Posting licensed content on any Website**: The following terms and conditions apply as follows: Licensing material from an Elsevier journal: All content posted to the web site must maintain the copyright information line on the bottom of each image; A hyper-text must be included to the Homepage of the journal from which you are licensing at http://www.sciencedirect.com/science/journal/xxxxx or the Elsevier homepage for books at http://www.elsevier.com; Central Storage: This license does not include permission for a scanned version of the material to be stored in a central repository such as that provided by Heron/XanEdu.
Licensing material from an Elsevier book: A hyper-text link must be included to the Elsevier homepage at http://www.elsevier.com . All content posted to the web site must maintain the copyright information line on the bottom of each image.

Posting licensed content on Electronic reserve: In addition to the above the following clauses are applicable: The web site must be password-protected and made available only to bona fide students registered on a relevant course. This permission is granted for 1 year only. You may obtain a new license for future website posting.
17. **For journal authors:** the following clauses are applicable in addition to the above:
Preprints:
A preprint is an author's own write-up of research results and analysis, it has not been peer-reviewed, nor has it had any other value added to it by a publisher (such as formatting,

copyright, technical enhancement etc.).
Authors can share their preprints anywhere at any time. Preprints should not be added to or enhanced in any way in order to appear more like, or to substitute for, the final versions of articles however authors can update their preprints on arXiv or RePEc with their Accepted Author Manuscript (see below).
If accepted for publication, we encourage authors to link from the preprint to their formal publication via its DOI. Millions of researchers have access to the formal publications on ScienceDirect, and so links will help users to find, access, cite and use the best available version. Please note that Cell Press, The Lancet and some society-owned have different preprint policies. Information on these policies is available on the journal homepage.
Accepted Author Manuscripts: An accepted author manuscript is the manuscript of an article that has been accepted for publication and which typically includes author-incorporated changes suggested during submission, peer review and editor-author communications.
Authors can share their accepted author manuscript:

- immediately
  - via their non-commercial person homepage or blog
  - by updating a preprint in arXiv or RePEc with the accepted manuscript
  - via their research institute or institutional repository for internal institutional uses or as part of an invitation-only research collaboration work-group
  - directly by providing copies to their students or to research collaborators for their personal use
  - for private scholarly sharing as part of an invitation-only work group on commercial sites with which Elsevier has an agreement
- after the embargo period
  - via non-commercial hosting platforms such as their institutional repository
  - via commercial sites with which Elsevier has an agreement

In all cases accepted manuscripts should:

- link to the formal publication via its DOI
- bear a CC-BY-NC-ND license - this is easy to do
- if aggregated with other manuscripts, for example in a repository or other site, be shared in alignment with our hosting policy not be added to or enhanced in any way to appear more like, or to substitute for, the published journal article.

Published journal article (JPA): A published journal article (PJA) is the definitive final record of published research that appears or will appear in the journal and embodies all value-adding publishing activities including peer review co-ordination, copy-editing, formatting, (if relevant) pagination and online enrichment.
Policies for sharing publishing journal articles differ for subscription and gold open access articles:
Subscription Articles: If you are an author, please share a link to your article rather than the full-text. Millions of researchers have access to the formal publications on ScienceDirect, and so links will help your users to find, access, cite, and use the best available version.
Theses and dissertations which contain embedded PJAs as part of the formal submission can be posted publicly by the awarding institution with DOI links back to the formal publications on ScienceDirect.
If you are affiliated with a library that subscribes to ScienceDirect you have additional private sharing rights for others' research accessed under that agreement. This includes use for classroom teaching and internal training at the institution (including use in course packs and courseware programs), and inclusion of the article for grant funding purposes.
Gold Open Access Articles: May be shared according to the author-selected end-user

license and should contain a CrossMark logo, the end user license, and a DOI link to the formal publication on ScienceDirect.
Please refer to Elsevier's posting policy for further information.
18. **For book authors** the following clauses are applicable in addition to the above: Authors are permitted to place a brief summary of their work online only. You are not allowed to download and post the published electronic version of your chapter, nor may you scan the printed edition to create an electronic version. **Posting to a repository:** Authors are permitted to post a summary of their chapter only in their institution's repository.
19. **Thesis/Dissertation**: If your license is for use in a thesis/dissertation your thesis may be submitted to your institution in either print or electronic form. Should your thesis be published commercially, please reapply for permission. These requirements include permission for the Library and Archives of Canada to supply single copies, on demand, of the complete thesis and include permission for Proquest/UMI to supply single copies, on demand, of the complete thesis. Should your thesis be published commercially, please reapply for permission. Theses and dissertations which contain embedded PJAs as part of the formal submission can be posted publicly by the awarding institution with DOI links back to the formal publications on ScienceDirect.

Elsevier Open Access Terms and Conditions
You can publish open access with Elsevier in hundreds of open access journals or in nearly 2000 established subscription journals that support open access publishing. Permitted third party re-use of these open access articles is defined by the author's choice of Creative Commons user license. See our open access license policy for more information.
Terms & Conditions applicable to all Open Access articles published with Elsevier:
Any reuse of the article must not represent the author as endorsing the adaptation of the article nor should the article be modified in such a way as to damage the author's honour or reputation. If any changes have been made, such changes must be clearly indicated.
The author(s) must be appropriately credited and we ask that you include the end user license and a DOI link to the formal publication on ScienceDirect.
If any part of the material to be used (for example, figures) has appeared in our publication with credit or acknowledgement to another source it is the responsibility of the user to ensure their reuse complies with the terms and conditions determined by the rights holder.
Additional Terms & Conditions applicable to each Creative Commons user license:
CC BY: The CC-BY license allows users to copy, to create extracts, abstracts and new works from the Article, to alter and revise the Article and to make commercial use of the Article (including reuse and/or resale of the Article by commercial entities), provided the user gives appropriate credit (with a link to the formal publication through the relevant DOI), provides a link to the license, indicates if changes were made and the licensor is not represented as endorsing the use made of the work. The full details of the license are available at http://creativecommons.org/licenses/by/4.0.
CC BY NC SA: The CC BY-NC-SA license allows users to copy, to create extracts, abstracts and new works from the Article, to alter and revise the Article, provided this is not done for commercial purposes, and that the user gives appropriate credit (with a link to the formal publication through the relevant DOI), provides a link to the license, indicates if changes were made and the licensor is not represented as endorsing the use made of the work. Further, any new works must be made available on the same conditions. The full details of the license are available at http://creativecommons.org/licenses/by-nc-sa/4.0.
CC BY NC ND: The CC BY-NC-ND license allows users to copy and distribute the Article, provided this is not done for commercial purposes and further does not permit distribution of the Article if it is changed or edited in any way, and provided the user gives appropriate credit (with a link to the formal publication through the relevant DOI), provides a link to the license, and that the licensor is not represented as endorsing the use made of the work. The full details of the license are available at http://creativecommons.org/licenses/by-nc-nd/4.0.
Any commercial reuse of Open Access articles published with a CC BY NC SA or CC BY

NC ND license requires permission from Elsevier and will be subject to a fee.
Commercial reuse includes:

- Associating advertising with the full text of the Article
- Charging fees for document delivery or access
- Article aggregation
- Systematic distribution via e-mail lists or share buttons

Posting or linking by commercial companies for use by customers of those companies.

20. **Other Conditions**:

v1.8

Questions? customercare@copyright.com or +1-855-239-3415 (toll free in the US) or +1-978-646-2777.

D.5. Paper V Copyright Information: Behavior of concentrically loaded geopolymer-concrete circular columns reinforced longitudinally and transversely with GFRP bars

Paper V: Maranan, G. B., Manalo, A. C., Benmokrane, B., Karunasena W. M., and Mendis, P. (2016). Behavior of concentrically loaded geopolymer-concrete circular columns reinforced longitudinally and transversely with GFRP bars. Engineering Structures, Vol. 117, pp. 422-436. (IF: 1.838, SNIP: 2.396)

ELSEVIER LICENSE
TERMS AND CONDITIONS

Mar 25, 2016

This is a License Agreement between Ginghis B Maranan ("You") and Elsevier ("Elsevier") provided by Copyright Clearance Center ("CCC"). The license consists of your order details, the terms and conditions provided by Elsevier, and the payment terms and conditions.

All payments must be made in full to CCC. For payment instructions, please see information listed at the bottom of this form.

Supplier	Elsevier Limited The Boulevard,Langford Lane Kidlington,Oxford,OX5 1GB,UK
Registered Company Number	1982084
Customer name	Ginghis B Maranan
Customer address	537-561 West Street Darling Heights Toowoomba, Queensland 4350
License number	3836210514440
License date	Mar 25, 2016
Licensed content publisher	Elsevier
Licensed content publication	Engineering Structures
Licensed content title	Behavior of concentrically loaded geopolymer-concrete circular columns reinforced longitudinally and transversely with GFRP bars
Licensed content author	G.B. Maranan,A.C. Manalo,B. Benmokrane,W. Karunasena,P. Mendis
Licensed content date	15 June 2016
Licensed content volume number	117
Licensed content issue number	n/a
Number of pages	15
Start Page	422
End Page	436
Type of Use	reuse in a thesis/dissertation
Portion	full article
Format	electronic
Are you the author of this Elsevier article?	Yes
Will you be translating?	No
Title of your thesis/dissertation	Structural behaviour of geopolymer concrete beams and columns reinforced with glass fibre reinforced polymer (GFRP) bars
Expected completion date	Mar 2016
Estimated size (number of pages)	200
Elsevier VAT number	GB 494 6272 12

Permissions price	0.00 AUD
VAT/Local Sales Tax	0.00 AUD / 0.00 GBP
Total	0.00 AUD

Terms and Conditions

INTRODUCTION

1. The publisher for this copyrighted material is Elsevier. By clicking "accept" in connection with completing this licensing transaction, you agree that the following terms and conditions apply to this transaction (along with the Billing and Payment terms and conditions established by Copyright Clearance Center, Inc. ("CCC"), at the time that you opened your Rightslink account and that are available at any time at http://myaccount.copyright.com).

GENERAL TERMS

2. Elsevier hereby grants you permission to reproduce the aforementioned material subject to the terms and conditions indicated.
3. Acknowledgement: If any part of the material to be used (for example, figures) has appeared in our publication with credit or acknowledgement to another source, permission must also be sought from that source. If such permission is not obtained then that material may not be included in your publication/copies. Suitable acknowledgement to the source must be made, either as a footnote or in a reference list at the end of your publication, as follows:
"Reprinted from Publication title, Vol /edition number, Author(s), Title of article / title of chapter, Pages No., Copyright (Year), with permission from Elsevier [OR APPLICABLE SOCIETY COPYRIGHT OWNER]." Also Lancet special credit - "Reprinted from The Lancet, Vol. number, Author(s), Title of article, Pages No., Copyright (Year), with permission from Elsevier."
4. Reproduction of this material is confined to the purpose and/or media for which permission is hereby given.
5. Altering/Modifying Material: Not Permitted. However figures and illustrations may be altered/adapted minimally to serve your work. Any other abbreviations, additions, deletions and/or any other alterations shall be made only with prior written authorization of Elsevier Ltd. (Please contact Elsevier at permissions@elsevier.com)
6. If the permission fee for the requested use of our material is waived in this instance, please be advised that your future requests for Elsevier materials may attract a fee.
7. Reservation of Rights: Publisher reserves all rights not specifically granted in the combination of (i) the license details provided by you and accepted in the course of this licensing transaction, (ii) these terms and conditions and (iii) CCC's Billing and Payment terms and conditions.
8. License Contingent Upon Payment: While you may exercise the rights licensed immediately upon issuance of the license at the end of the licensing process for the transaction, provided that you have disclosed complete and accurate details of your proposed use, no license is finally effective unless and until full payment is received from you (either by publisher or by CCC) as provided in CCC's Billing and Payment terms and conditions. If full payment is not received on a timely basis, then any license preliminarily granted shall be deemed automatically revoked and shall be void as if never granted. Further, in the event that you breach any of these terms and conditions or any of CCC's Billing and Payment terms and conditions, the license is automatically revoked and shall be void as if never granted. Use of materials as described in a revoked license, as well as any use of the materials beyond the scope of an unrevoked license, may constitute copyright infringement and publisher reserves the right to take any and all action to protect its copyright in the materials.
9. Warranties: Publisher makes no representations or warranties with respect to the licensed material.
10. Indemnity: You hereby indemnify and agree to hold harmless publisher and CCC, and their respective officers, directors, employees and agents, from and against any and all

claims arising out of your use of the licensed material other than as specifically authorized pursuant to this license.
11. No Transfer of License: This license is personal to you and may not be sublicensed, assigned, or transferred by you to any other person without publisher's written permission.
12. No Amendment Except in Writing: This license may not be amended except in a writing signed by both parties (or, in the case of publisher, by CCC on publisher's behalf).
13. Objection to Contrary Terms: Publisher hereby objects to any terms contained in any purchase order, acknowledgment, check endorsement or other writing prepared by you, which terms are inconsistent with these terms and conditions or CCC's Billing and Payment terms and conditions. These terms and conditions, together with CCC's Billing and Payment terms and conditions (which are incorporated herein), comprise the entire agreement between you and publisher (and CCC) concerning this licensing transaction. In the event of any conflict between your obligations established by these terms and conditions and those established by CCC's Billing and Payment terms and conditions, these terms and conditions shall control.
14. Revocation: Elsevier or Copyright Clearance Center may deny the permissions described in this License at their sole discretion, for any reason or no reason, with a full refund payable to you. Notice of such denial will be made using the contact information provided by you. Failure to receive such notice will not alter or invalidate the denial. In no event will Elsevier or Copyright Clearance Center be responsible or liable for any costs, expenses or damage incurred by you as a result of a denial of your permission request, other than a refund of the amount(s) paid by you to Elsevier and/or Copyright Clearance Center for denied permissions.

LIMITED LICENSE

The following terms and conditions apply only to specific license types:
15. **Translation**: This permission is granted for non-exclusive world **English** rights only unless your license was granted for translation rights. If you licensed translation rights you may only translate this content into the languages you requested. A professional translator must perform all translations and reproduce the content word for word preserving the integrity of the article.
16. **Posting licensed content on any Website**: The following terms and conditions apply as follows: Licensing material from an Elsevier journal: All content posted to the web site must maintain the copyright information line on the bottom of each image; A hyper-text must be included to the Homepage of the journal from which you are licensing at http://www.sciencedirect.com/science/journal/xxxxx or the Elsevier homepage for books at http://www.elsevier.com; Central Storage: This license does not include permission for a scanned version of the material to be stored in a central repository such as that provided by Heron/XanEdu.
Licensing material from an Elsevier book: A hyper-text link must be included to the Elsevier homepage at http://www.elsevier.com . All content posted to the web site must maintain the copyright information line on the bottom of each image.

Posting licensed content on Electronic reserve: In addition to the above the following clauses are applicable: The web site must be password-protected and made available only to bona fide students registered on a relevant course. This permission is granted for 1 year only. You may obtain a new license for future website posting.
17. **For journal authors:** the following clauses are applicable in addition to the above:
Preprints:
A preprint is an author's own write-up of research results and analysis, it has not been peer-reviewed, nor has it had any other value added to it by a publisher (such as formatting, copyright, technical enhancement etc.).
Authors can share their preprints anywhere at any time. Preprints should not be added to or enhanced in any way in order to appear more like, or to substitute for, the final versions of articles however authors can update their preprints on arXiv or RePEc with their Accepted

Author Manuscript (see below).
If accepted for publication, we encourage authors to link from the preprint to their formal publication via its DOI. Millions of researchers have access to the formal publications on ScienceDirect, and so links will help users to find, access, cite and use the best available version. Please note that Cell Press, The Lancet and some society-owned have different preprint policies. Information on these policies is available on the journal homepage.
Accepted Author Manuscripts: An accepted author manuscript is the manuscript of an article that has been accepted for publication and which typically includes author-incorporated changes suggested during submission, peer review and editor-author communications.
Authors can share their accepted author manuscript:

- immediately
  - via their non-commercial person homepage or blog
  - by updating a preprint in arXiv or RePEc with the accepted manuscript
  - via their research institute or institutional repository for internal institutional uses or as part of an invitation-only research collaboration work-group
  - directly by providing copies to their students or to research collaborators for their personal use
  - for private scholarly sharing as part of an invitation-only work group on commercial sites with which Elsevier has an agreement
- after the embargo period
  - via non-commercial hosting platforms such as their institutional repository
  - via commercial sites with which Elsevier has an agreement

In all cases accepted manuscripts should:

- link to the formal publication via its DOI
- bear a CC-BY-NC-ND license - this is easy to do
- if aggregated with other manuscripts, for example in a repository or other site, be shared in alignment with our hosting policy not be added to or enhanced in any way to appear more like, or to substitute for, the published journal article.

Published journal article (JPA): A published journal article (PJA) is the definitive final record of published research that appears or will appear in the journal and embodies all value-adding publishing activities including peer review co-ordination, copy-editing, formatting, (if relevant) pagination and online enrichment.
Policies for sharing publishing journal articles differ for subscription and gold open access articles:
Subscription Articles: If you are an author, please share a link to your article rather than the full-text. Millions of researchers have access to the formal publications on ScienceDirect, and so links will help your users to find, access, cite, and use the best available version.
Theses and dissertations which contain embedded PJAs as part of the formal submission can be posted publicly by the awarding institution with DOI links back to the formal publications on ScienceDirect.
If you are affiliated with a library that subscribes to ScienceDirect you have additional private sharing rights for others' research accessed under that agreement. This includes use for classroom teaching and internal training at the institution (including use in course packs and courseware programs), and inclusion of the article for grant funding purposes.
Gold Open Access Articles: May be shared according to the author-selected end-user license and should contain a CrossMark logo, the end user license, and a DOI link to the formal publication on ScienceDirect.
Please refer to Elsevier's posting policy for further information.
18. **For book authors** the following clauses are applicable in addition to the above:

Authors are permitted to place a brief summary of their work online only. You are not allowed to download and post the published electronic version of your chapter, nor may you scan the printed edition to create an electronic version. **Posting to a repository:** Authors are permitted to post a summary of their chapter only in their institution's repository.
19. **Thesis/Dissertation**: If your license is for use in a thesis/dissertation your thesis may be submitted to your institution in either print or electronic form. Should your thesis be published commercially, please reapply for permission. These requirements include permission for the Library and Archives of Canada to supply single copies, on demand, of the complete thesis and include permission for Proquest/UMI to supply single copies, on demand, of the complete thesis. Should your thesis be published commercially, please reapply for permission. Theses and dissertations which contain embedded PJAs as part of the formal submission can be posted publicly by the awarding institution with DOI links back to the formal publications on ScienceDirect.

Elsevier Open Access Terms and Conditions
You can publish open access with Elsevier in hundreds of open access journals or in nearly 2000 established subscription journals that support open access publishing. Permitted third party re-use of these open access articles is defined by the author's choice of Creative Commons user license. See our open access license policy for more information.
Terms & Conditions applicable to all Open Access articles published with Elsevier:
Any reuse of the article must not represent the author as endorsing the adaptation of the article nor should the article be modified in such a way as to damage the author's honour or reputation. If any changes have been made, such changes must be clearly indicated.
The author(s) must be appropriately credited and we ask that you include the end user license and a DOI link to the formal publication on ScienceDirect.
If any part of the material to be used (for example, figures) has appeared in our publication with credit or acknowledgement to another source it is the responsibility of the user to ensure their reuse complies with the terms and conditions determined by the rights holder.
Additional Terms & Conditions applicable to each Creative Commons user license:
CC BY: The CC-BY license allows users to copy, to create extracts, abstracts and new works from the Article, to alter and revise the Article and to make commercial use of the Article (including reuse and/or resale of the Article by commercial entities), provided the user gives appropriate credit (with a link to the formal publication through the relevant DOI), provides a link to the license, indicates if changes were made and the licensor is not represented as endorsing the use made of the work. The full details of the license are available at http://creativecommons.org/licenses/by/4.0.
CC BY NC SA: The CC BY-NC-SA license allows users to copy, to create extracts, abstracts and new works from the Article, to alter and revise the Article, provided this is not done for commercial purposes, and that the user gives appropriate credit (with a link to the formal publication through the relevant DOI), provides a link to the license, indicates if changes were made and the licensor is not represented as endorsing the use made of the work. Further, any new works must be made available on the same conditions. The full details of the license are available at http://creativecommons.org/licenses/by-nc-sa/4.0.
CC BY NC ND: The CC BY-NC-ND license allows users to copy and distribute the Article, provided this is not done for commercial purposes and further does not permit distribution of the Article if it is changed or edited in any way, and provided the user gives appropriate credit (with a link to the formal publication through the relevant DOI), provides a link to the license, and that the licensor is not represented as endorsing the use made of the work. The full details of the license are available at http://creativecommons.org/licenses/by-nc-nd/4.0.
Any commercial reuse of Open Access articles published with a CC BY NC SA or CC BY NC ND license requires permission from Elsevier and will be subject to a fee.
Commercial reuse includes:

- Associating advertising with the full text of the Article

- Charging fees for document delivery or access
- Article aggregation
- Systematic distribution via e-mail lists or share buttons

Posting or linking by commercial companies for use by customers of those companies.

20. **Other Conditions**:

v1.8

Questions? customercare@copyright.com or +1-855-239-3415 (toll free in the US) or +1-978-646-2777.